SURFACE FIELD MEASUREMENTS ON SCALE MODEL EC-135 AIRCRAFT FOR VPD AND SRF DATA INTERPRETATION

Valdis V. Liepa

The Radiation Laboratory
Department of Electrical and Computer Engineering
University of Michigan
Ann Arbor, Michigan 48109

July 1977

ABSTRACT

Data have been obtained for the current and charge induced on a scale model EC-135 aircraft when illuminated by a plane electromagnetic wave in a simulated free space environment. The measurements were made on a 1/216 scale model over the frequency range 450 - 4250 MHz, simulating 2.1 - 19.7 MHz full scale. The test points and directions of excitation and polarization were chosen to correspond to those used in the full scale measurements at the VPD and SRF facilities at Kirtland AFB.

PREFACE

It is a pleasure to acknowledge the enthusiasm given by Messrs. K. Powers, R. Stoddard, J. Tedesco, and K. Young in performing the measurements, computer programming, data processing, and other tasks related to obtaining these data. Special thanks go to Mr. I. LaHaie who spent many frustrating hours in the process of interfacing the HP9830A calculator with the University of Michigan computer. The assistance provided by the Computing Center personnel, especially Mr. Dave Flower, is also acknowledged.

TABLE OF CONTENTS

ILLUSTRATIONS

SECTION I

INTRODUCTION

The data presented here were obtained for the Autonetics Group of Rockwell International to assist in extrapolating [1] the results of tests made in EMP simulators, and the test points and excitation conditions were chosen to correspond to those used in measurements made in the VPD and SRF facilities at Kirtland AFB. The data were recorded, reduced and plotted digitally, and have also been furnished to Rockwell in digital form on computer cards, as well as stored on (IBM compatible) magnetic tape. It should be emphasized that the data are in raw form. So as not to lose information that may be relevant to the development of analytical techniques such as SEM, no smoothing has been carried out to remove the minor perturbations attributable to measurement noise, nor have any corrections been applied to account for probe integration. Based on previous measurements performed using clean cylindrical and spherical bodies, probe correction factors have been developed [2] which could be applied to the data in digital form were it found desirable to do so.

---

1. Carl E. Baum, "Extrapolation Techniques for Interpreting the Results of Tests in EMP Simulators in Terms of EMP Criteria", AFWL Sensors and Simulation Notes, Note 222, 1977.

2. Valdis V. Liepa, "Sweep Frequency Surface Field Measurements", University of Michigan Radiation Laboratory Report No. 013378-1-F, AFWL-TR-75-217, 1975.

SECTION II

MEASUREMENTS

The measurements were made using a single 1/216 scale model 707 aircraft modified by the addition of HF wires and a refueling boom to simulate the EC-135. Based on the dimensions of the EC-135, the actual scaling factors for the model are 1/215.11 for the length and 1/225.29 for the wingspan and for measurements on the fuselage and wings the corresponding scale factor was used to convert a measurement frequency to a full scale one.

For the most part the measurement techniques are the same as previously used [3], but two changes that were made are the use of a new and larger anechoic chamber [4] and the direct digitization and recording of the data. The measurements were performed over three overlapping bands 450 - 1100, 1000 - 2200 and 2000 - 4250 MHz with the model and sensor held fixed while data was obtained for all three bands. In contrast to previous studies where the probe was moved from one test point to another to complete the data gathering in each frequency band before moving to the next, the new procedure avoids the possibility of probe positioning error that can lead to discrepancies in the overlapping portions of the bands. On the other hand, the use of only a single model no longer enables us to employ the data spread to estimate the sensitivity to model differences and sensor positioning.

---

3. Valdis V. Liepa, "Surface Field Measurements on Scale Model EC-135 Aircraft", University of Michigan Radiation Laboratory Report No. 014182-1-F, AFWL-TR-77-101, 1977.

4. Valdis V. Liepa, "Surface Field Measurements on Scale Model E-4 Aircraft", University of Michigan Radiation Laboratory Report No. 014182-2-F, AFWL-TR-77-111, 1977.

The currents were measured using loops 0.31 cm in outside diameter made from 0.76 cm diameter 50 ohm semi-rigid coax, and the charge (or normal electric field) using a 0.2 cm long monopole made by extending the center conductor of the coax. Various views of the model with current and charge probes in position are shown in Figures 1 through 4 and details of the particular measurement situation are given below each figure.

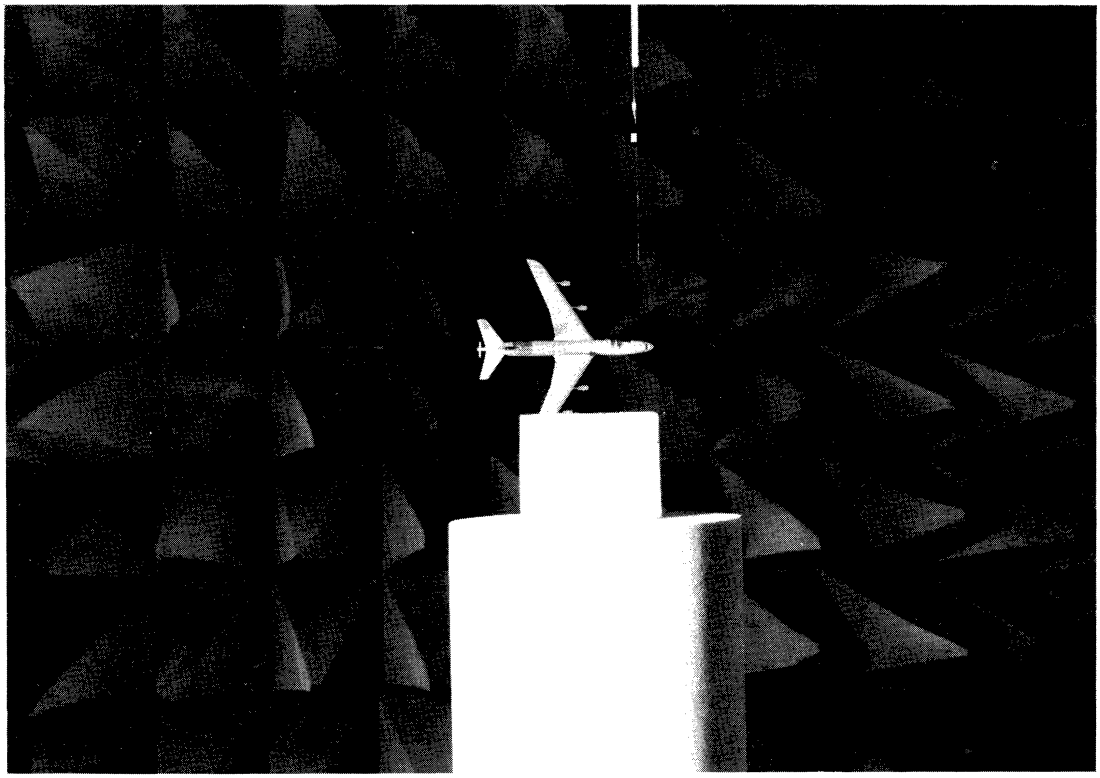

Figure 1.

An EC-135 mounted on a styrofoam pedestal in the anechoic chamber for topside incidence, E parallel to the fuselage. The vertical wire in the upper part of the photograph is a magnetic sensor. The photograph was taken from the transmitting antenna direction.

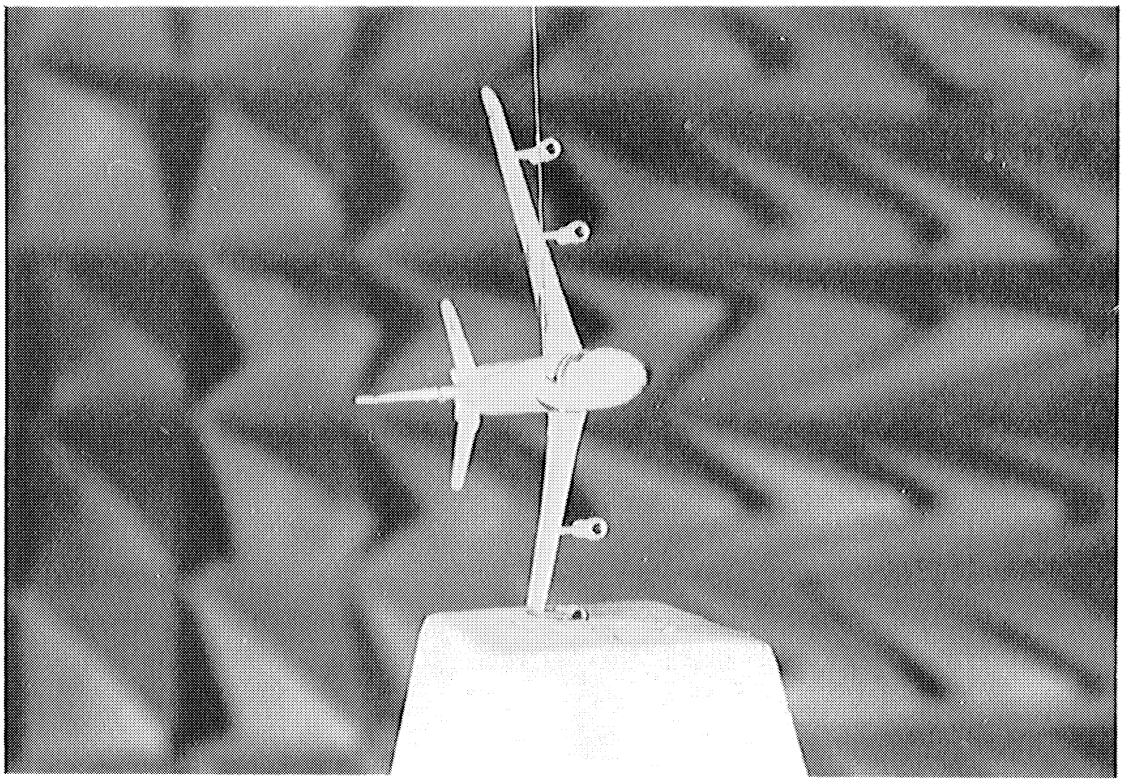

Figure 2.

A loop sensor placed for current measurement at TP:F520T, top incidence, E parallel to the fuselage. For this view the incidence is from the left.

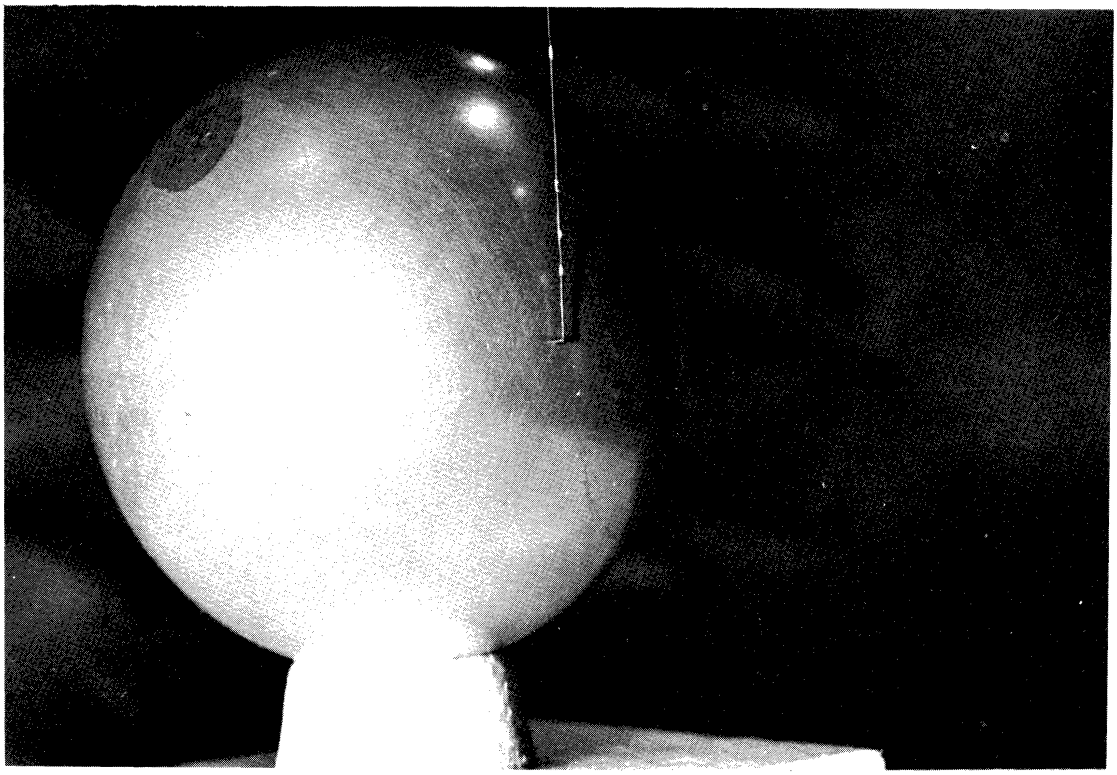

Figure 3.

A current measurement is made in front of a 6-inch diameter sphere to calibrate the system. In case of charge measurements, a 3-inch diameter sphere which can be split in two halves to insert the sensor is used. The calibration measurement is then made with the monopole placed at the shadow boundary of the sphere.

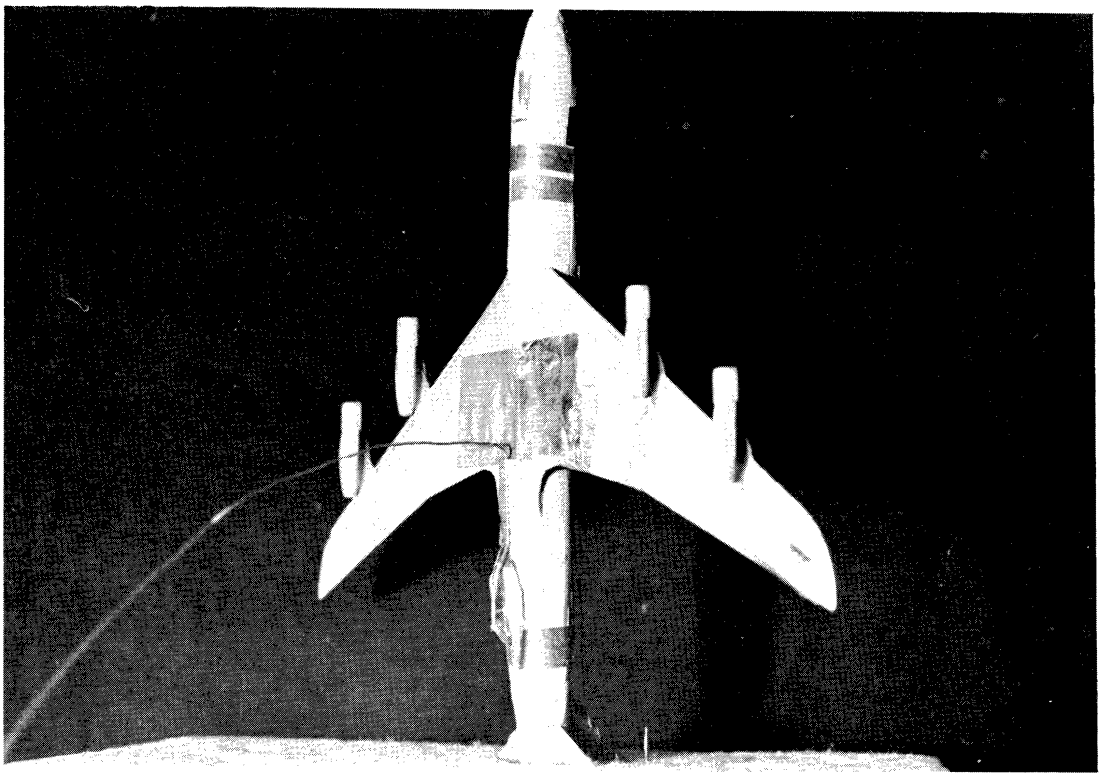

Figure 4.

To minimize the lead interaction with the model in the charge measurements, the coax is removed perpendicular to the fuselage. In this particular situation the charge would be measured at TP:F1350T, E perpendicular to the fuselage.

SECTION III

DATA

Results are presented for 36 current and 24 charge measurements, and the cases considered are summarized in Table 1, which can also serve as a guide in locating a particular data set. The abbreviations used in the Table and in the subsequent plots are as follows:

PARF - electric field parallel to the fuselage

PERPF - electric field perpendicular to the fuselage

PARV - electric field paralled to the vertical stabilizer

TOP - top incidence

NOSE - nose-on or forward incidence

SIDEL - broadside incidence, left side

In the identification of the test points, letter references are:

F - fuselage

HL - horizontal stabilizer, left

WL - wing, left

VL - vertical stabilizer, left side

and the letter T or B following a test point number indicates a top or bottom measurement respectively.

The particular measurement situation is also described in the title printed on each figure. As an example, consider Figure 6. The title at the top gives the test point location (TP:F520T), the polarization (PARF), the illumination (TOP), the quantity measured (J_A), and the file names where the data is stored (E1207, E1209, E1211). As a futher aid, a sketch of the aircraft is included showing the measurement point and the directions of excita-

tion and polarization.

The current amplitudes are normalized to the incident magnetic field H_o and the charge amplitudes to the incident electric field E_o. The incident field phase reference (or origin) is TP:F520T. A time convention $e^{i\omega t}$ is employed, corresponding to a phase decrease on moving away from the source.

Figure 5 shows the components of the skin currents measured at the various test locations. The words "axial" (J_A) and "circumferential" (J_C) used in describing these components are somewhat arbitrary. Thus, on the wings and horizontal and vertical stabilizers, the components J_A and J_C are actually perpendicular and parallel to the fuselage, respectively. If the component in any other direction is required, this can be obtained from

$$J_\alpha = J_A \cos\alpha + J_C \sin\alpha$$

where α is the angle between the directions of J_A and J_α measured positively towards J_C. In this equation, all currents are complex quantities, reconstructed from amplitude and phase data.

Due to the symmetric shape of the model one would expect that for certain excitations some of the fields measured on the fuselage should be zero. These cases are indicated by an asterisk (*) in Table 1 and also noted on the appropriate figures. However, due to the presence of the HF wires, the model is not really symmetric and many data that should be null show evidence of coupling from the wires to the fuselage (see Figures 22, 50). The measurements away from these wires, such as those near the nose and on the bottom of the fuselage, show less coupling and hence should be (theoretically) zero. The amplitudes of the order of 0.2 that are measured (see Figures 21, 26) are then indicative of the typical noise or background signal level present in the data.

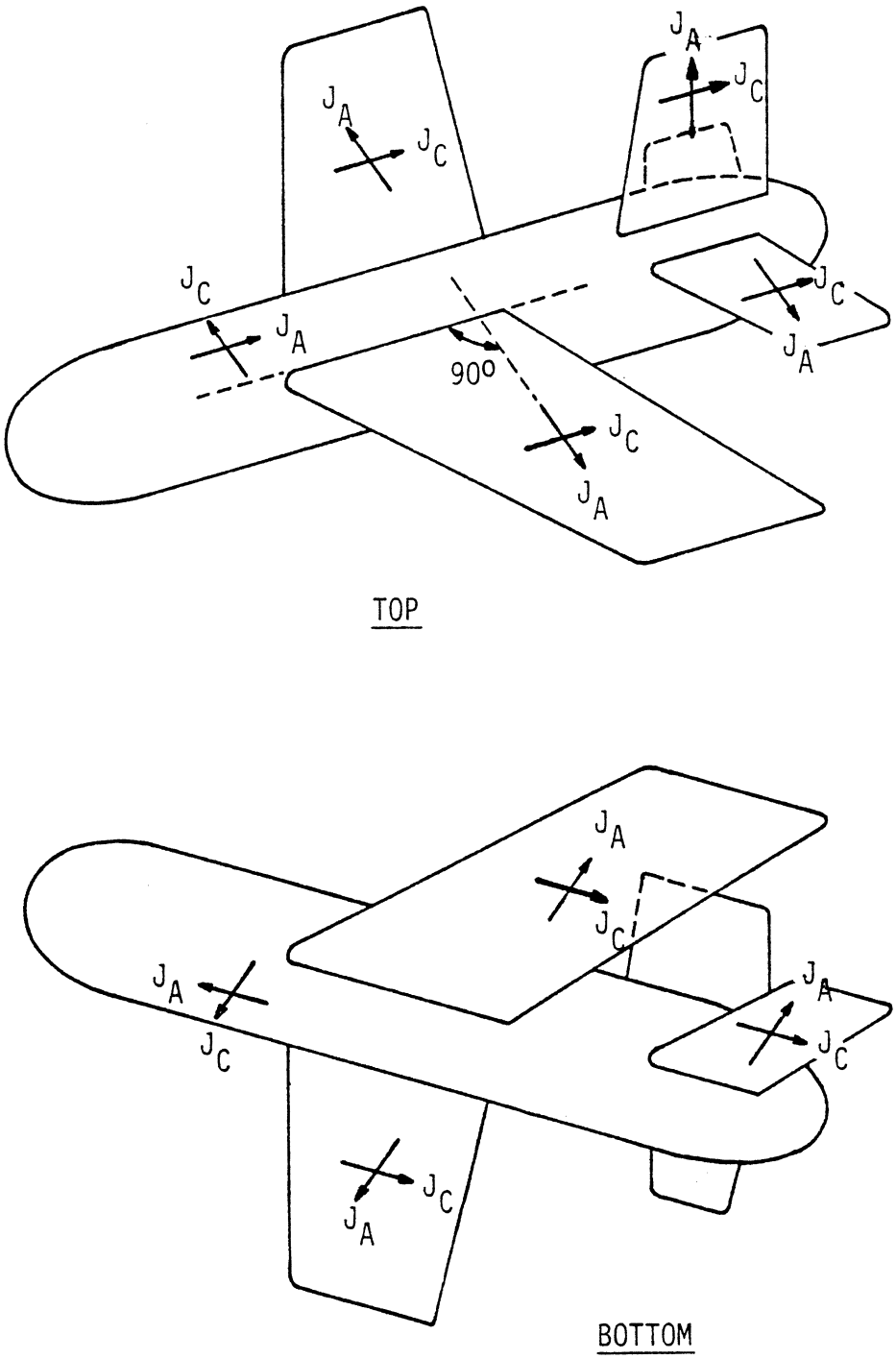

Figure 5: Directions of Measured Surface Current Components.

For those who may need the data in digital form, an illustration of a typical data set is provided by Table 2 showing the data used to generate Figure 30. It consists of three separate files, recorded in different bands and each stored in the format:

1. FILENAME (4A4)
2. Comments (18A4)
3. Comments (18A4)
4. TITLE for plotting (18A4)
5. FMIN, FMAX, AMPMIN, AMPMAX, PHASEMIN, PHASEMAX, NN
   (4F8.3, 2F8.2, I5)
6. F(1) AMP(1) PHASE(1) F(2) AMP(2) PHASE(2) F(3) AMP(3) PHASE (3)
   (3(2F8.3, F8.2)

data ↓

. . . F(NN) AMP(NN) PHASE(NN)

The data is stored on magnetic tape and can be provided to any authorized user.

```
1     E1211
2     EC135/216,F520T,PARF TOP,JA,1,A,6/23/77
3
4
5        2.104    5.151    3.214    9.144   -28.59    50.09  138
6        2.104    4.804    50.09    2.126    4.511    47.75    2.148    4.634    48.90
7        2.170    4.673    47.64    2.193    4.854    47.17    2.215    4.837    47.99
8        2.237    4.841    47.19    2.259    5.015    49.19    2.282    5.146    49.08
9        2.304    5.427    47.96    2.326    5.567    47.93    2.348    5.579    46.19
10       2.371    5.854    44.85    2.393    5.904    45.49    2.415    5.955    43.54
11       2.437    6.157    43.67    2.460    6.093    44.90    2.482    6.415    43.72
12       2.504    6.783    44.45    2.526    6.864    43.26    2.548    7.205    40.28
13       2.571    7.388    38.89    2.593    7.334    35.90    2.615    7.483    36.01
14       2.637    7.511    35.92    2.660    7.624    32.82    2.682    7.899    32.63
15       2.704    7.959    31.34    2.726    8.129    28.45    2.749    8.358    27.36
16       2.771    8.224    24.97    2.793    8.375    22.39    2.815    8.350    21.81
17       2.838    8.268    19.83    2.860    8.589    18.96    2.882    8.619    17.59
18       2.904    8.626    13.73    2.927    8.834    12.57    2.949    8.656    10.22
19       2.971    8.461     6.58    2.993    8.364     5.84    3.016    8.080     4.21
20       3.038    8.021     2.09    3.060    7.980     1.67    3.082    7.847    -0.53
21       3.105    7.895    -2.83    3.127    7.672    -4.02    3.149    7.437    -6.49
22       3.171    7.309    -8.06    3.194    6.922    -9.72    3.216    6.692   -11.97
23       3.238    6.468   -12.01    3.260    6.096   -13.04    3.283    5.904   -14.45
24       3.305    5.601   -14.96    3.327    5.289   -15.96    3.349    4.993   -15.94
25       3.372    4.554   -14.81    3.394    4.134   -13.78    3.416    3.787   -10.02
26       3.438    3.359    -3.27    3.461    3.214     7.71    3.483    3.647    21.70
27       3.505    4.774    25.40    3.527    5.645    16.50    3.550    5.439     8.03
28       3.572    4.857     4.86    3.594    4.469     7.11    3.616    4.266    12.37
29       3.639    4.235    17.54    3.661    4.433    22.92    3.683    4.706    26.51
30       3.705    5.111    28.42    3.728    5.551    30.43    3.750    5.975    30.96
31       3.772    6.446    30.30    3.794    6.955    29.15    3.817    7.401    27.21
32       3.839    7.841    24.98    3.861    8.137    22.56    3.883    8.406    19.66
33       3.906    8.665    16.96    3.928    8.812    14.37    3.950    8.940    11.59
34       3.972    9.093     8.93    3.995    9.018     6.36    4.017    9.091     4.51
35       4.039    9.144     2.67    4.061    9.073     0.43    4.083    9.066    -1.80
36       4.106    9.040    -3.32    4.128    8.953    -5.44    4.150    8.910    -7.45
37       4.172    8.768    -9.16    4.195    8.589   -11.06    4.217    8.396   -12.46
38       4.239    8.209   -13.35    4.261    8.065   -14.04    4.284    7.980   -14.23
39       4.306    7.861   -14.72    4.328    7.798   -15.20    4.350    7.792   -15.99
40       4.373    7.805   -17.27    4.395    7.731   -18.15    4.417    7.640   -18.84
41       4.439    7.518   -19.52    4.462    7.415   -20.11    4.484    7.316   -21.10
42       4.506    7.252   -21.69    4.528    7.142   -22.29    4.551    7.033   -22.89
43       4.573    6.928   -23.39    4.595    6.841   -23.50    4.617    6.757   -23.71
44       4.640    6.720   -23.73    4.662    6.685   -23.76    4.684    6.651   -24.39
45       4.706    6.603   -25.23    4.729    6.526   -26.17    4.751    6.465   -26.72
46       4.773    6.391   -26.78    4.795    6.246   -26.55    4.818    6.205   -26.22
47       4.840    6.192   -26.41    4.862    6.166   -26.60    4.884    6.126   -27.10
48       4.907    6.073   -27.61    4.929    6.007   -27.92    4.951    5.915   -28.05
49       4.973    5.865   -28.09    4.996    5.815   -28.03    5.018    5.753   -27.98
50       5.040    5.744   -28.05    5.062    5.695   -28.12    5.085    5.674   -28.30
51       5.107    5.639   -28.28    5.129    5.566   -28.58    5.151    5.544   -28.59
```

Table 2. Data used for Figure 8 (3 files)

```
1     E1209
2     EC135/216,F520T,PARF TOP,JA,2,A,6/23/77
3
4
5        4.651  10.256   1.395   6.772  -61.67   12.74  127
6        4.651   6.772  -23.94   4.695   6.719  -24.60   4.740   6.488  -26.09
7        4.784   6.282  -26.31   4.829   6.184  -25.66   4.873   6.175  -26.35
8        4.918   6.040  -27.67   4.962   5.856  -27.42   5.007   5.744  -27.01
9        5.051   5.713  -26.93   5.096   5.643  -27.29   5.140   5.498  -27.99
10       5.185   5.468  -27.11   5.229   5.513  -27.47   5.274   5.443  -30.76
11       5.318   5.263  -30.08   5.363   5.158  -29.62   5.407   5.160  -29.19
12       5.452   5.160  -29.19   5.496   5.122  -29.70   5.541   5.083  -30.34
13       5.585   5.031  -30.89   5.630   4.920  -31.45   5.674   4.777  -30.73
14       5.719   4.689  -29.31   5.763   4.643  -29.51   5.808   4.575  -28.00
15       5.852   4.663  -25.21   5.896   4.807  -25.41   5.941   4.896  -29.01
16       5.985   4.871  -28.40   6.030   4.856  -29.20   6.074   4.905  -34.58
17       6.119   4.753  -30.46   6.163   4.699  -32.62   6.208   4.731  -31.97
18       6.252   4.740  -31.31   6.297   4.769  -32.03   6.341   4.775  -33.14
19       6.386   4.736  -34.03   6.430   4.707  -34.20   6.475   4.764  -35.45
20       6.519   4.810  -37.88   6.564   4.659  -37.89   6.608   4.564  -39.58
21       6.653   4.501  -40.05   6.697   4.470  -40.69   6.742   4.429  -41.41
22       6.786   4.328  -41.71   6.831   4.329  -42.48   6.875   4.250  -41.63
23       6.920   4.232  -45.16   6.964   4.109  -45.27   7.009   4.055  -45.26
24       7.053   4.030  -46.33   7.098   3.907  -47.78   7.142   3.805  -47.72
25       7.187   3.751  -45.84   7.231   3.724  -47.45   7.276   3.656  -50.15
26       7.320   3.566  -48.84   7.365   3.660  -48.72   7.409   3.622  -55.90
27       7.454   3.393  -61.67   7.498   3.100  -56.84   7.542   2.940  -61.01
28       7.587   2.707  -56.89   7.631   2.558  -56.97   7.676   2.485  -54.86
29       7.720   2.432  -54.06   7.765   2.310  -54.57   7.809   2.216  -54.09
30       7.854   2.102  -52.52   7.898   2.035  -50.67   7.943   2.004  -51.84
31       7.987   1.803  -52.72   8.032   1.576  -47.52   8.076   1.534  -38.54
32       8.121   1.653  -36.08   8.165   1.636  -37.54   8.210   1.476  -34.81
33       8.254   1.468  -28.31   8.299   1.452  -25.92   8.343   1.395  -19.74
34       8.388   1.499  -12.69   8.432   1.687  -11.35   8.477   1.747  -12.83
35       8.521   1.697  -12.22   8.566   1.689  -10.32   8.610   1.709  -10.04
36       8.655   1.647   -7.86   8.699   1.646   -1.90   8.744   1.751    3.56
37       8.788   1.914    3.80   8.833   2.111   -0.95   8.877   2.108    1.98
38       8.922   2.100   -1.98   8.966   2.039    2.65   9.011   2.068    0.88
39       9.055   2.054    4.31   9.100   2.155    8.34   9.144   2.372    9.08
40       9.188   2.448    5.62   9.233   2.434    4.96   9.277   2.437    6.01
41       9.322   2.507    7.57   9.366   2.486    3.54   9.411   2.408    7.01
42       9.455   2.534   10.10   9.500   2.666    9.89   9.544   2.679    8.80
43       9.589   2.741   11.12   9.633   2.870   12.15   9.678   3.011    9.49
44       9.722   2.996    8.95   9.767   3.058    9.42   9.811   3.164    8.20
45       9.856   3.199    7.70   9.900   3.325    6.91   9.945   3.363    4.33
46       9.989   3.416   -0.03  10.034   3.158   -4.08  10.078   2.808   -1.32
47      10.123   2.694    5.26  10.167   2.751   10.54  10.212   2.955   12.74
48      10.256   3.075   12.54
```

Table 2. Data used for Figure 8 (cont.)

```
1     E1207
2     EC135/216,F520T,PARF TOP,JA,3,A,6/23/77
3
4     EC-135 TP:F520T PARF TOP JA;E1207,1209,1211
5        9.298   19.773    1.056    5.369   -45.41    12.54   135
6        9.298    2.402     3.05    9.376    2.341     6.01   9.454   2.552    8.60
7        9.532    2.638     8.92    9.610    2.827     9.08   9.688   2.961    7.08
8        9.767    3.065     6.72    9.845    3.253     4.60   9.923   3.298    0.52
9       10.001    3.022    -5.82   10.079    2.608     1.58  10.158   2.797    9.02
10      10.236    3.028    10.99   10.314    3.280    10.89  10.392   3.364   11.51
11      10.470    3.666    12.54   10.548    3.951     9.99  10.627   4.080    7.93
12      10.705    4.167     6.27   10.783    4.278     5.30  10.861   4.540    4.42
13      10.939    4.732     1.31   11.017    4.745    -1.33  11.096   4.826   -3.20
14      11.174    5.001    -5.30   11.252    5.008    -7.63  11.330   5.096   -8.50
15      11.408    5.369   -11.60   11.487    5.351   -15.64  11.565   5.320  -18.91
16      11.643    5.275   -21.40   11.721    5.181   -25.13  11.799   4.892  -27.17
17      11.877    4.812   -28.13   11.956    4.666   -28.21  12.034   4.628  -29.70
18      12.112    4.401   -30.79   12.190    4.330   -29.88  12.268   4.318  -31.56
19      12.346    4.167   -31.54   12.425    4.218   -31.71  12.503   4.162  -34.16
20      12.581    3.956   -34.59   12.659    3.865   -36.20  12.737   3.899  -36.68
21      12.816    3.764   -37.84   12.894    3.692   -36.97  12.972   3.664  -37.77
22      13.050    3.586   -38.05   13.128    3.551   -37.70  13.206   3.516  -37.92
23      13.285    3.508   -38.22   13.363    3.436   -38.50  13.441   3.470  -38.06
24      13.519    3.433   -39.71   13.597    3.391   -40.26  13.676   3.281  -40.99
25      13.754    3.236   -39.63   13.832    3.275   -40.27  13.910   3.248  -40.72
26      13.988    3.200   -41.48   14.066    3.104   -41.55  14.145   3.138  -41.05
27      14.223    3.124   -42.36   14.301    3.060   -42.99  14.379   3.004  -43.85
28      14.457    2.937   -43.83   14.535    2.864   -44.34  14.614   2.805  -43.27
29      14.692    2.831   -43.62   14.770    2.766   -44.29  14.848   2.727  -44.68
30      14.926    2.645   -44.78   15.005    2.624   -42.99  15.083   2.615  -43.51
31      15.161    2.580   -44.04   15.239    2.522   -44.67  15.317   2.487  -43.51
32      15.395    2.481   -44.14   15.474    2.395   -44.16  15.552   2.364  -43.17
33      15.630    2.318   -42.97   15.708    2.298   -42.66  15.786   2.242  -42.64
34      15.864    2.197   -41.09   15.943    2.197   -40.13  16.021   2.192  -39.84
35      16.099    2.172   -39.34   16.177    2.143   -37.82  16.255   2.163  -36.98
36      16.334    2.159   -36.42   16.412    2.155   -34.95  16.490   2.228  -34.46
37      16.568    2.298   -35.06   16.646    2.328   -37.16  16.724   2.289  -38.04
38      16.803    2.289   -39.33   16.881    2.221   -40.41  16.959   2.197  -39.60
39      17.037    2.193   -39.89   17.115    2.200   -40.59  17.193   2.163  -42.31
40      17.272    2.078   -43.03   17.350    2.052   -42.47  17.428   2.056  -42.93
41      17.506    2.045   -44.00   17.584    1.966   -45.29  17.663   1.894  -44.69
42      17.741    1.876   -45.31   17.819    1.778   -45.15  17.897   1.728  -44.80
43      17.975    1.683   -43.27   18.053    1.712   -43.24  18.132   1.644  -43.82
44      18.210    1.612   -44.71   18.288    1.533   -45.41  18.366   1.444  -44.40
45      18.444    1.369   -42.60   18.523    1.353   -39.79  18.601   1.346  -40.18
46      18.679    1.270   -41.27   18.757    1.170   -40.04  18.835   1.064  -35.20
47      18.913    1.057   -28.95   18.992    1.056   -25.49  19.070   1.059  -21.52
48      19.148    1.072   -19.03   19.226    1.070   -16.13  19.304   1.086  -13.71
49      19.382    1.094    -9.38   19.461    1.150    -6.63  19.539   1.194   -5.28
50      19.617    1.209    -3.91   19.695    1.197    -2.04  19.773   1.238    1.64
```

Table 2. Data used for Figure 8 (cont.)

Table 1: DATA IDENTIFICATION

Measurement Point		Orientation 1 PARF; TOP			Orientation 2 PERPF; TOP			Orientation 3 PARV; NOSE			Orientation 4 PARV; SIDEL		
Rockwell	U of Mich	J_A	J_C	E	J_A	J_C	E	J_A	J_C	E	J_A	J_C	E
02x006	F520T	Fig. 6	18*	42	Fig. 21*	29	49*						
04x016	F1350T	7		43	22*	30	50*						
05x049	HL184T	8			23						Fig. 37		
06x049	HL184B	9											
10x045	WL900T	10		44			51	Fig.		56			62
11x040	WL450T	11		45	24	31	52	32		57	38		
12x037	WL227T	12		46			53	33		58			63
13x006	F520B	13	19*	47	25*		54*	34		59	39		64
16x022	F1631B	14											
20x005	F460B							35		60			
25x021	F1608B	15			26*								
26x016	F1350B	16	20*	48	27*		55*			61	40		65
07x052	VL149	17			28						41		
21x042	WL560T							36					

Footnotes:

HF Antenna Connected-all data
Airborne-all data
PARF - E parallel to fuselage
PERPF - E perpendicular to fuselage
PARV - E parallel to vertical stabilizer

SIDEL - left side incidence
TOP - top incidence
NOSE - nose-on incidence

*except for the presence of HF wires these are zero field measurements

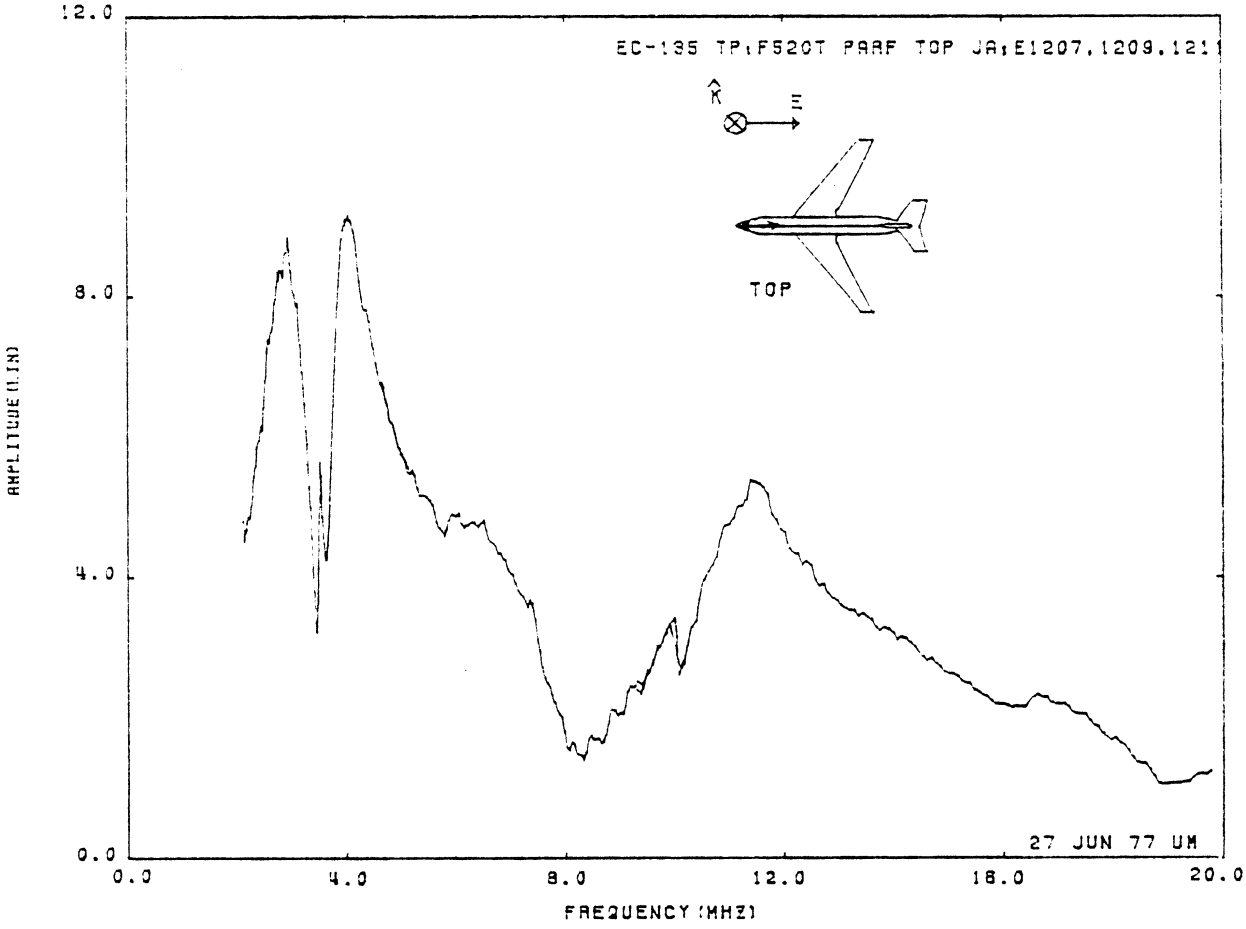

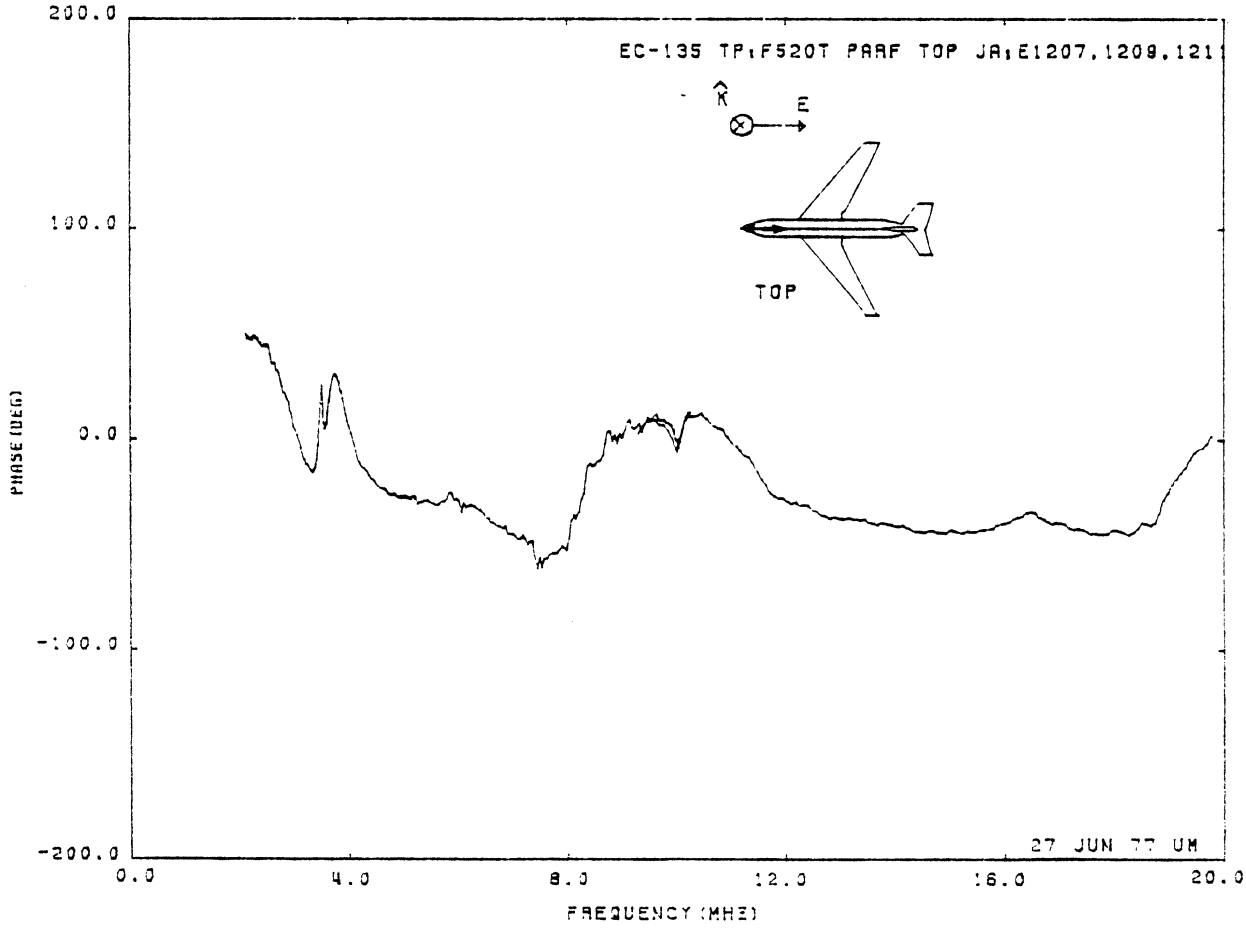

Figure 6: Axial Current at TP:F520T, Orientation 1.

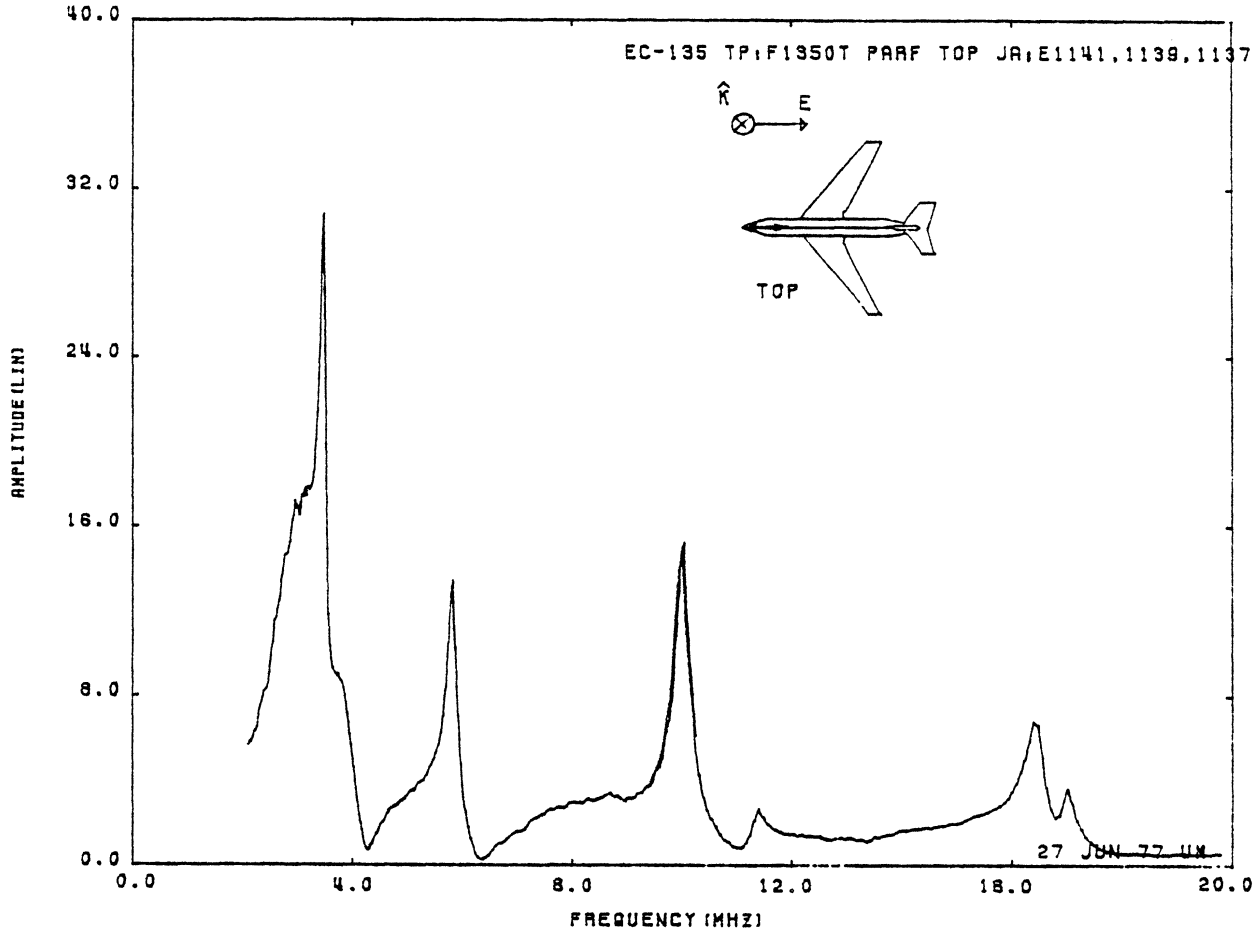

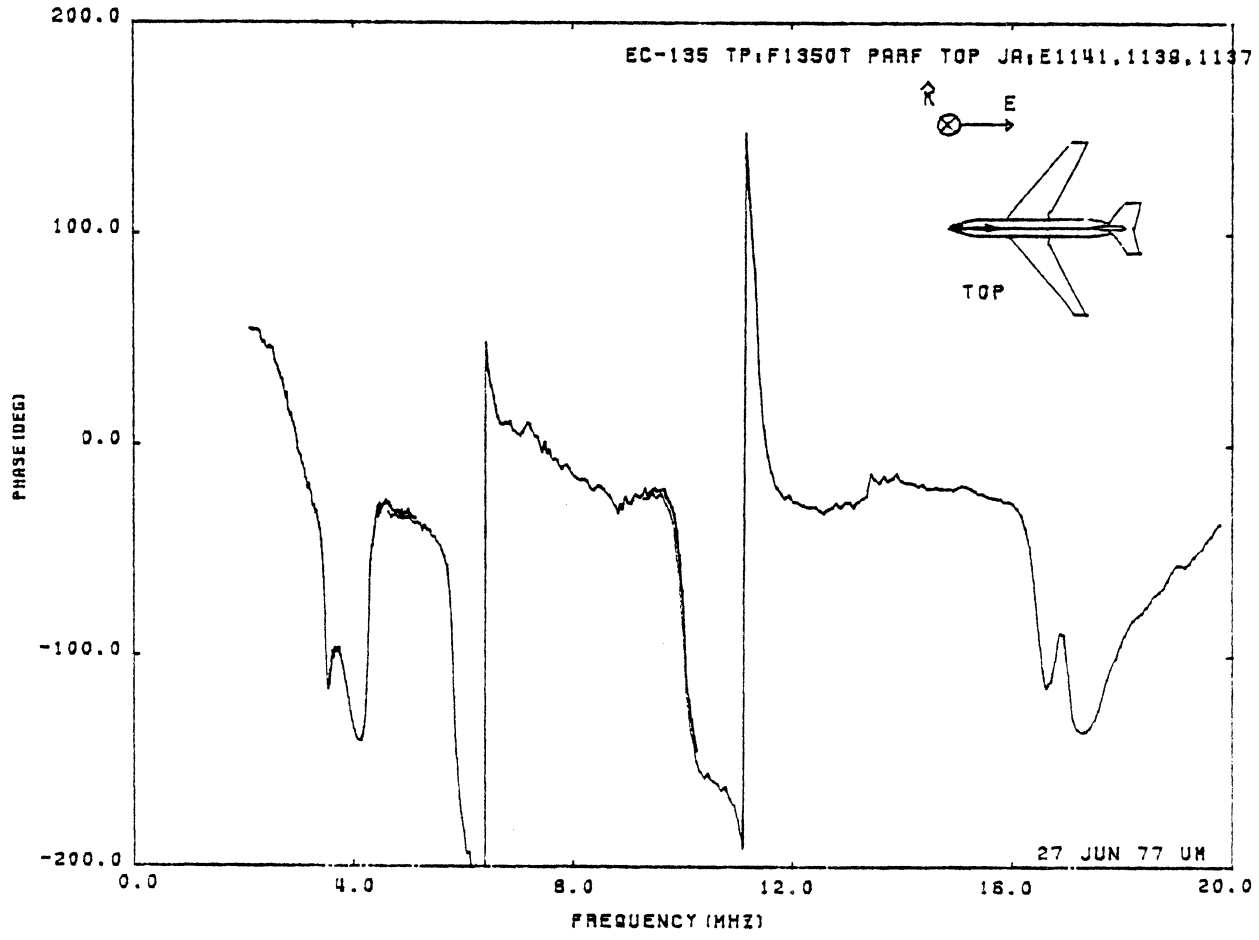

Figure 7: Axial Current at TP:F1350T, Orientation 1.

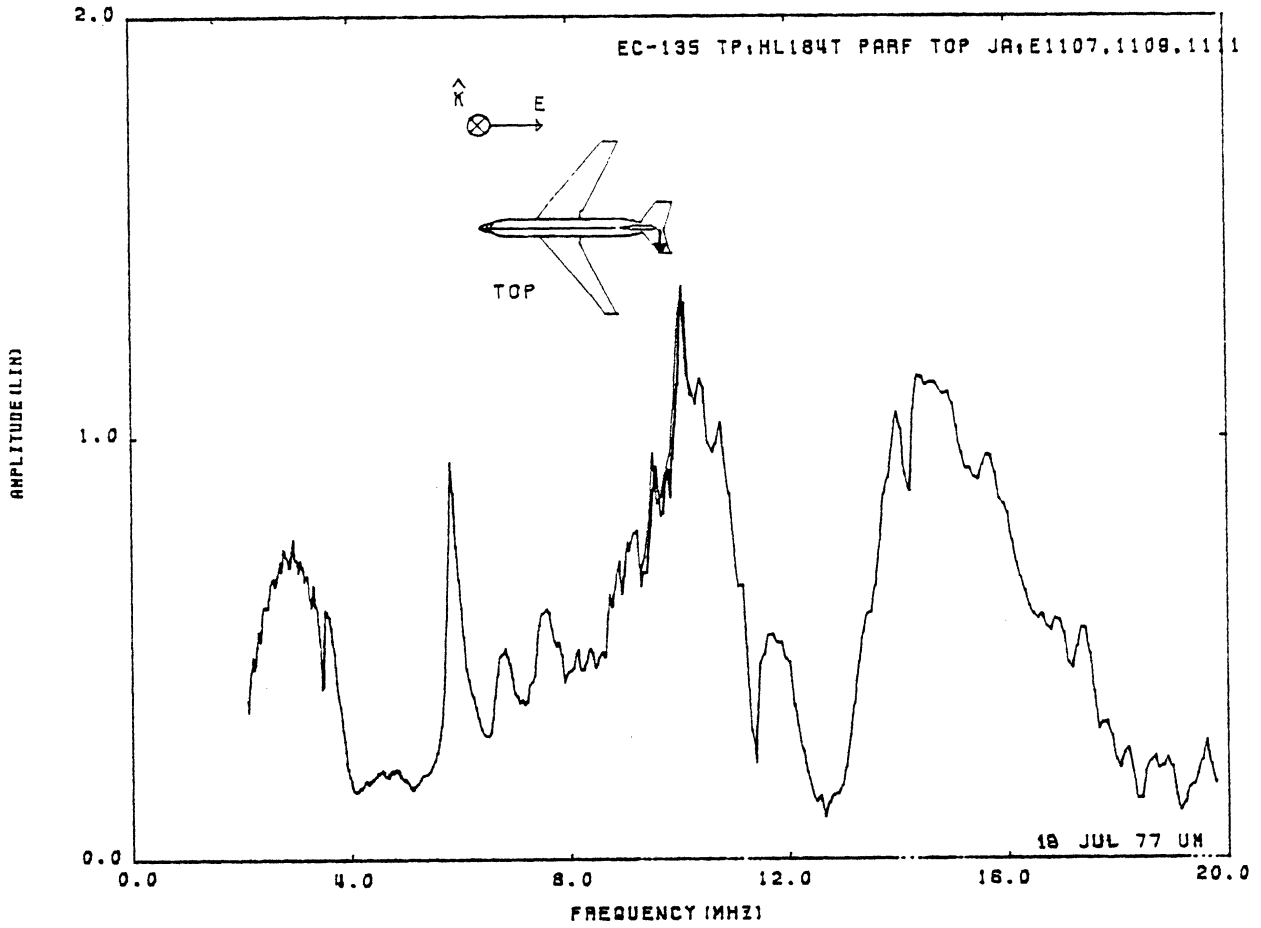

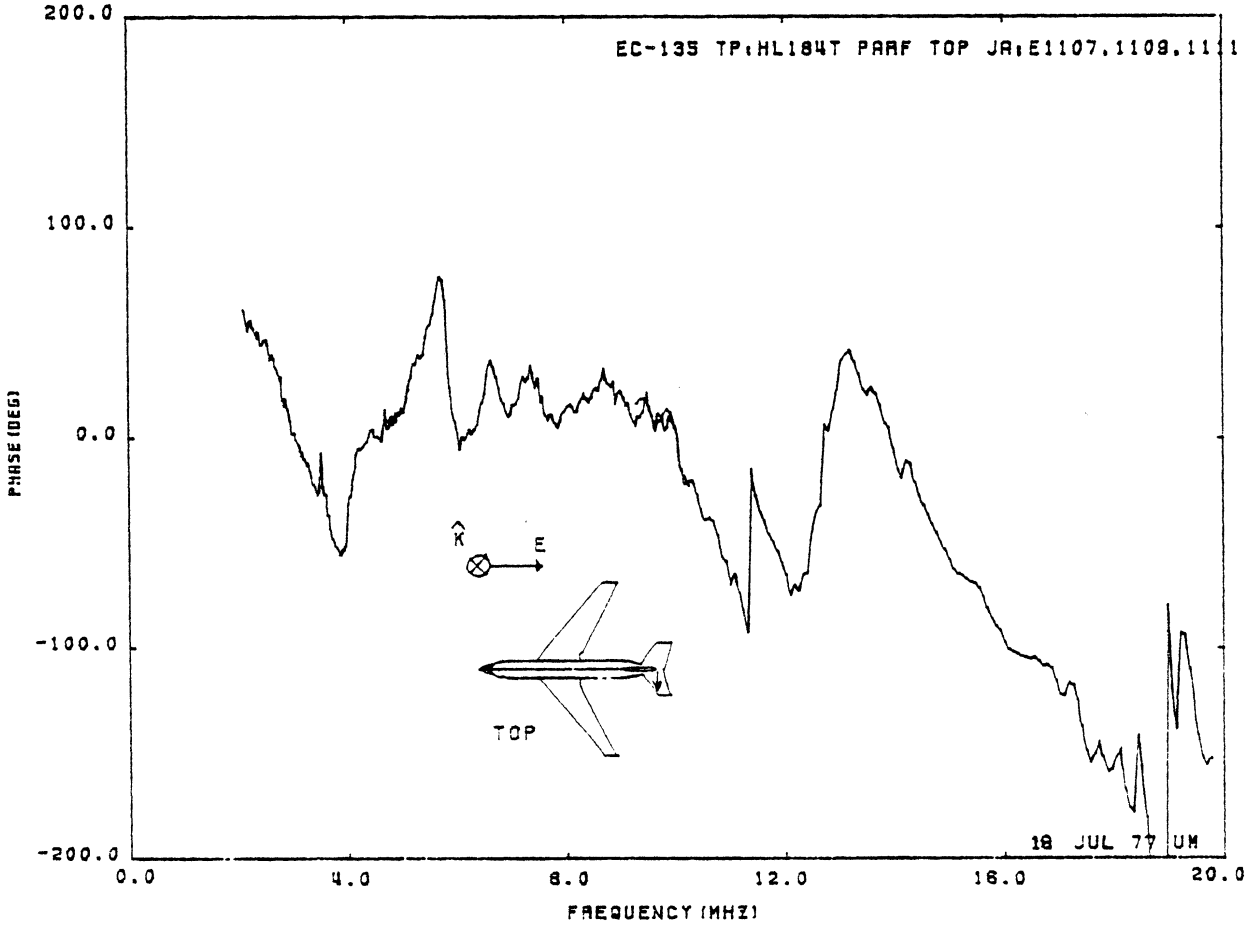

Figure 8: Axial Current at TP:HL184T, Orientation 1.

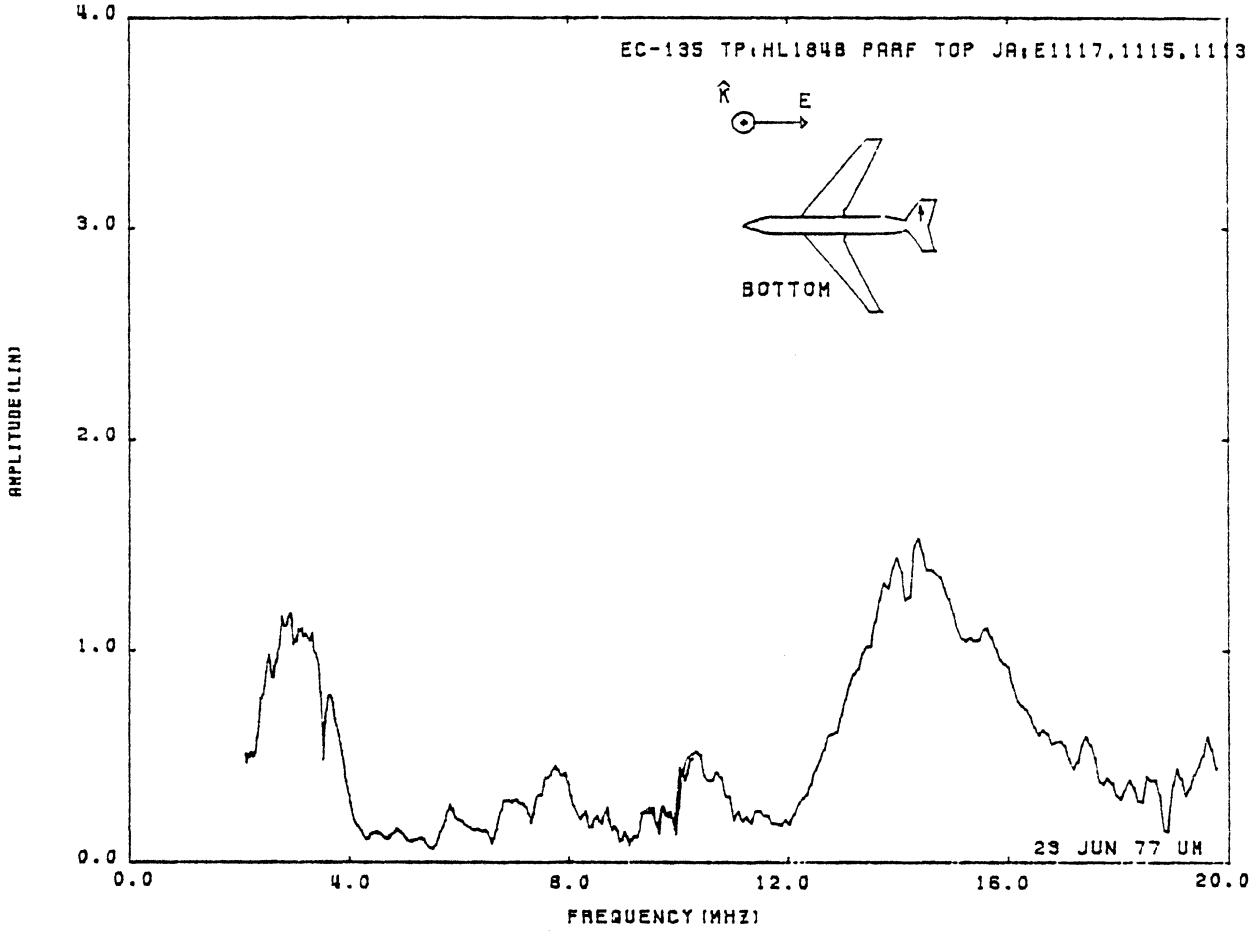

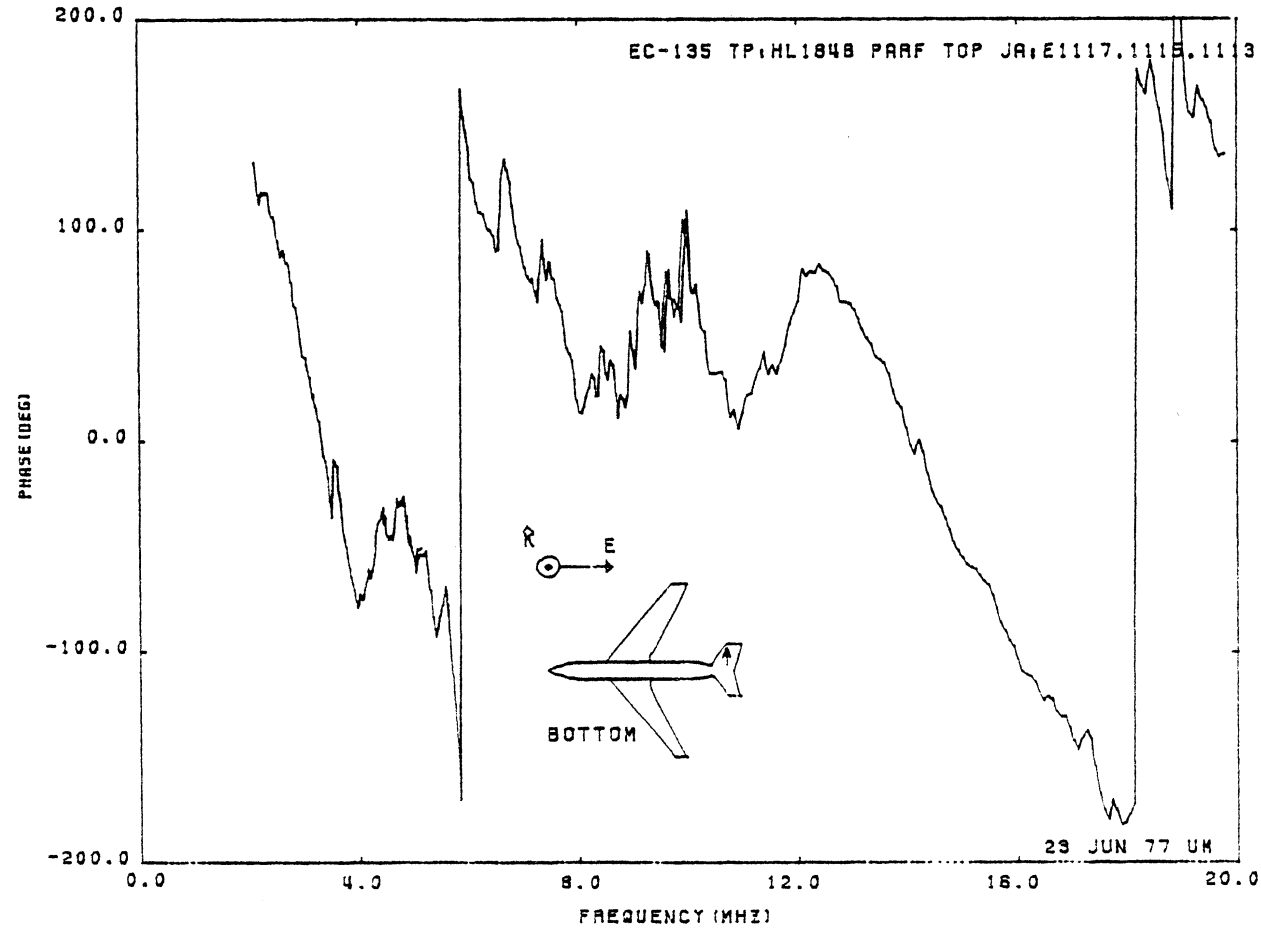

Figure 9: Axial Current at TP:HL184B, Orientation 1.

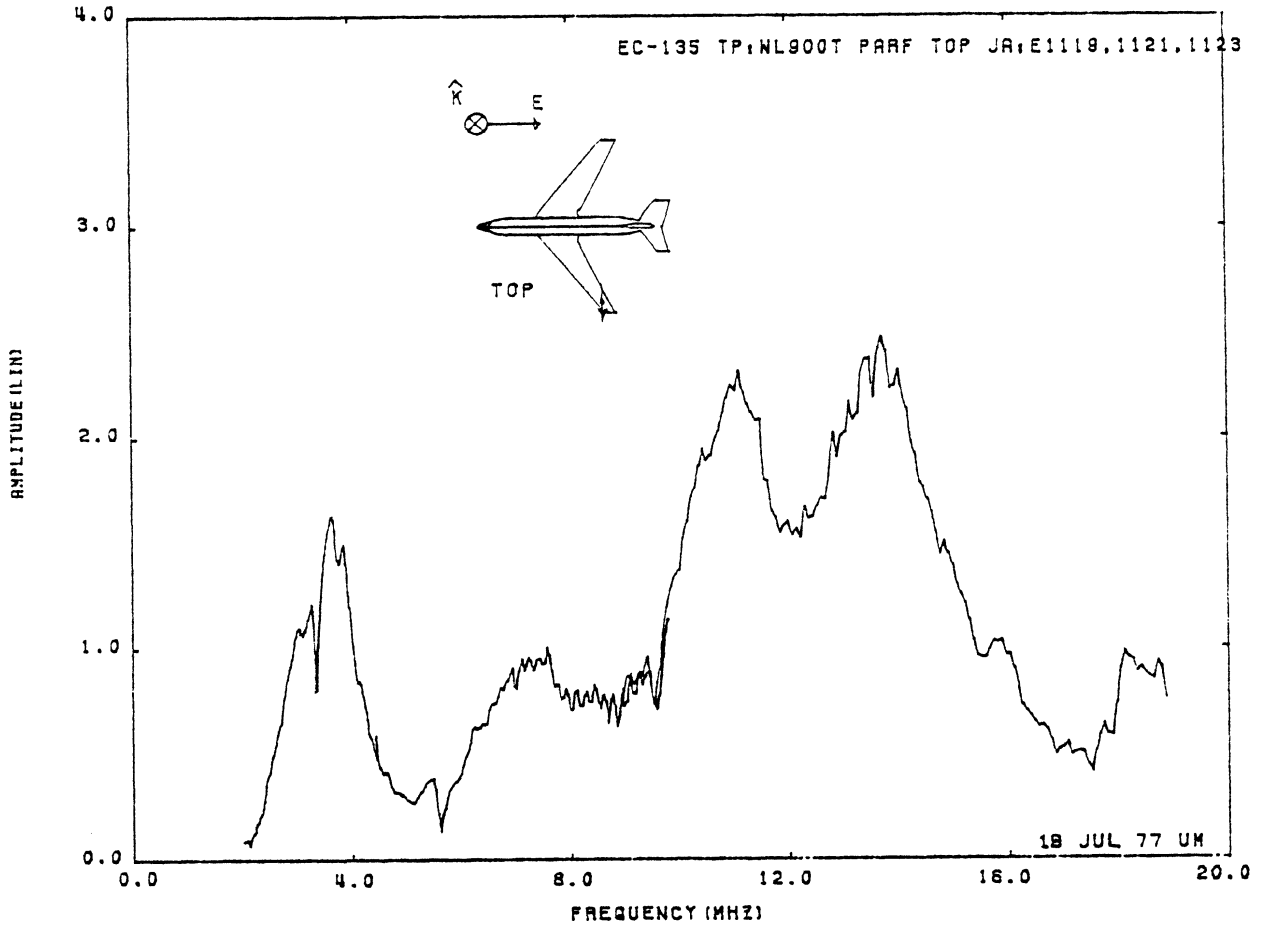

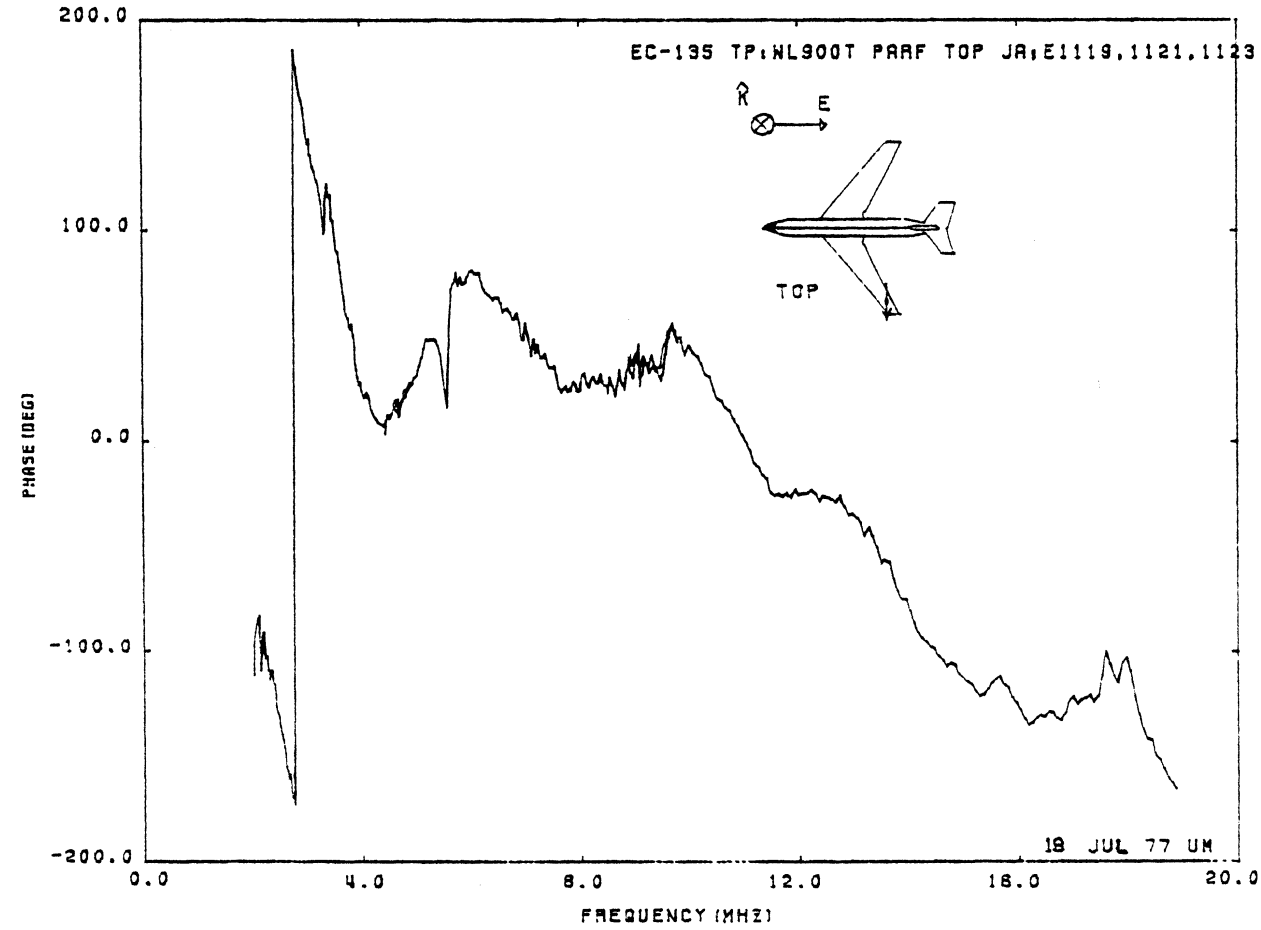

Figure 10: Axial Current at TP:WL900T, Orientation 1.

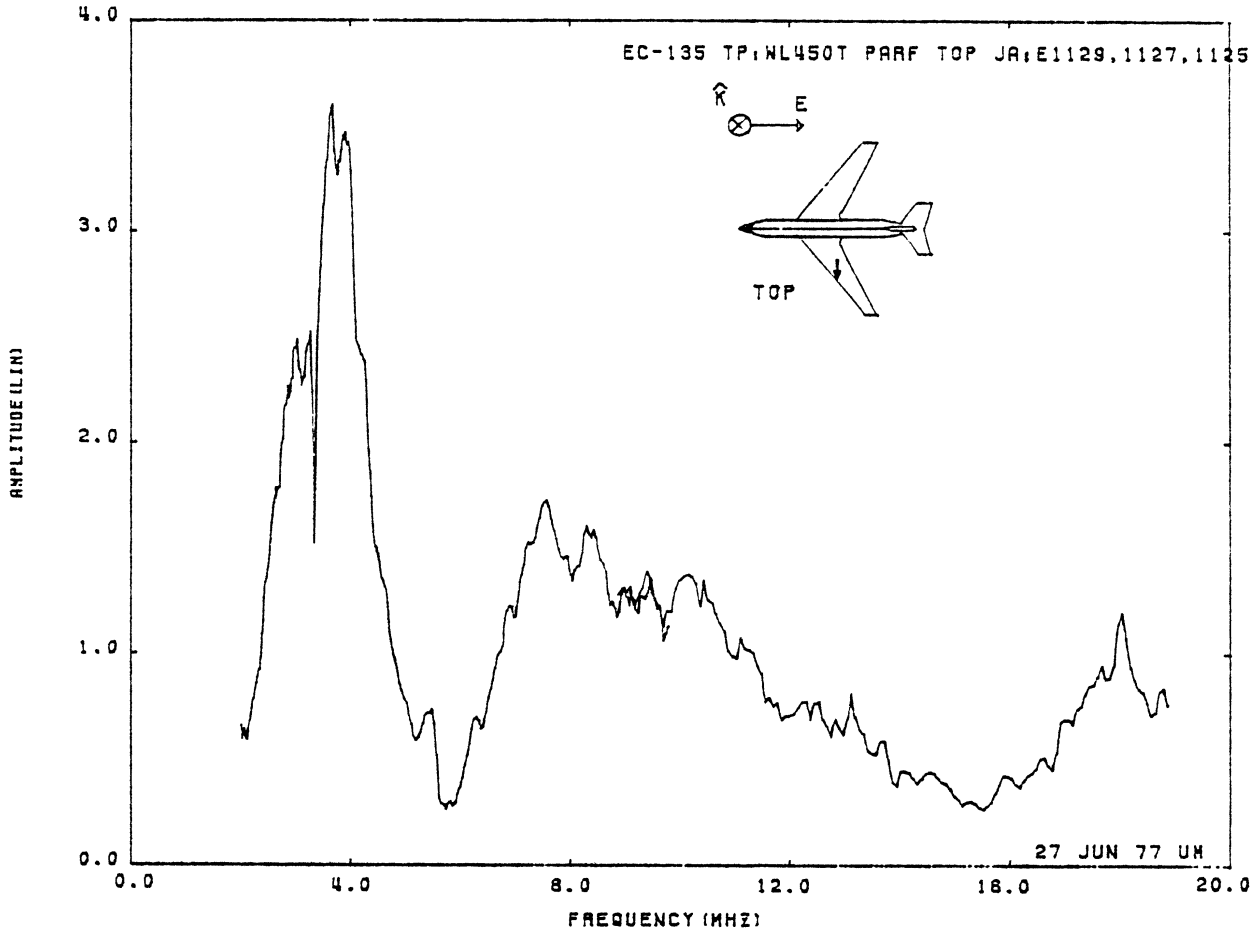

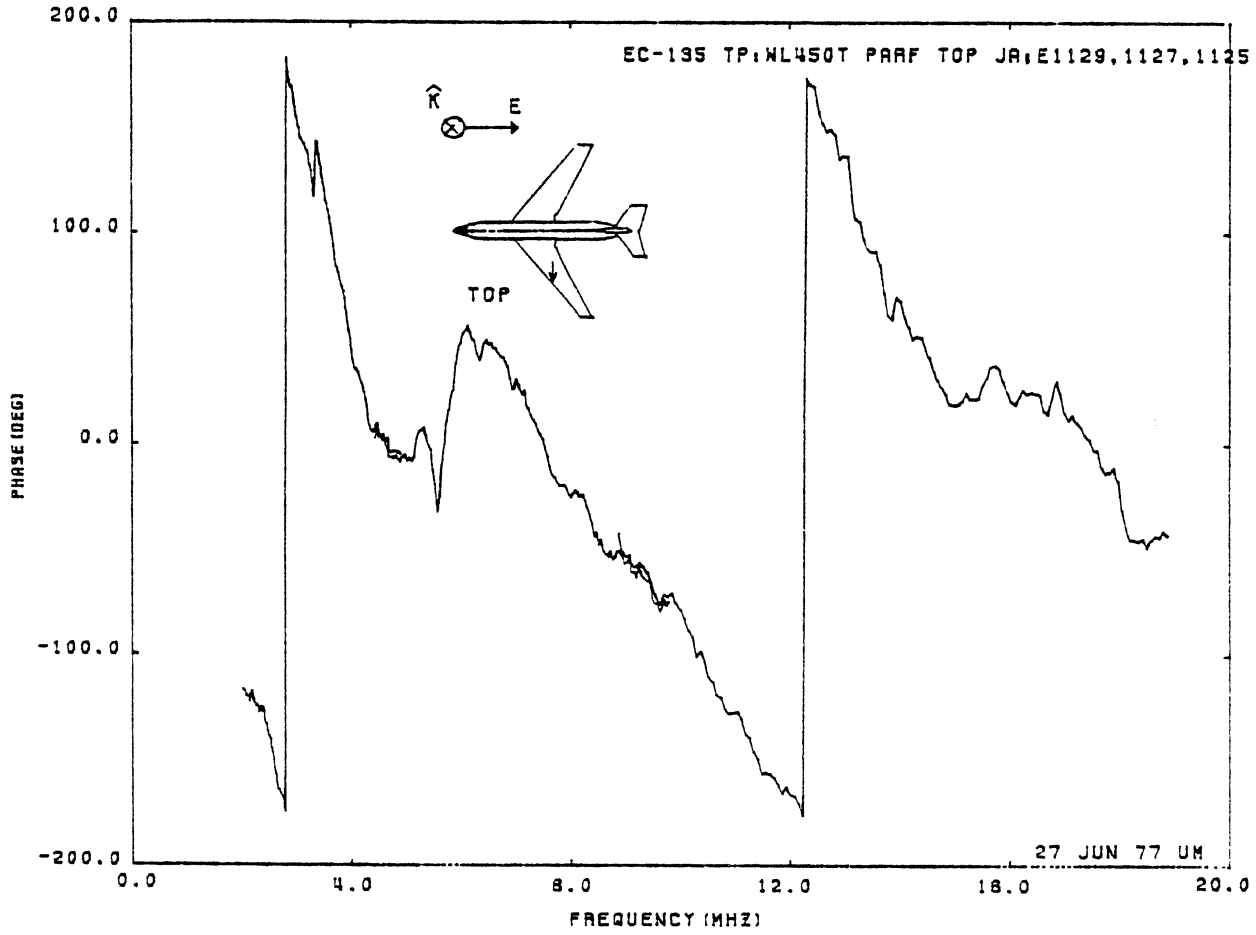

Figure 11: Axial Current at TP:WL450T, Orientation 1.

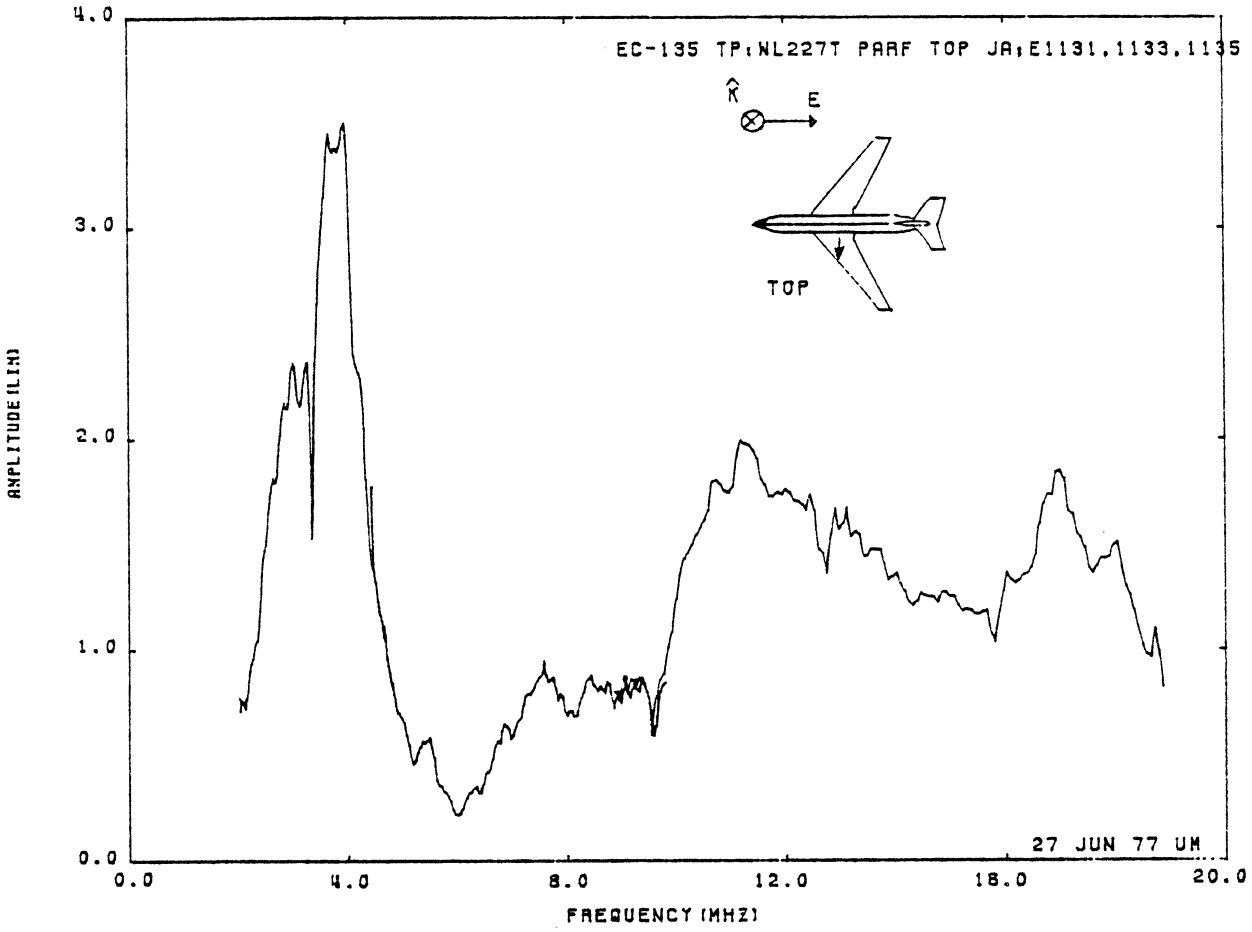

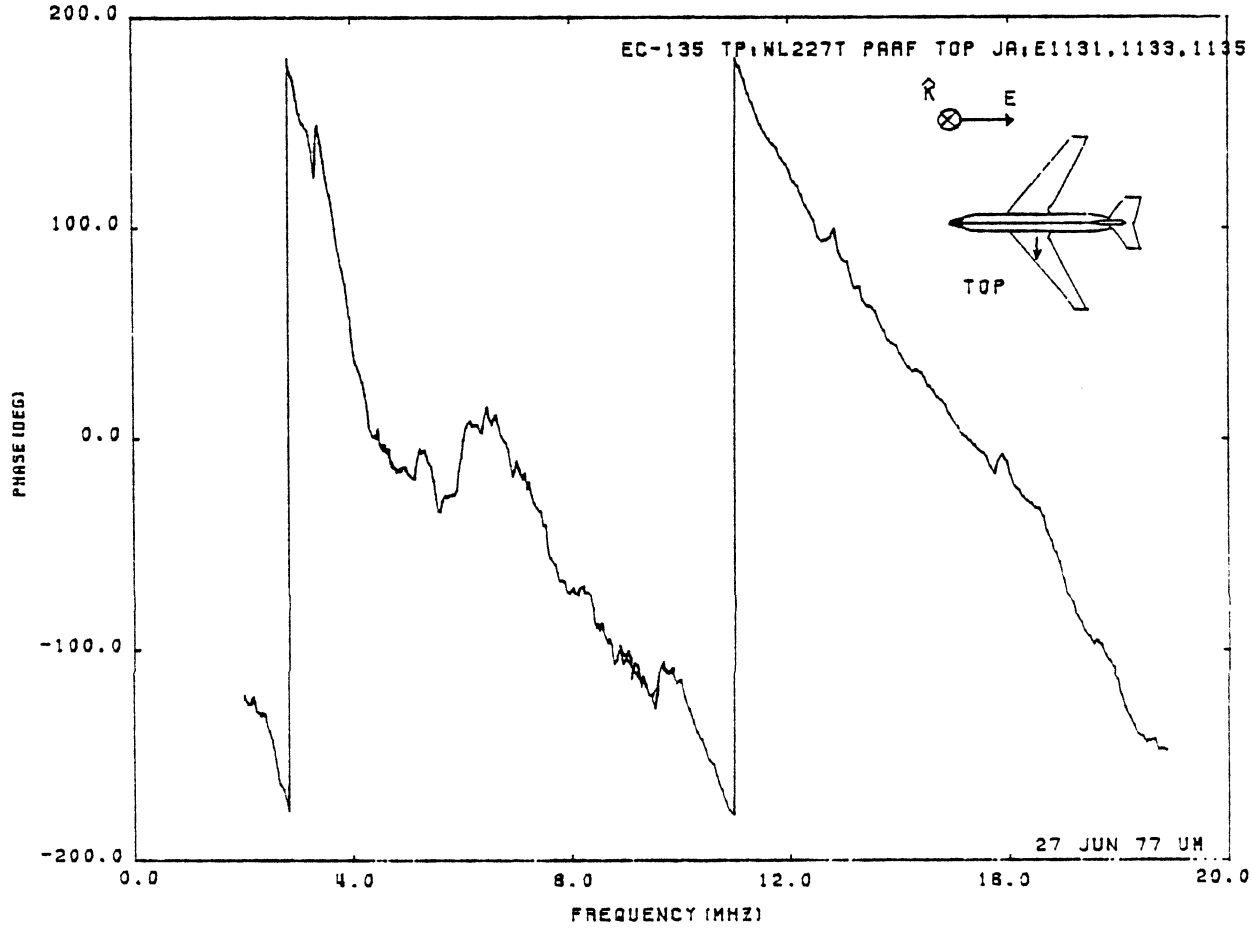

Figure 12: Axial Current at TP:WL227T, Orientation 1.

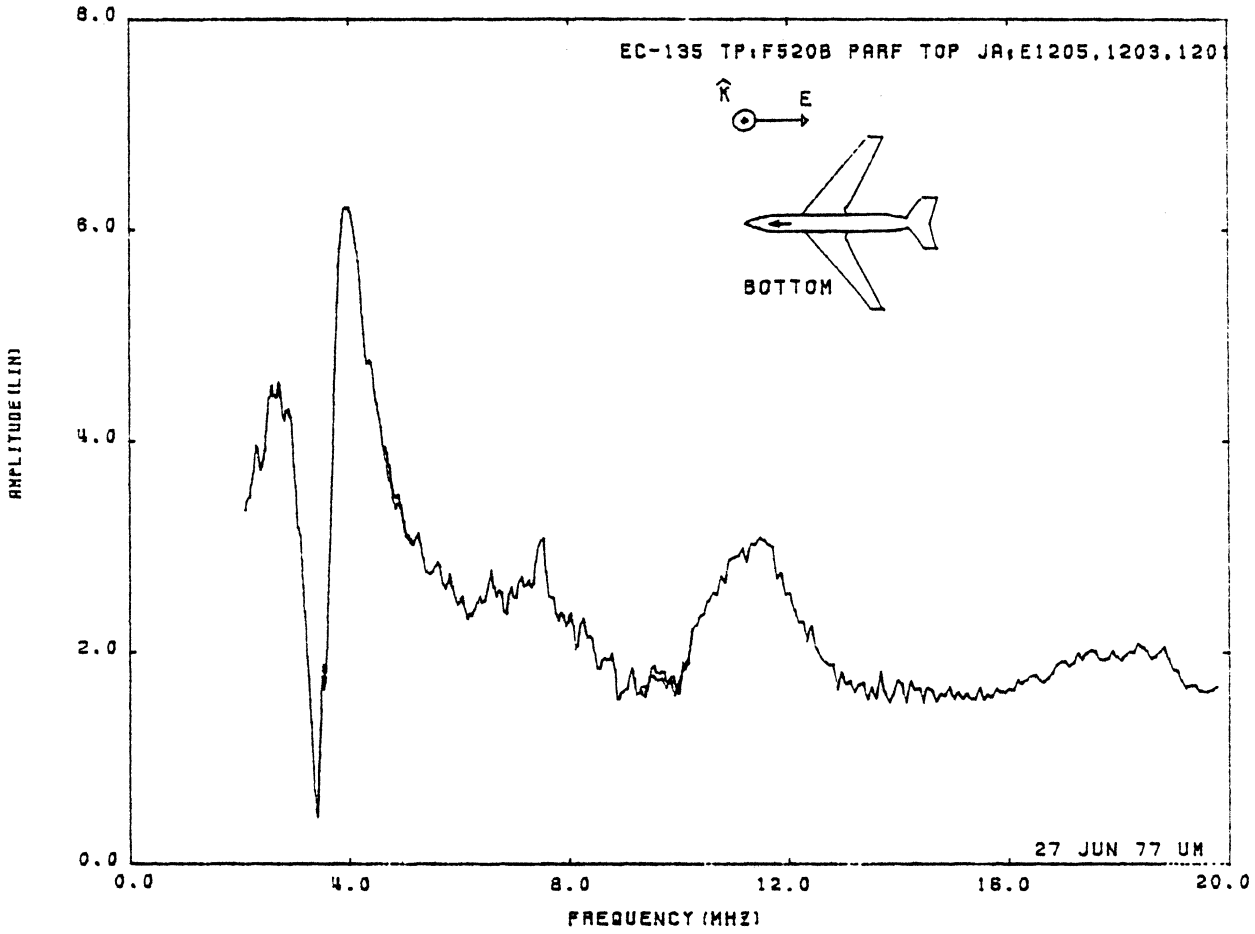

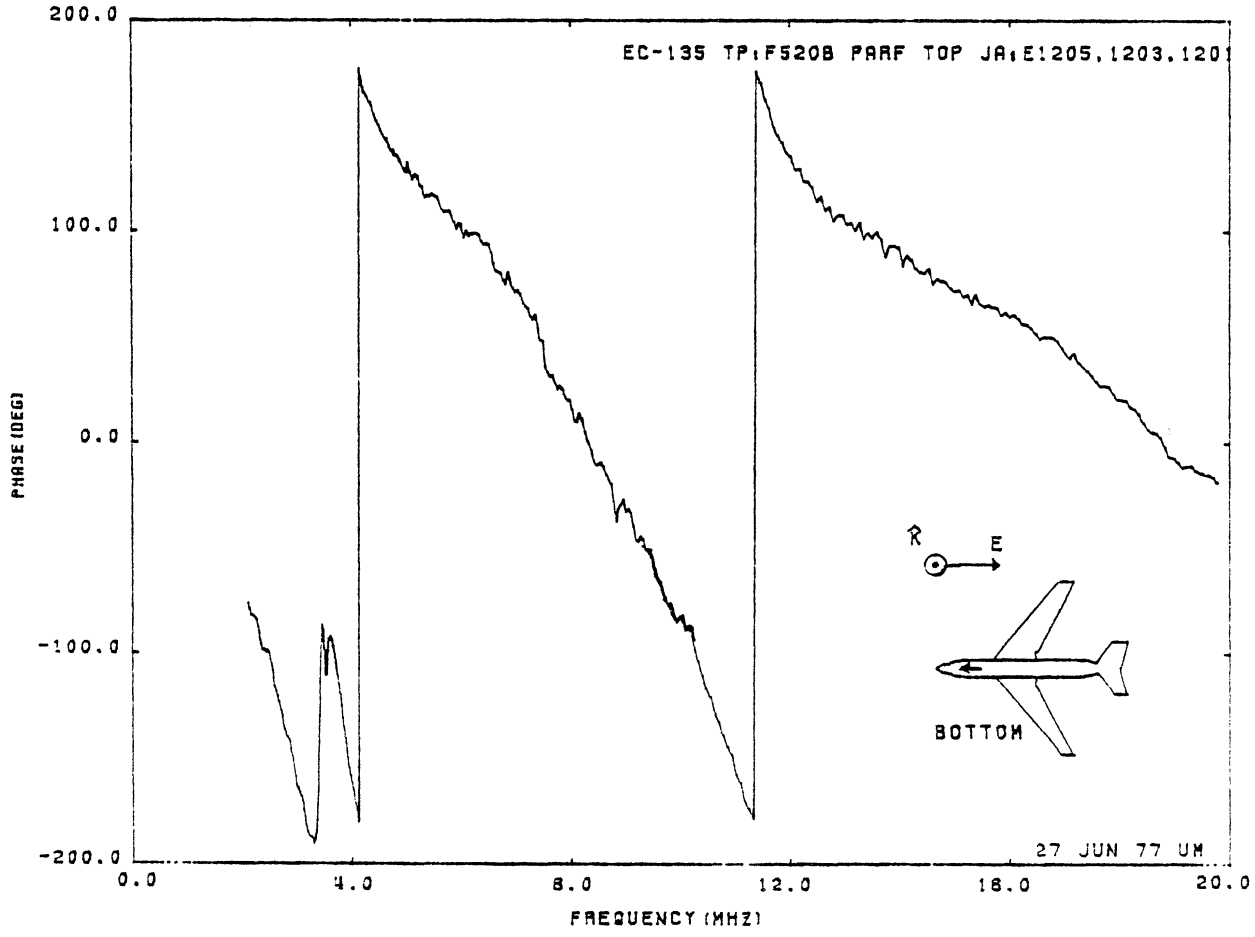

Figure 13: Axial Current at TP:F520B, Orientation 1.

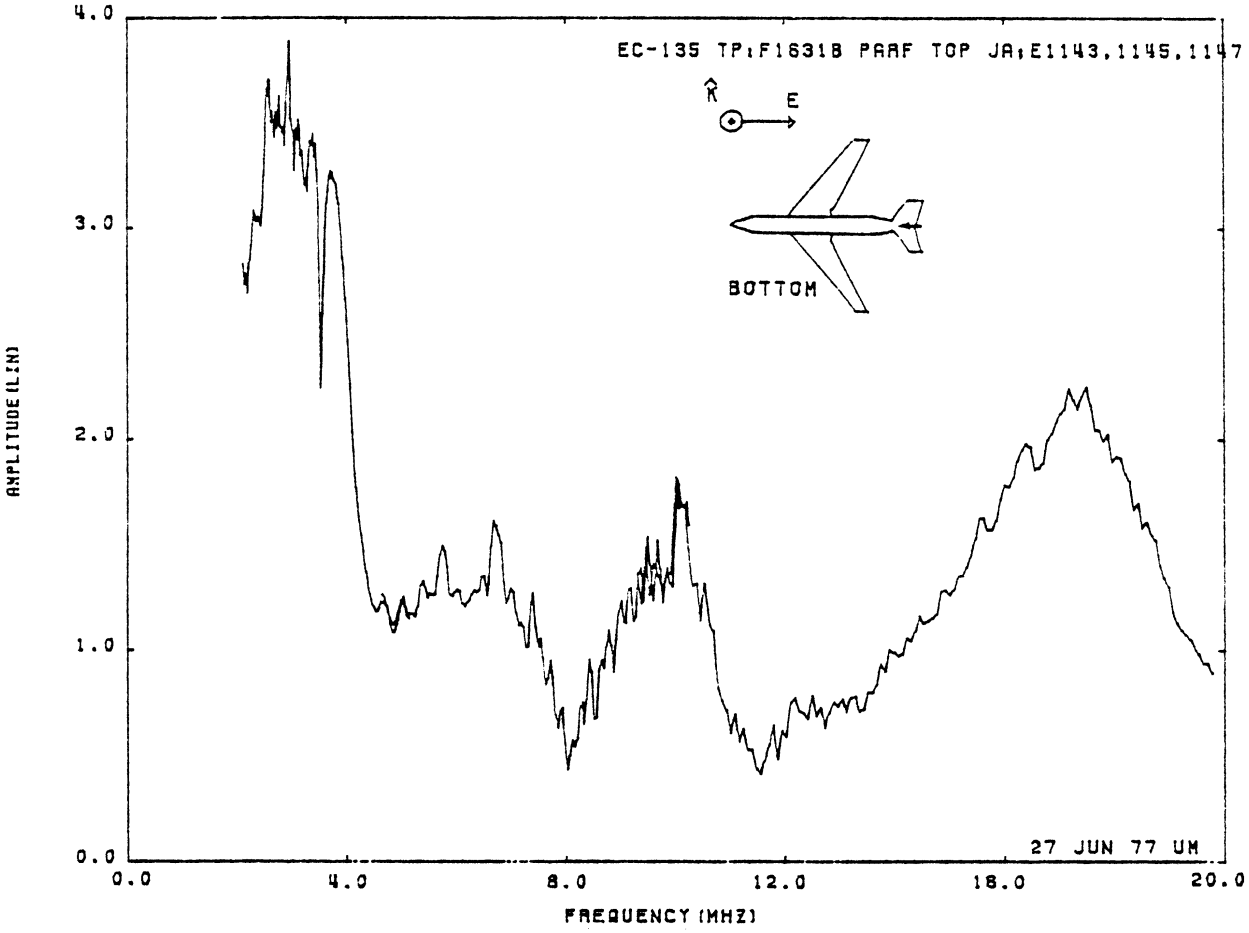

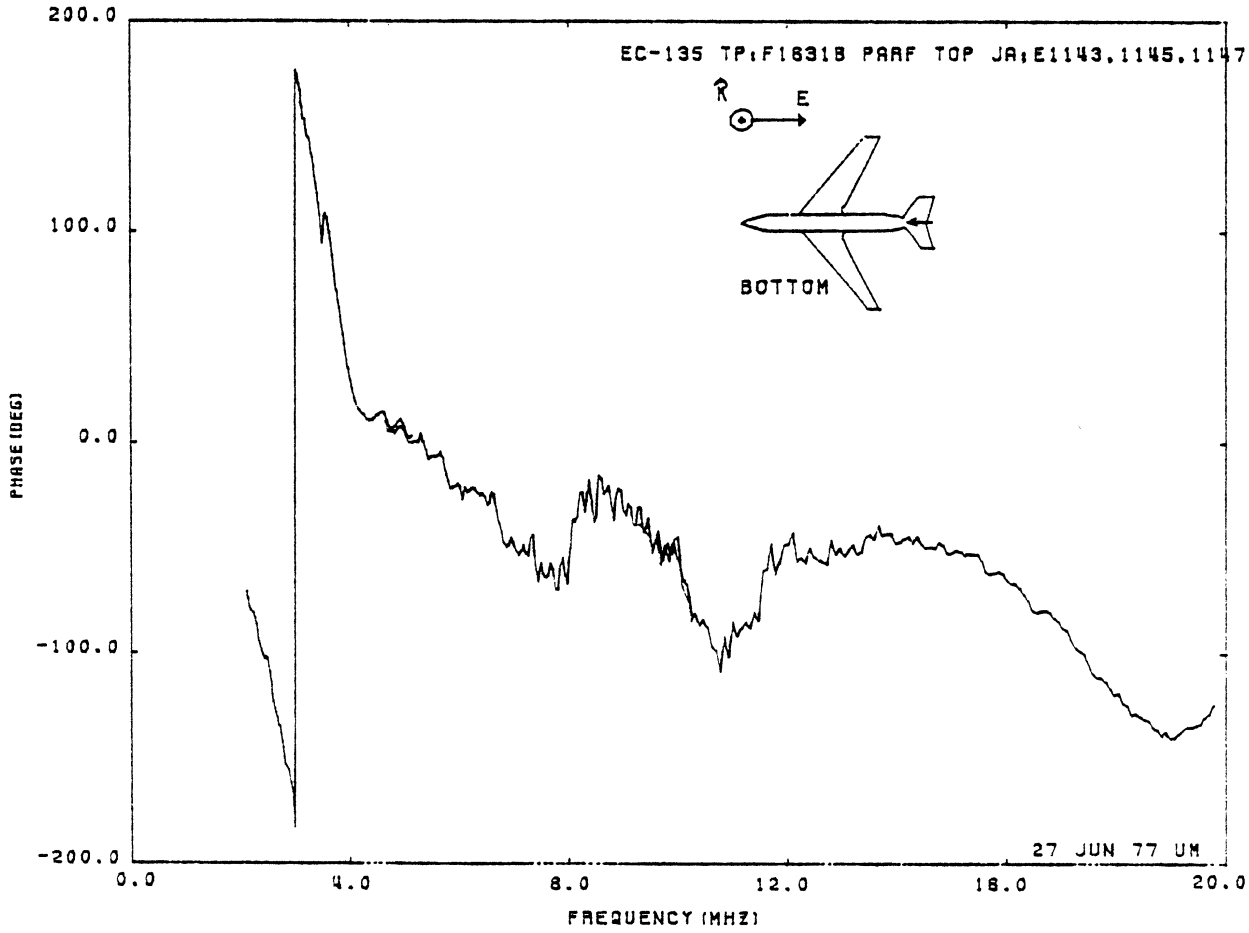

Figure 14: Axial Current at TP:F1631B, Orientation 1.

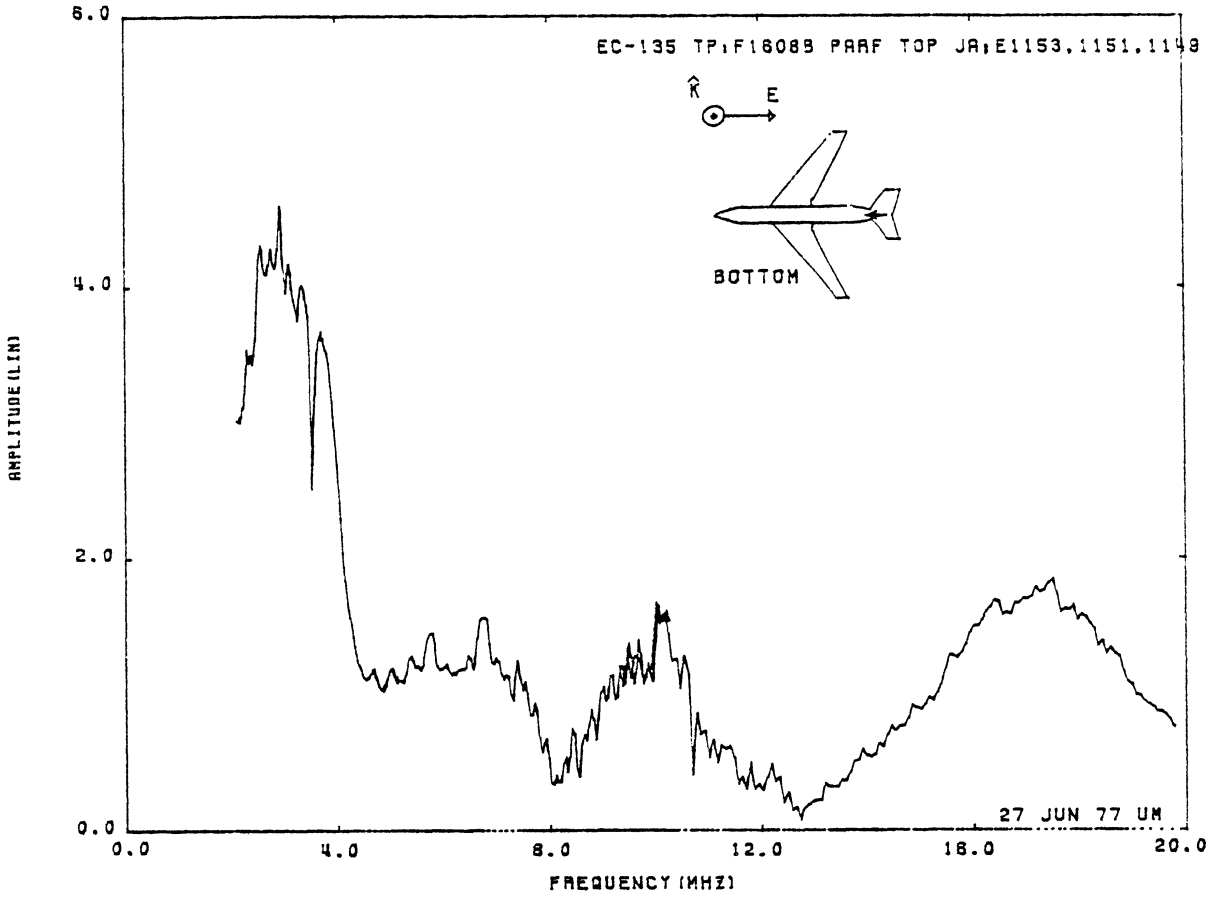

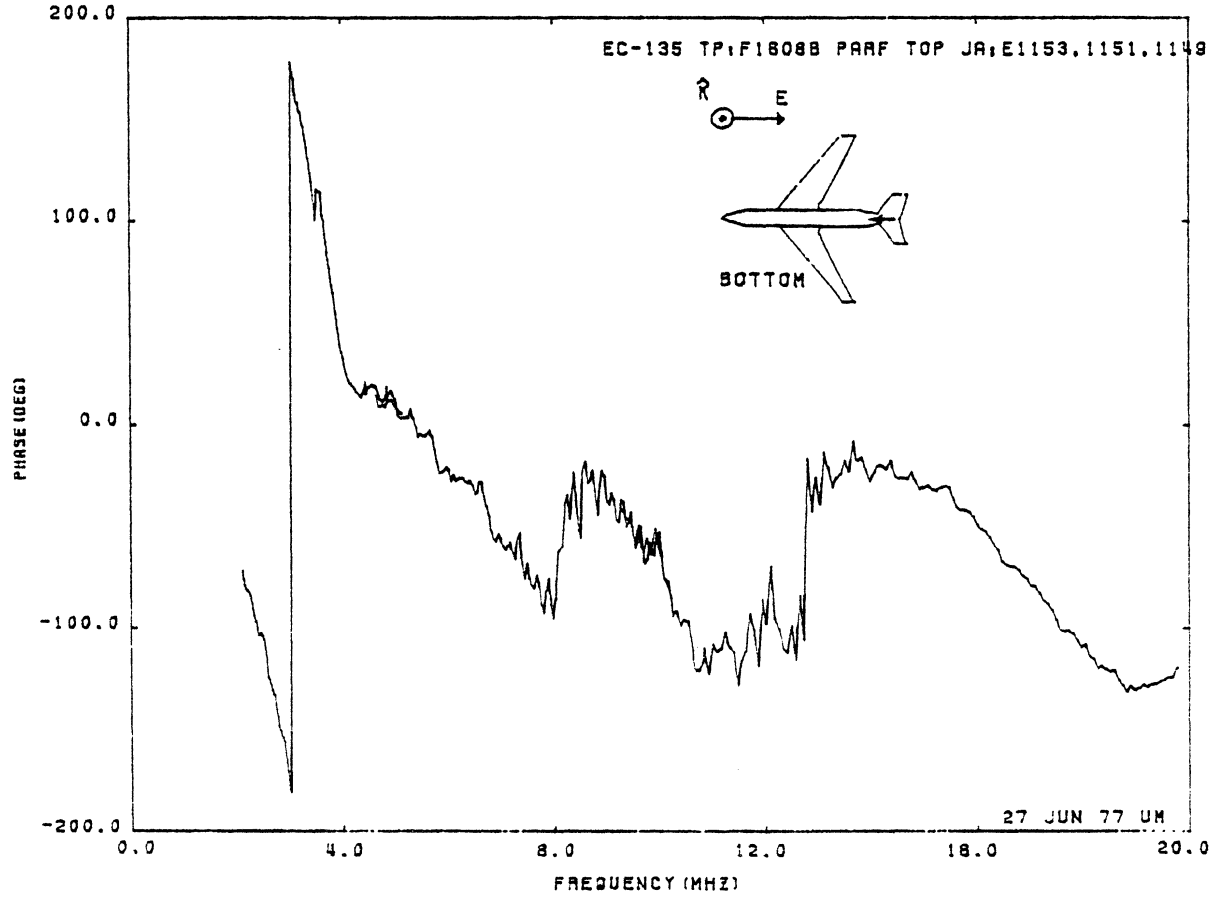

Figure 15: Circumferential Current at TP: F1608B, Orientation 1.

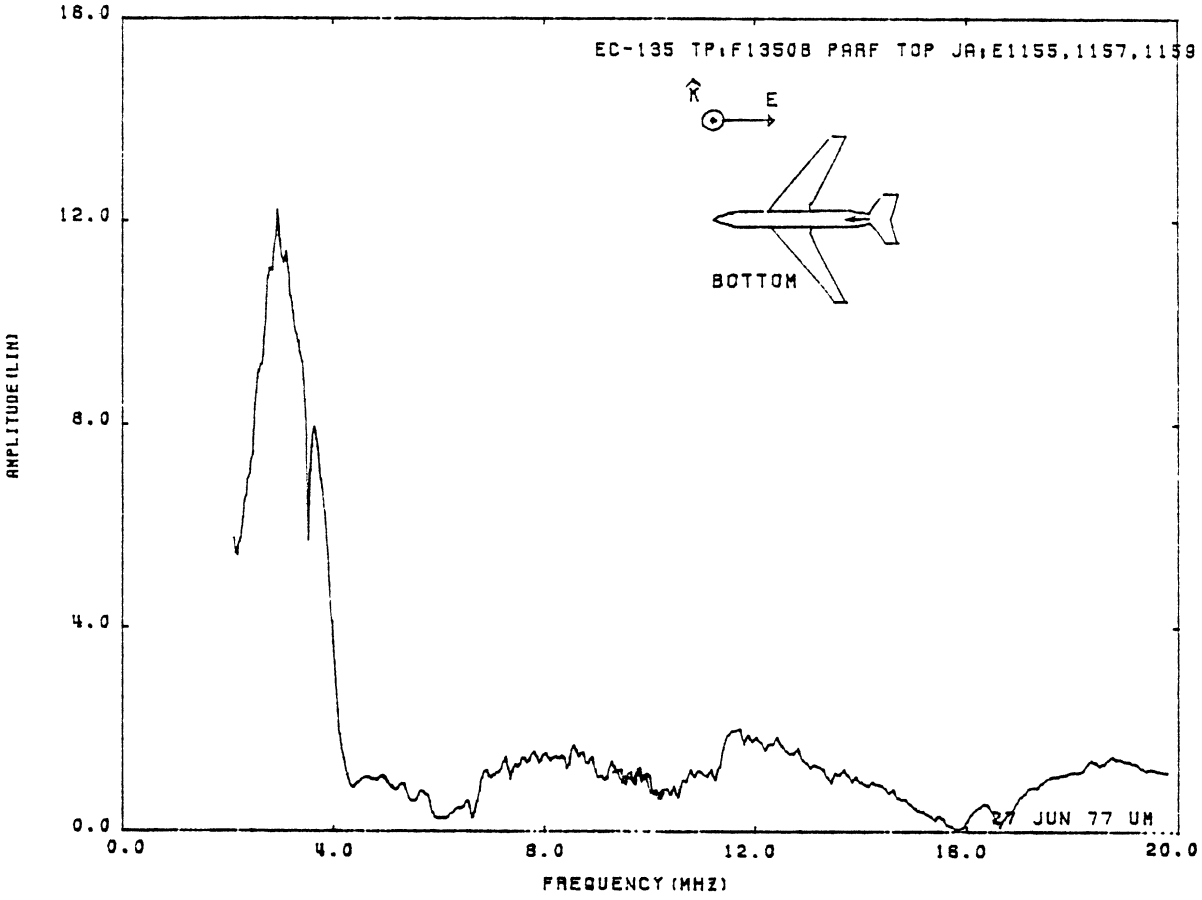

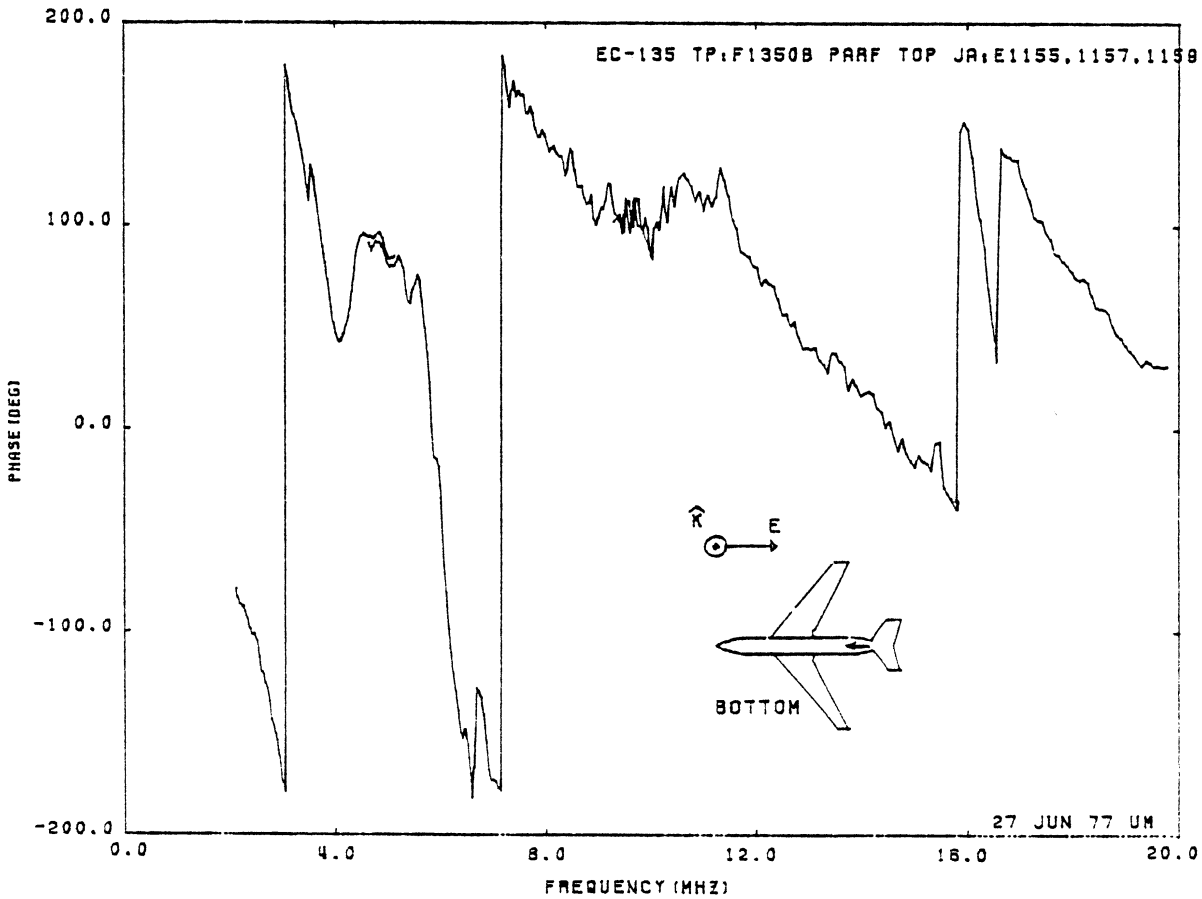

Figure 16 : Axial Current at TP:F1350B, Orientation 1.

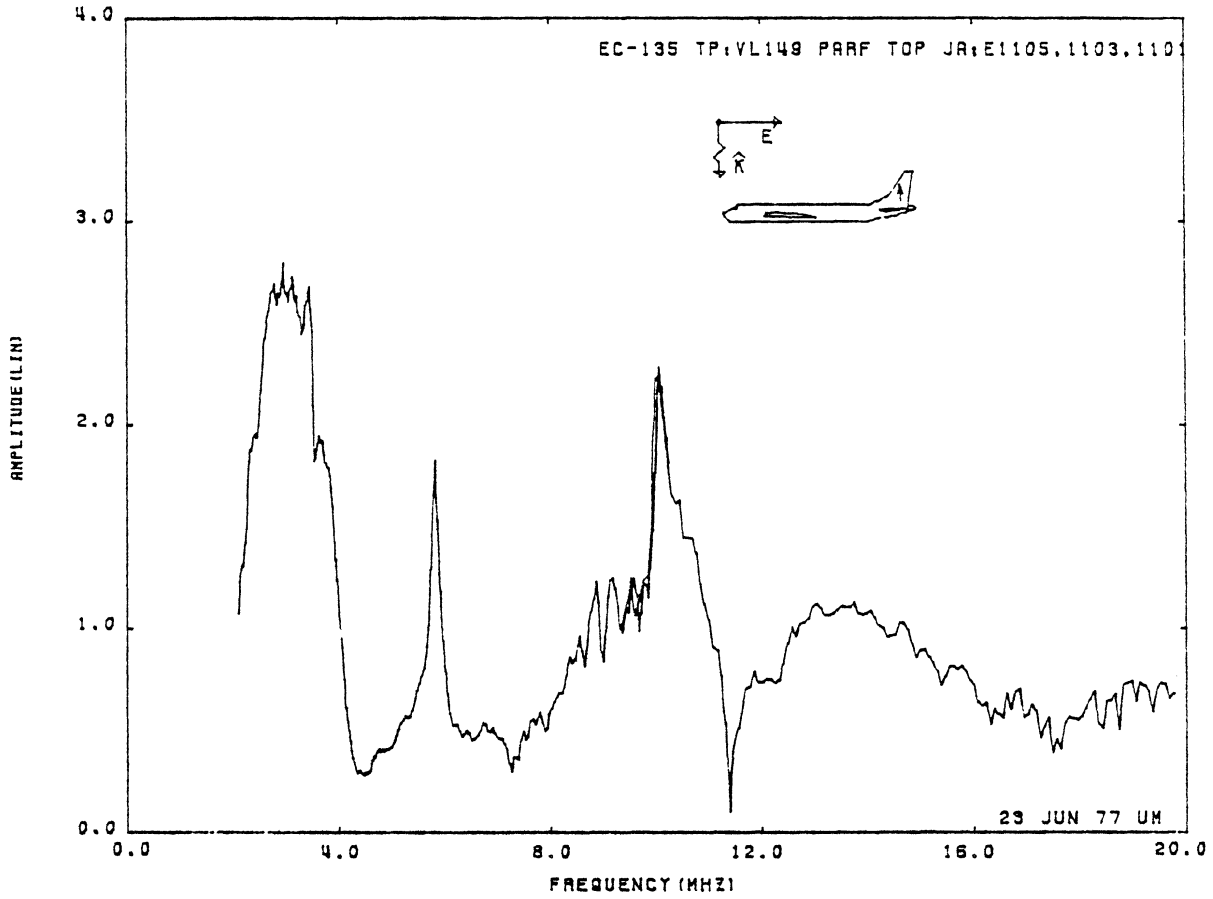

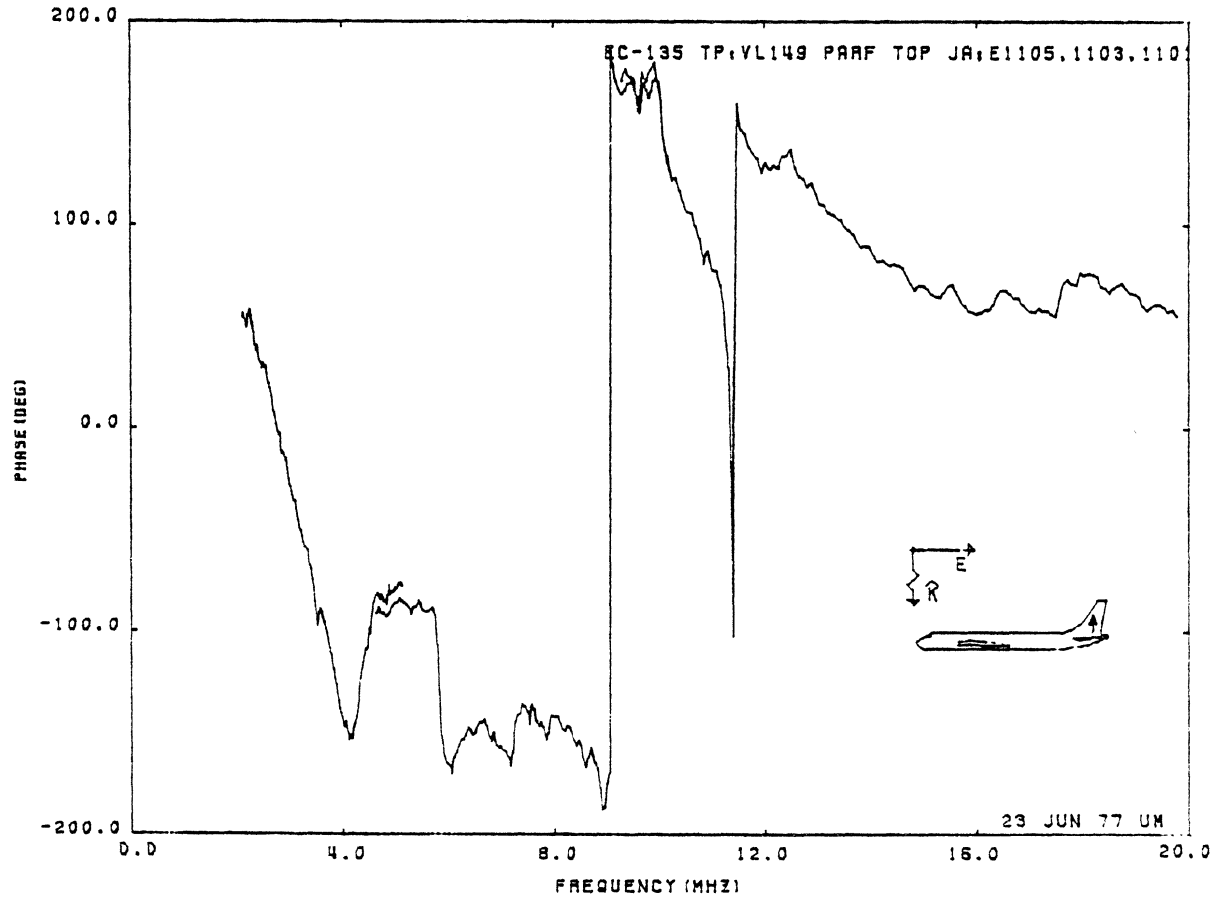

Figure 17: Axial Current at TP:VL149, Orientation 1.

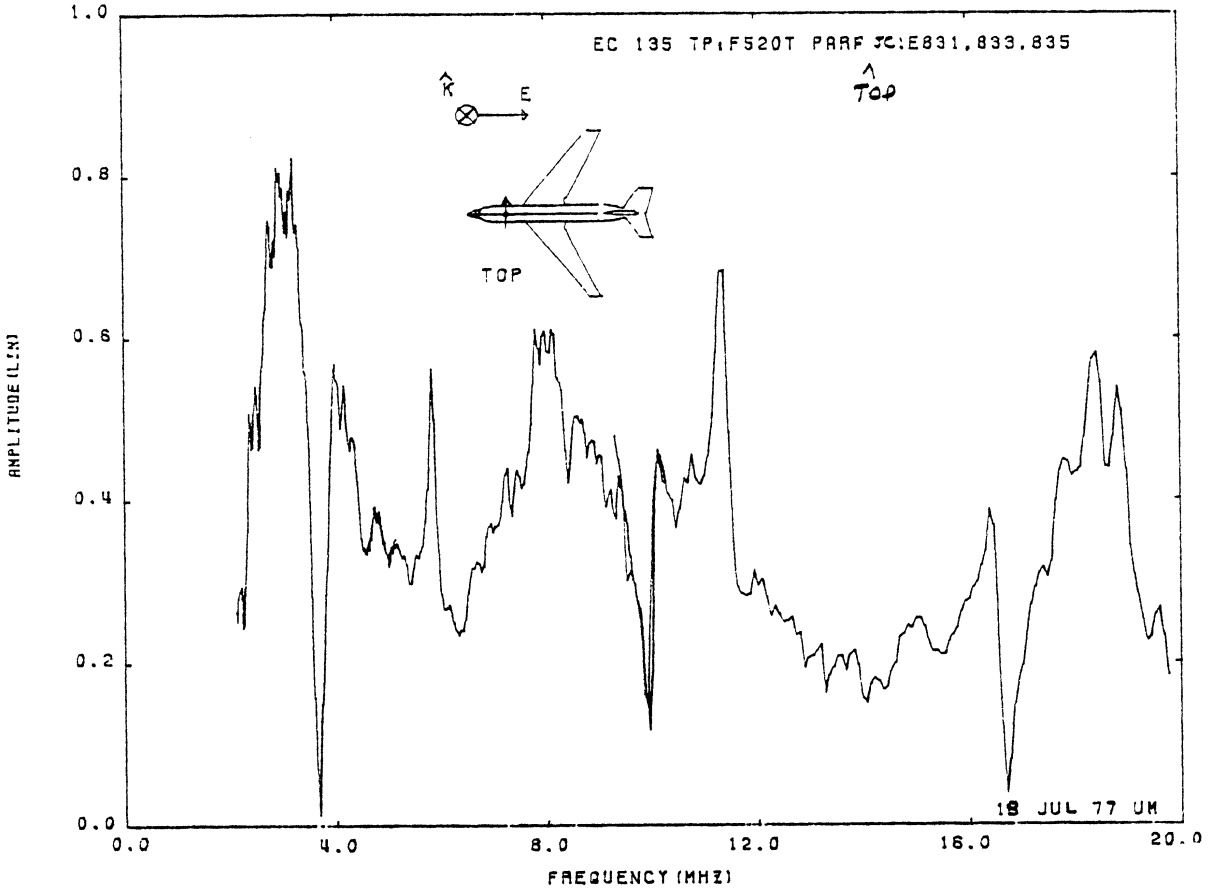

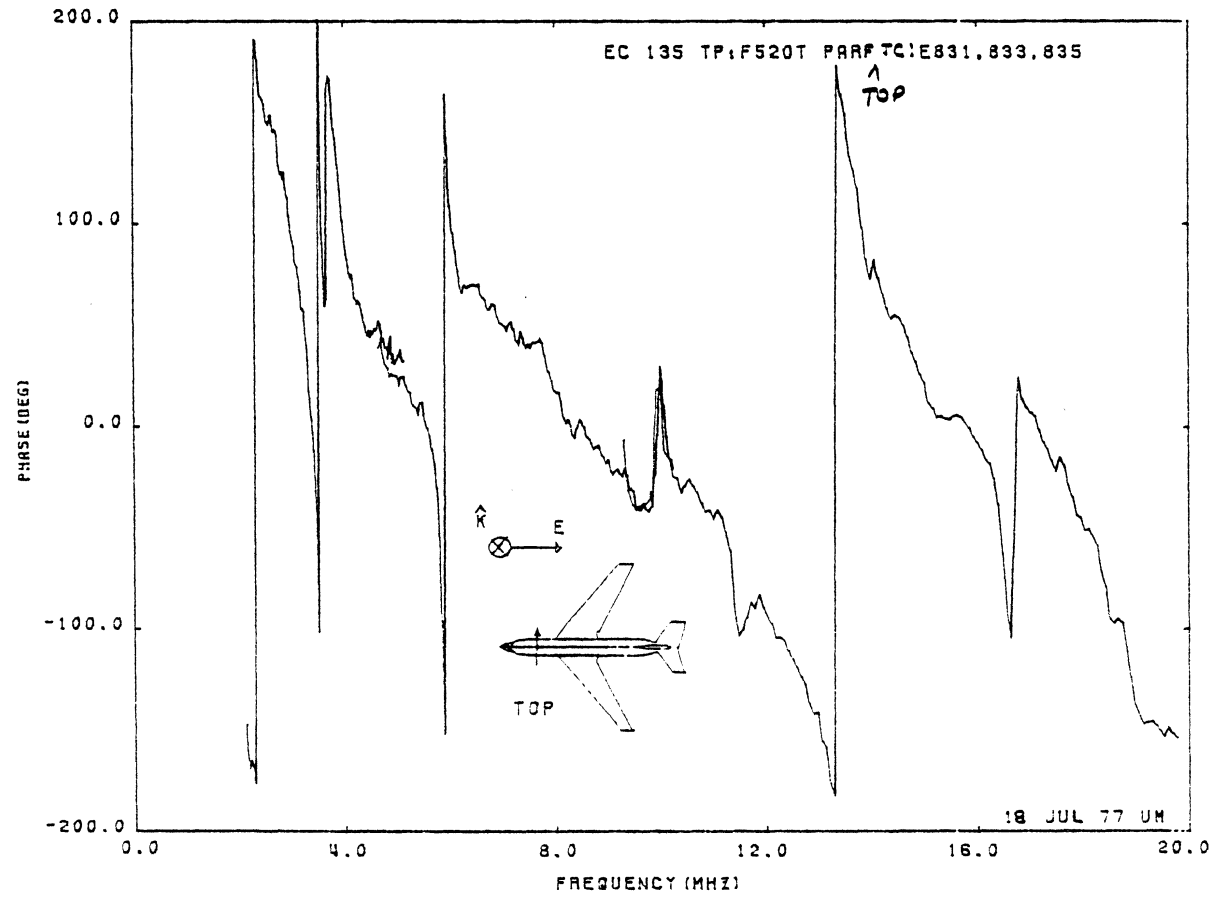

Figure 18: Circumferential Current at TP:F520T, Orientation 1.

(see *, page 15)

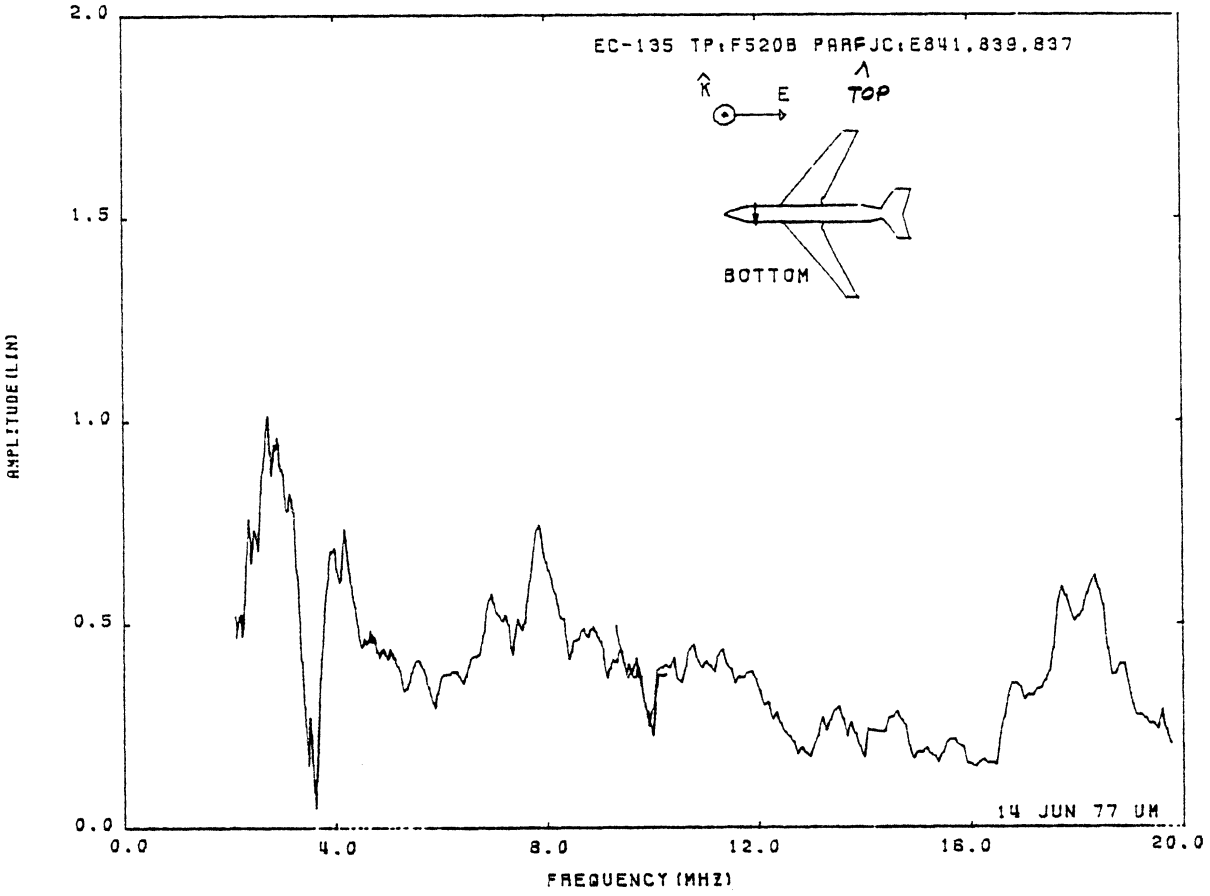

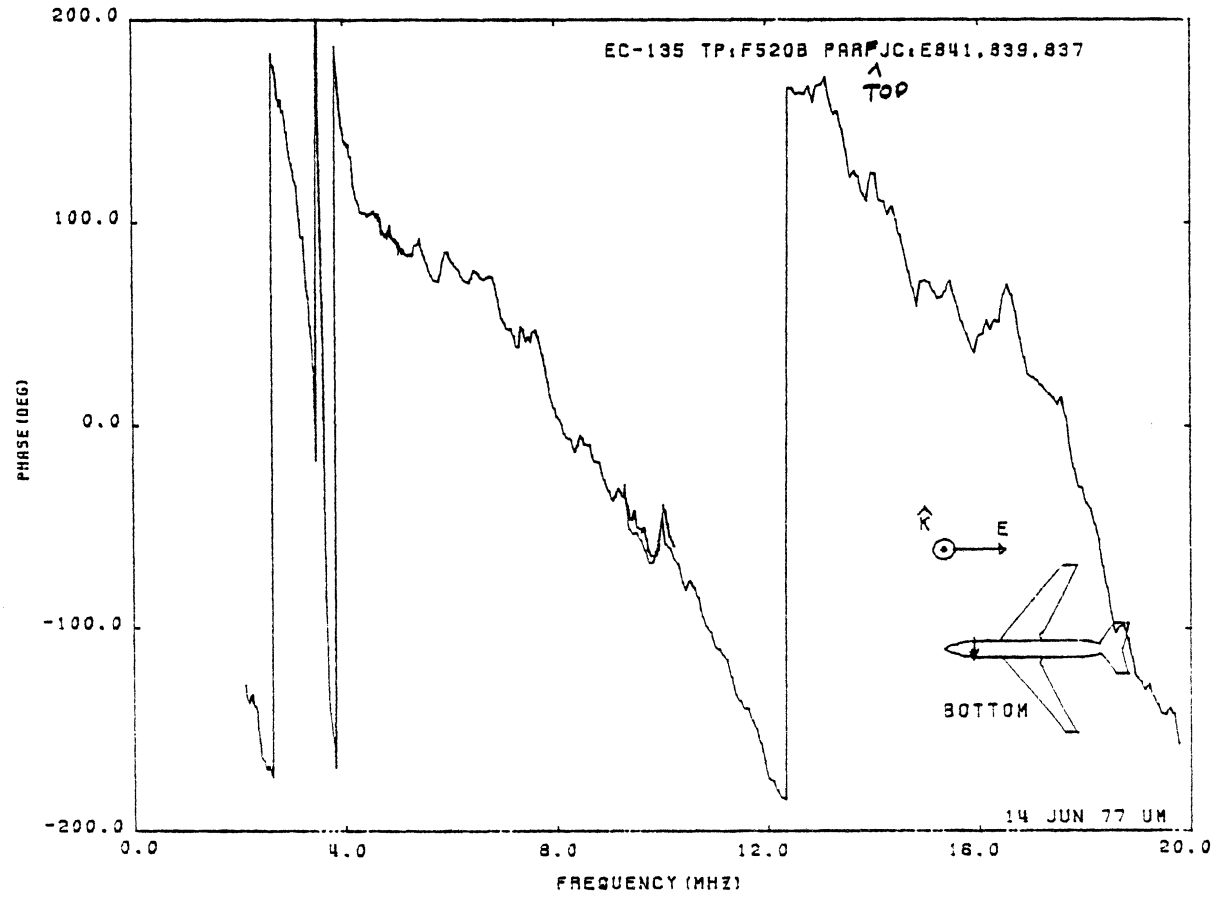

Figure 19 : Circumferential Current at TP:F520B, Orientation 1.
(see *, page 15)

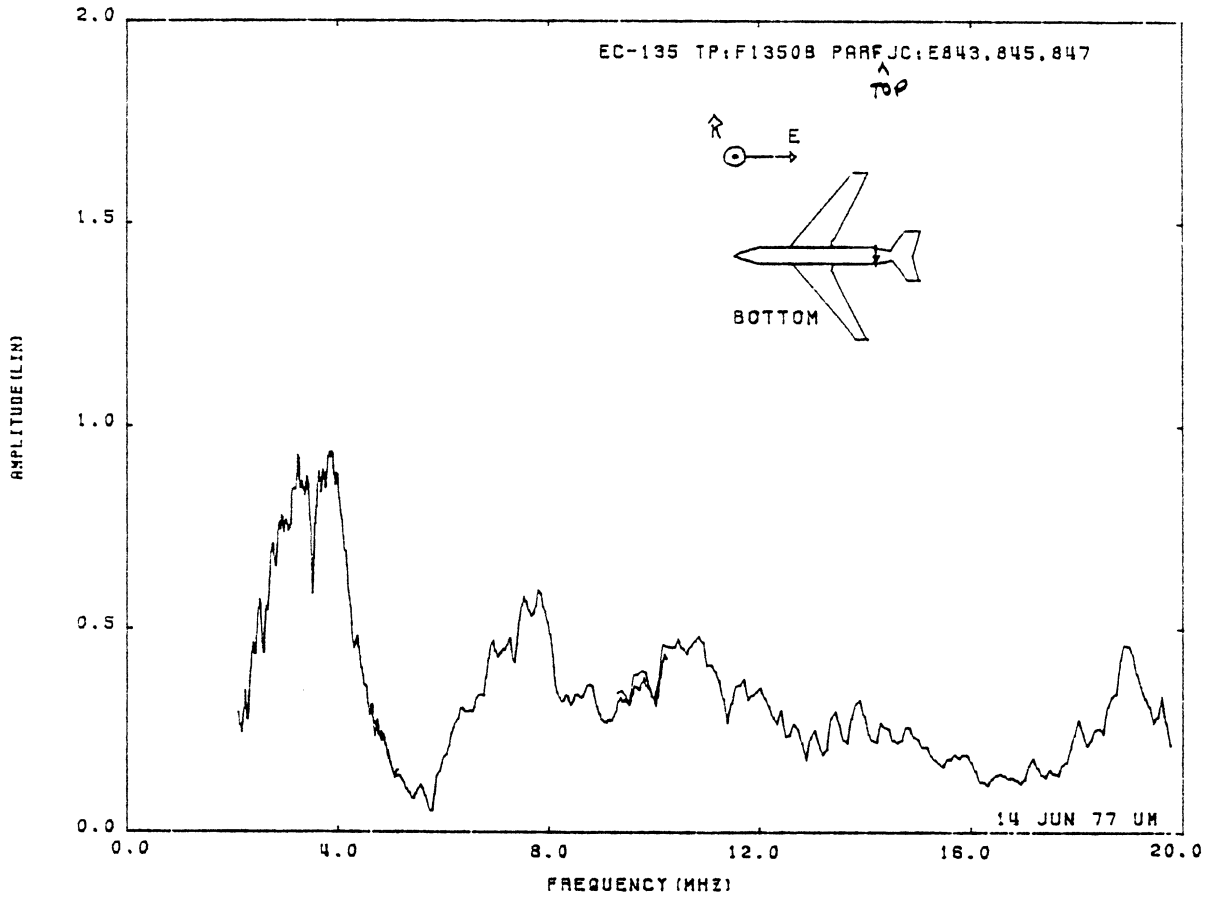

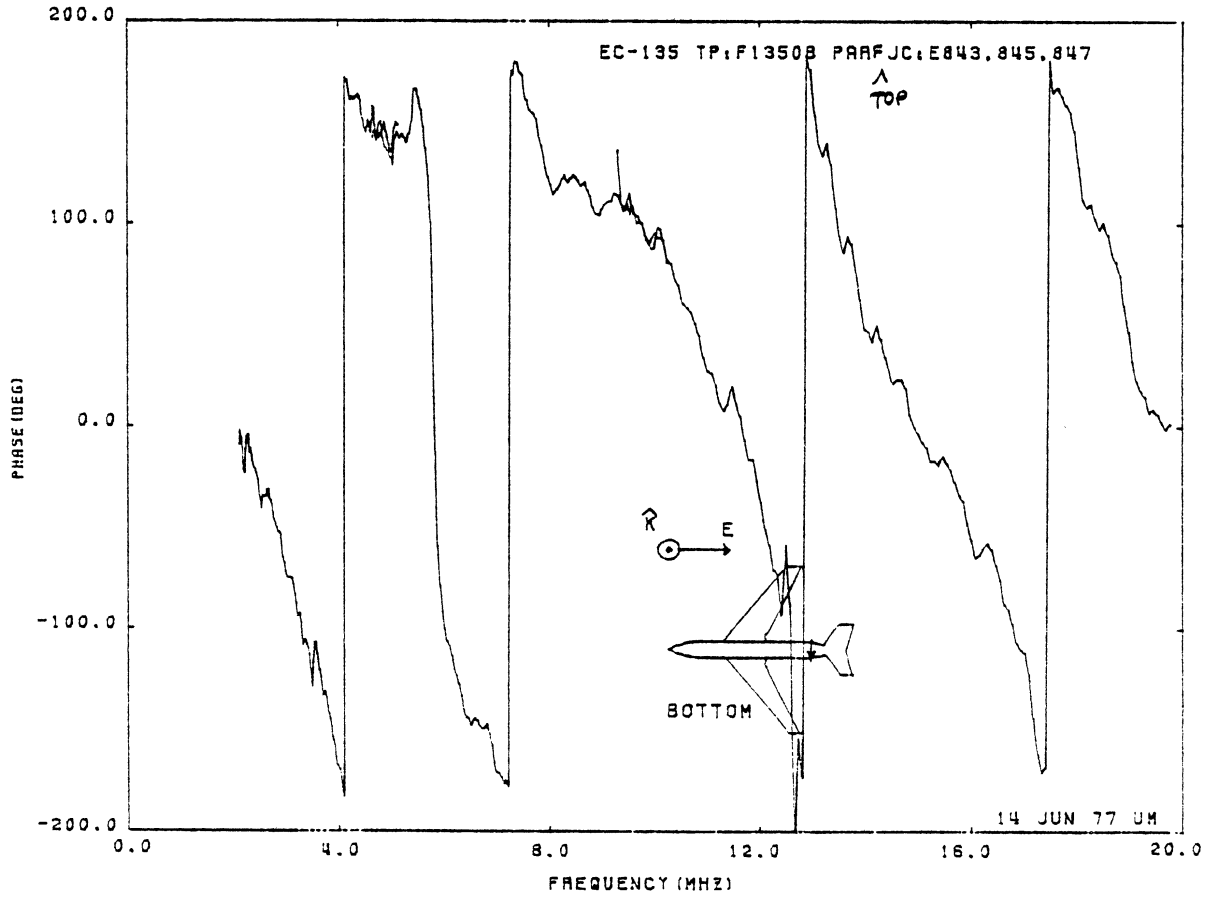

Figure 20: Circumferential Current at TP:F1350B, Orientation 1.

(see *, page 15)

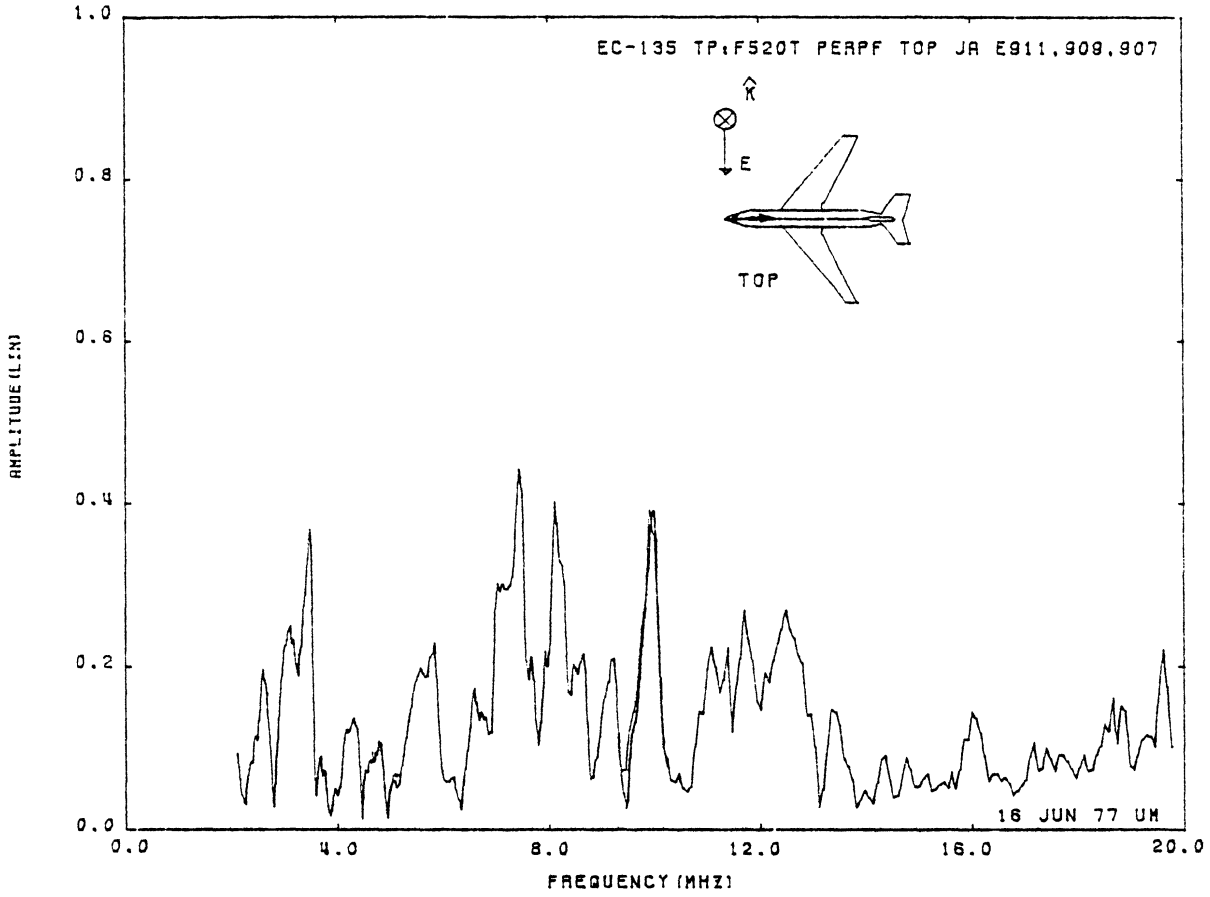

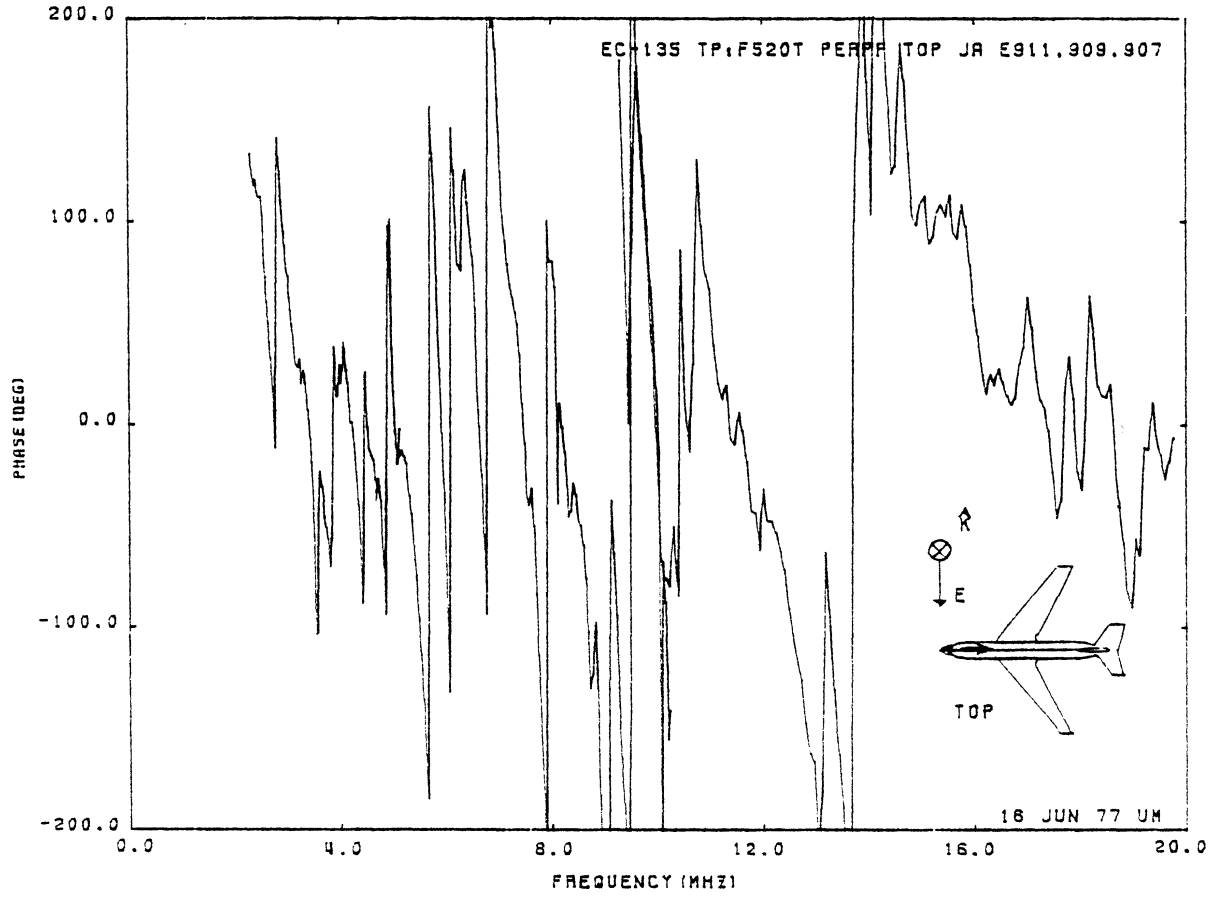

Figure 21: Axial Current at TP:F520T, Orientation 2.

(see *, page 15)

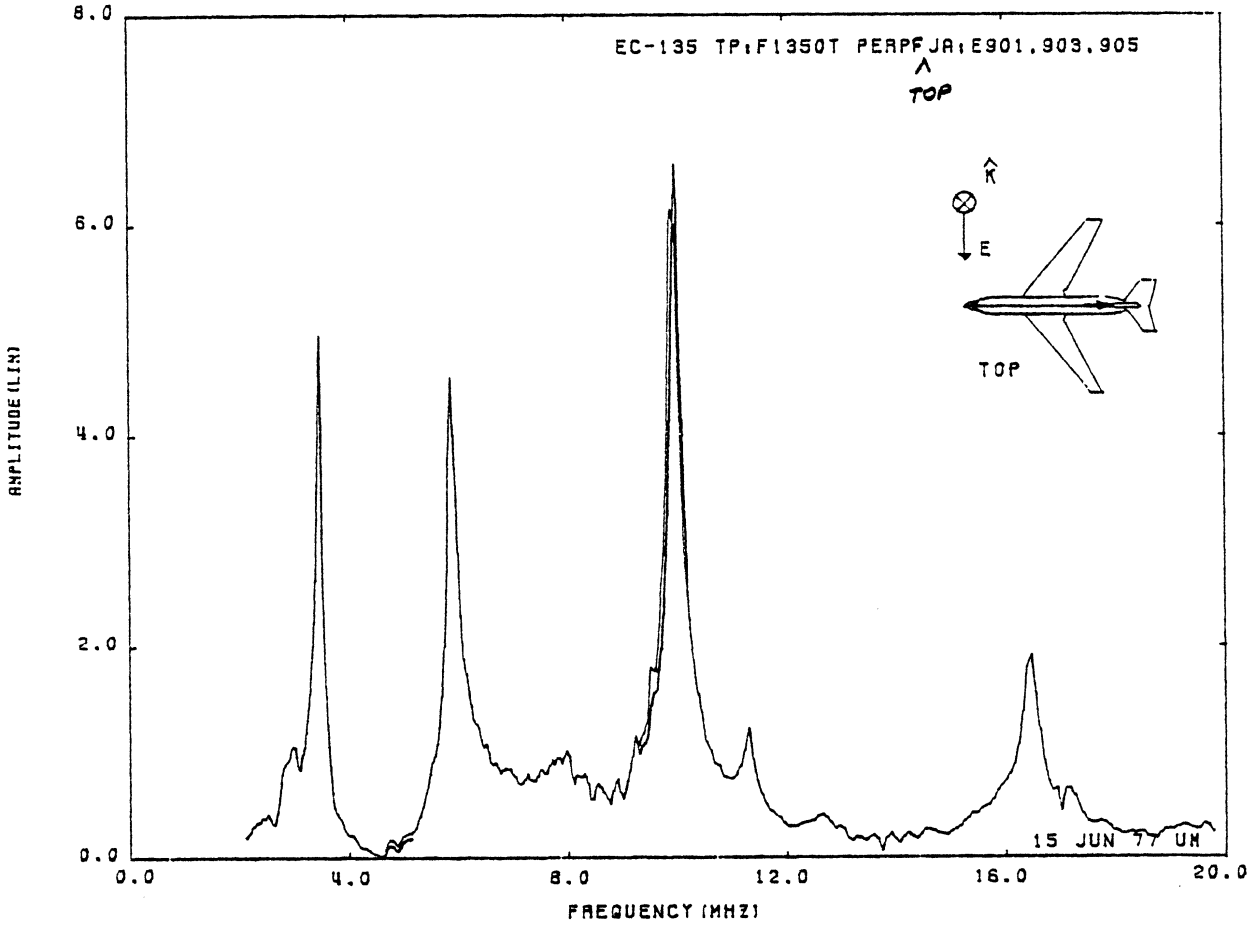

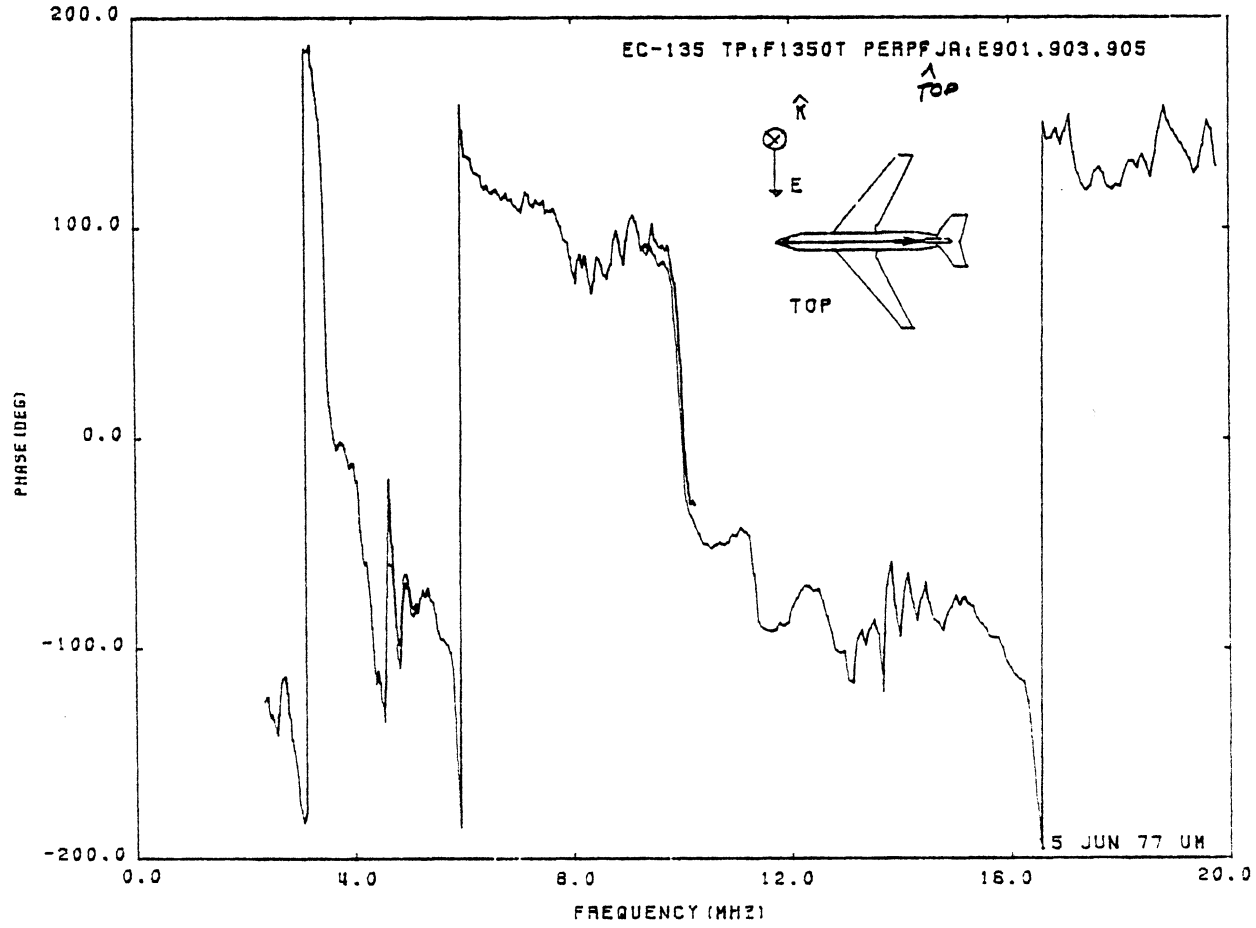

Figure 22: Axial Current at TP:F1350T, Orientation 2.

(see *, page 15)

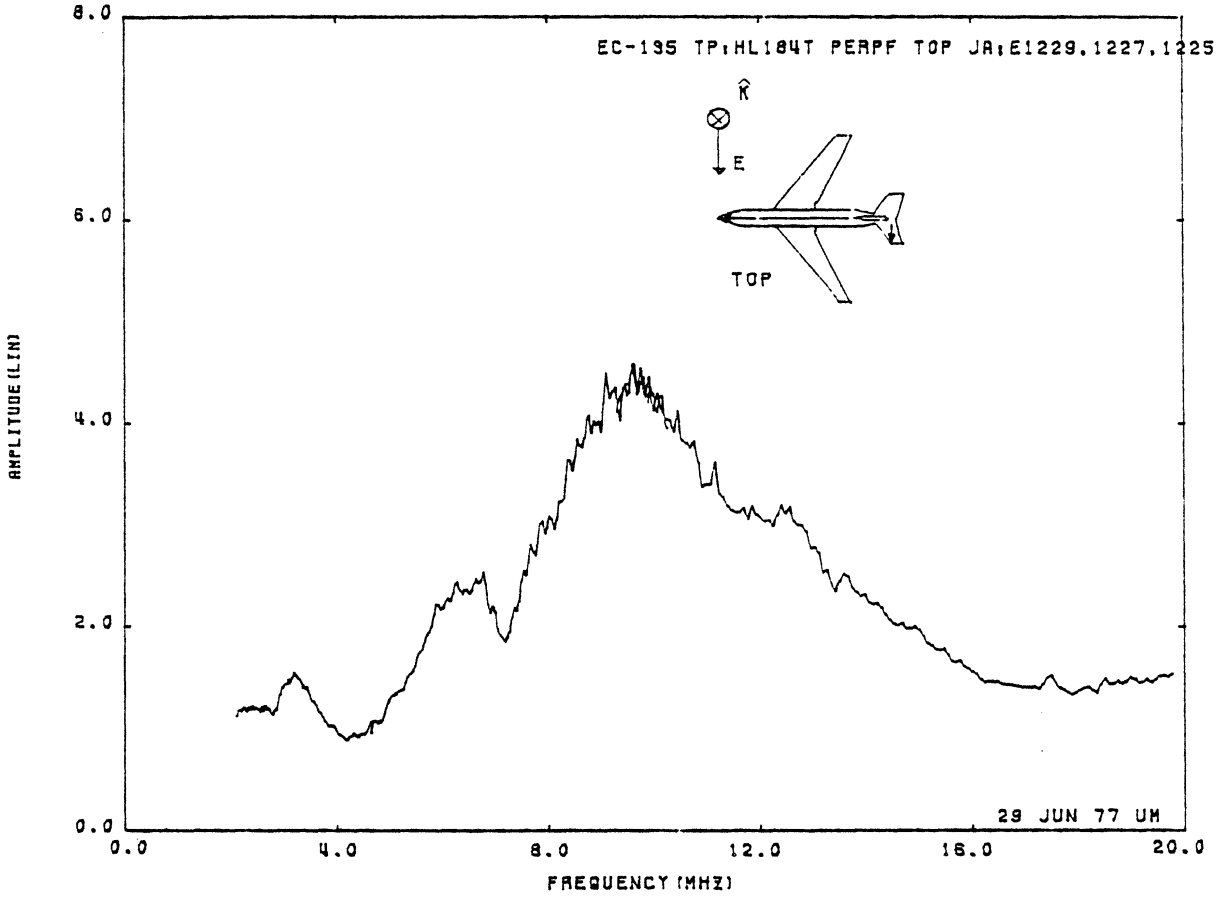

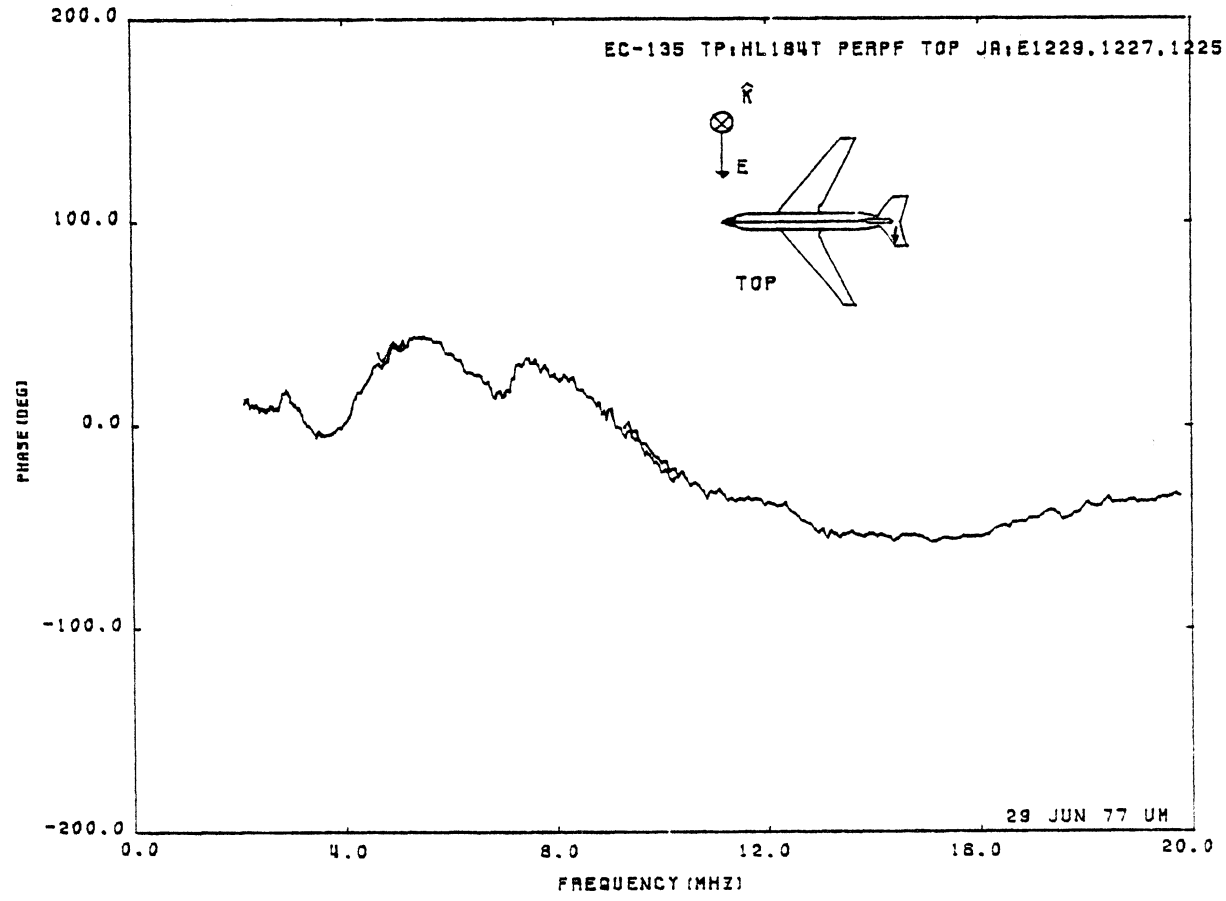

Figure 23: Axial Current at TP:HL184T, Orientation 2.

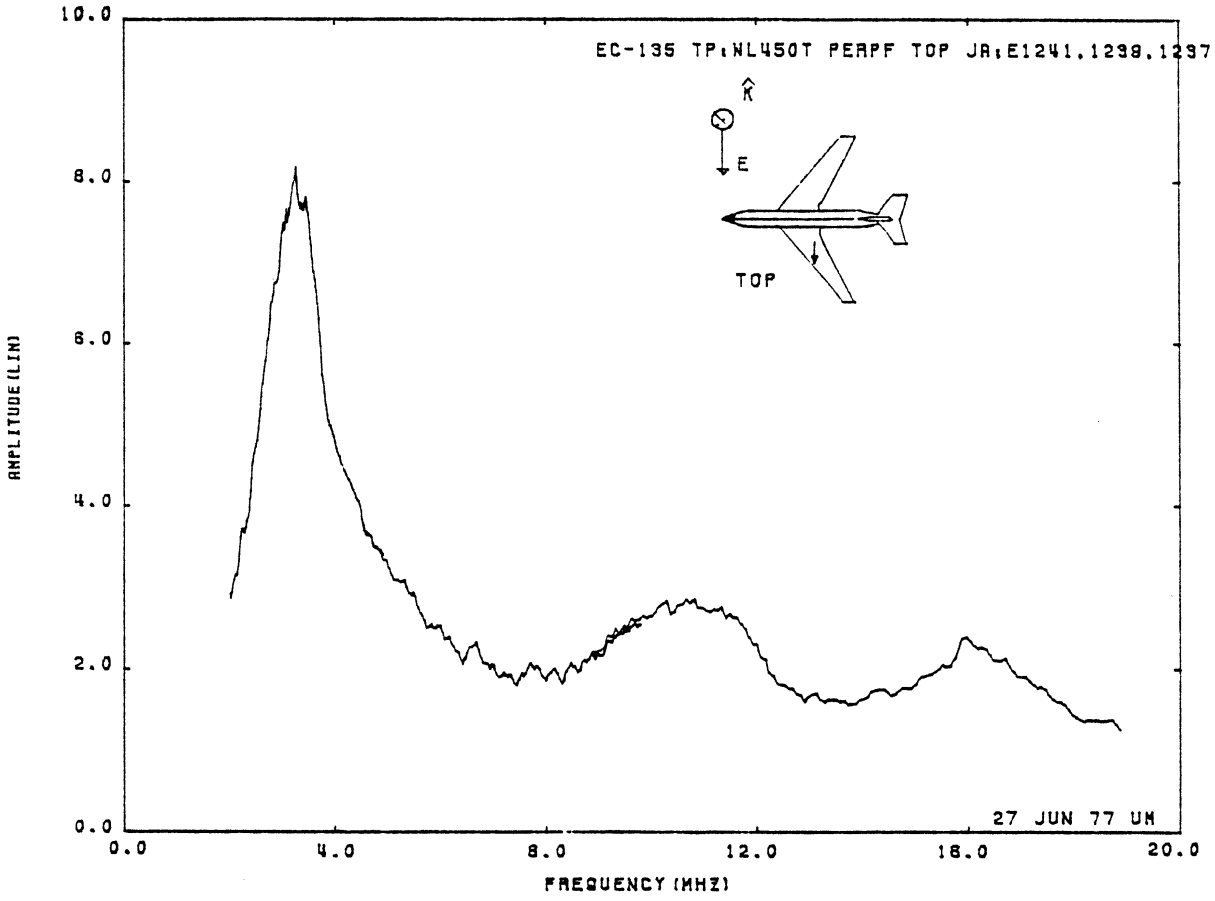

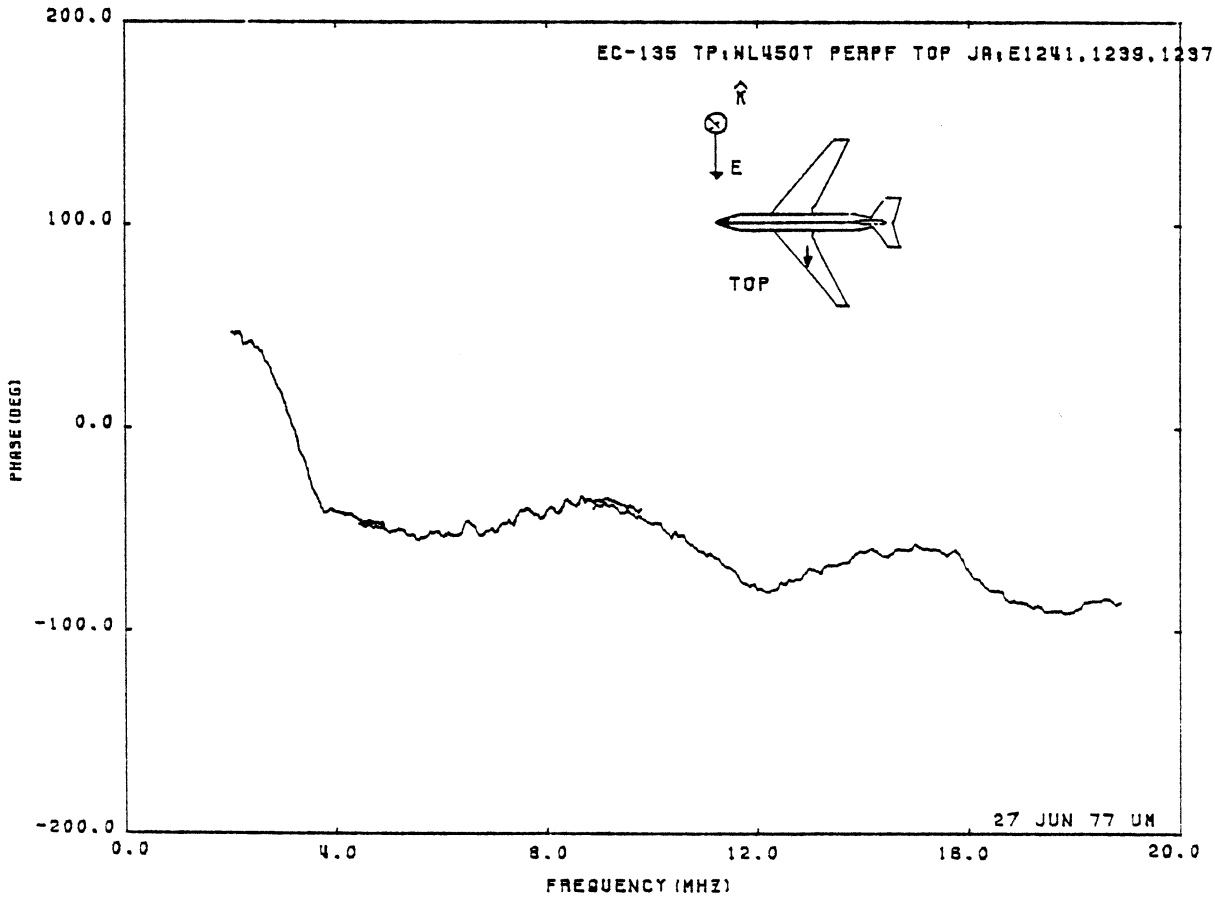

Figure 24: Axial Current at TP:WL450T, Orientation 2.

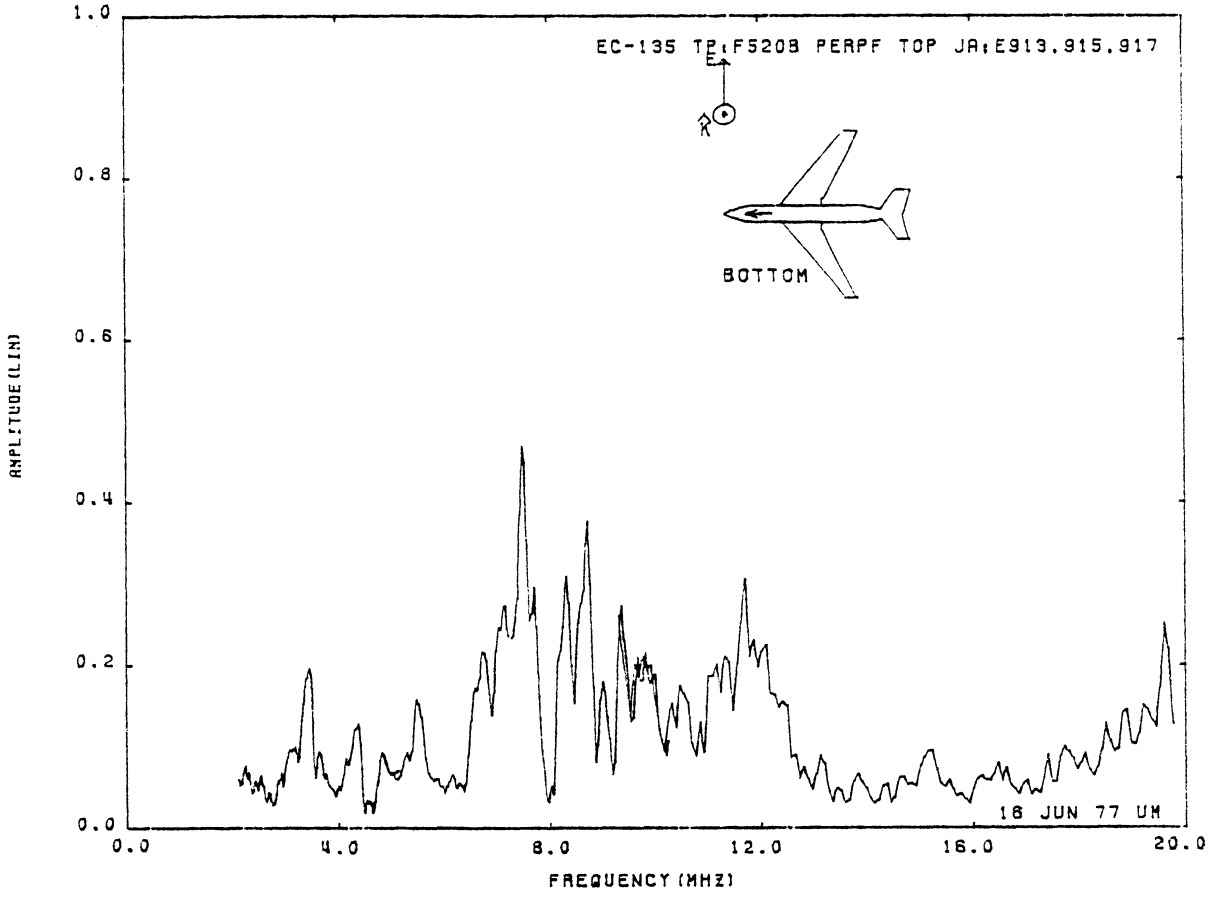

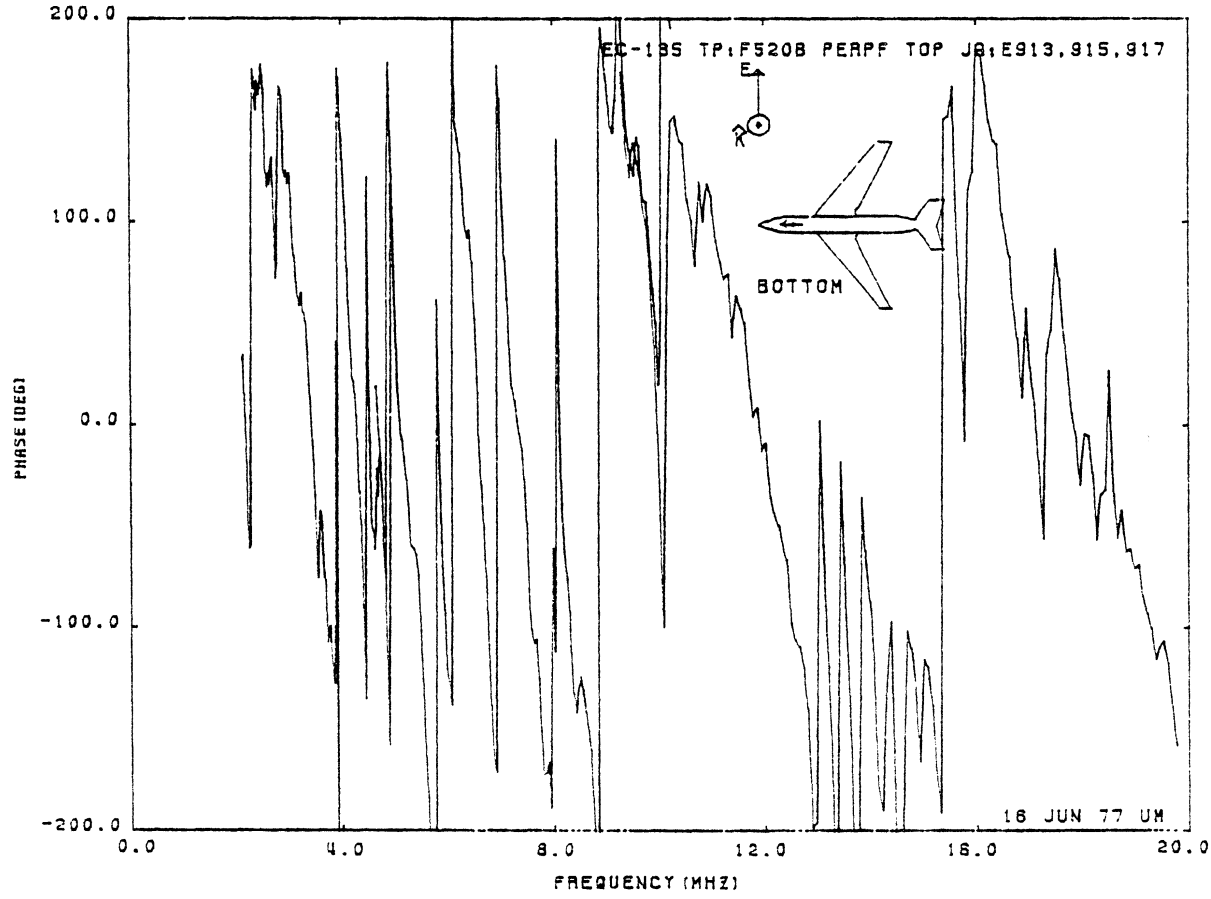

Figure 25: Axial Current at TP:F520B, Orientation 2.

(see *, page 15)

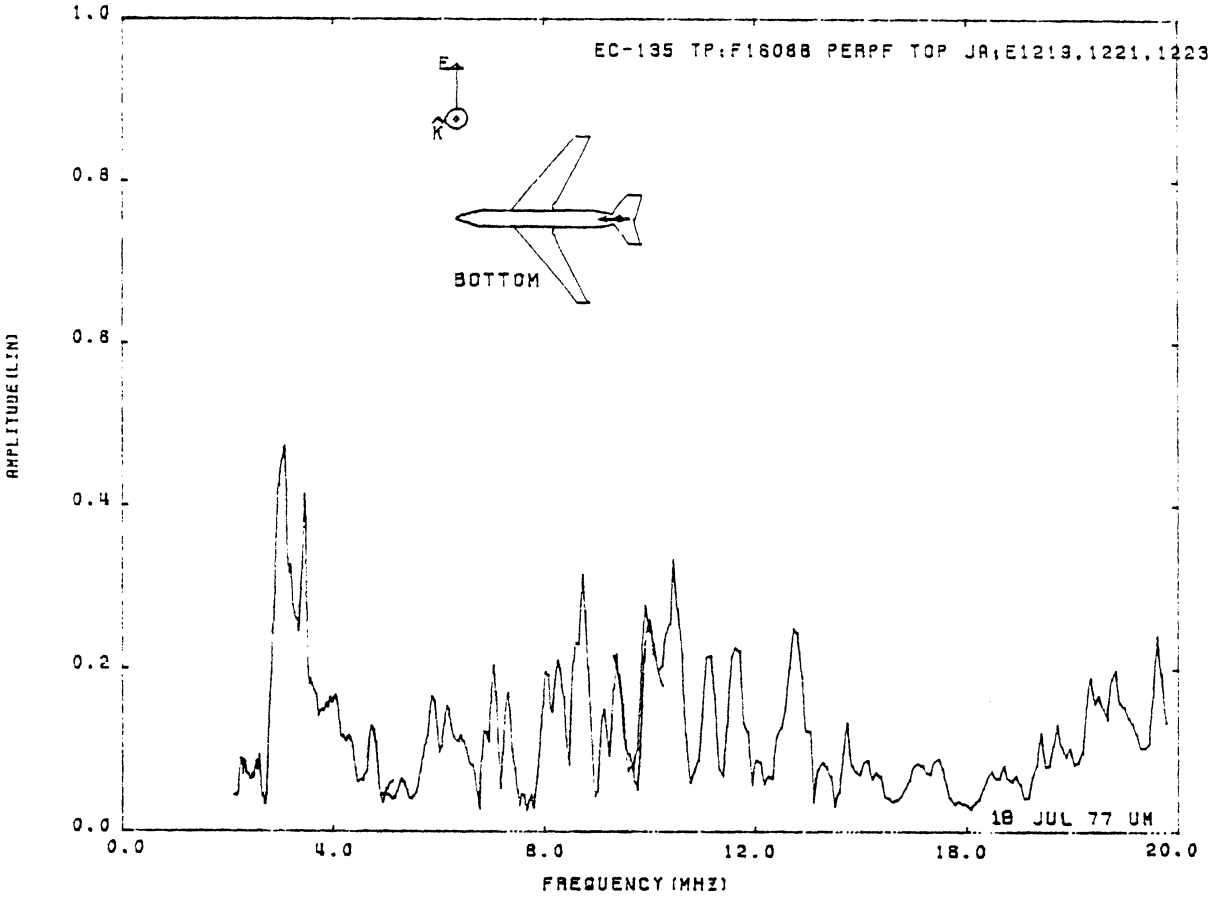

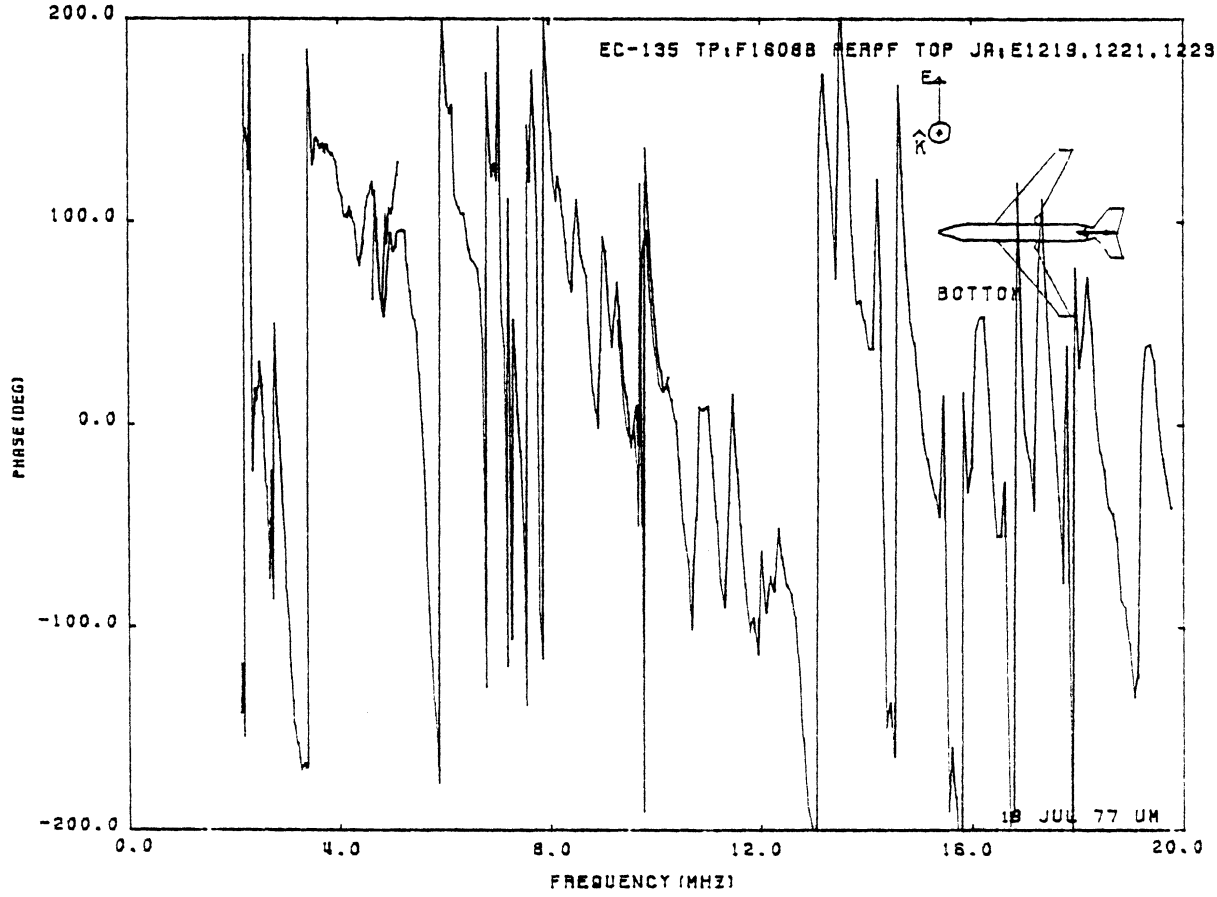

Figure 26: Axial Current at TP:F1608B, Orientation 2.

(see *, page 15)

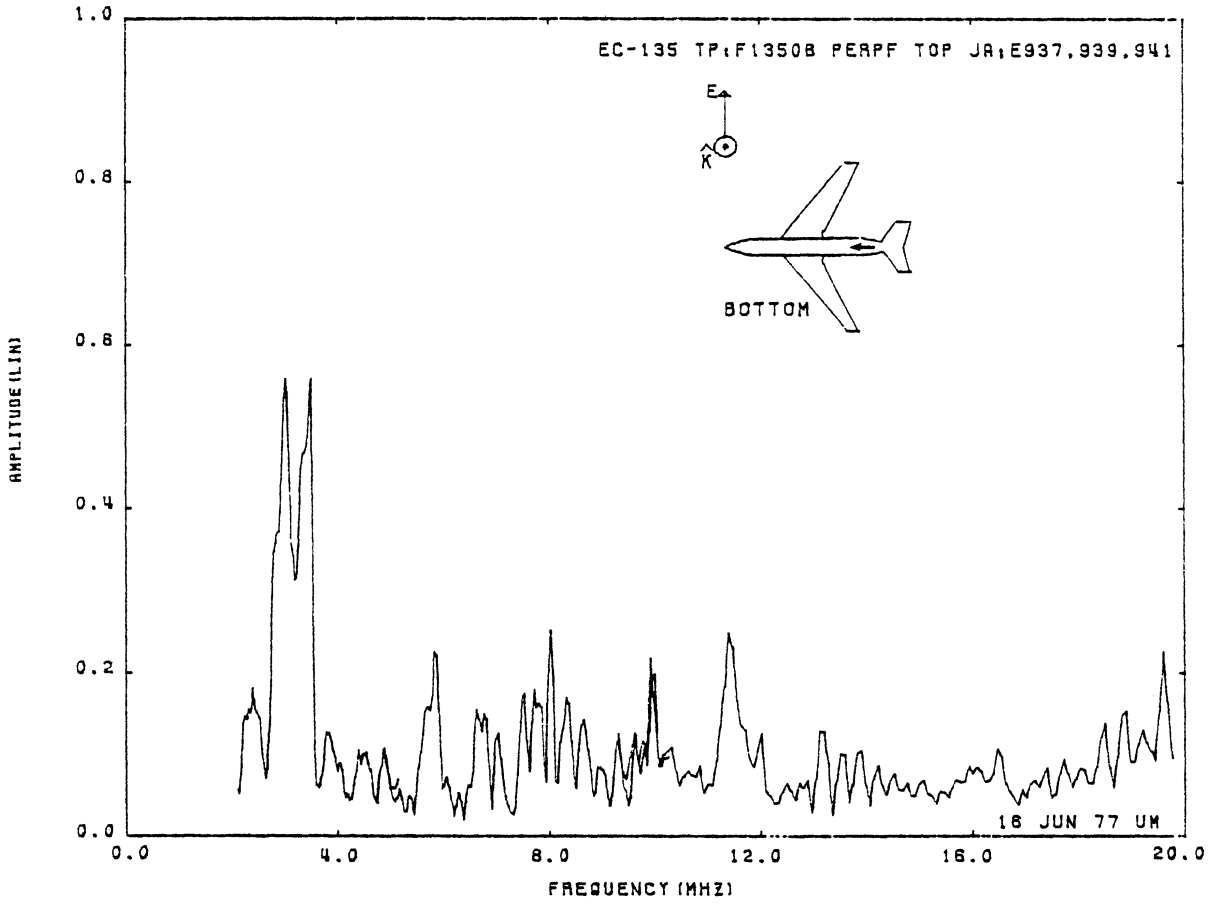

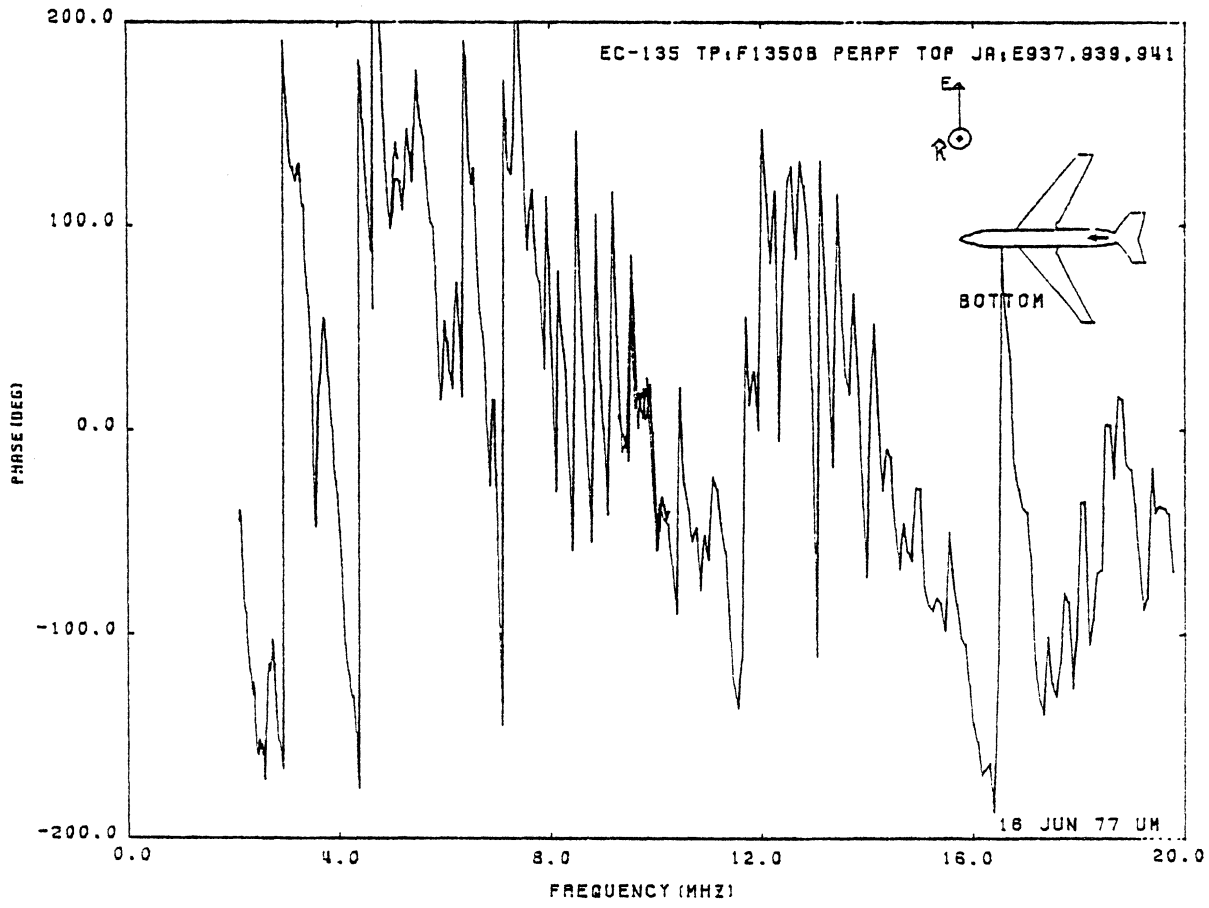

Figure 27: Axial Current at TP:F1350B, Orientation 2.

(see *, page 15)

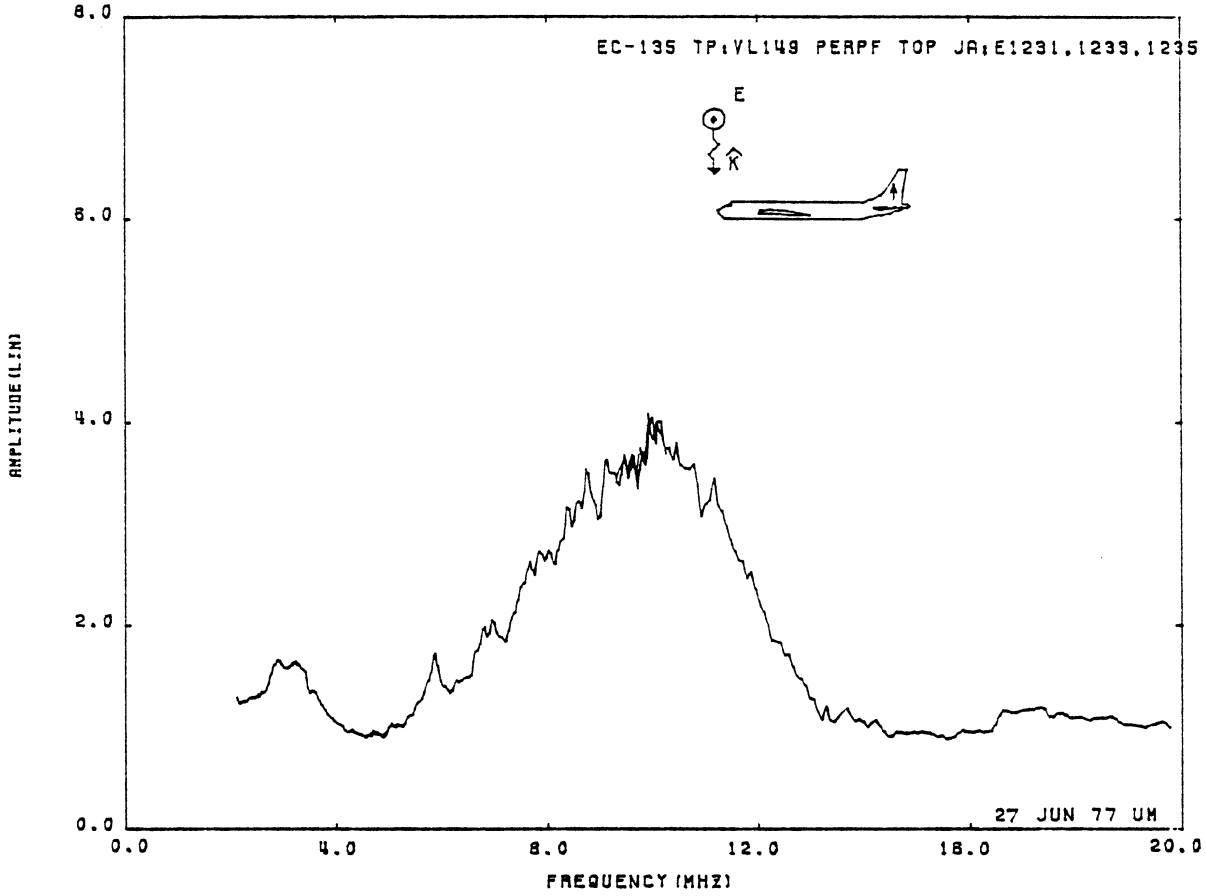

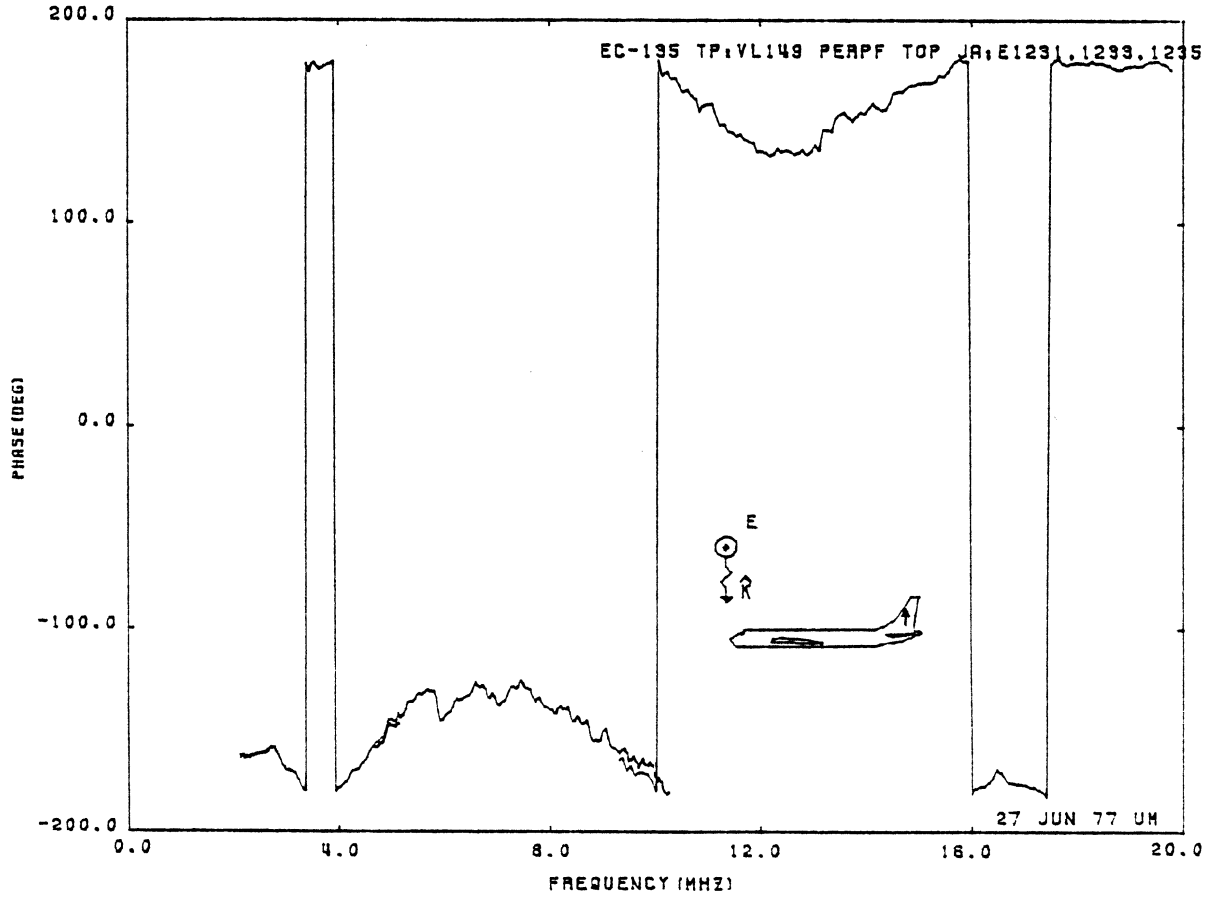

Figure 28: Axial Current at TP:VL149, Orientation 2.

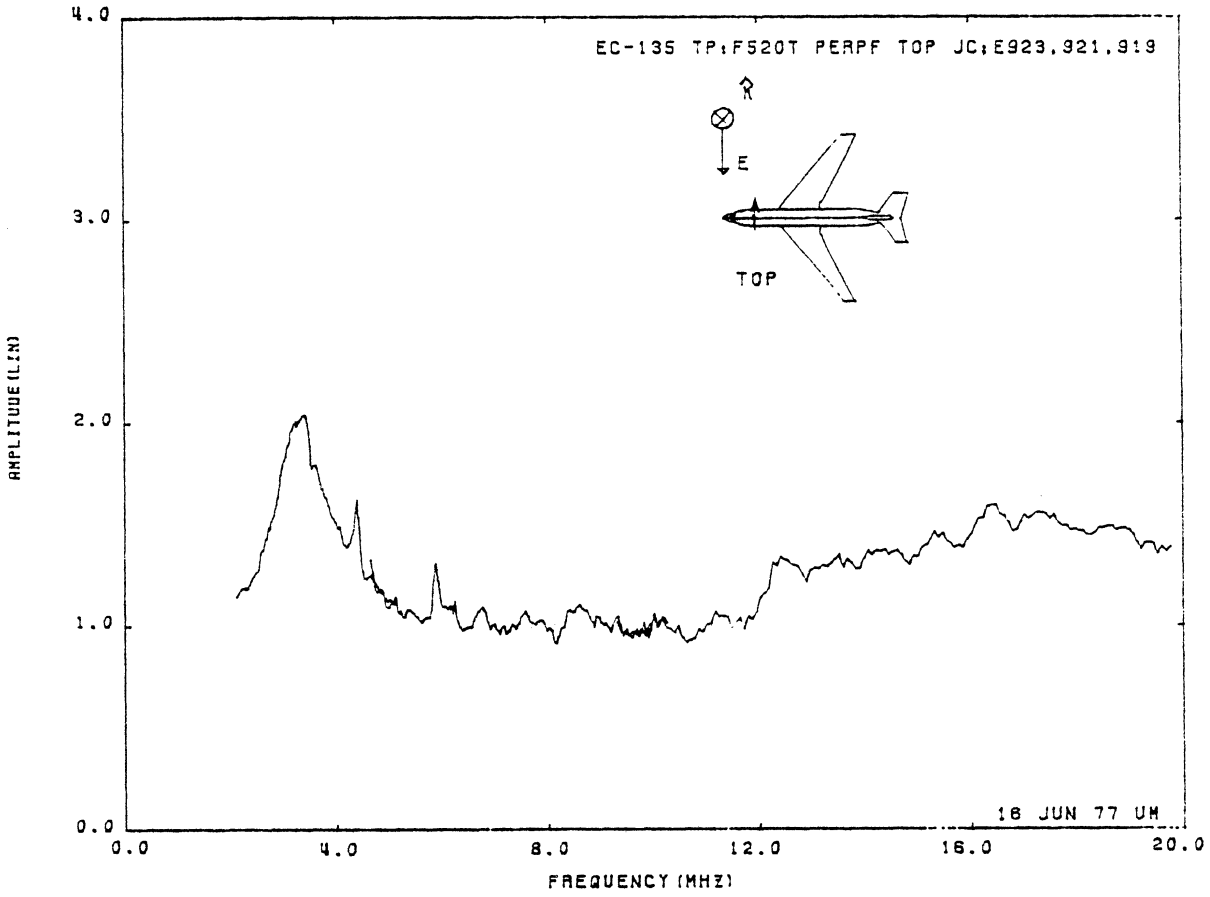

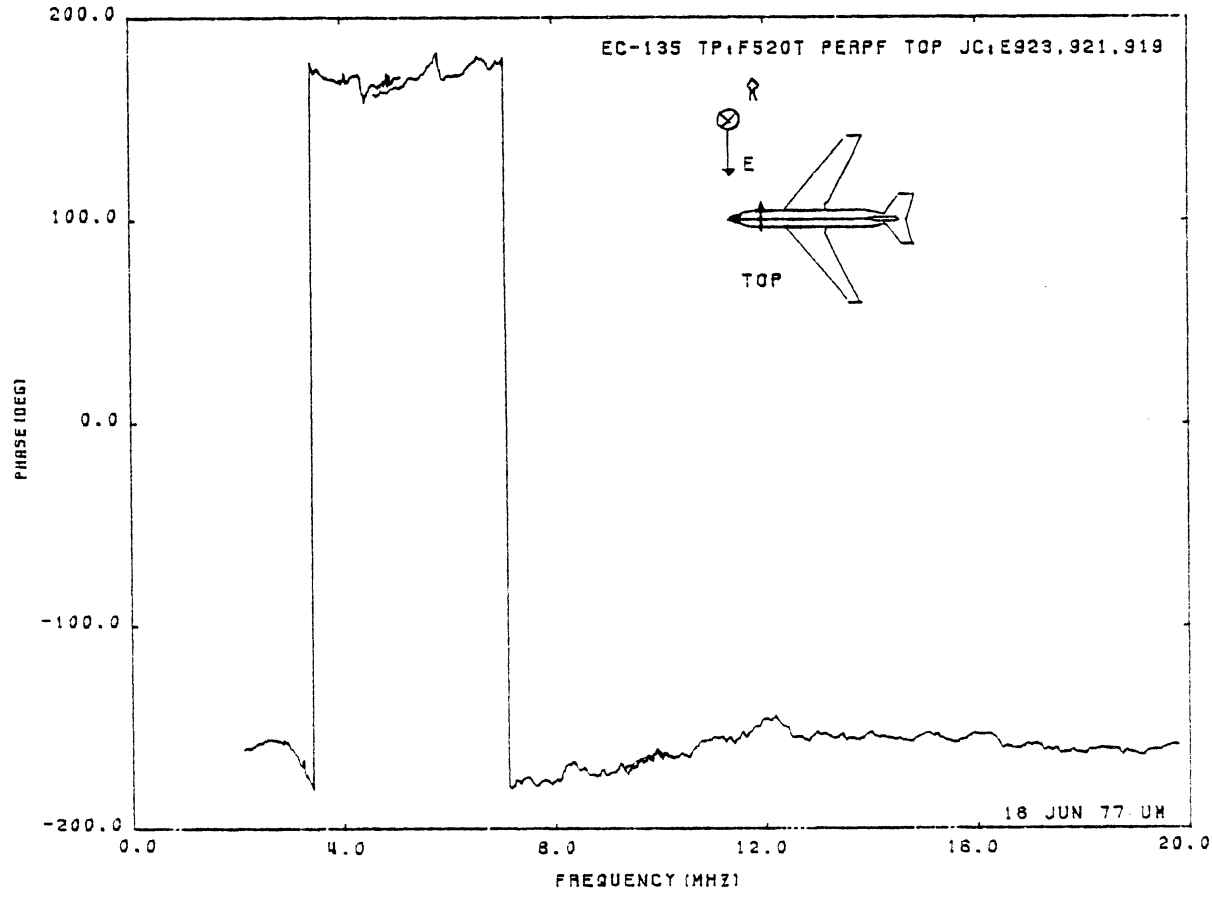

Figure 29 : Circumferential Current at TP:F520T, Orientation 2.

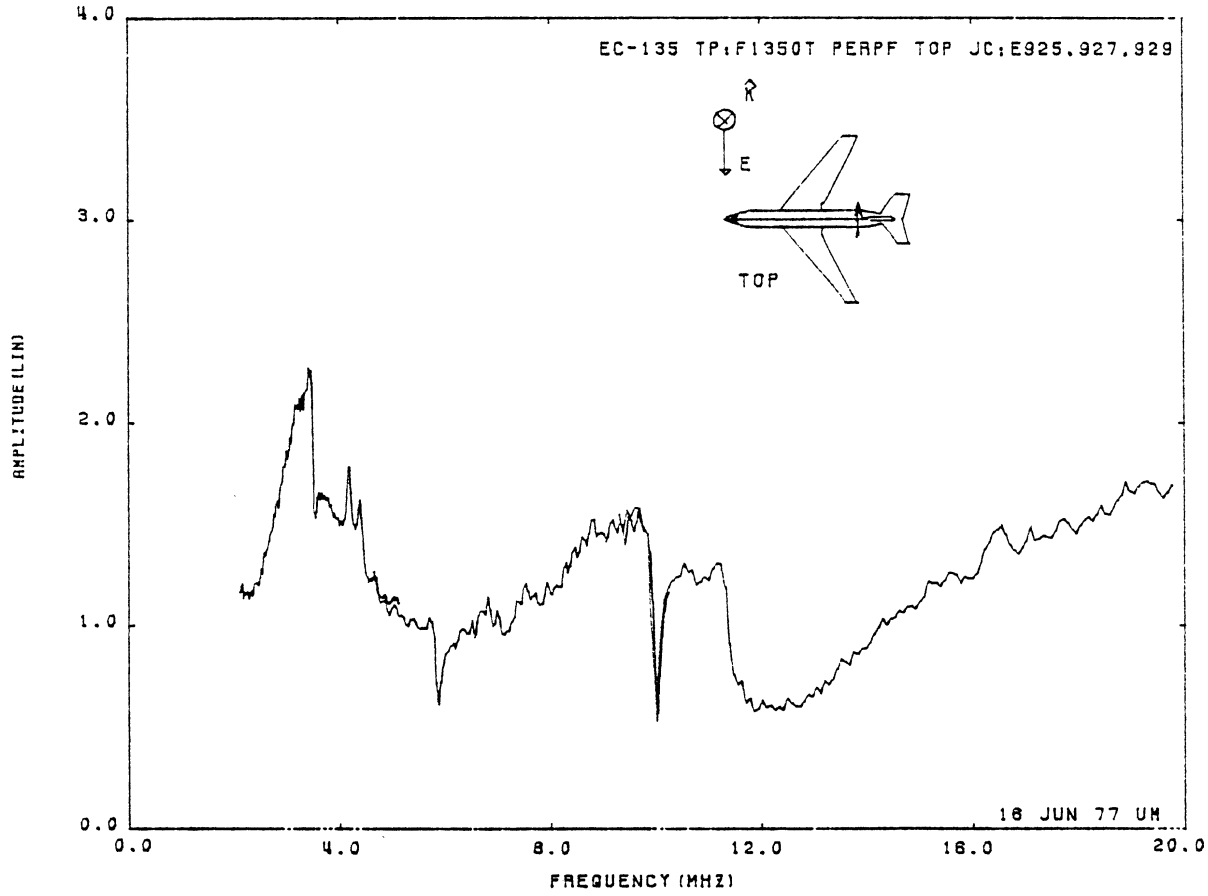

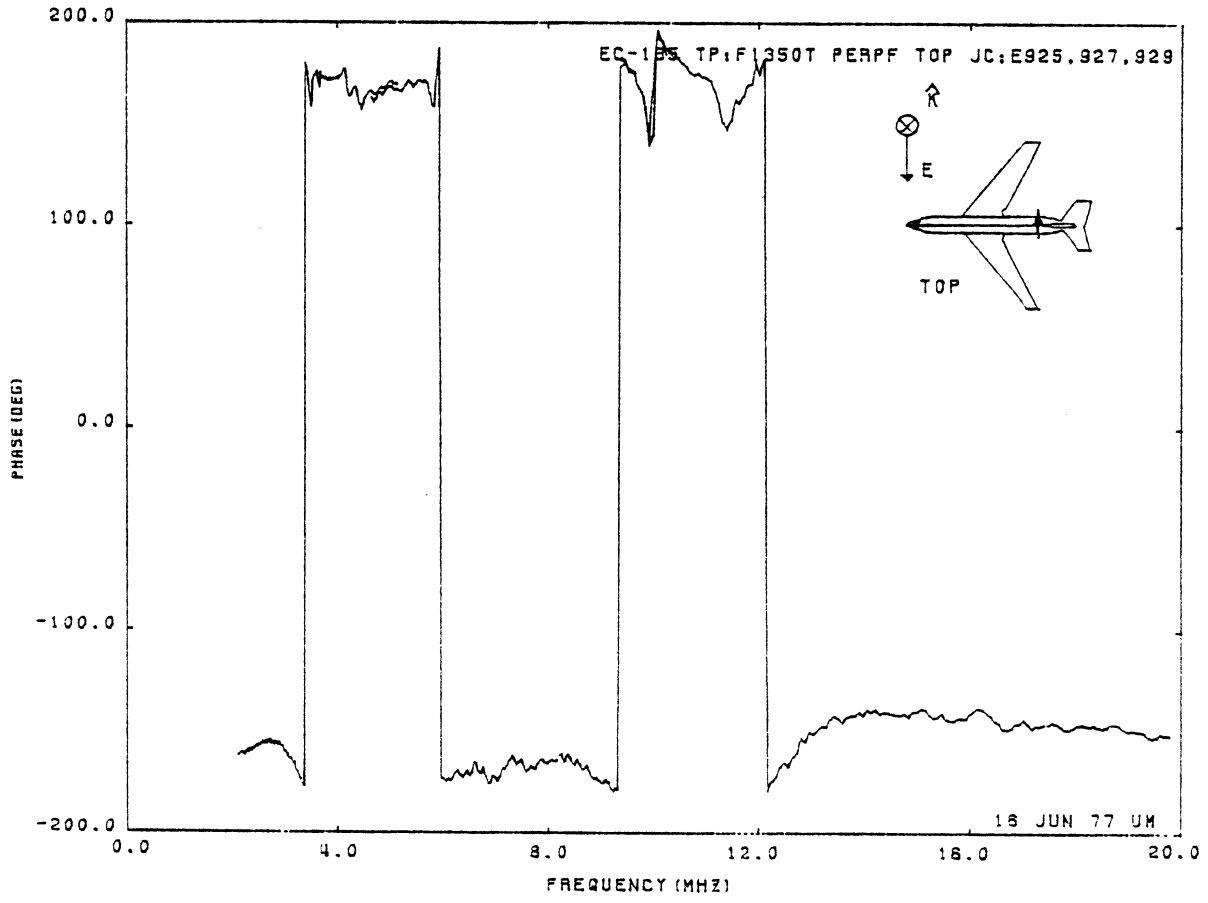

Figure 30: Circumferential Current at TP:F1350T, Orientation 2.

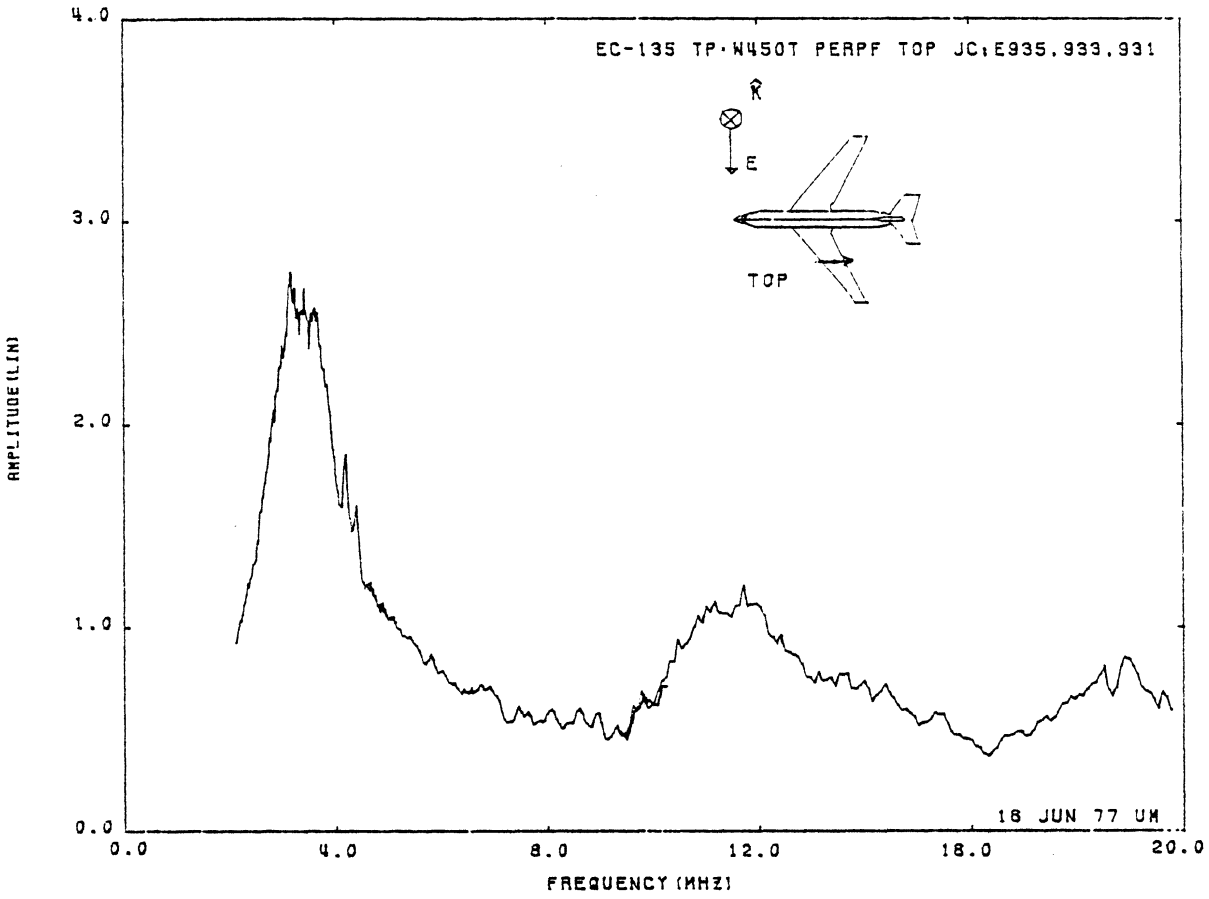

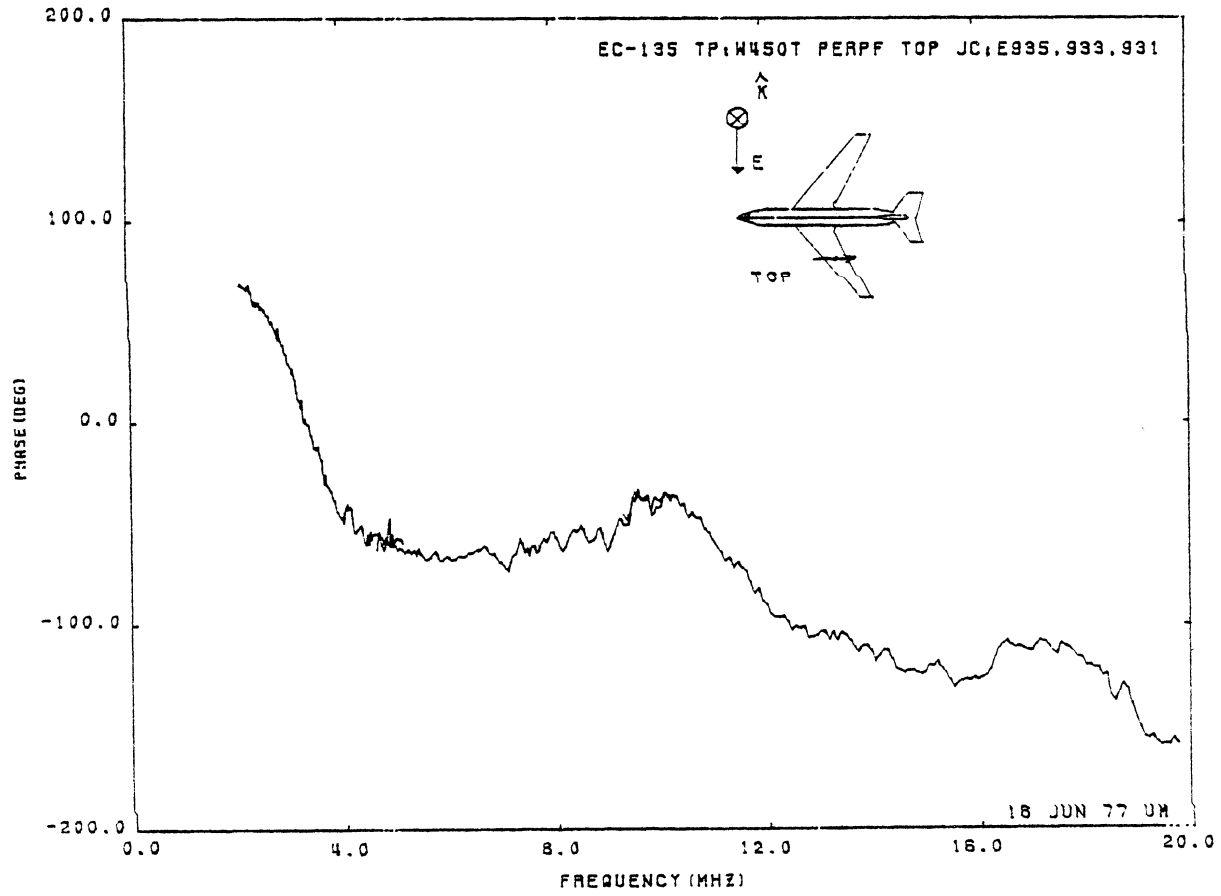

Figure 31: Circumferential Current at TP:WL450T, Orientation 2.

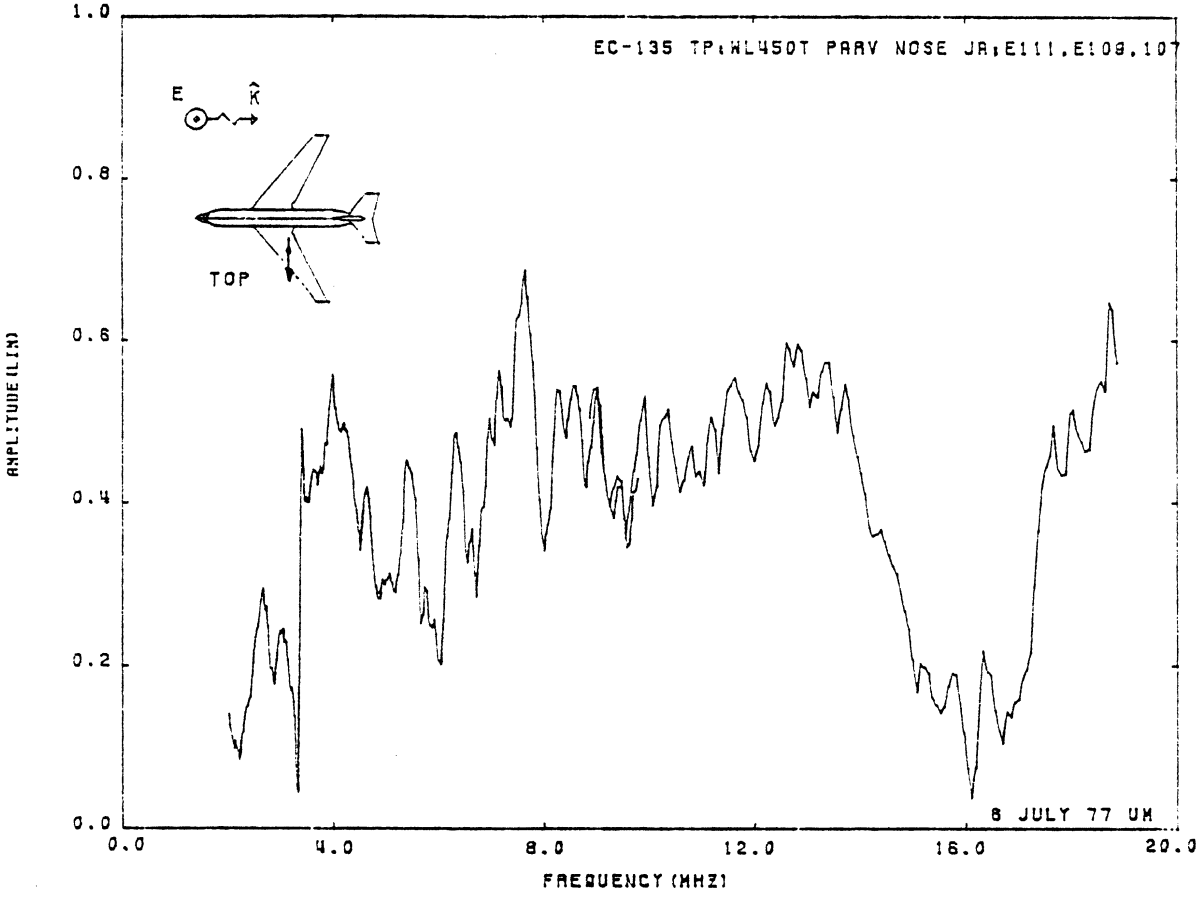

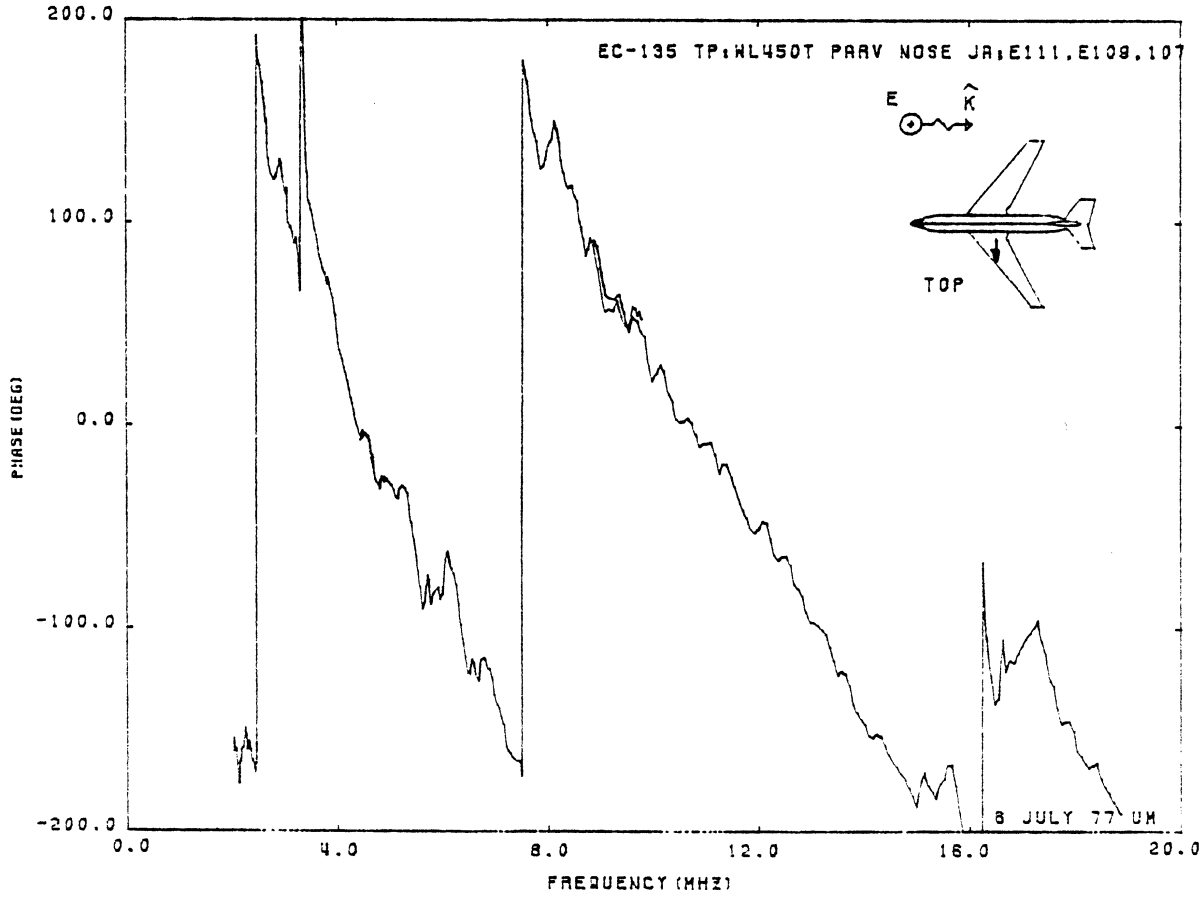

Figure 32: Axial Current at TP:WL450T, Orientation 3.

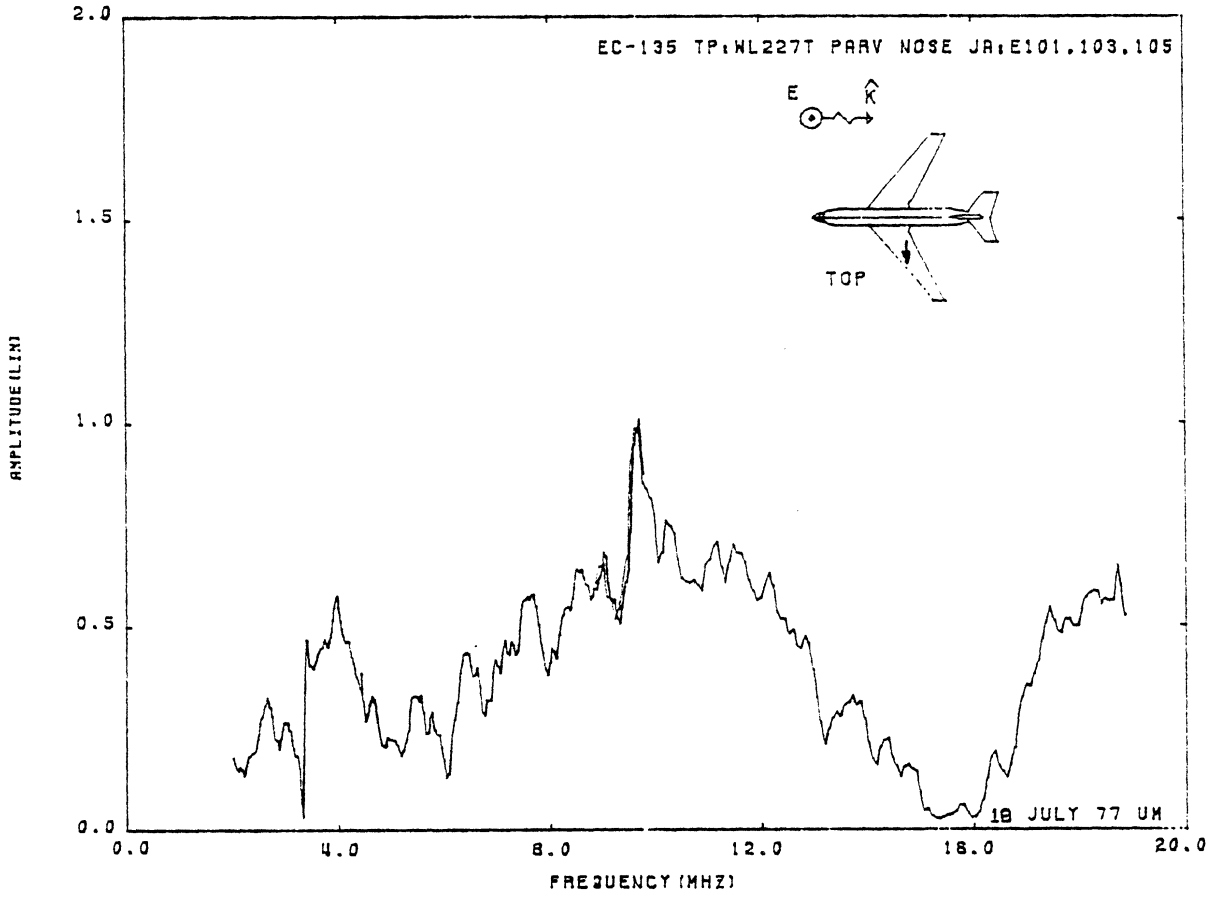

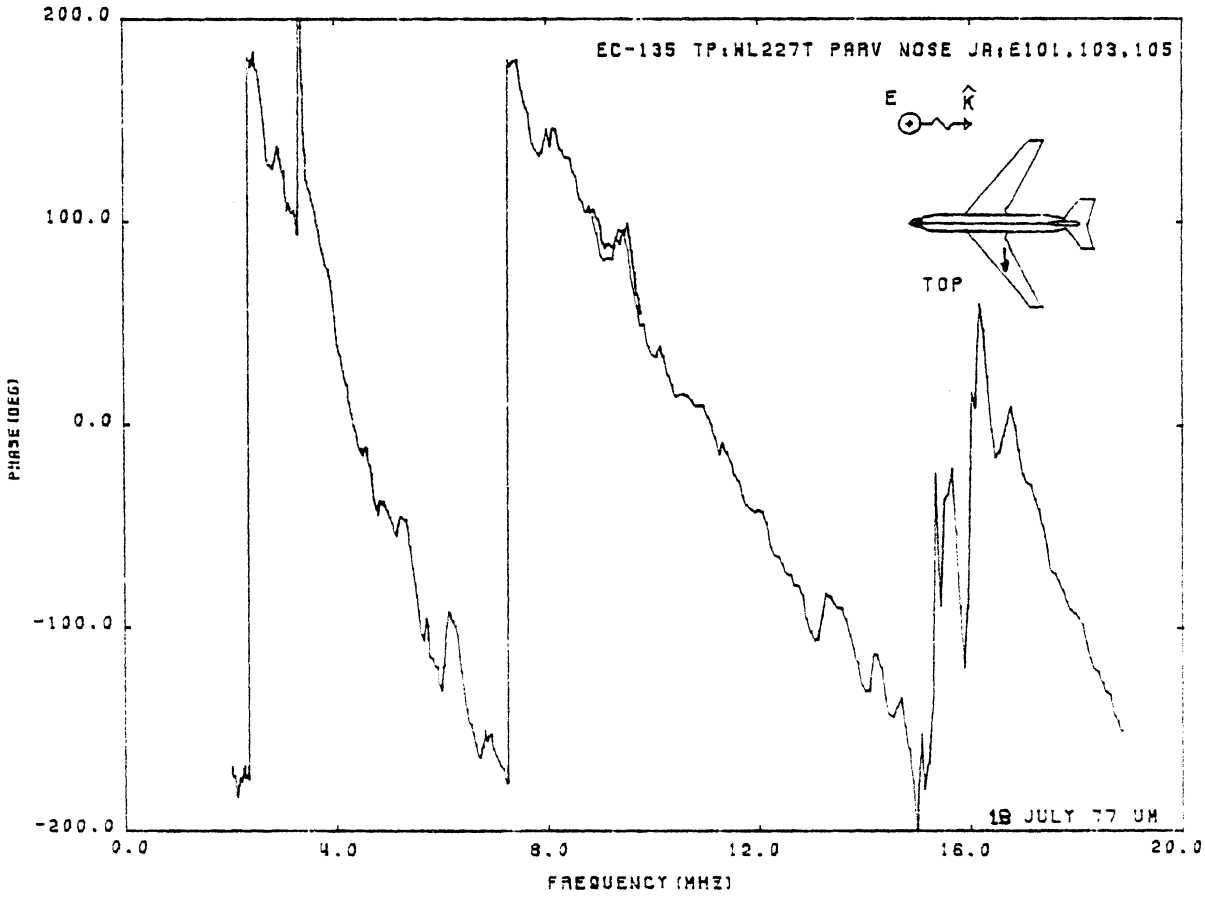

Figure 33: Axial Current at TP:WL227T, Orientation 3.

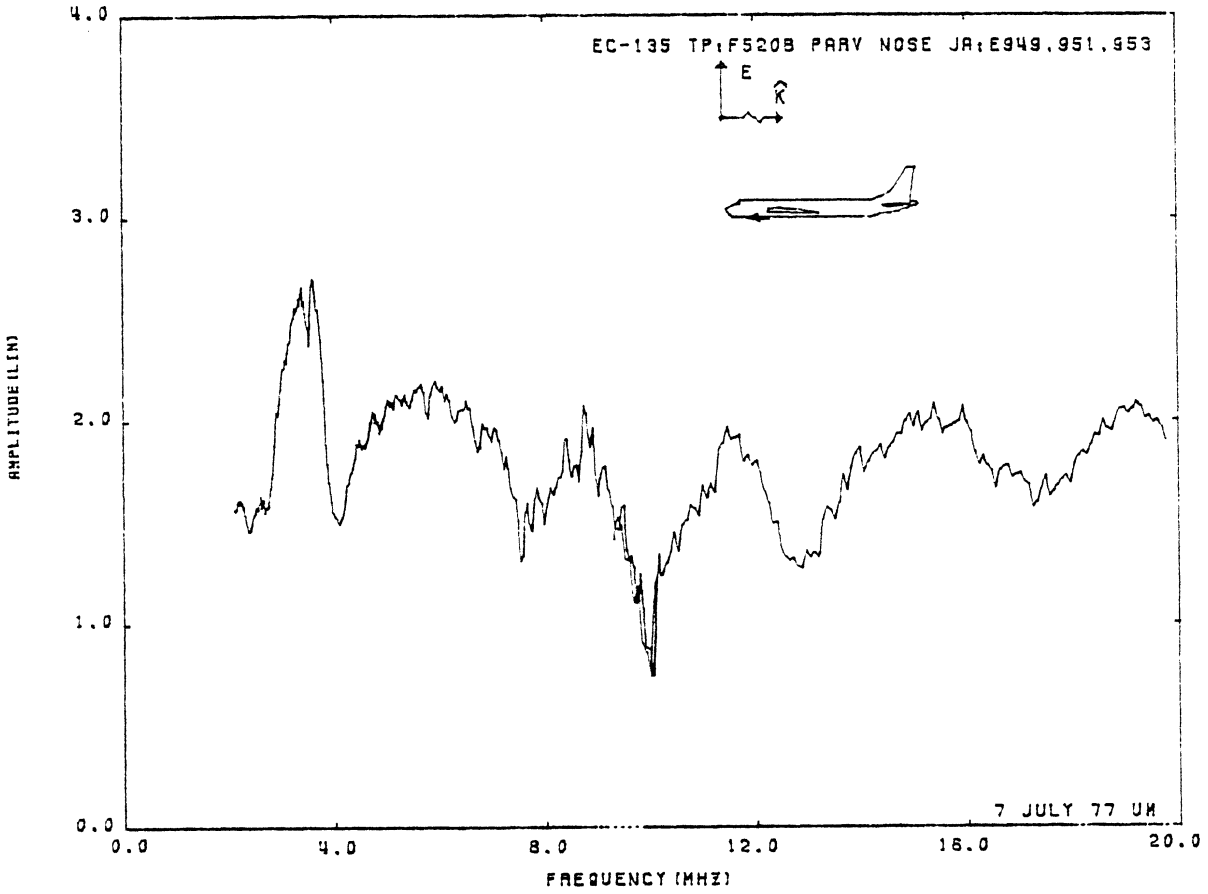

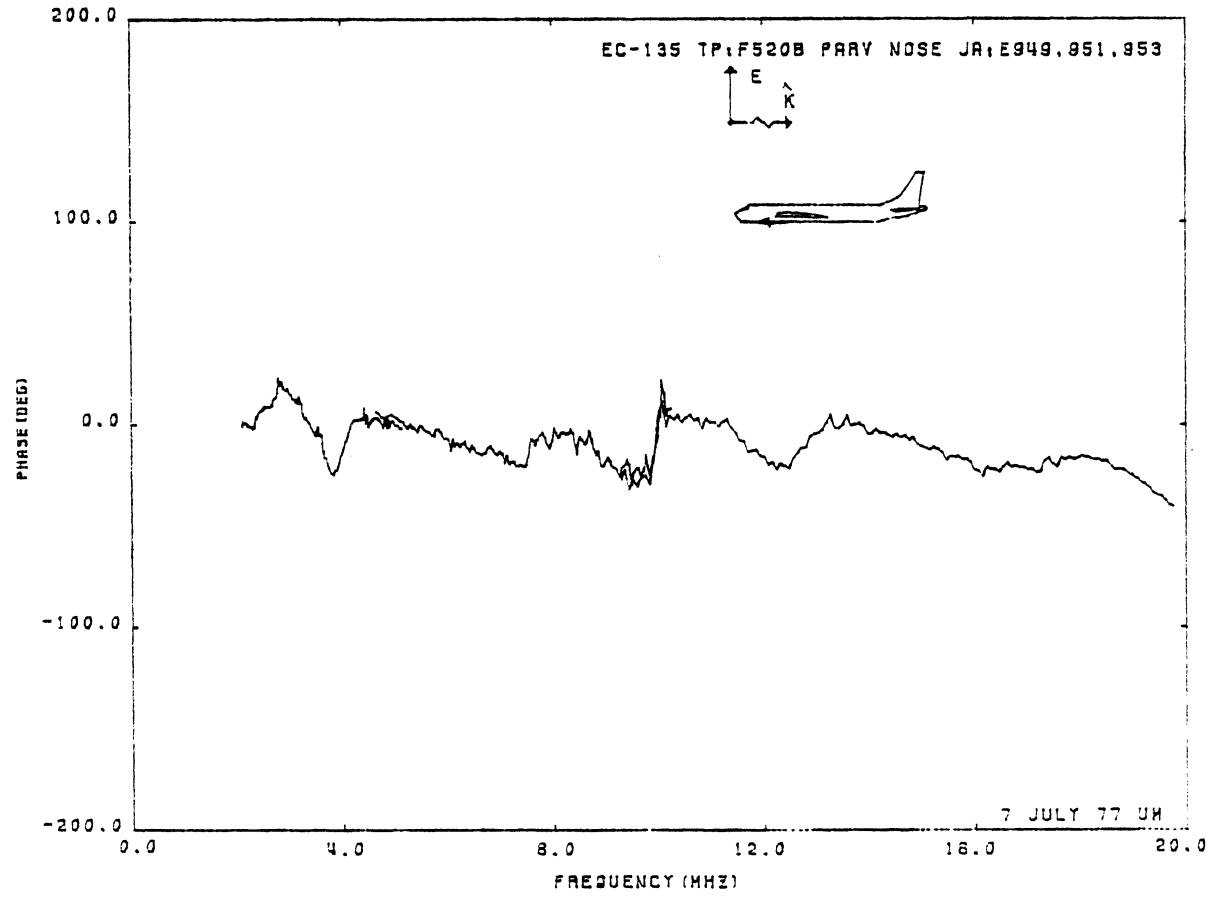

Figure 34: Axial Current at TP:F520B, Orientation 3.

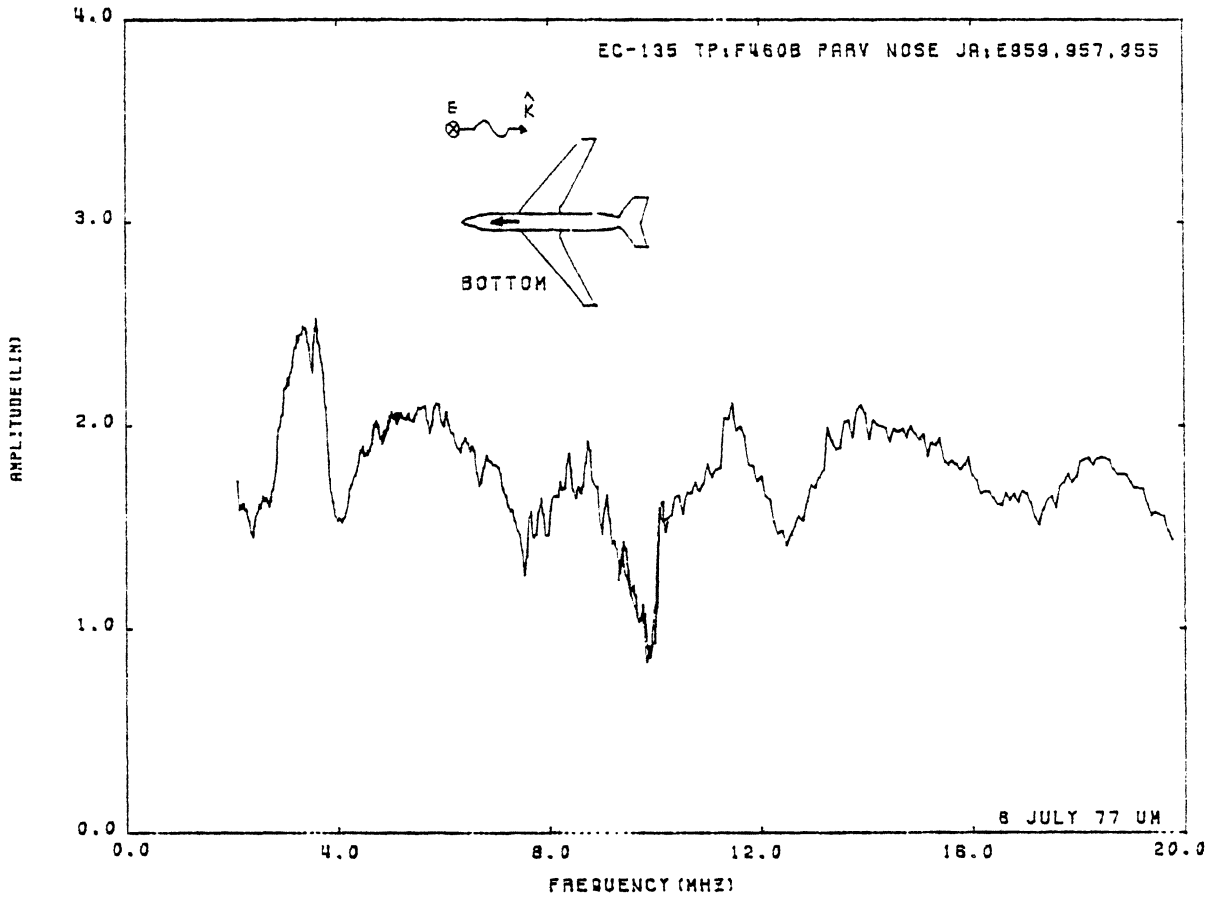

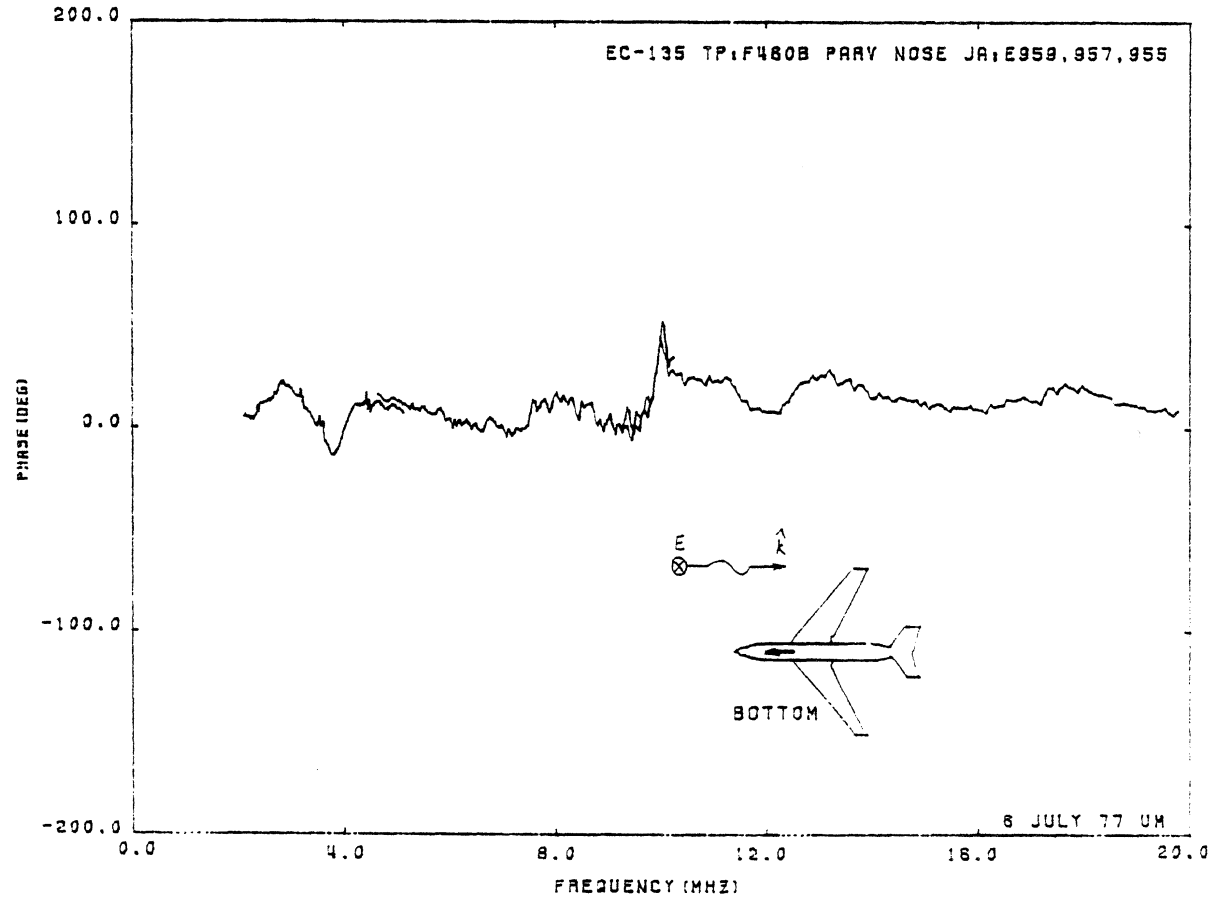

Figure 35: Axial Current at TP:F460B, Orientation 3.

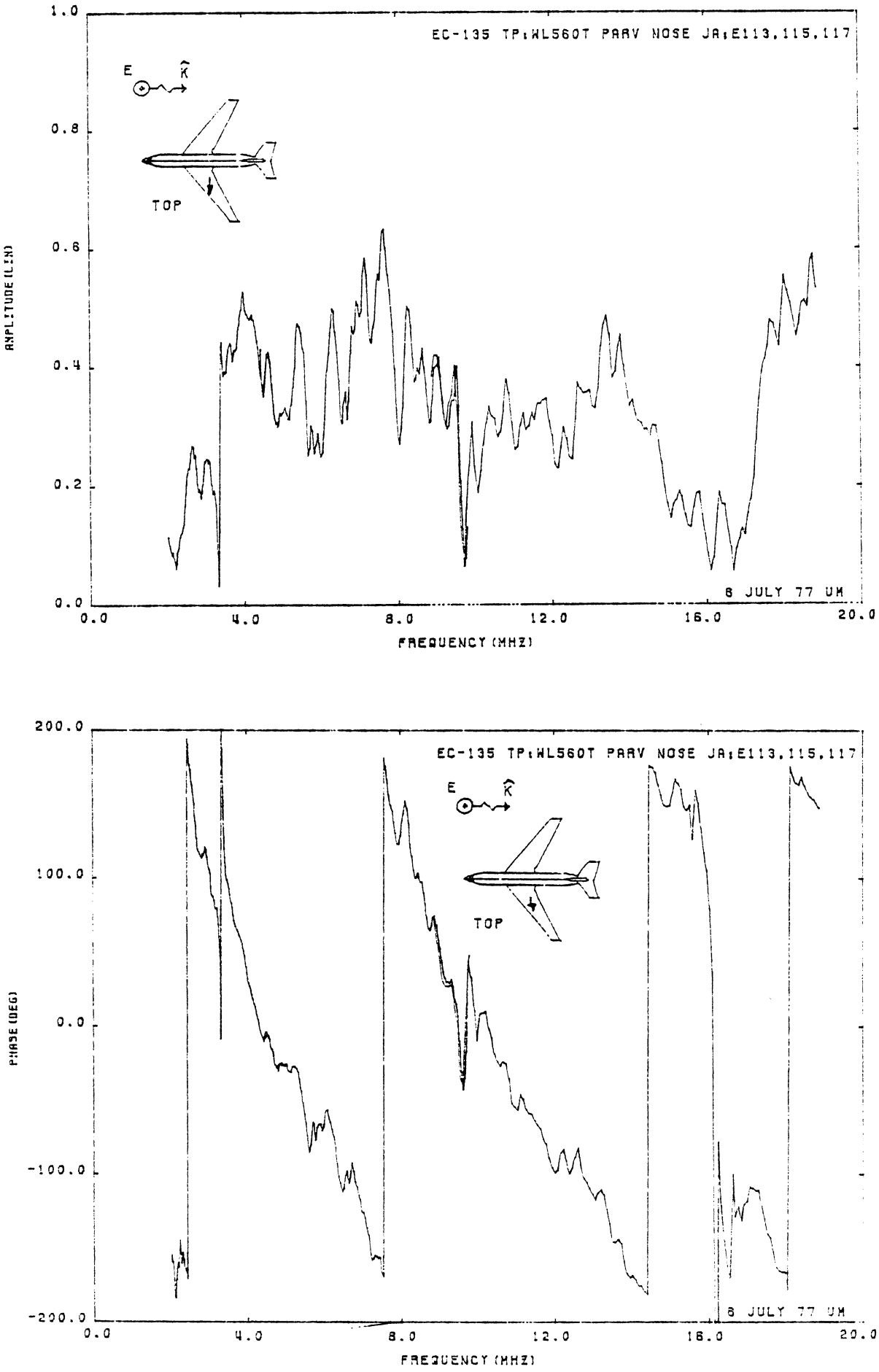

Figure 36: Axial Current at TP:WL560T, Orientation 3.

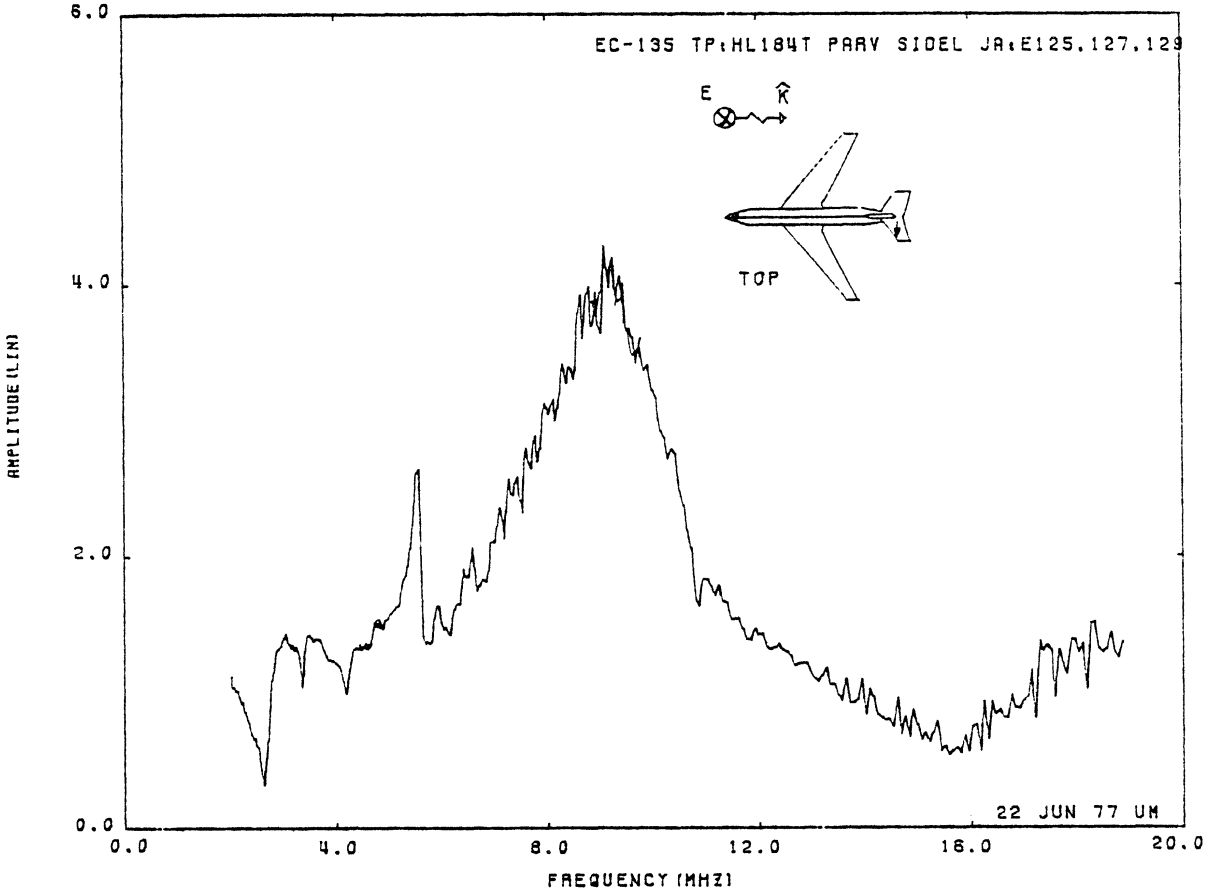

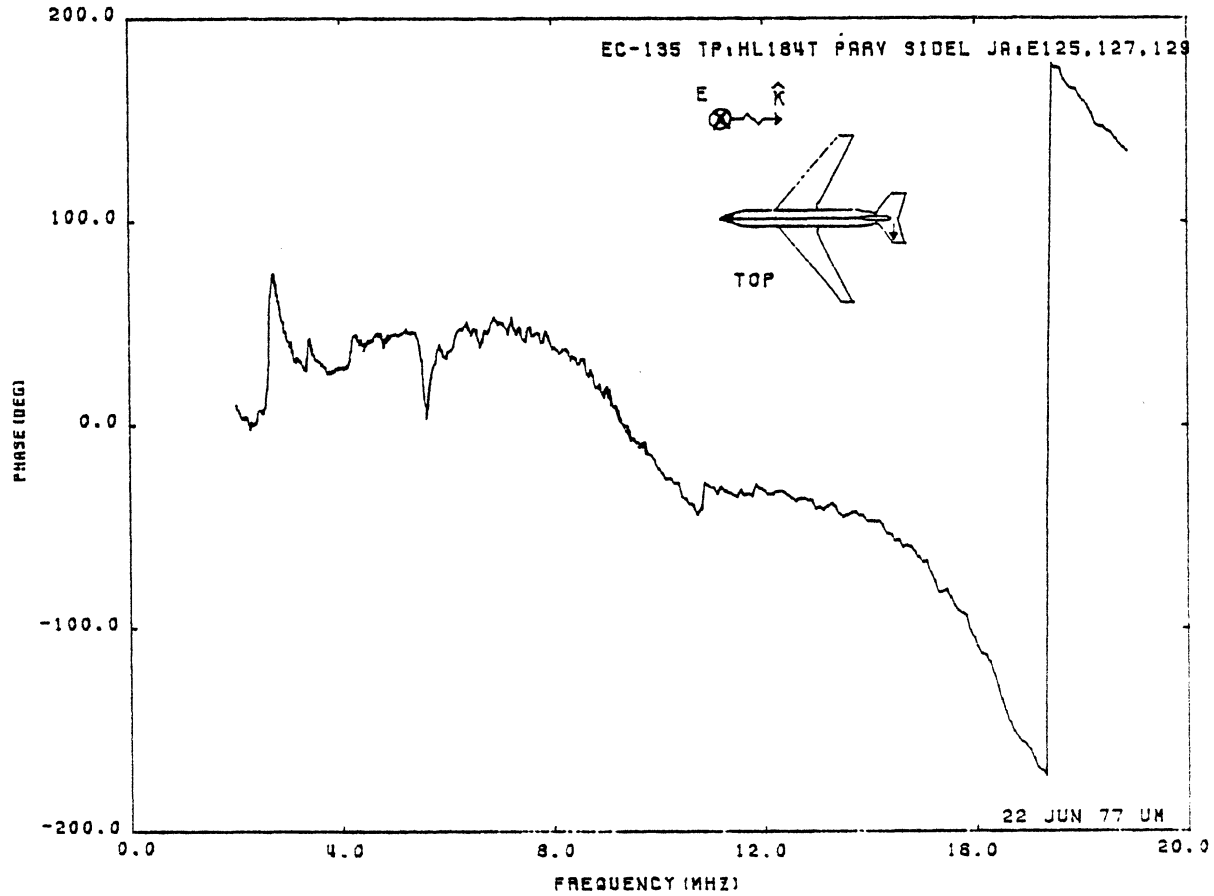

Figure 37: Axial Current at TP:HL184T, Orientation 4.

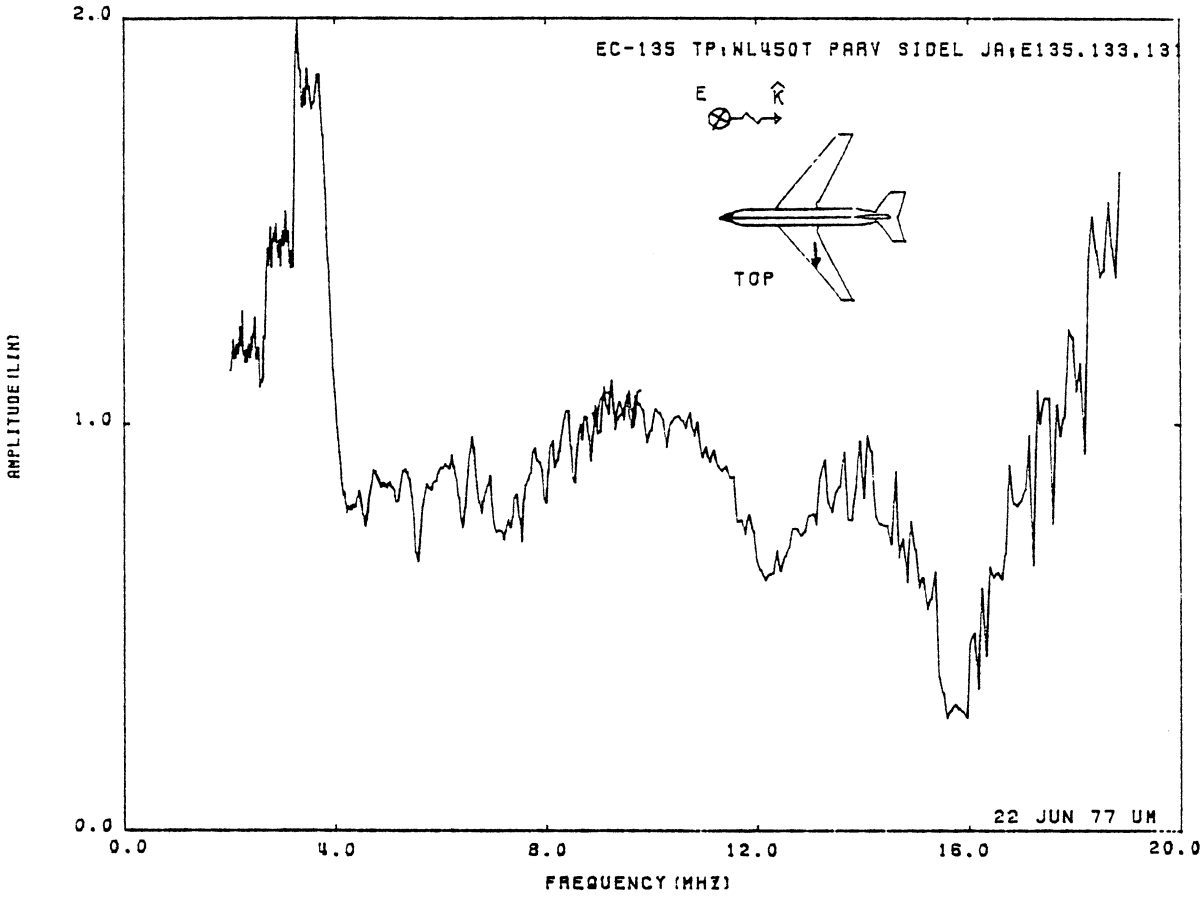

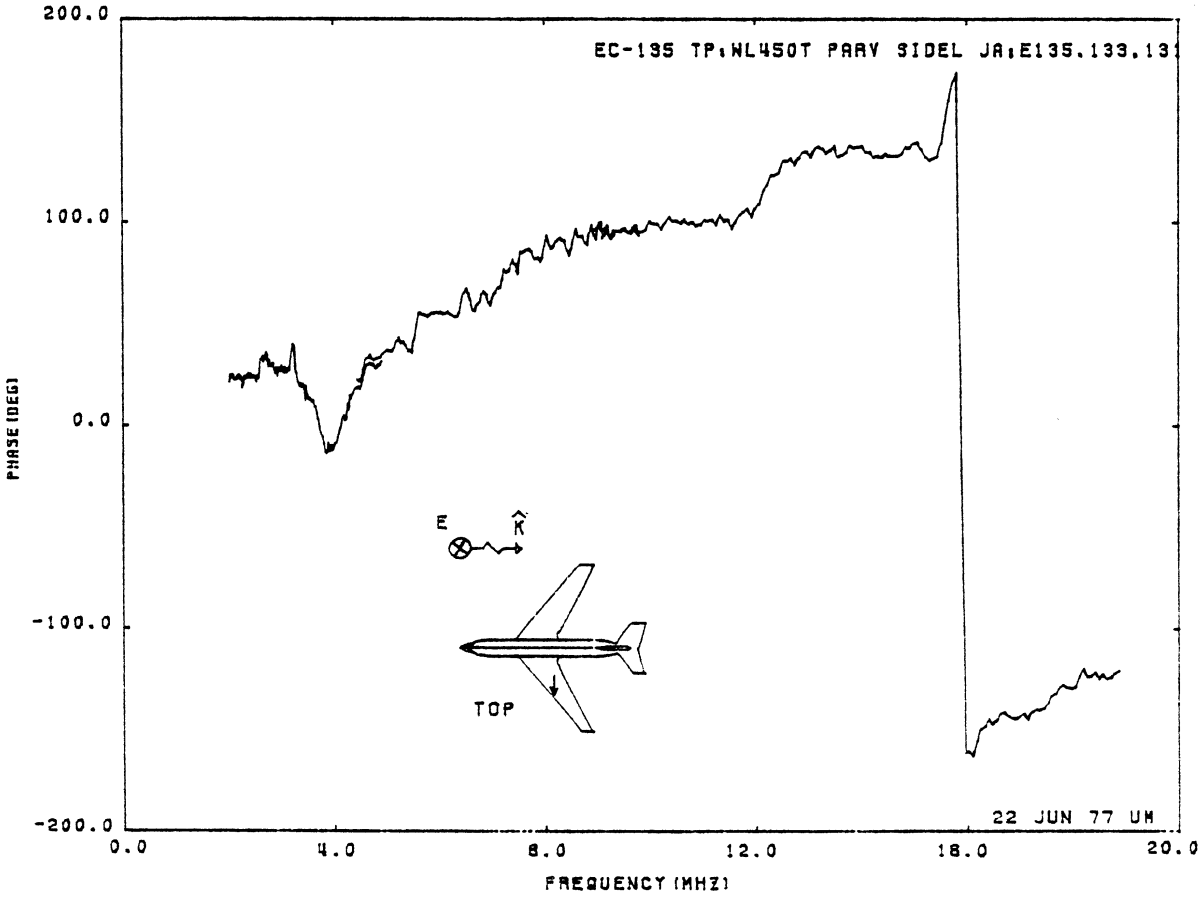

Figure 38: Axial Current at TP:WL450T, Orientation 4.

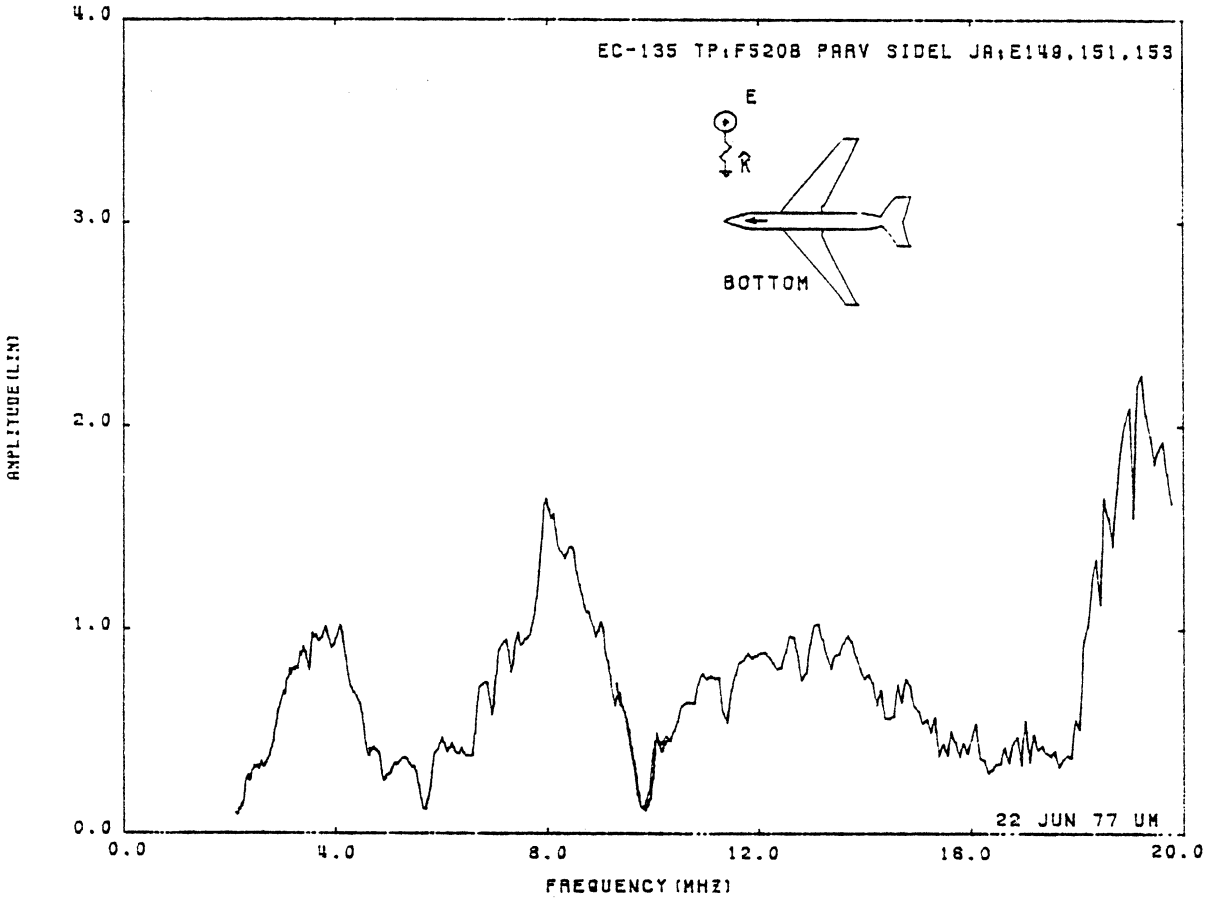

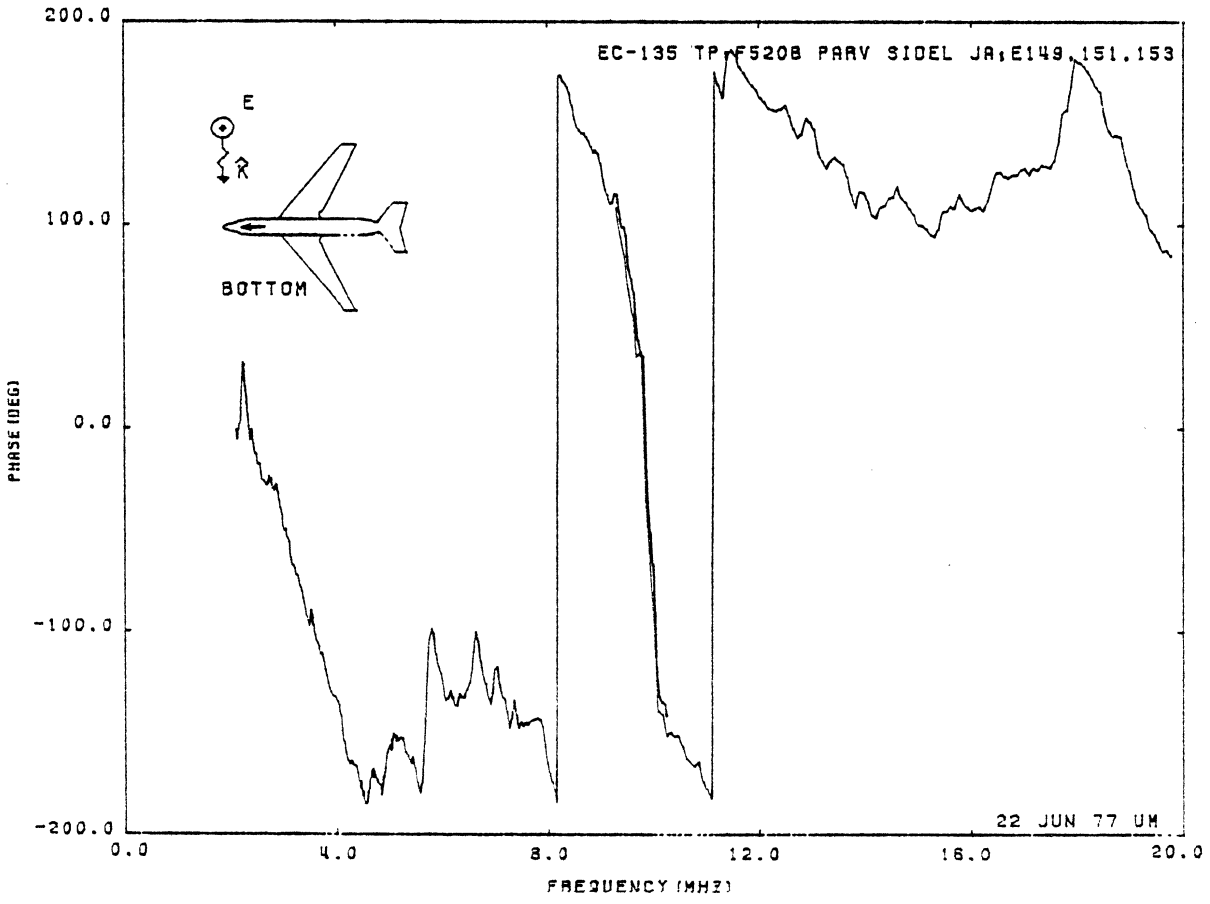

Figure 39: Axial Current at TP:F520B, Orientation 4.

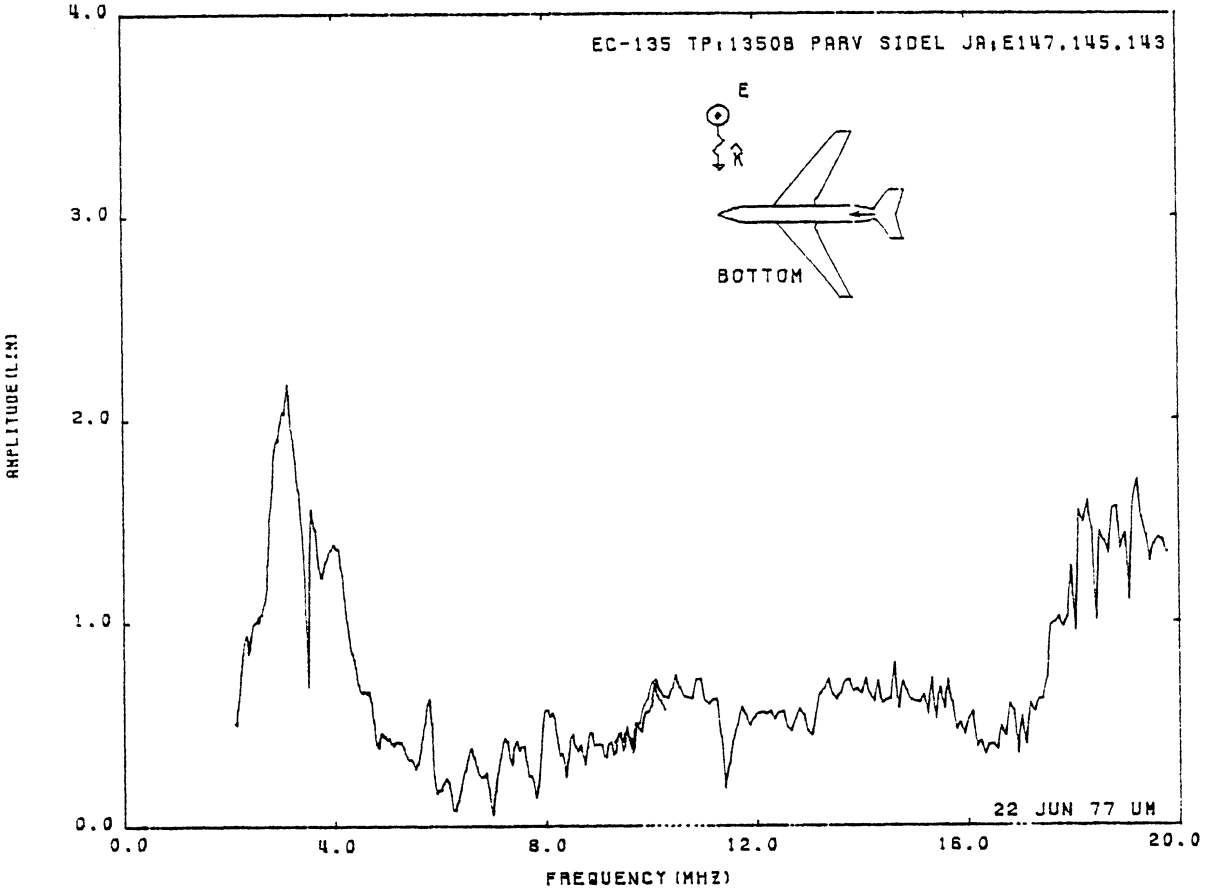

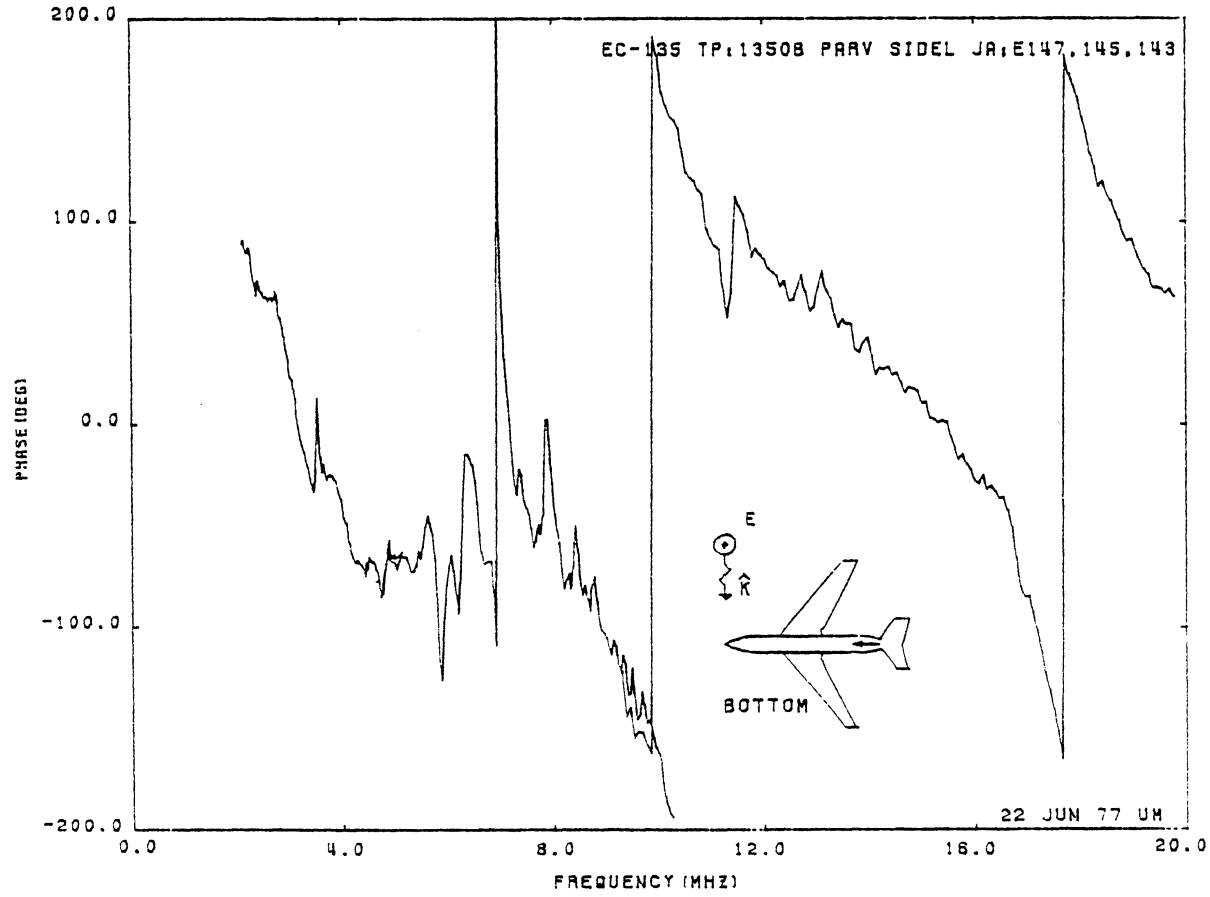

Figure 40: Axial Current at TP:F1350B, Orientation 4.

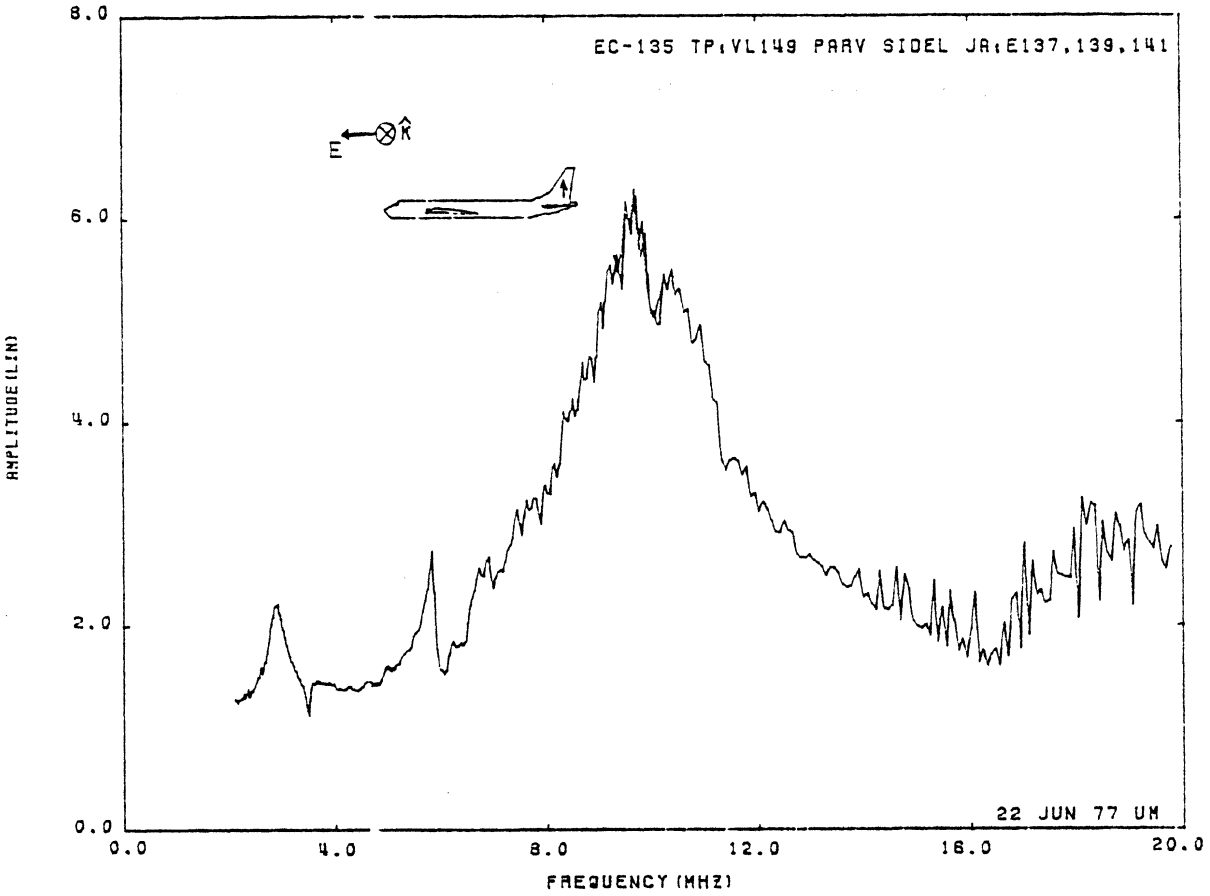

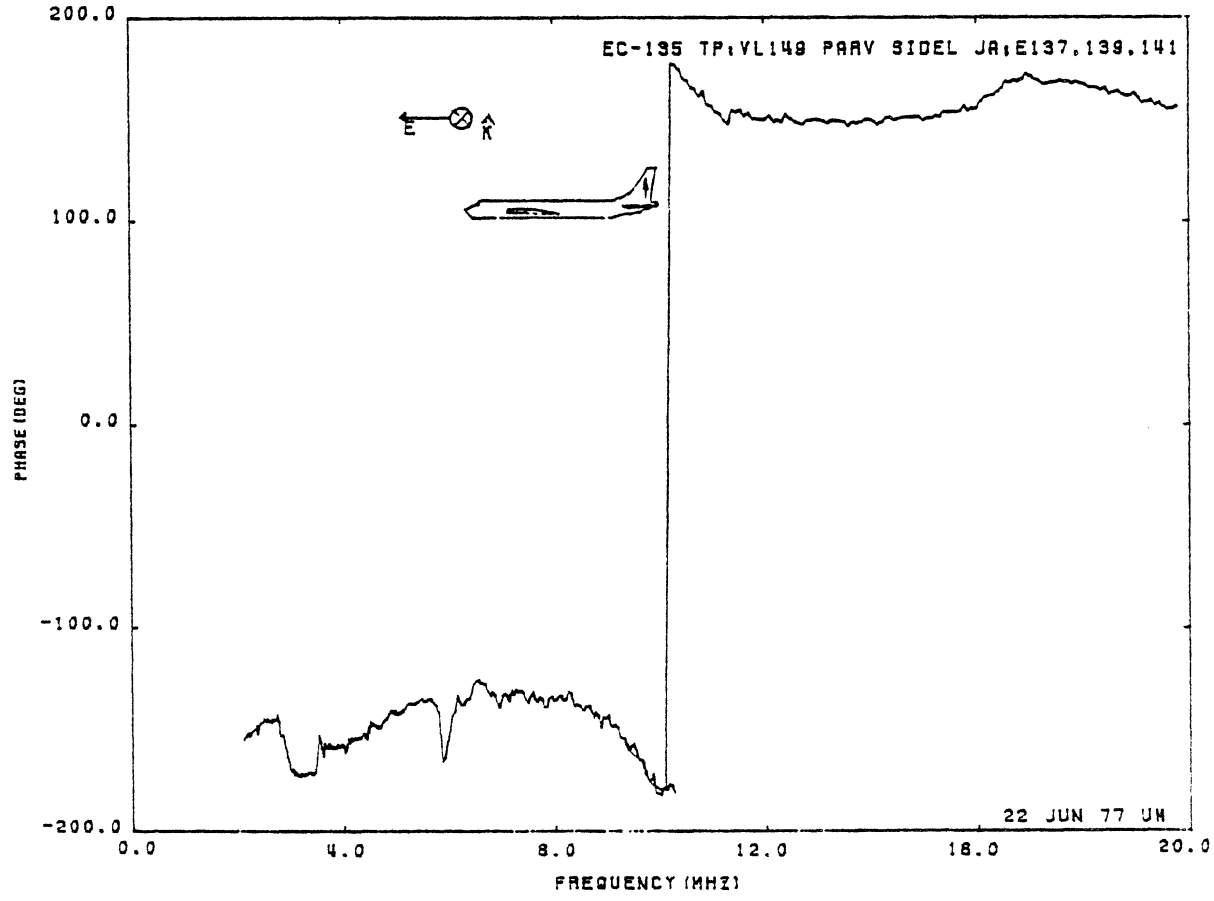

Figure 41: Axial Current at TP:VL149, Orientation 4.

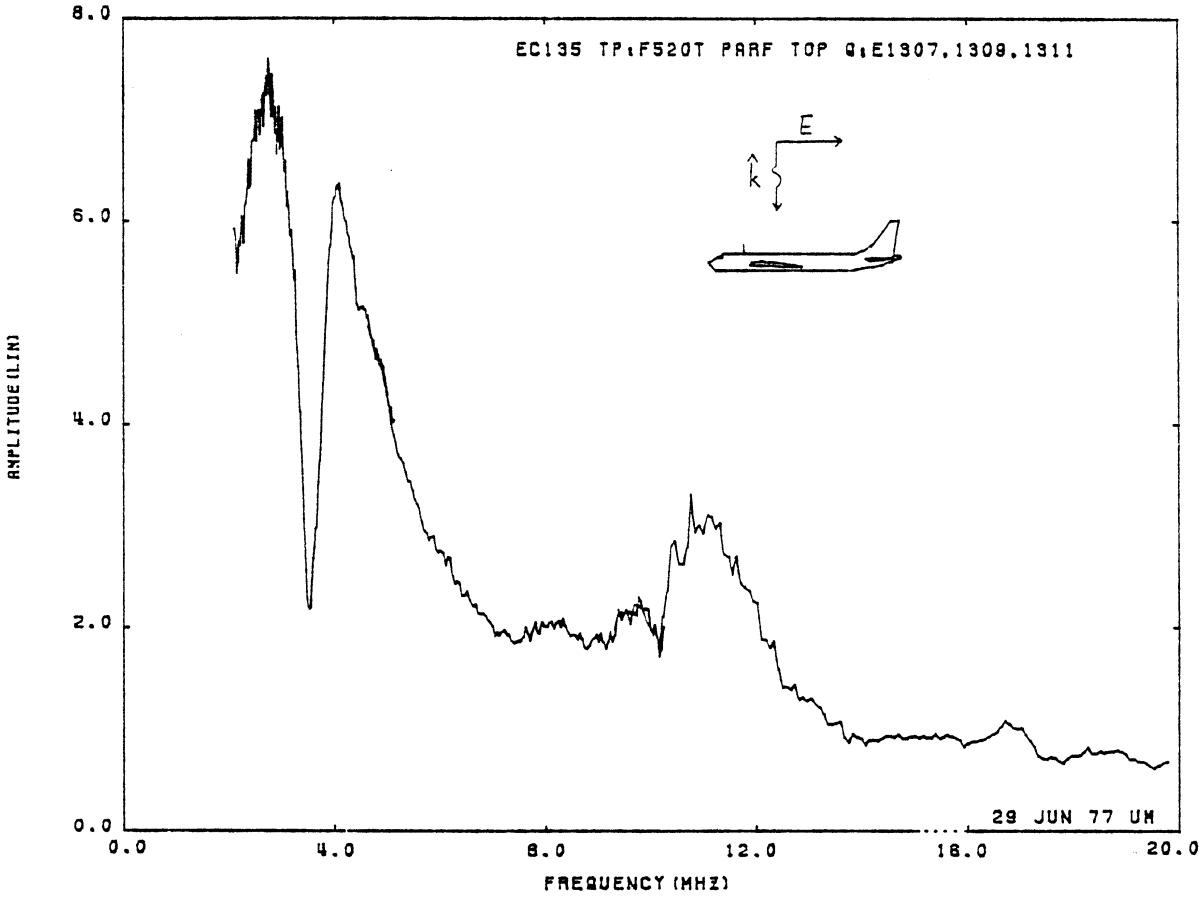

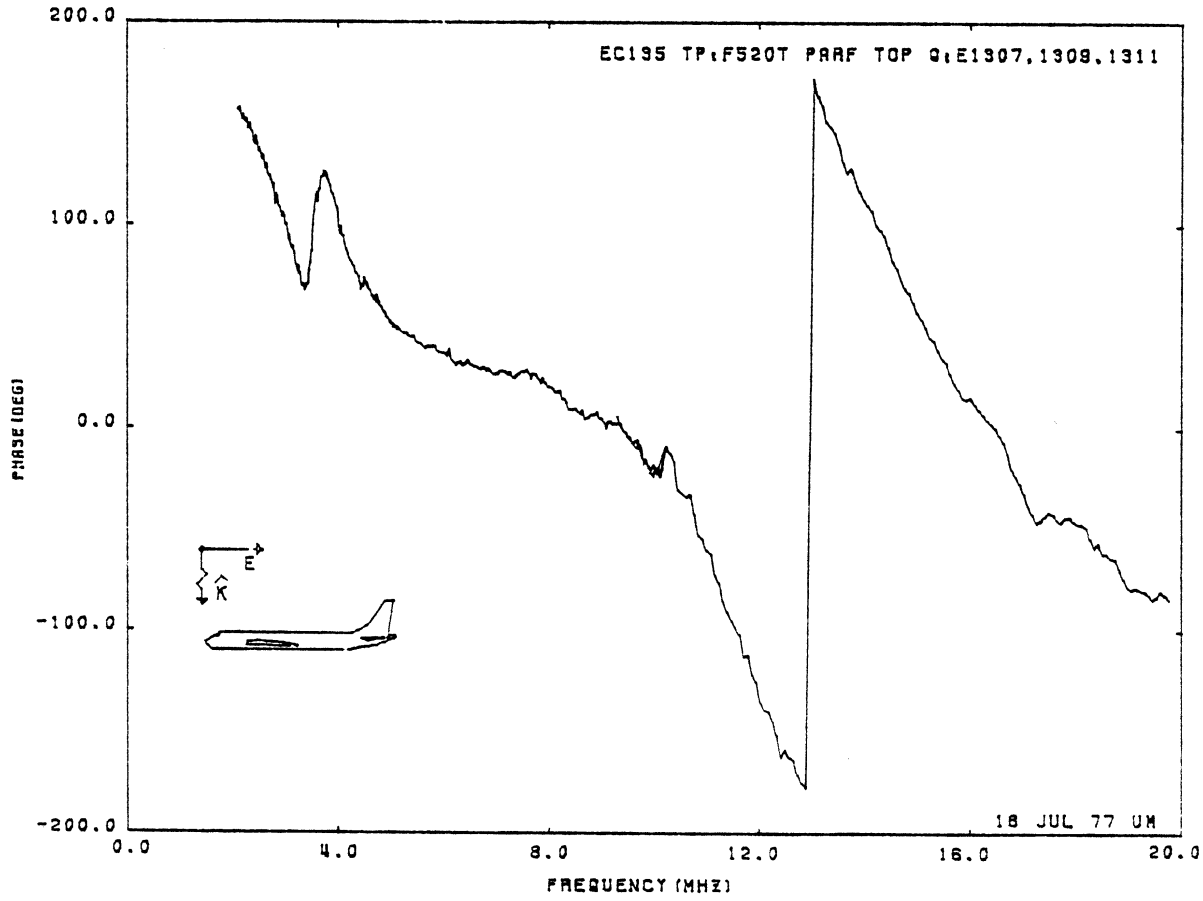

Figure 42: Charge at TP:F520T, Orientation 1.

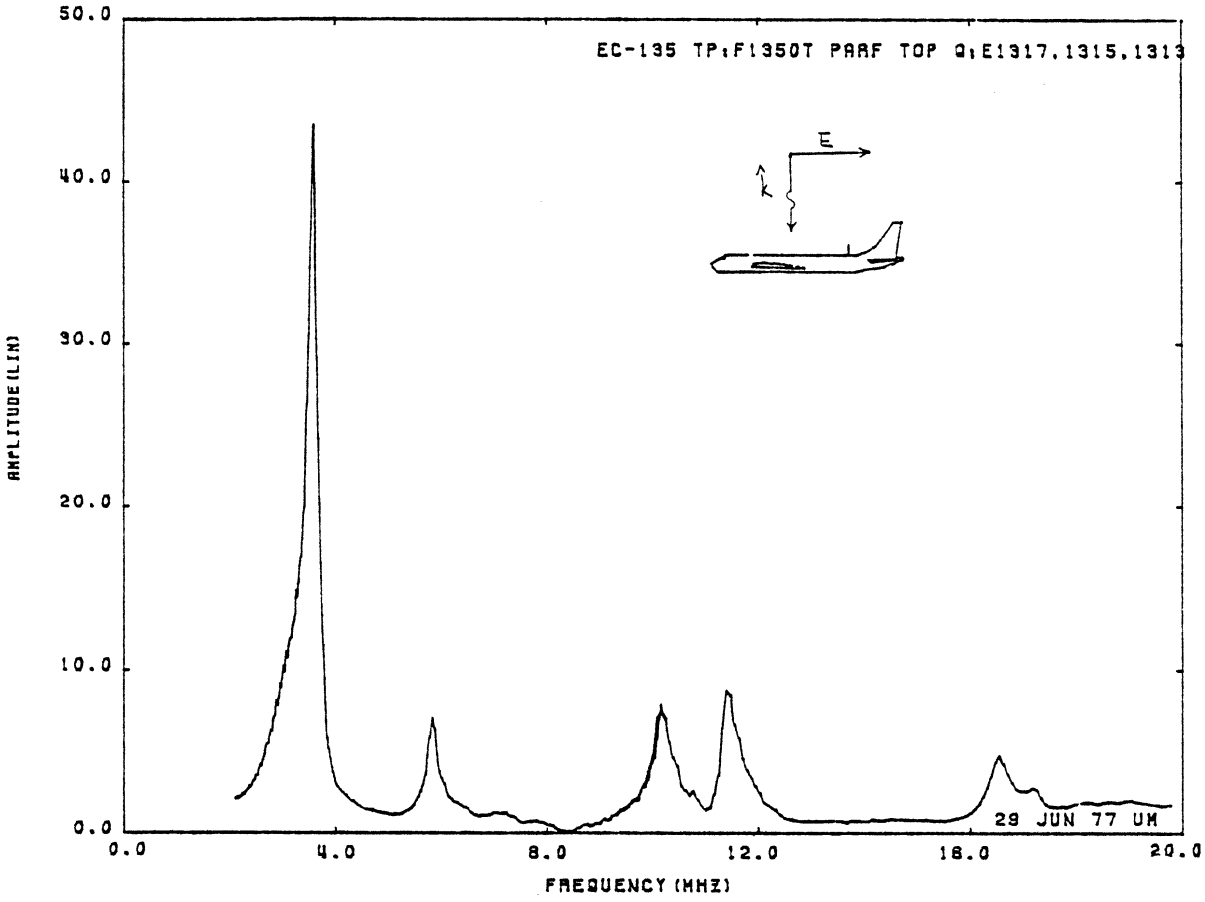

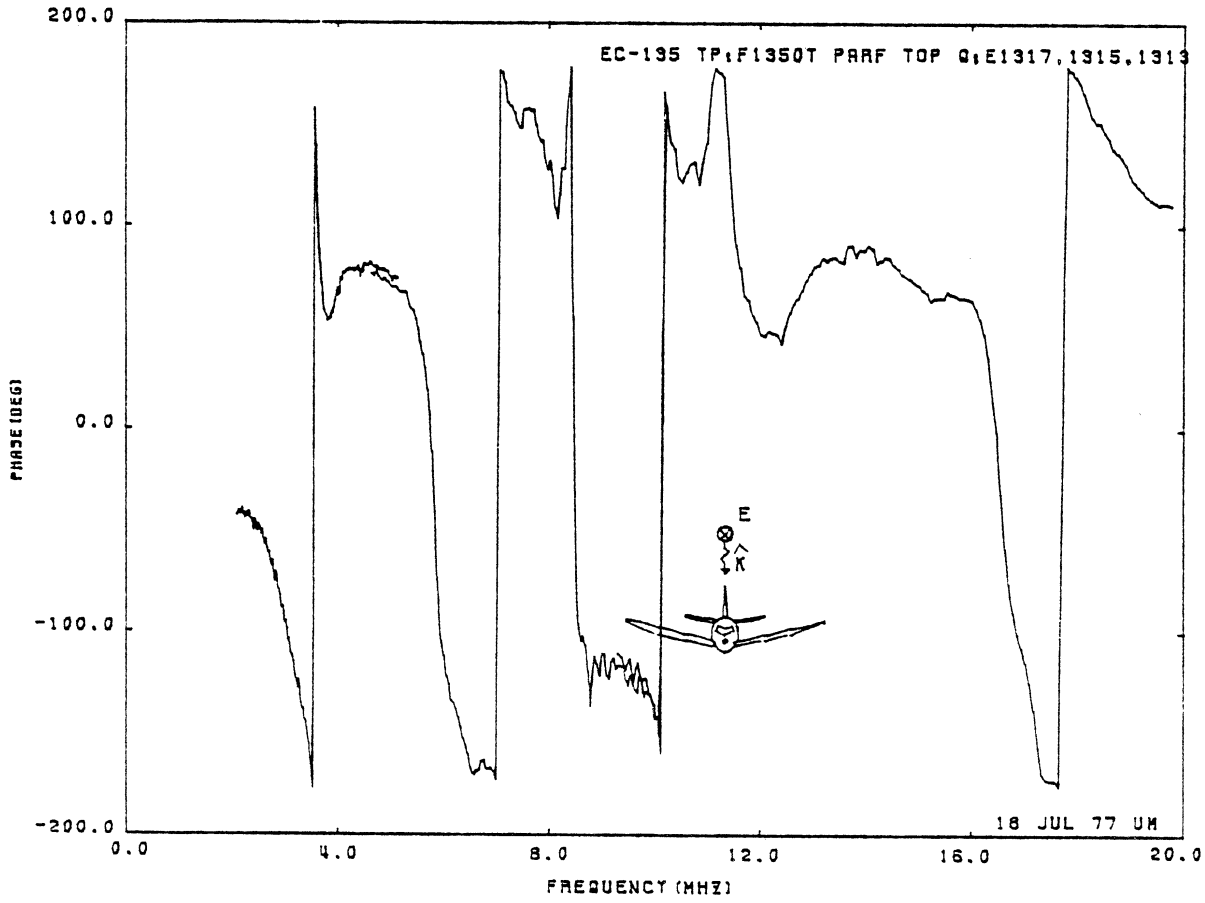

Figure 43: Charge at TP:F1350T, Orientation 1.

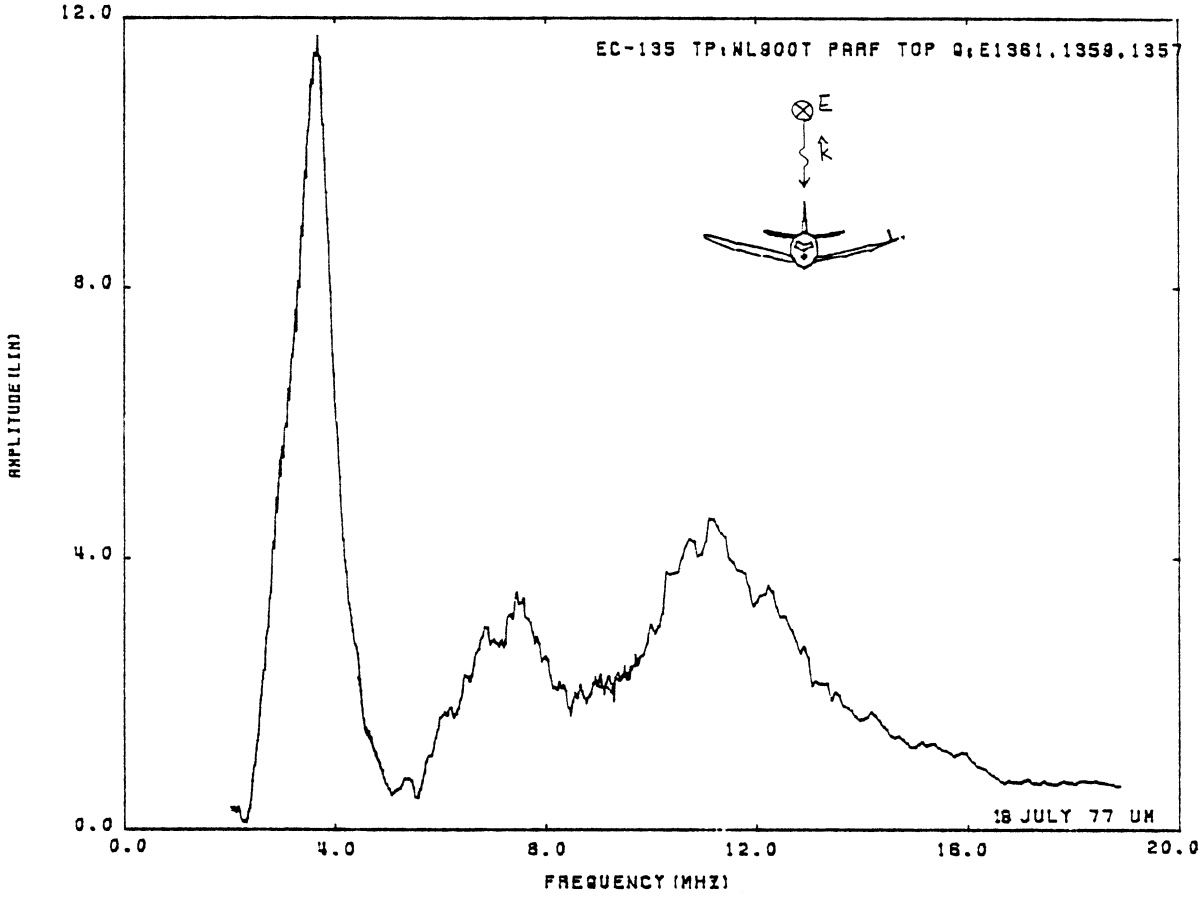

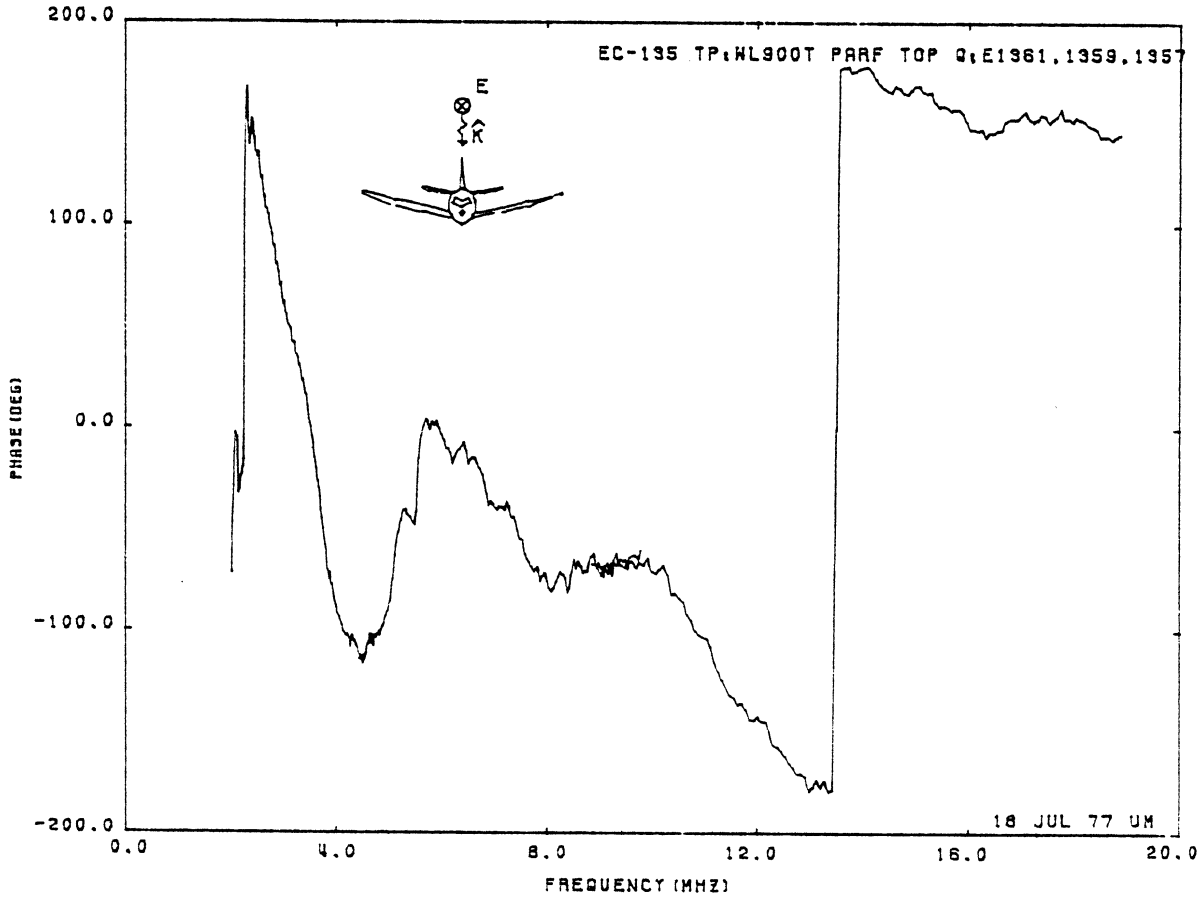

Figure 44: Charge at TP:WL900T, Orientation 1.

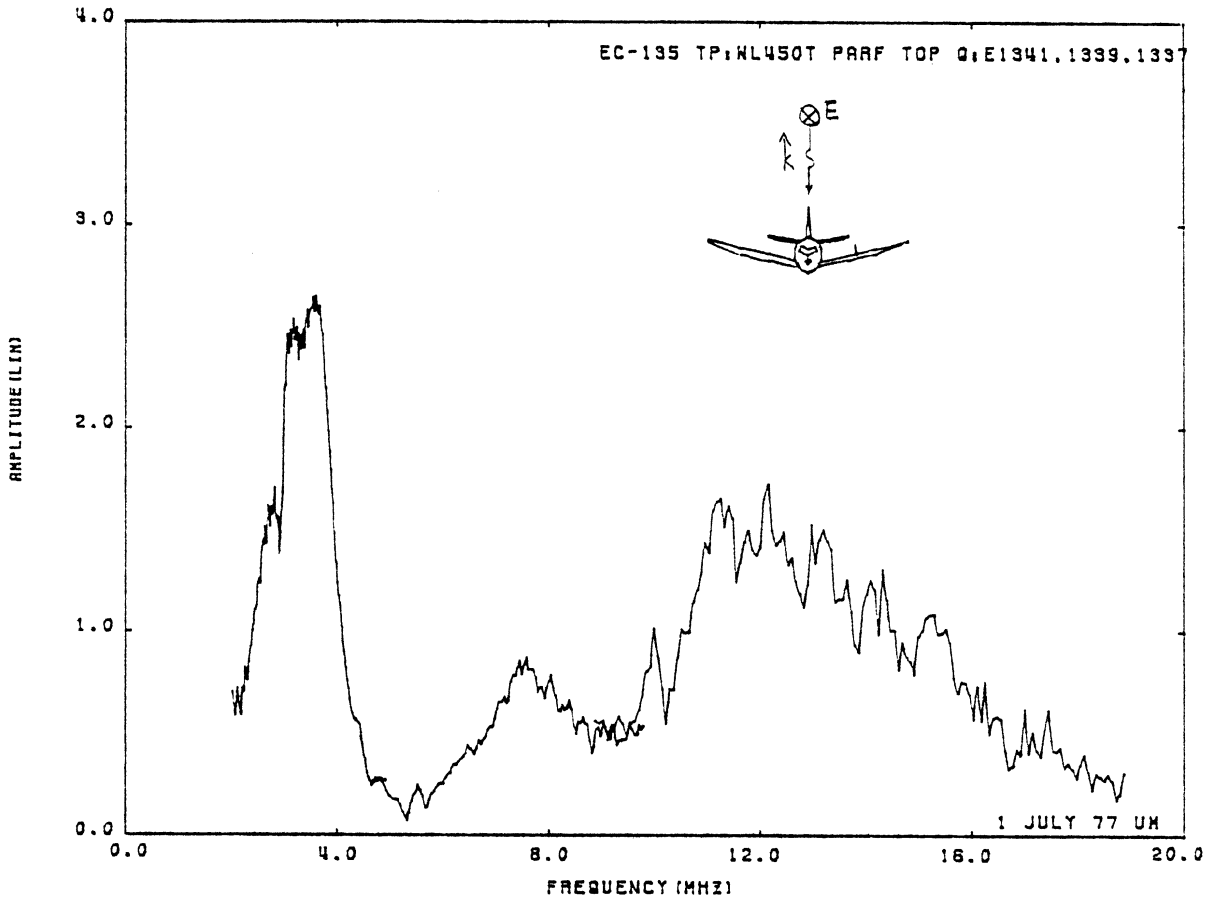

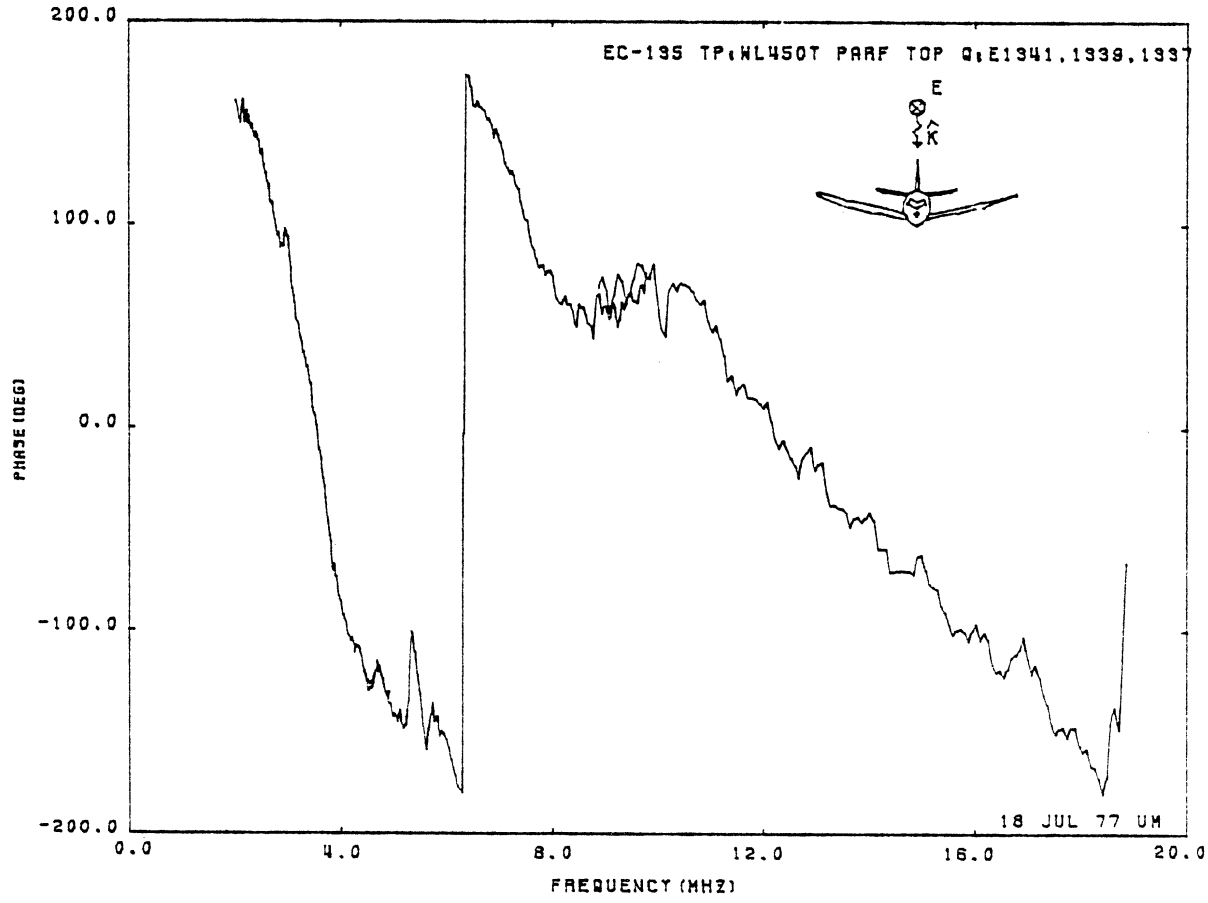

Figure 45: Charge at TP:WL450T, Orientation 1.

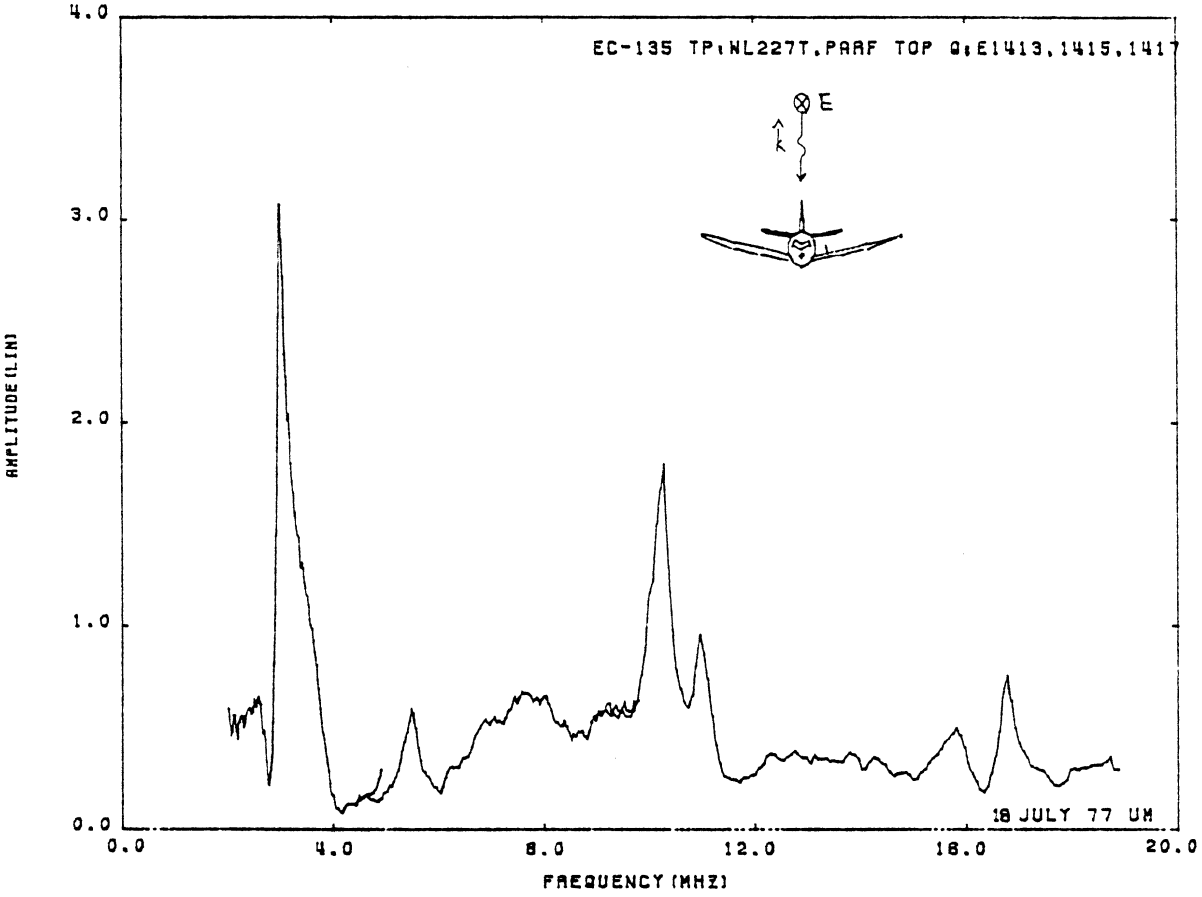

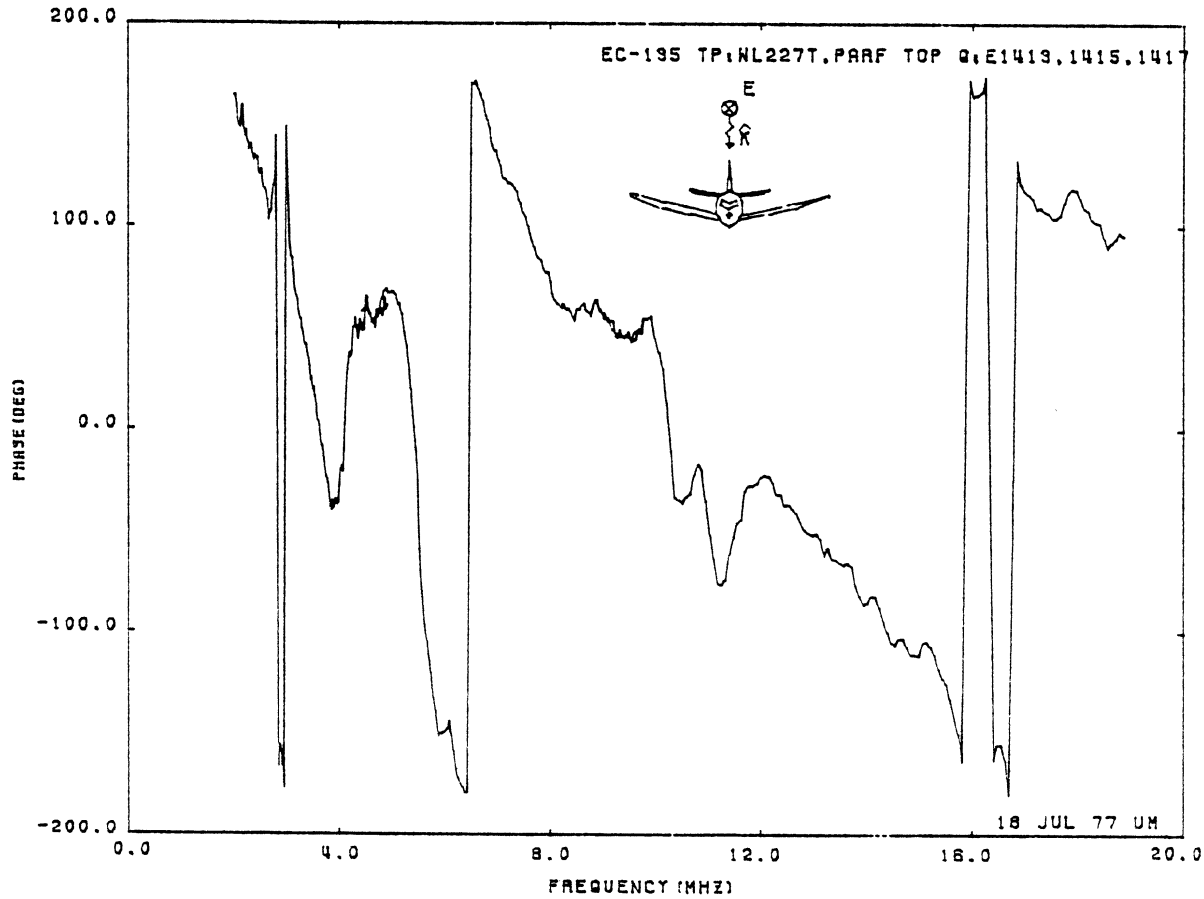

Figure 46: Charge at TP:WL227T, Orientation 1.

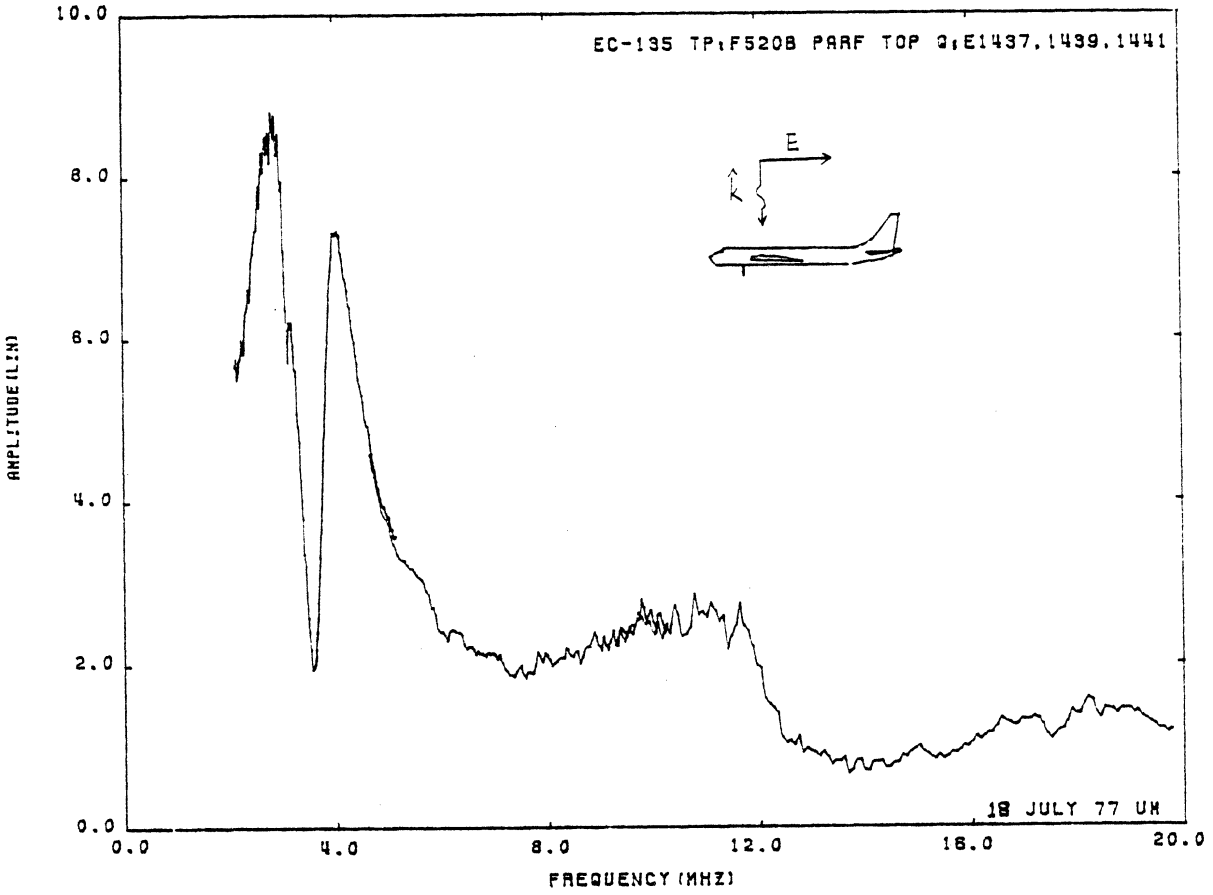

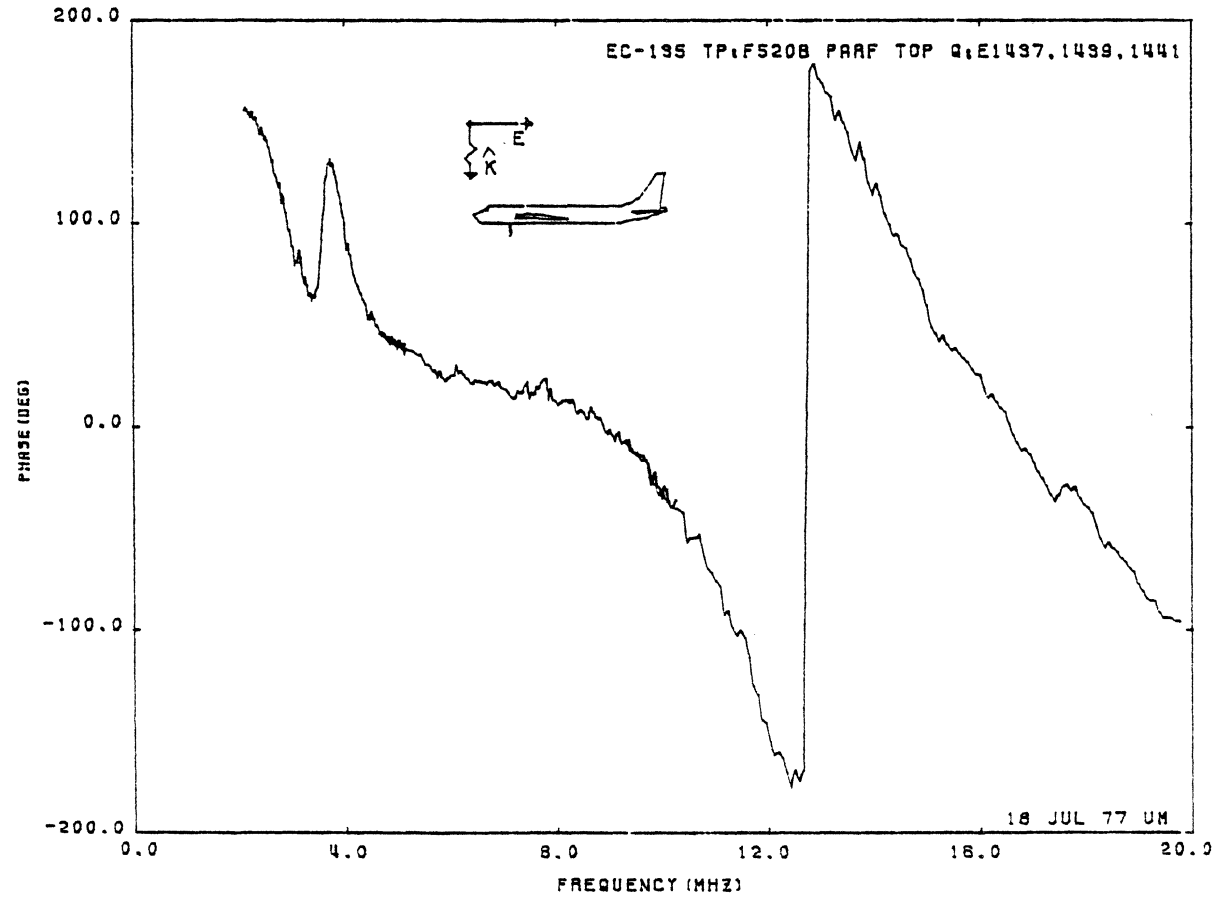

Figure 47: Charge at TP:F520B, Orientation 1.

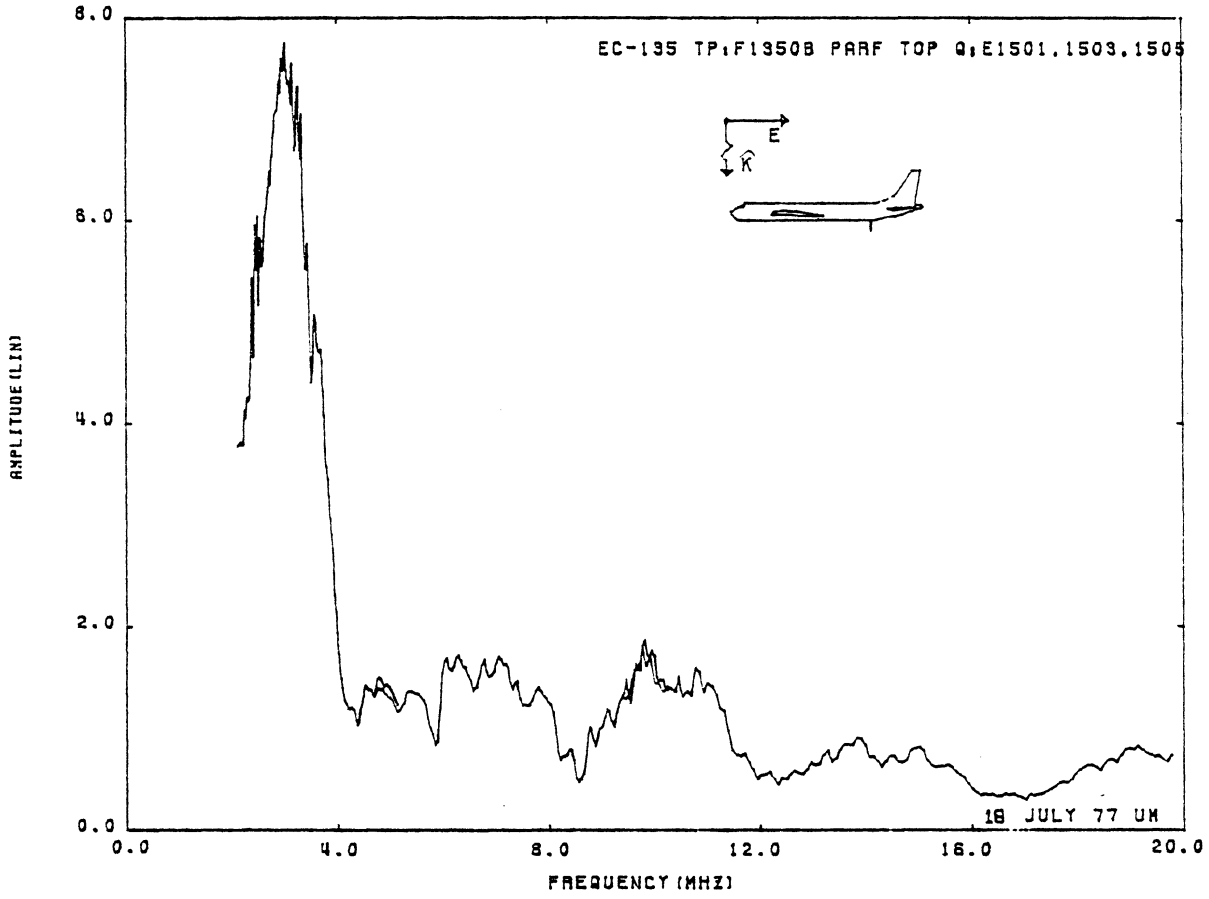

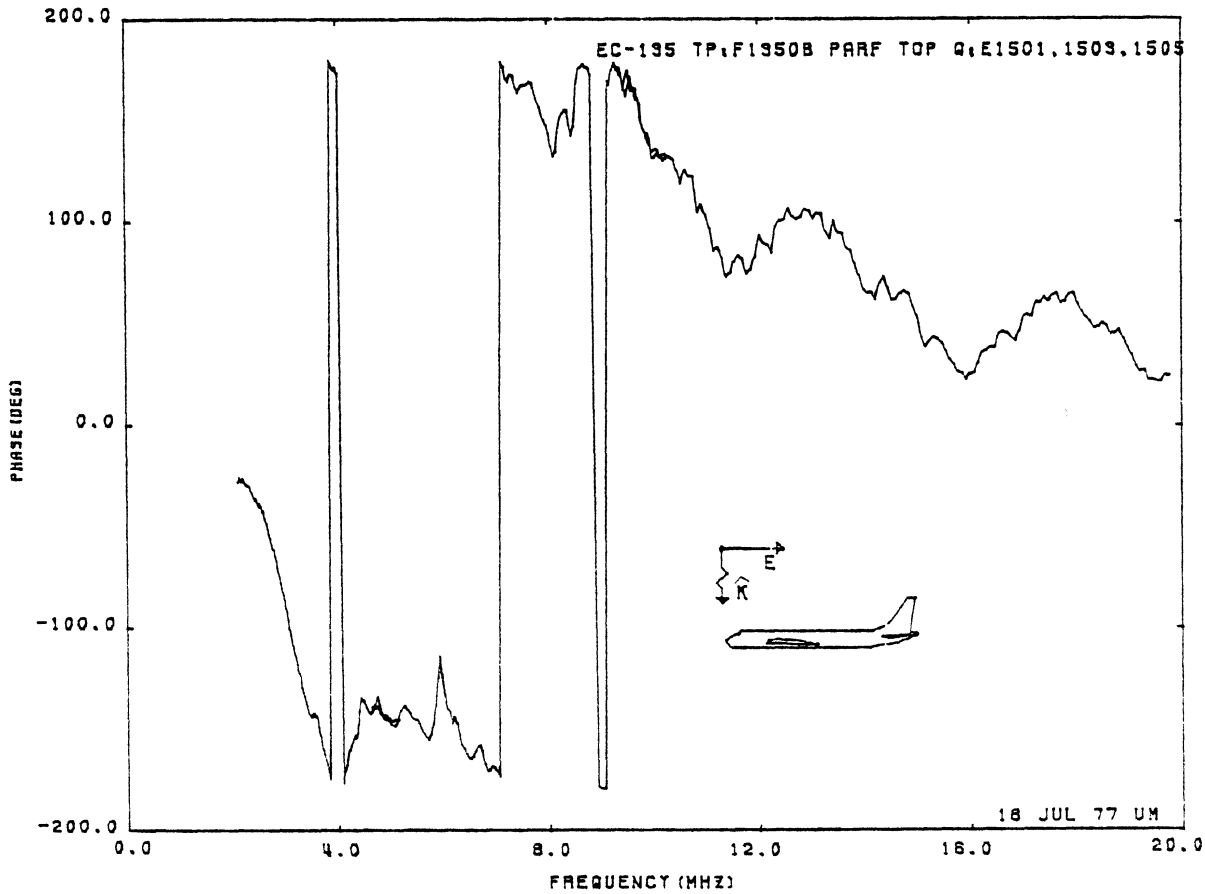

Figure 48: Charge at TP:F1350B, Orientation 1.

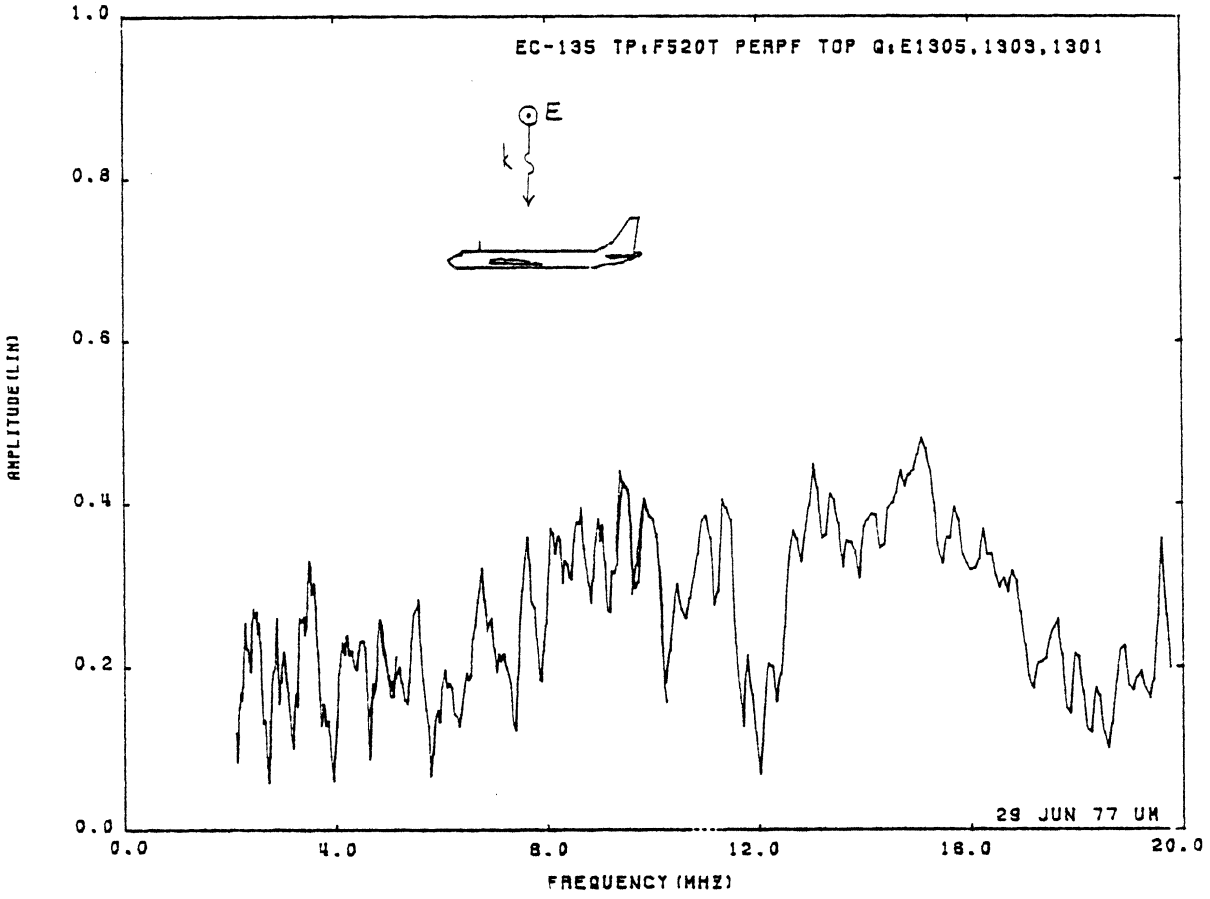

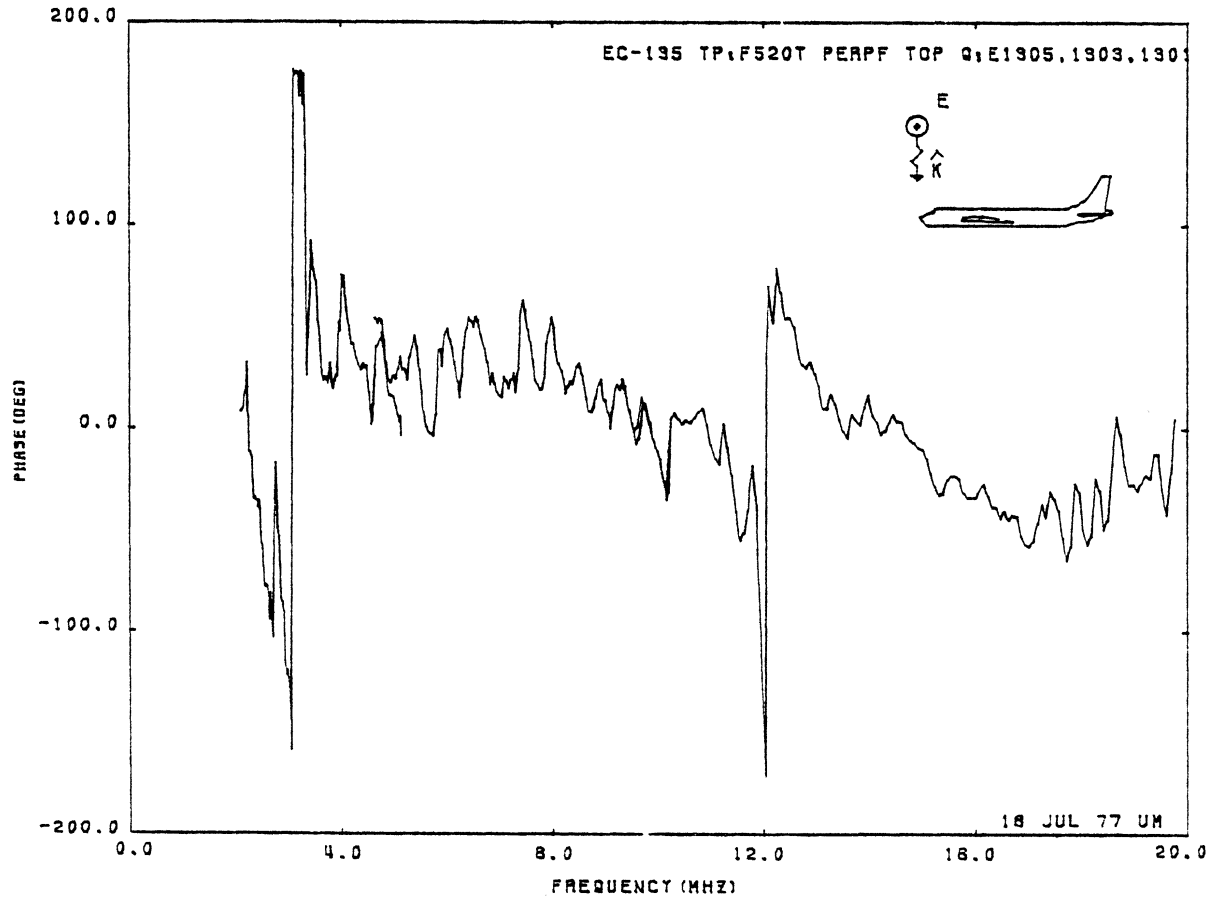

Figure 49: Charge at TP :F520T, Orientation 2.

 (see *, page 15)

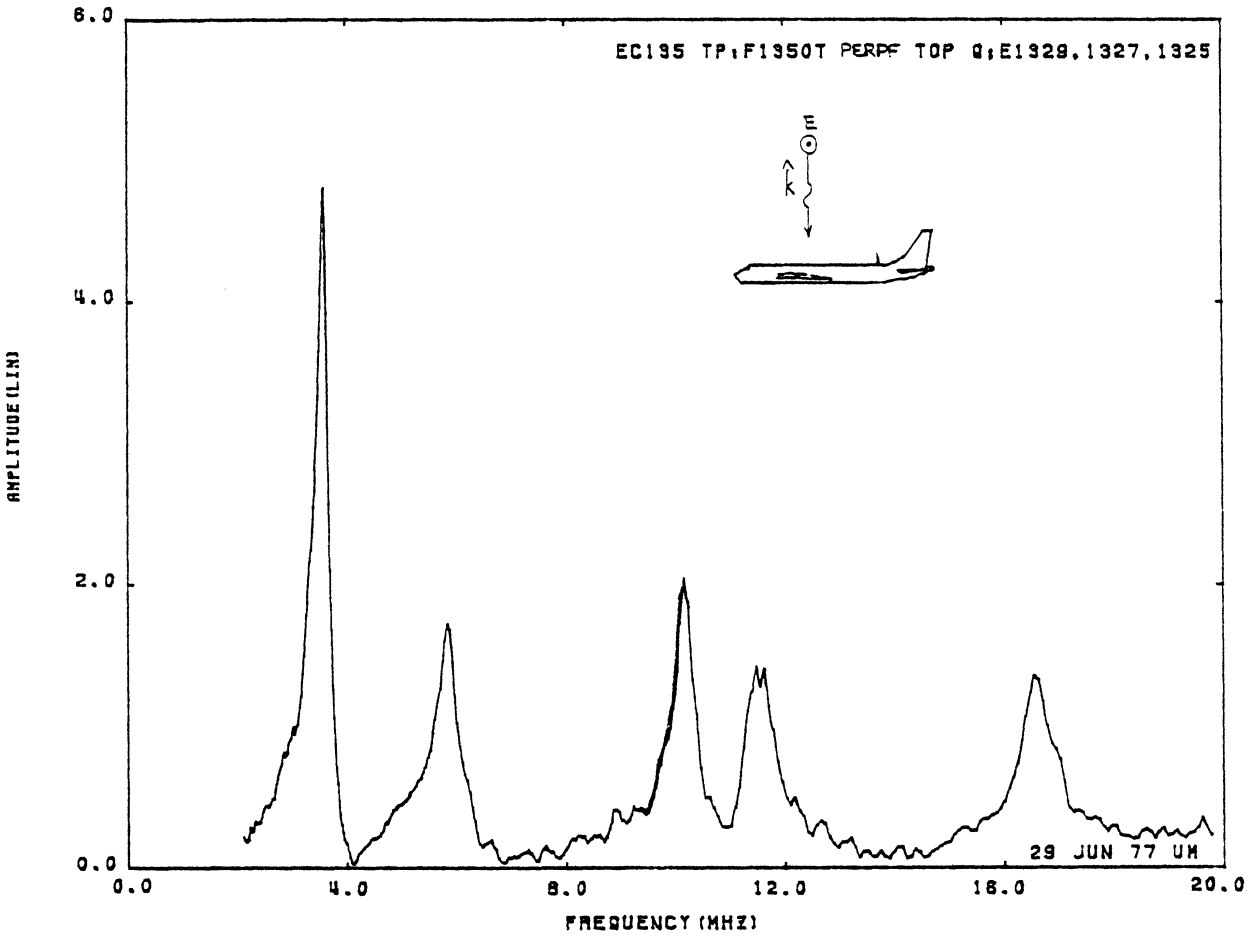

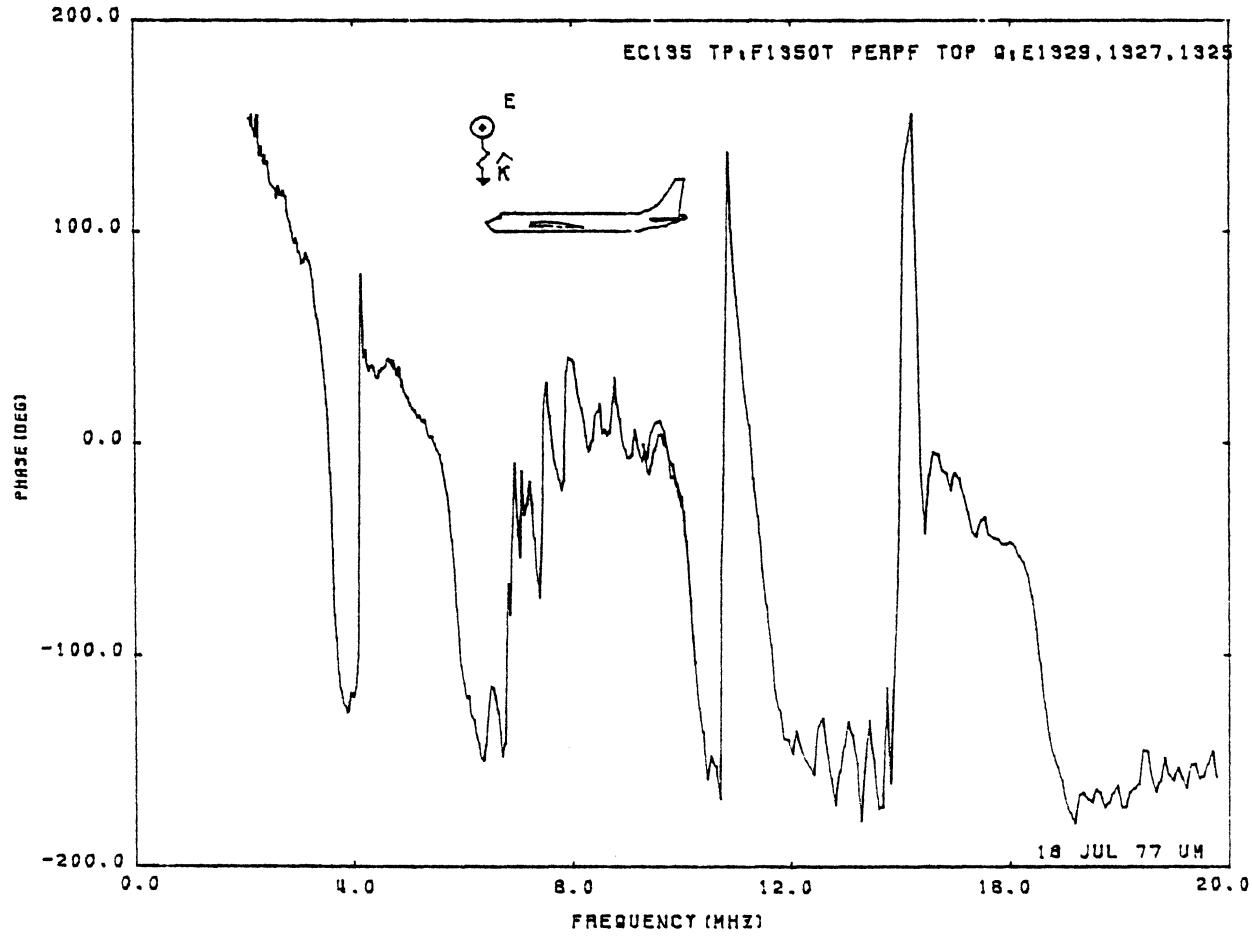

Figure 50: Charge at TP:F1350T, Orientation 2.

(see *, page 15)

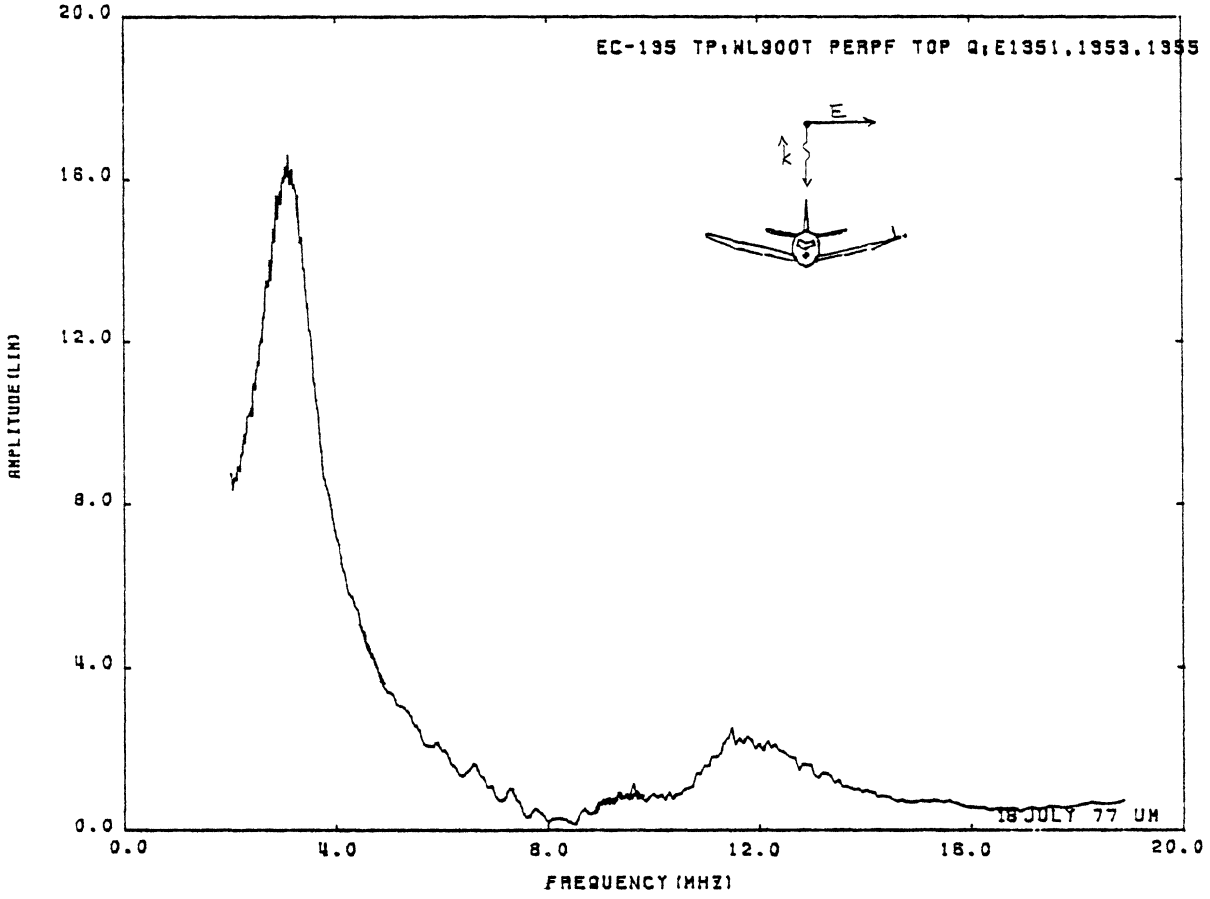

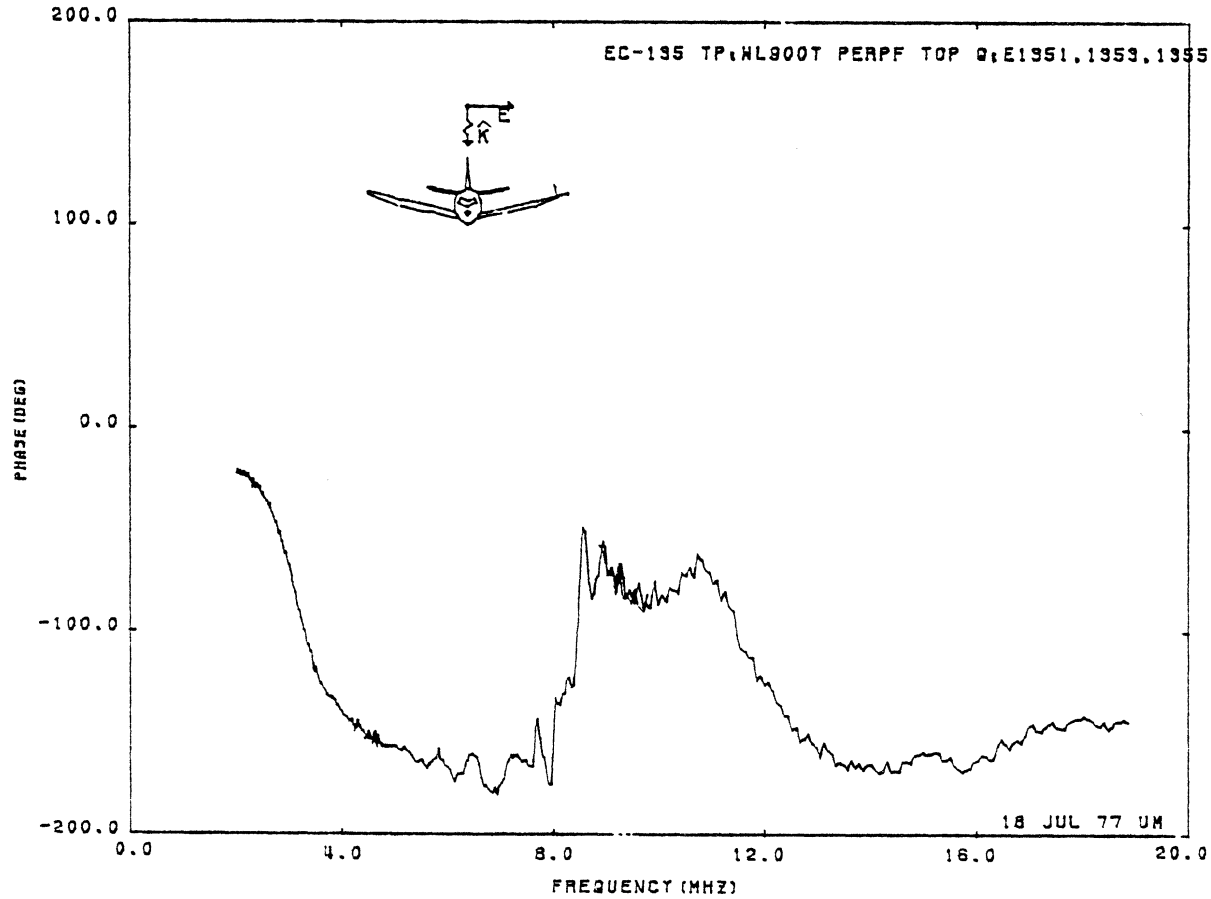

Figure 51: Charge at TP:WL900T, Orientation 2.

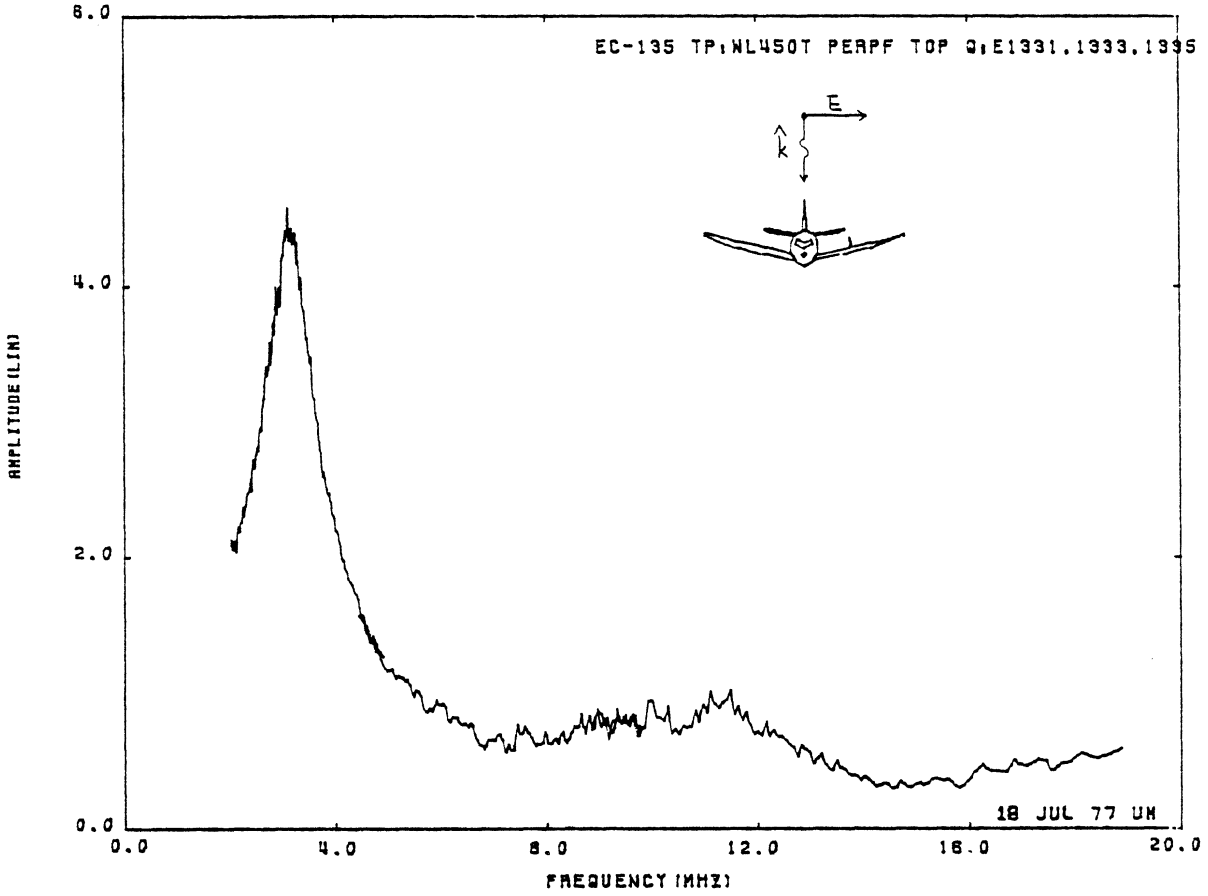

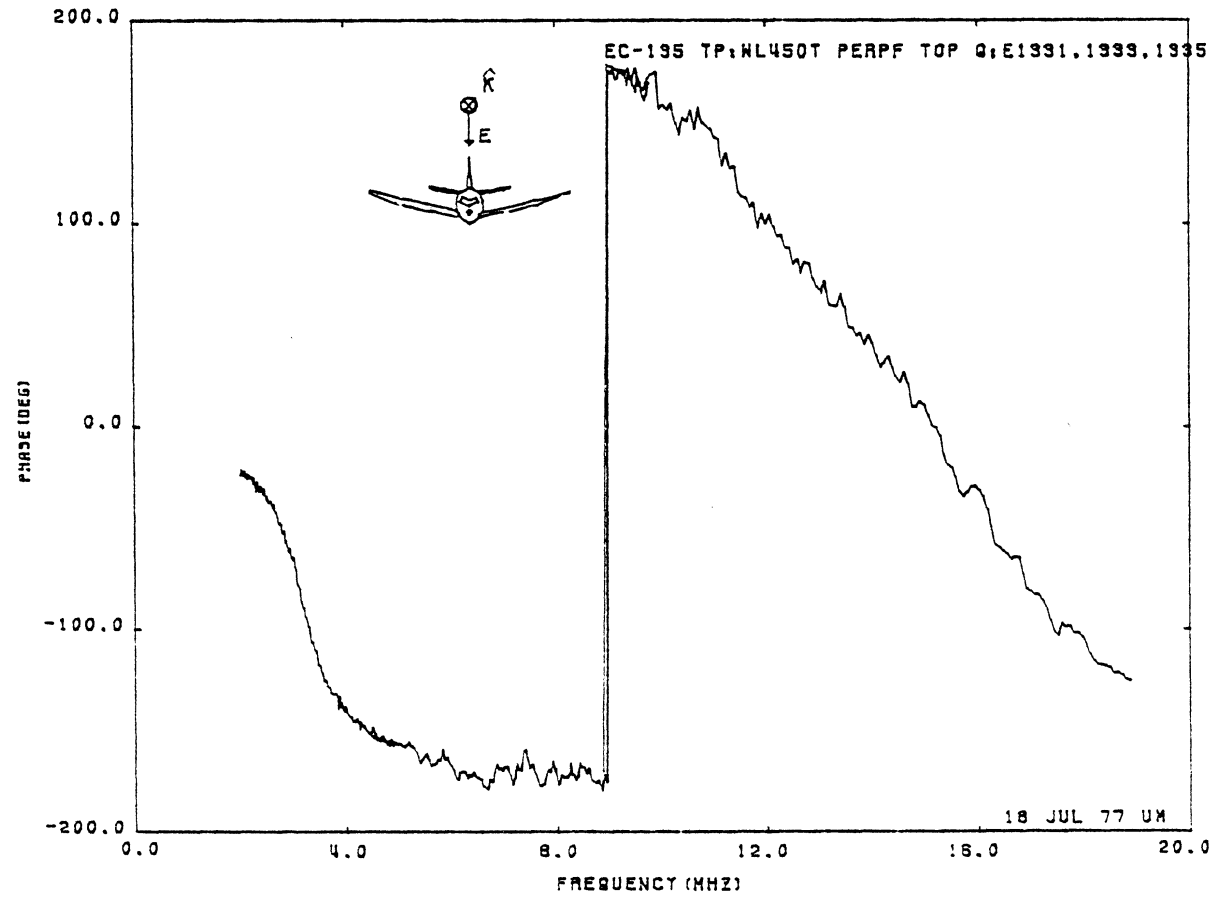

Figure 52: Charge at TP:WL450T, Orientation 2.

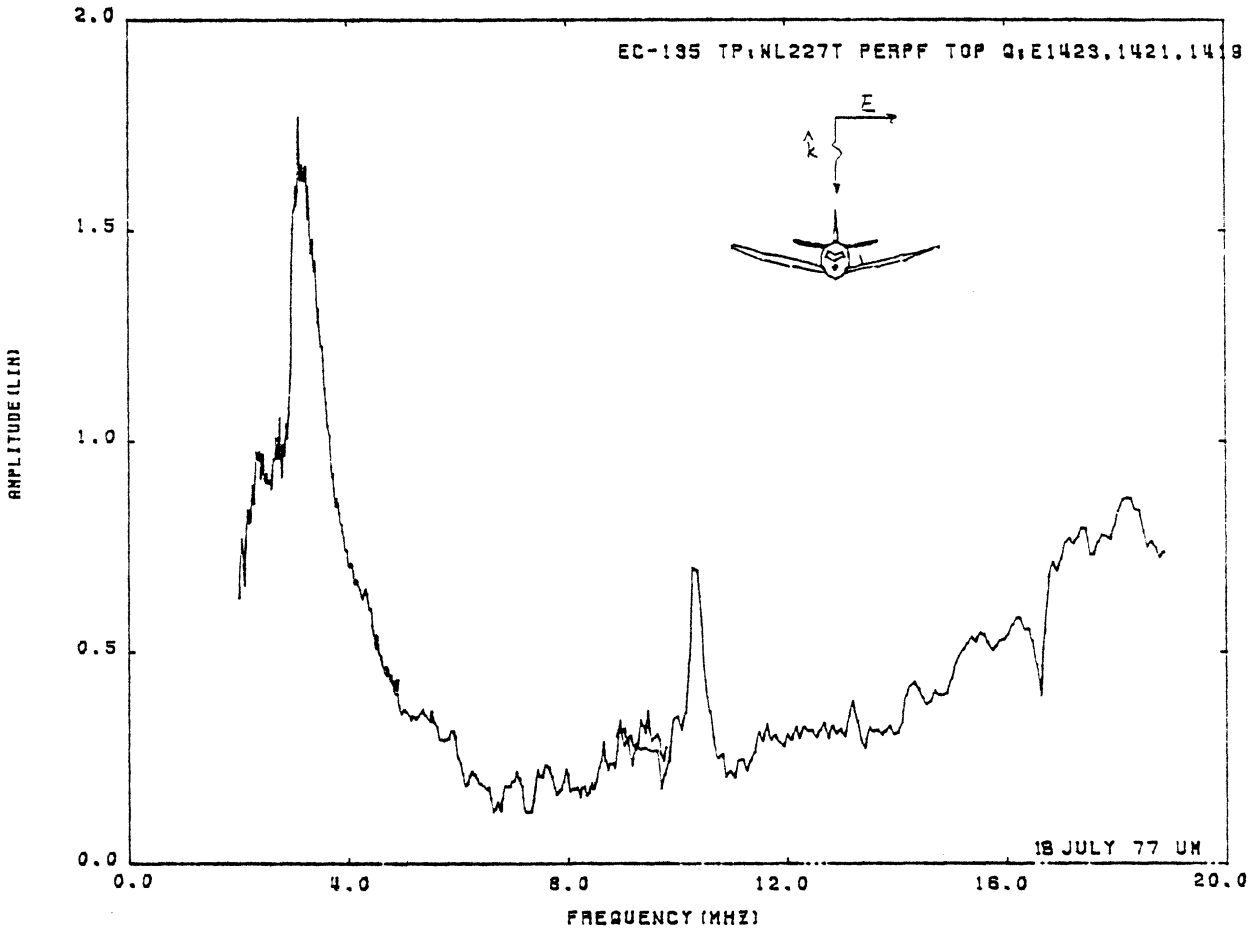

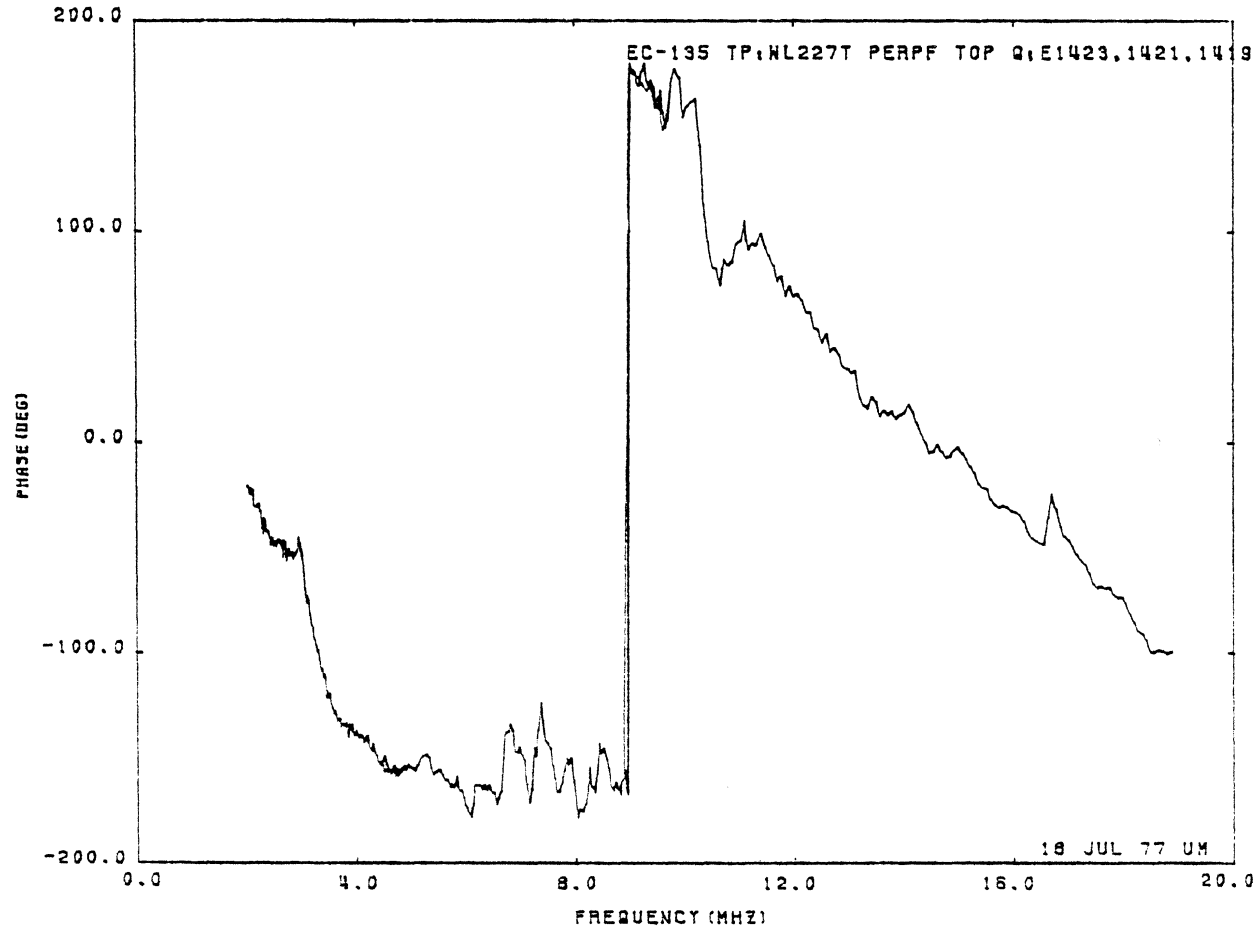

Figure 53: Charge at TP:WL227T, Orientation 2.

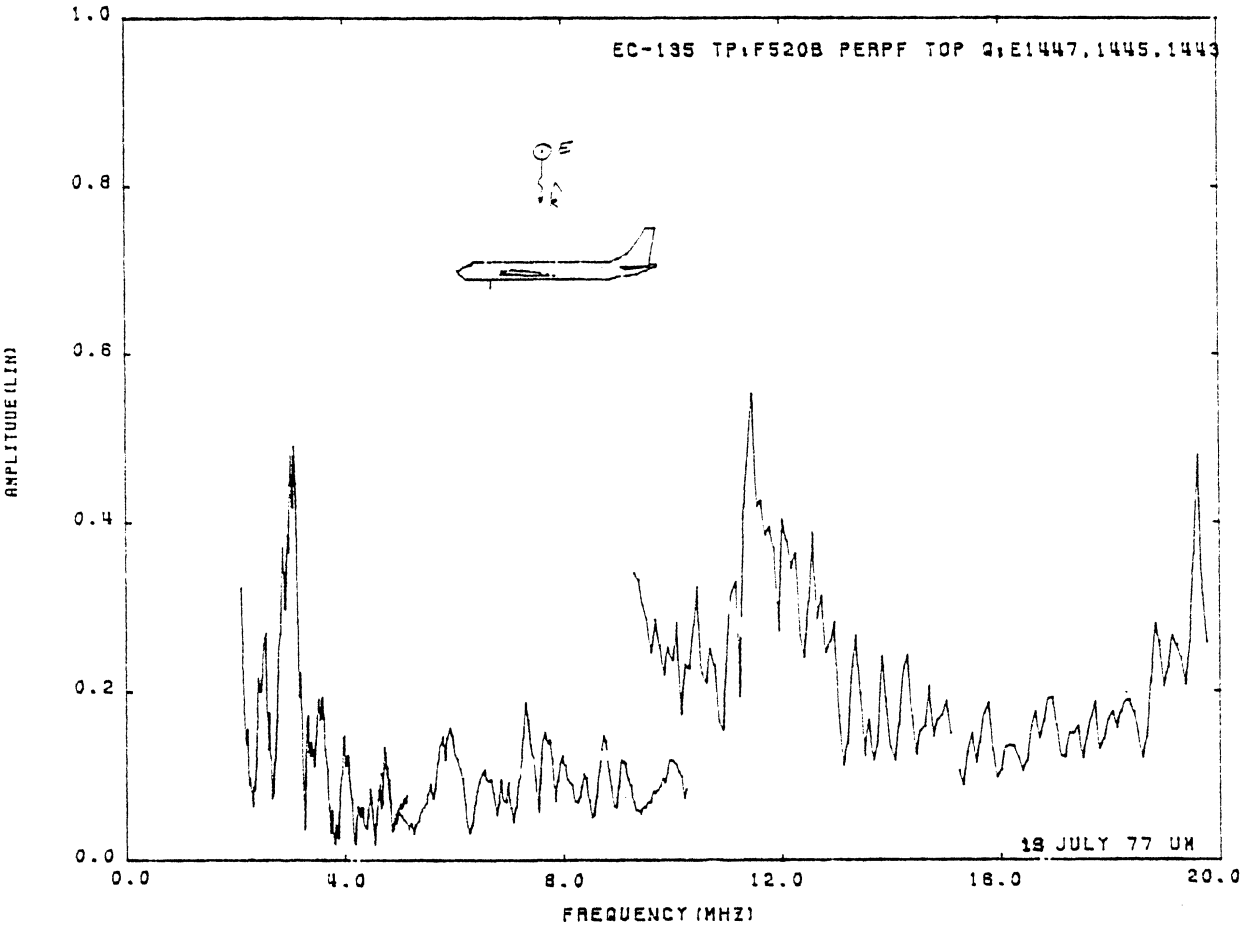

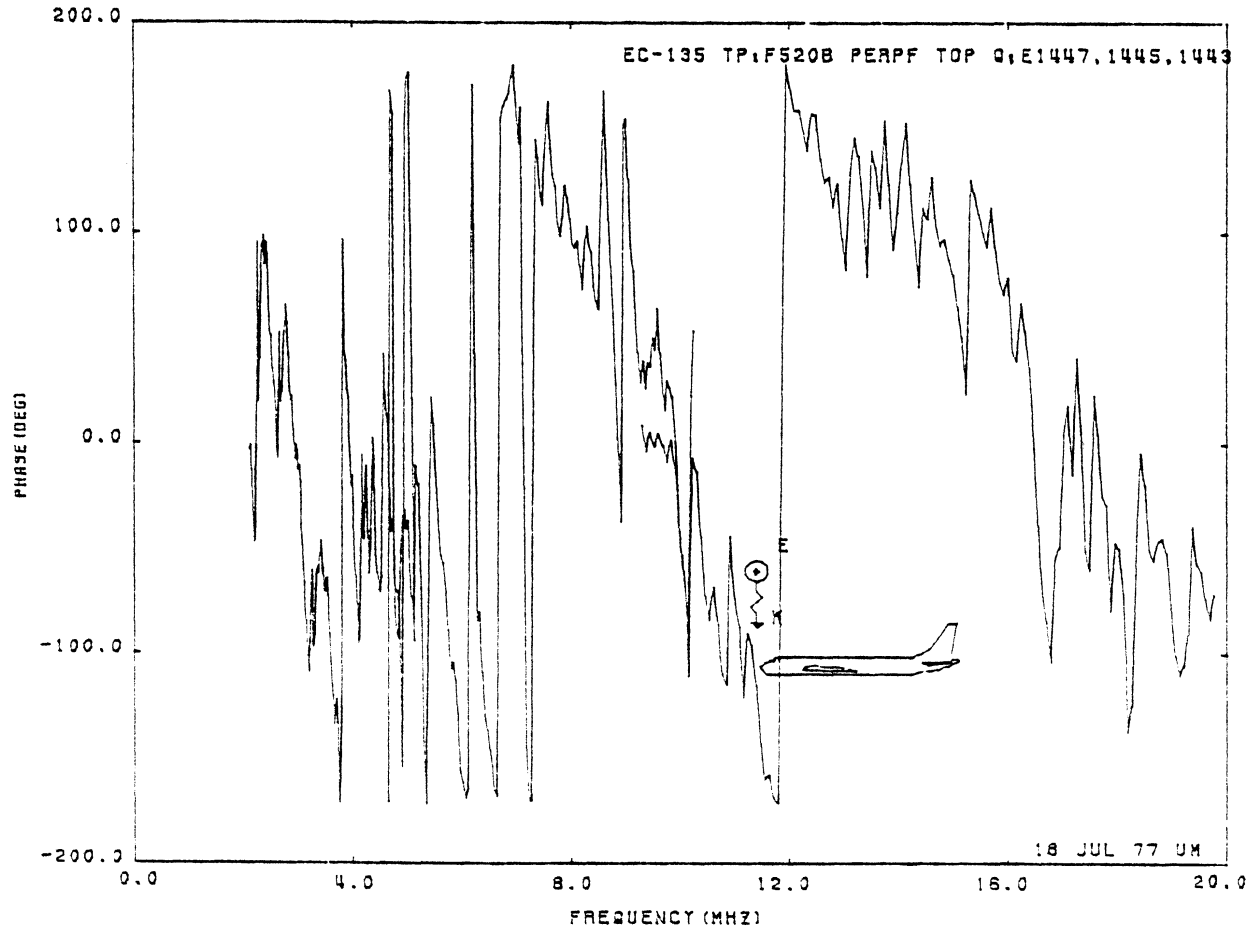

Figure 54: Charge at TP:F520B, Orientation 2.

(see *, page 15)

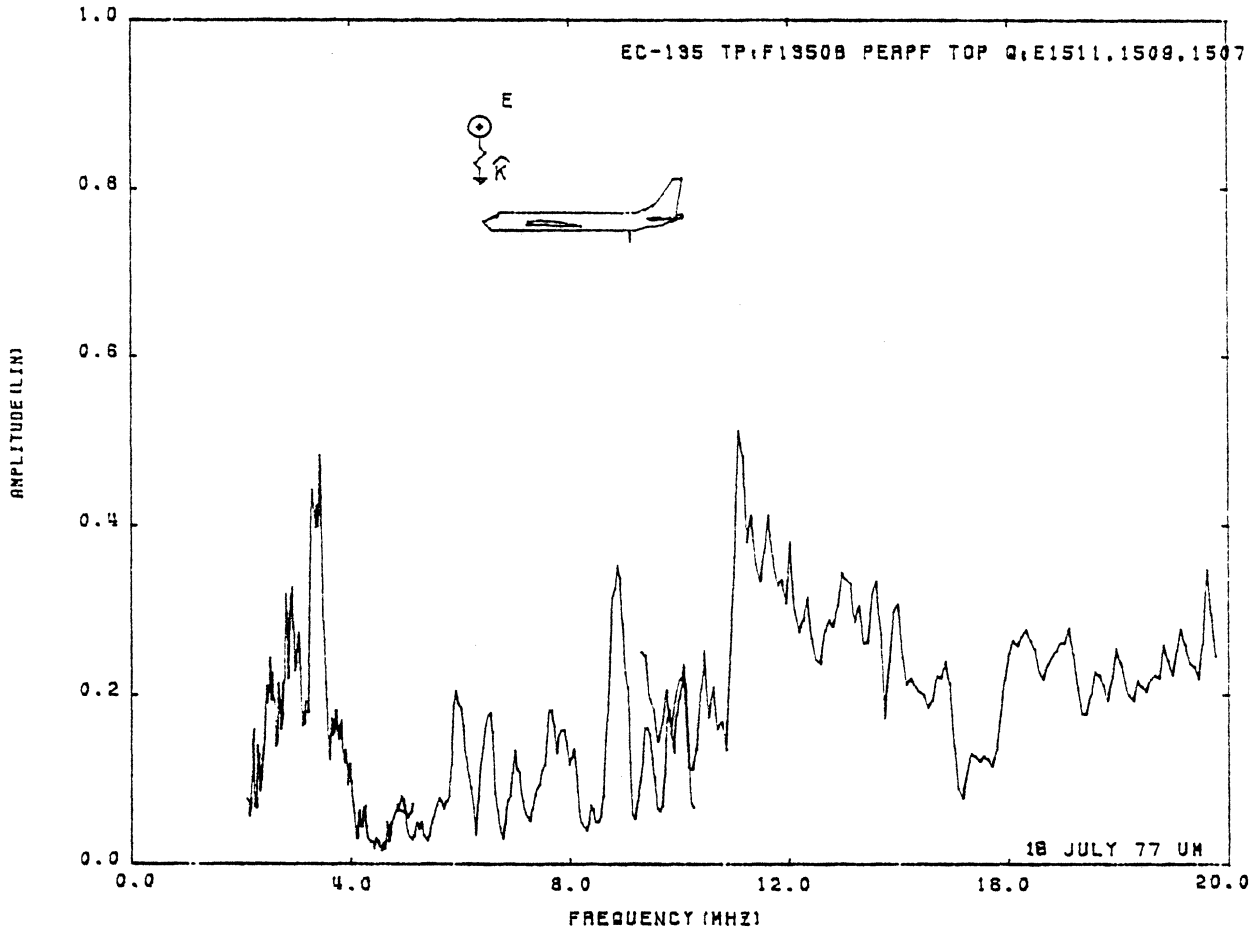

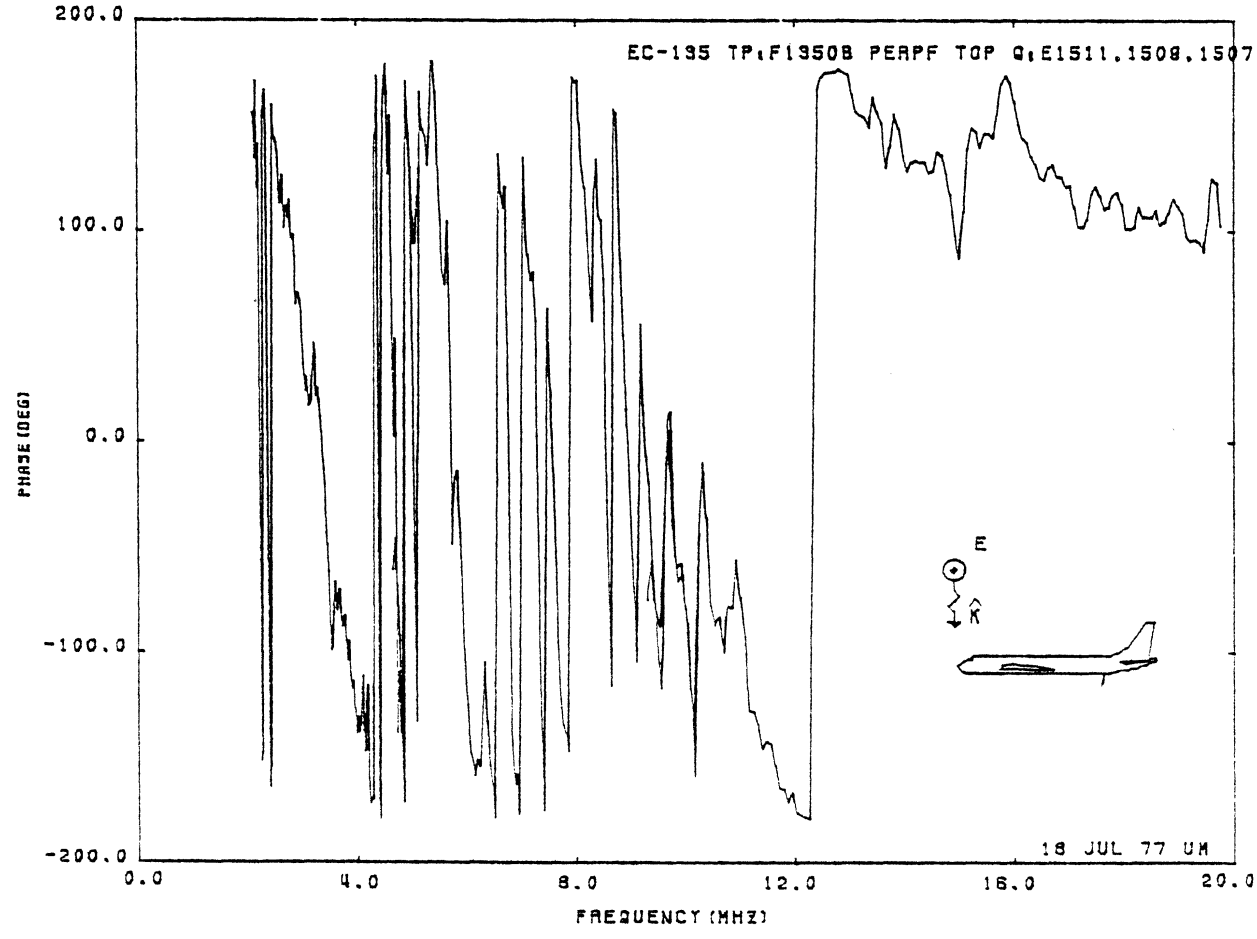

Figure 55: Charge at TP:F1350B, Orientation 2.

(see *, page 15)

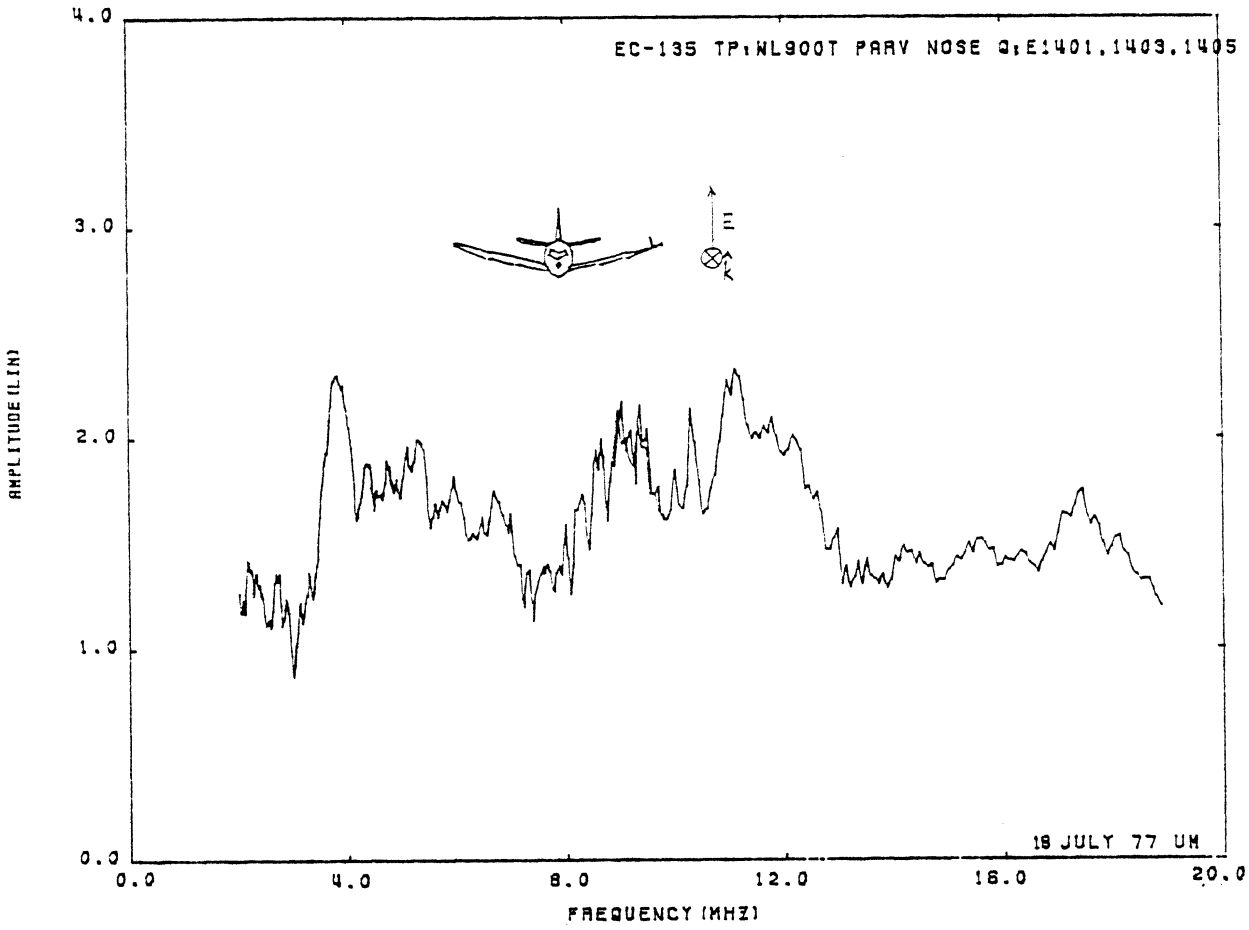

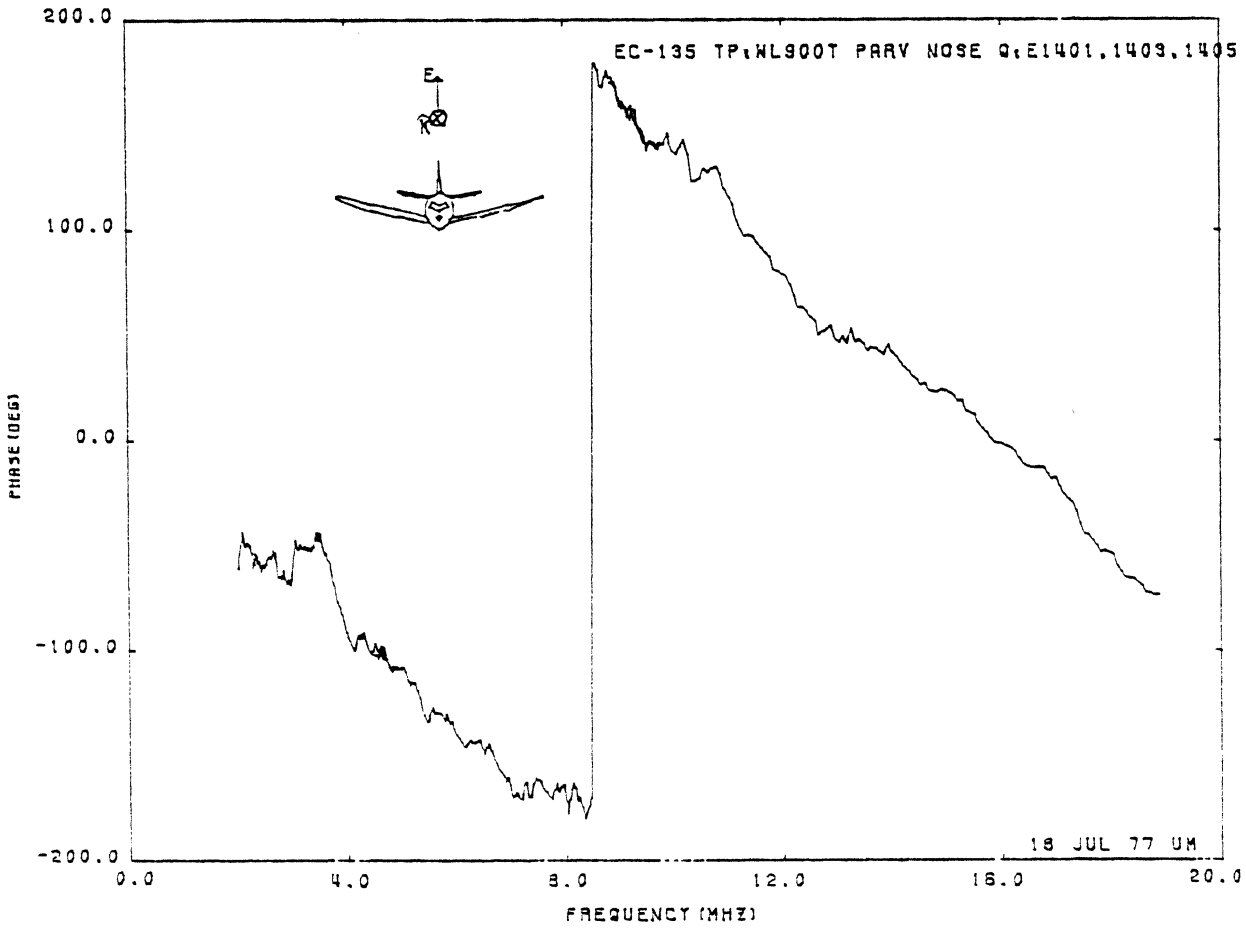

Figure 56: Charge at TP:WL900T, Orientation 3.

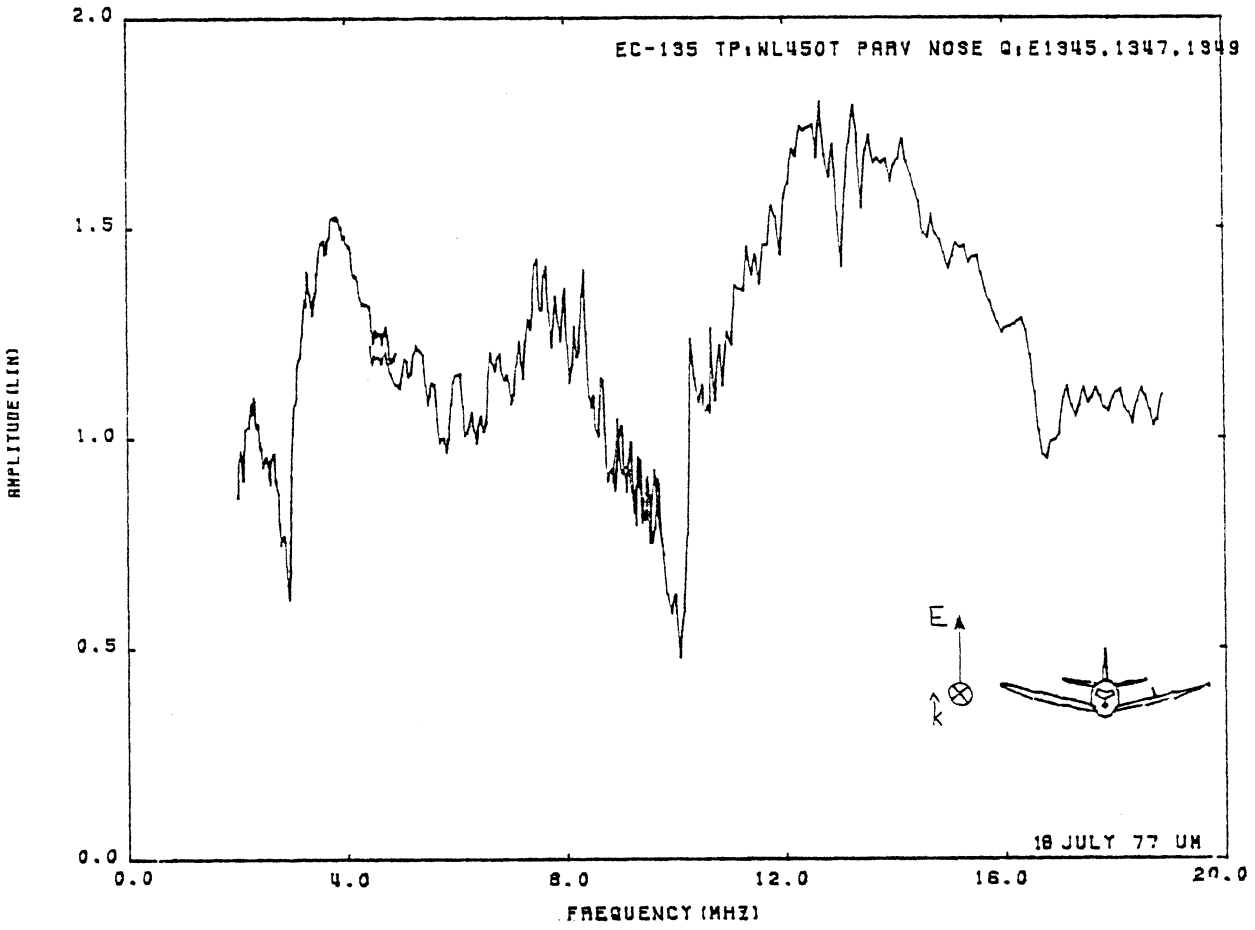

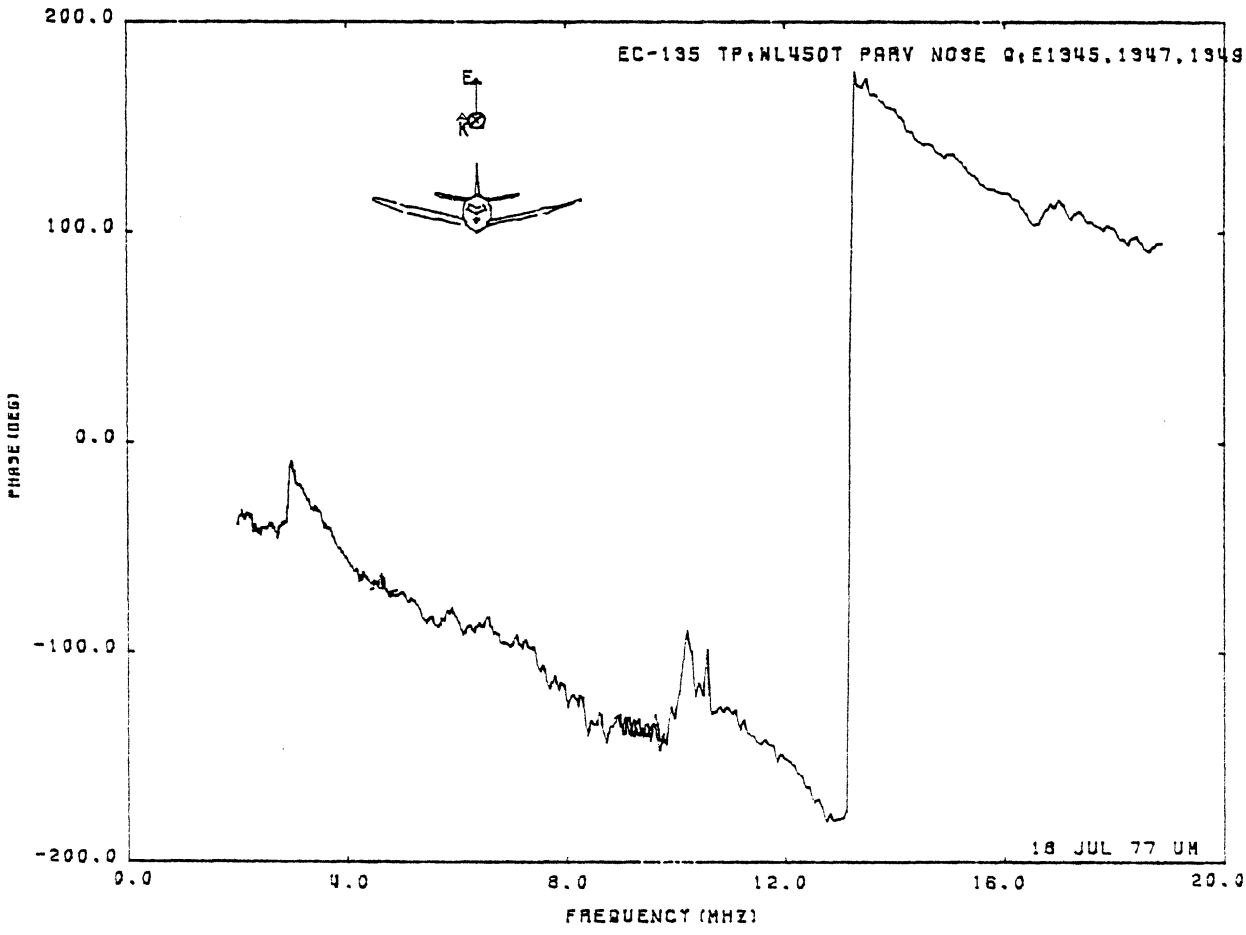

Figure 57: Charge at TP:WL450T, Orientation 3.

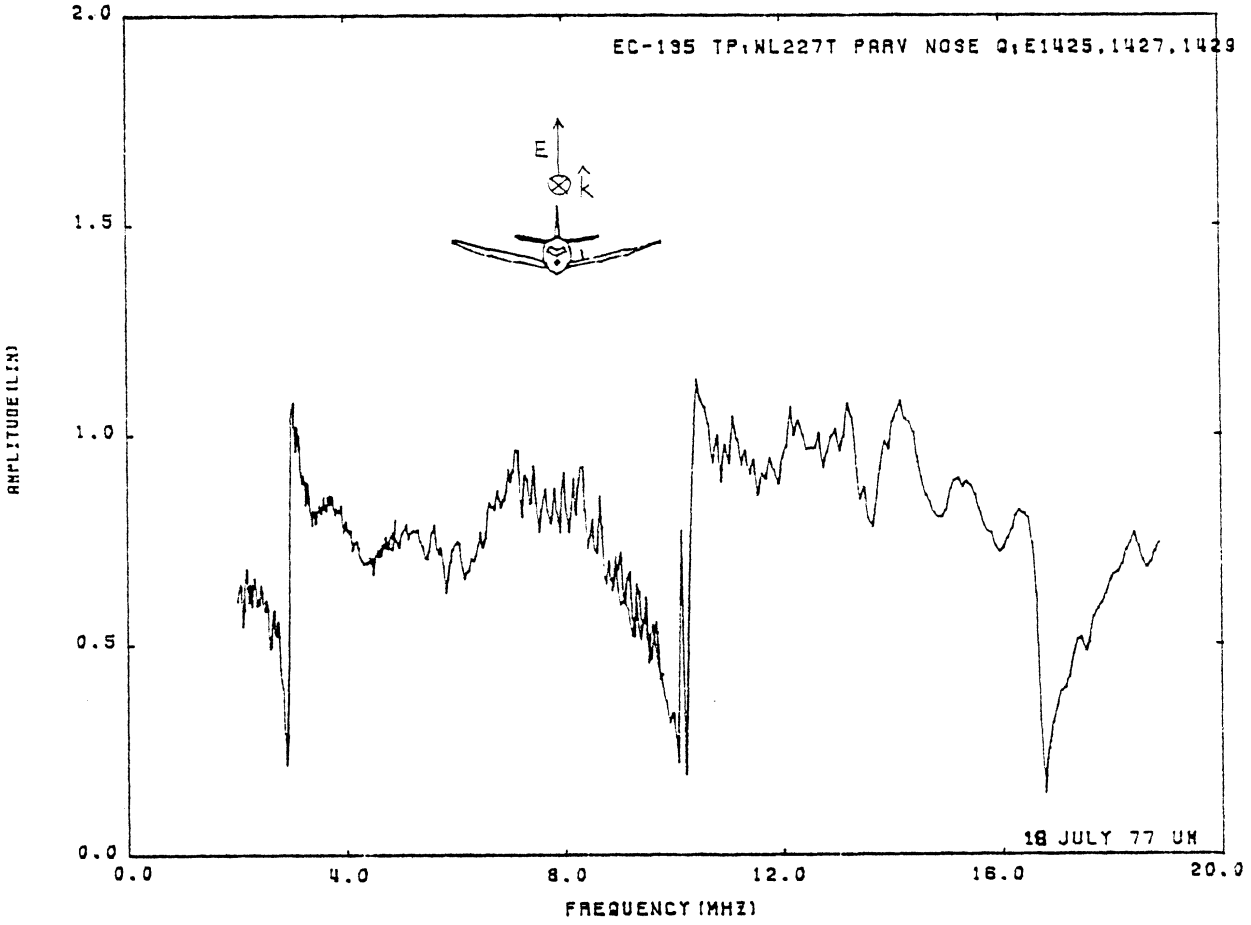

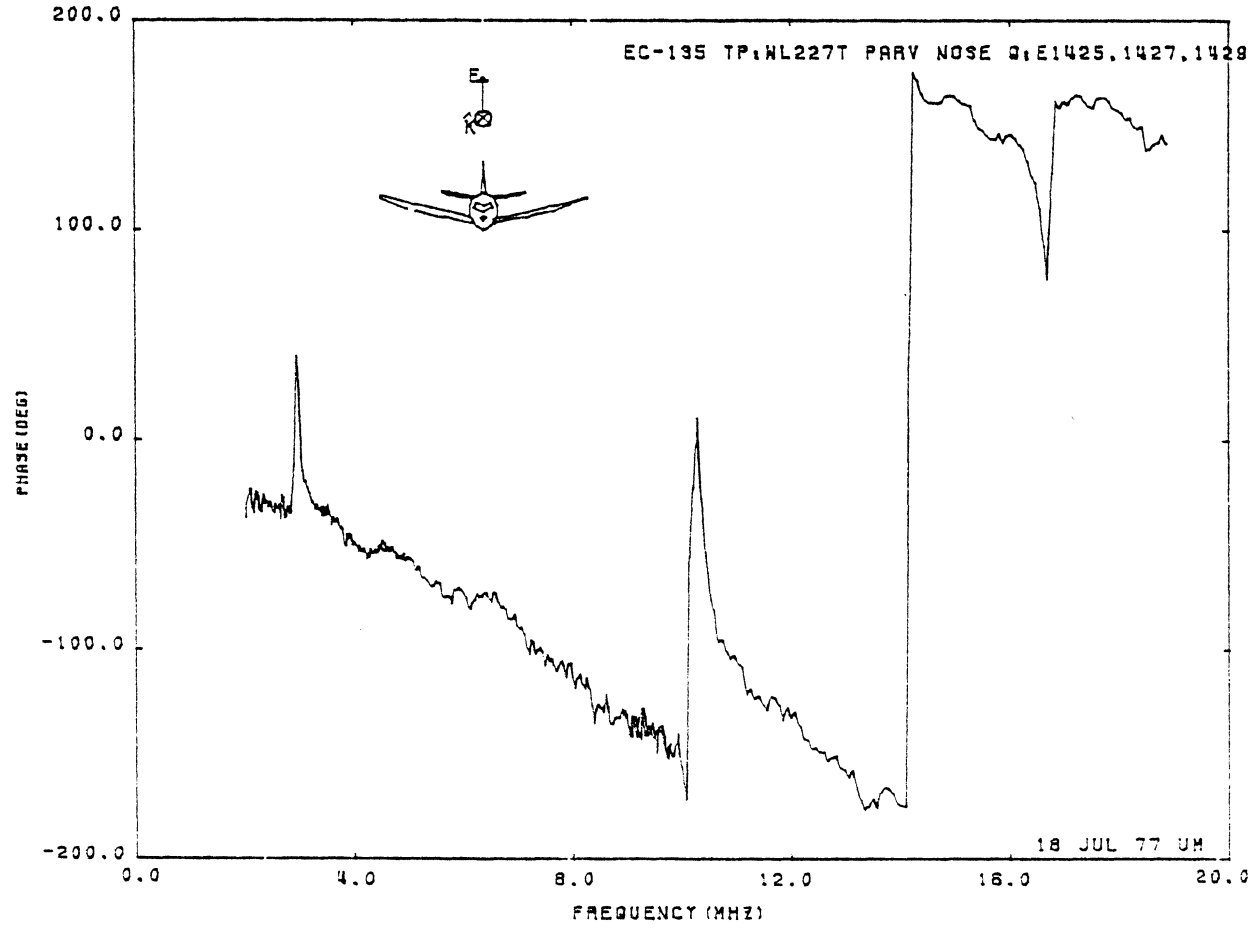

Figure 58: Charge at TP:WL227T, Orientation 3.

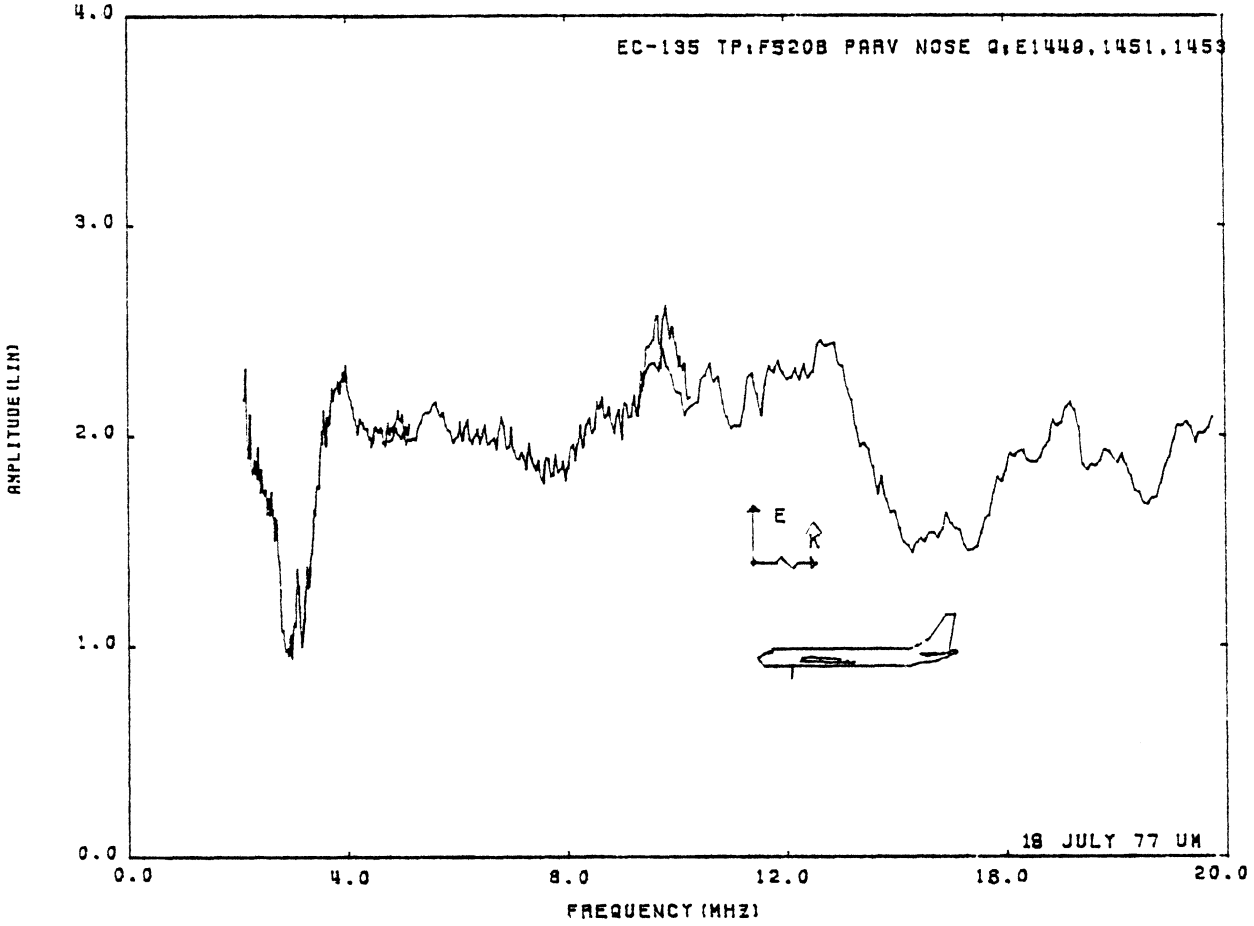

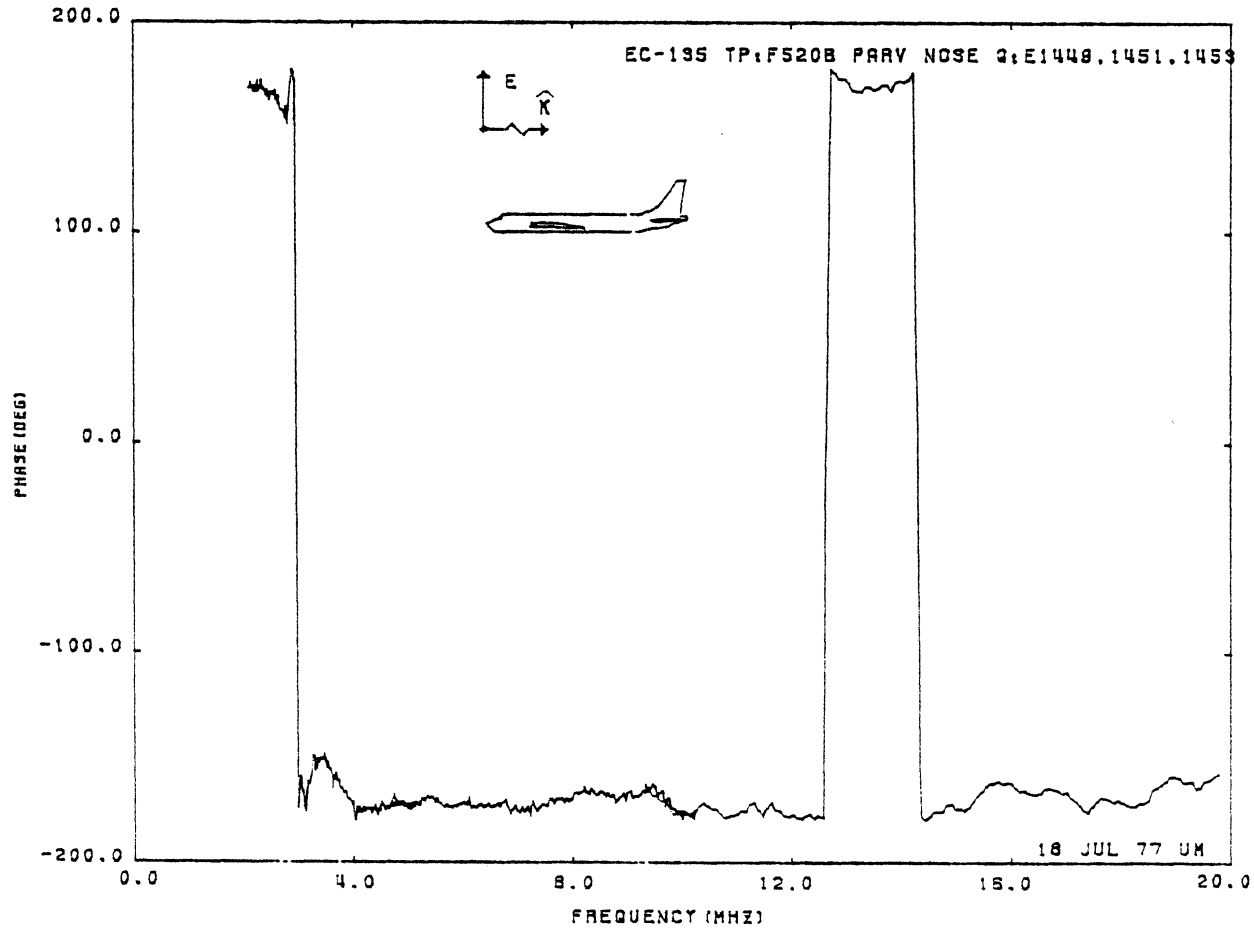

Figure 59: Charge at TP:F520B, Orientation 3.

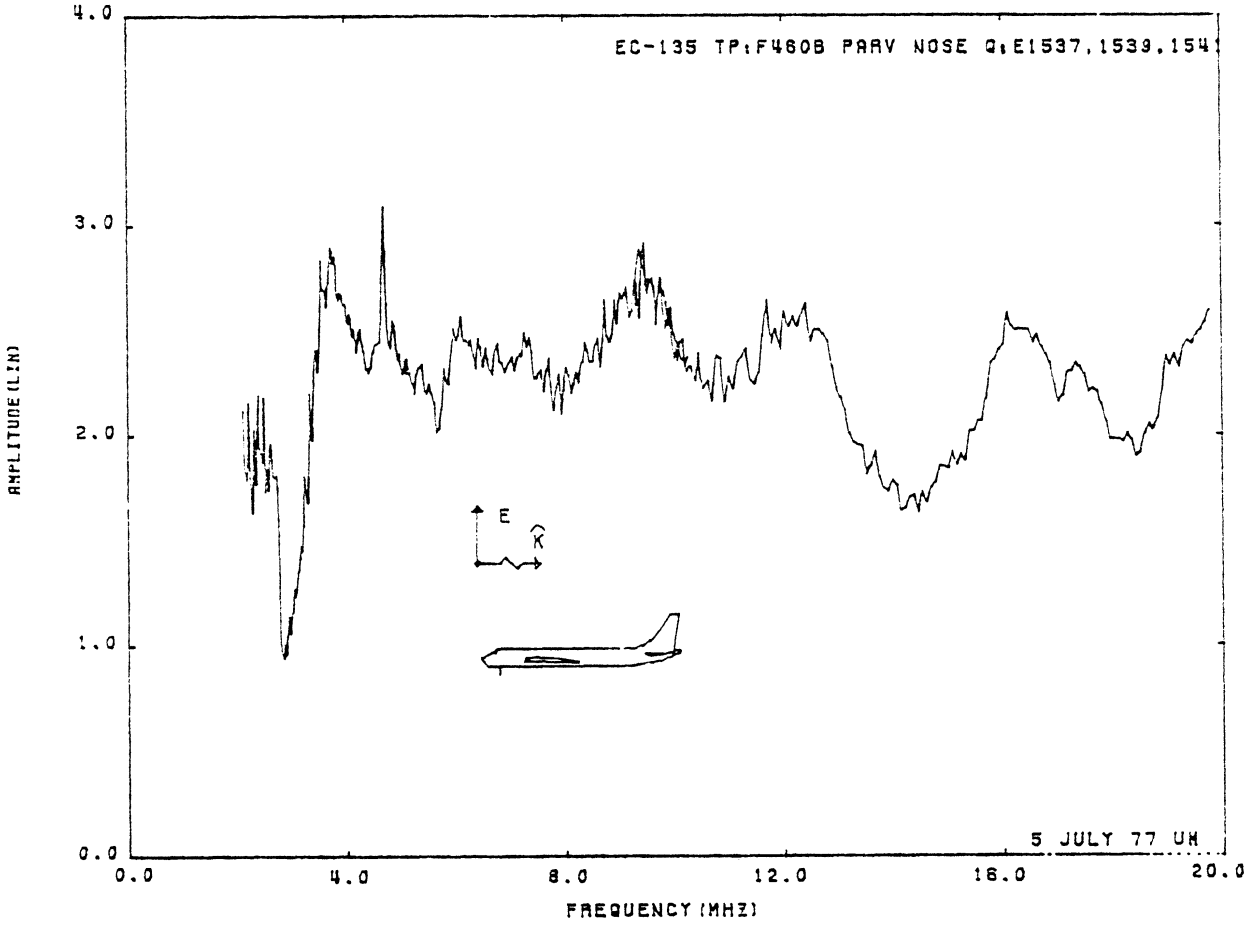

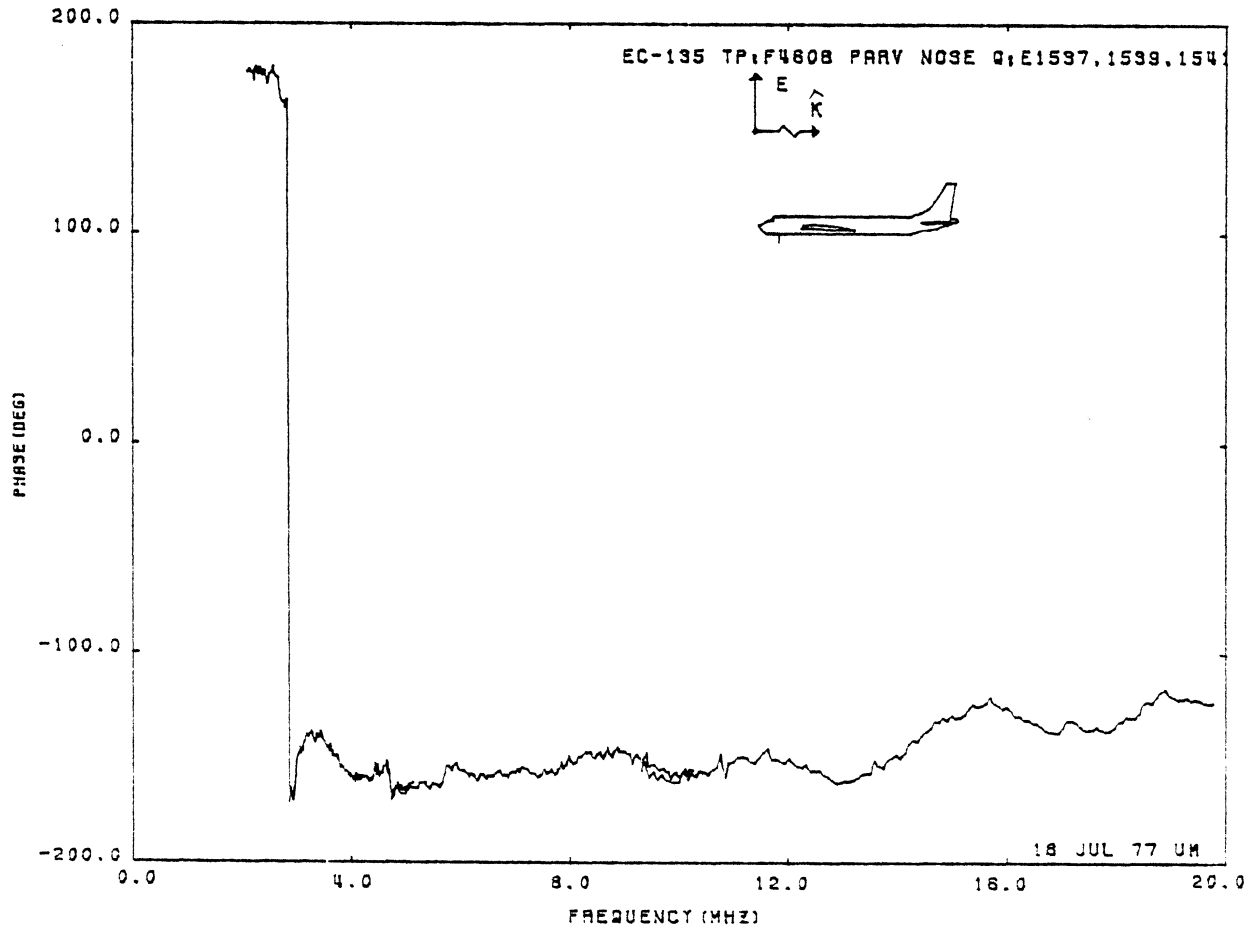

Figure 60: Charge at TP:F460B, Orientation 3.

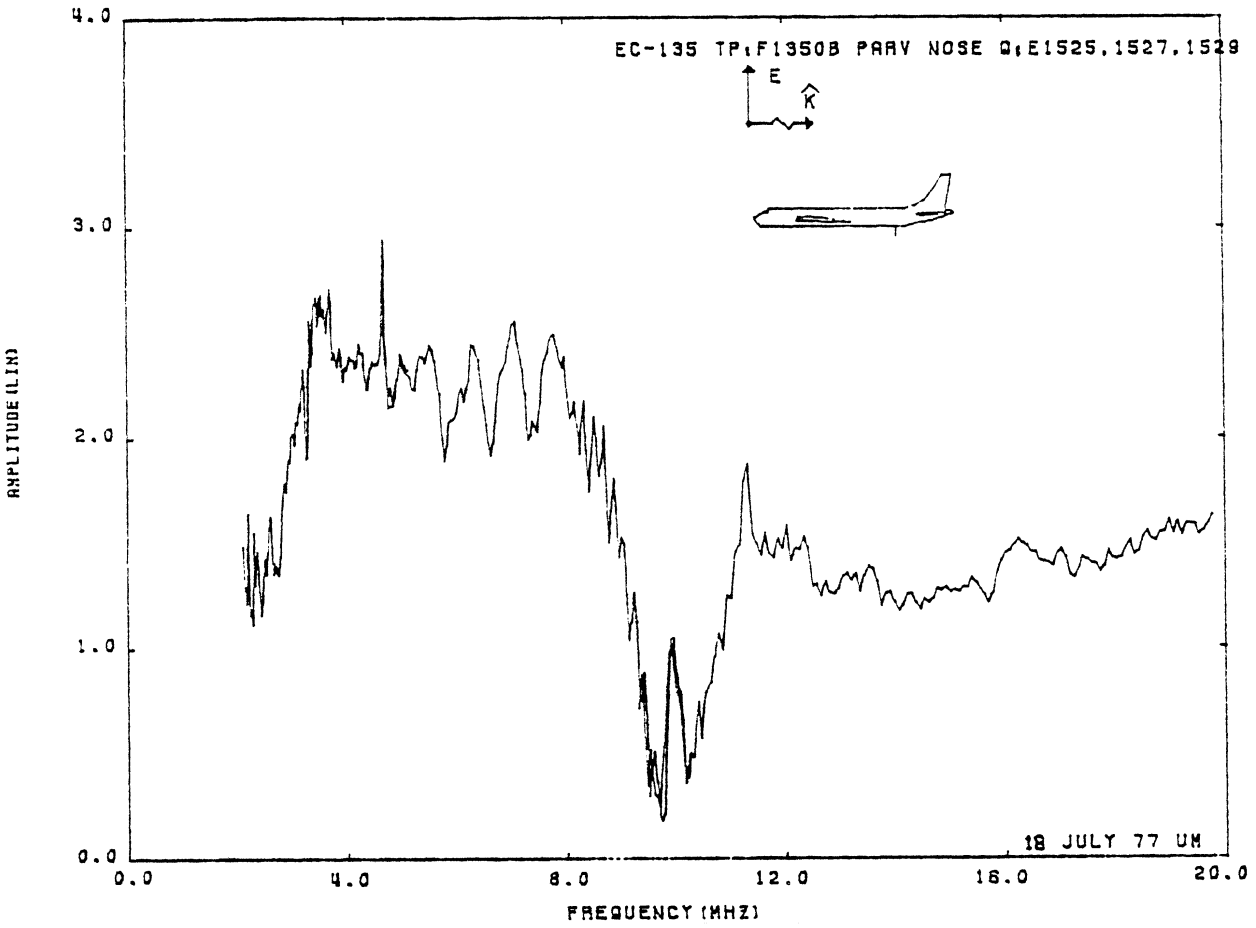

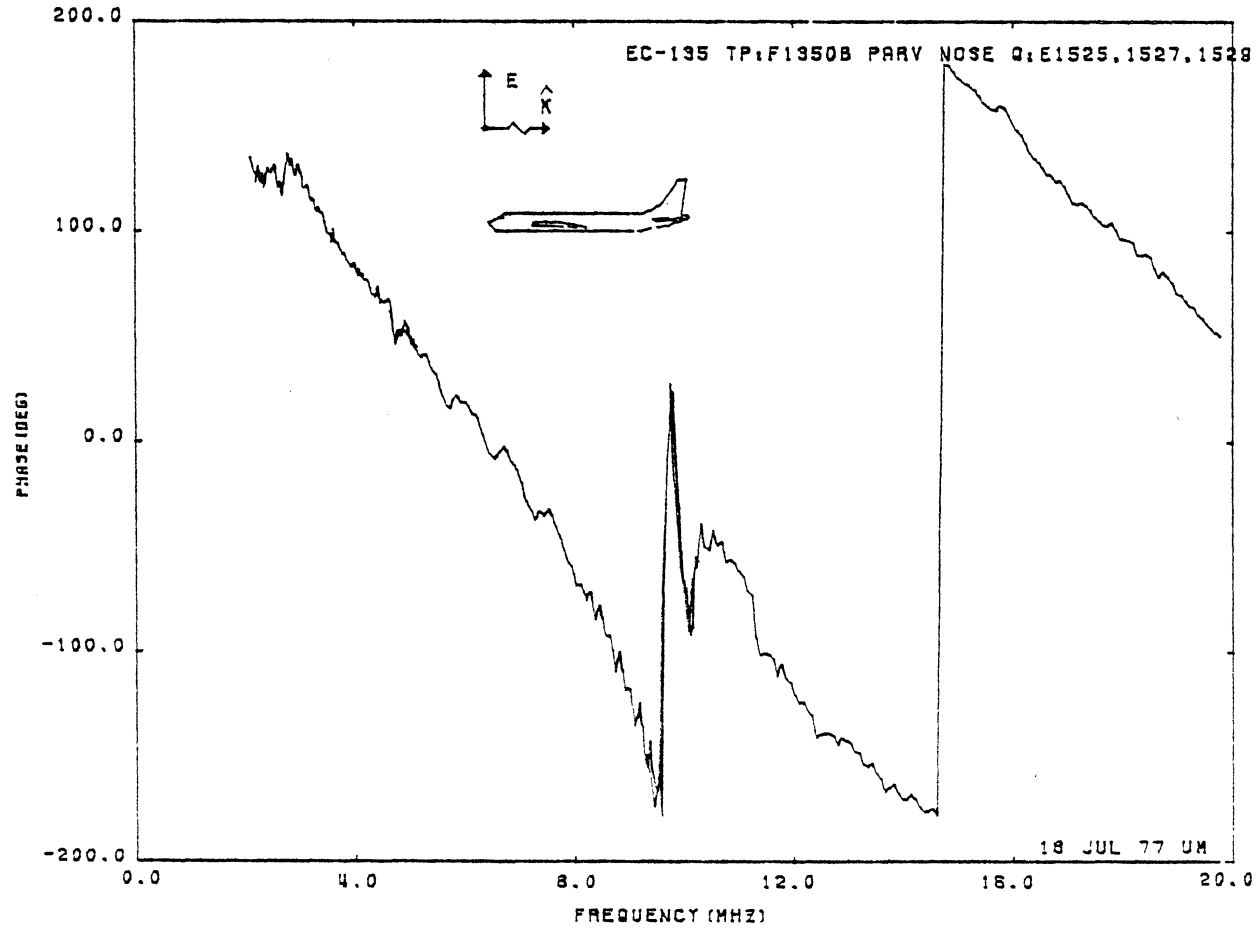

Figure 61: Charge at TP:F1350B, Orientation 3.

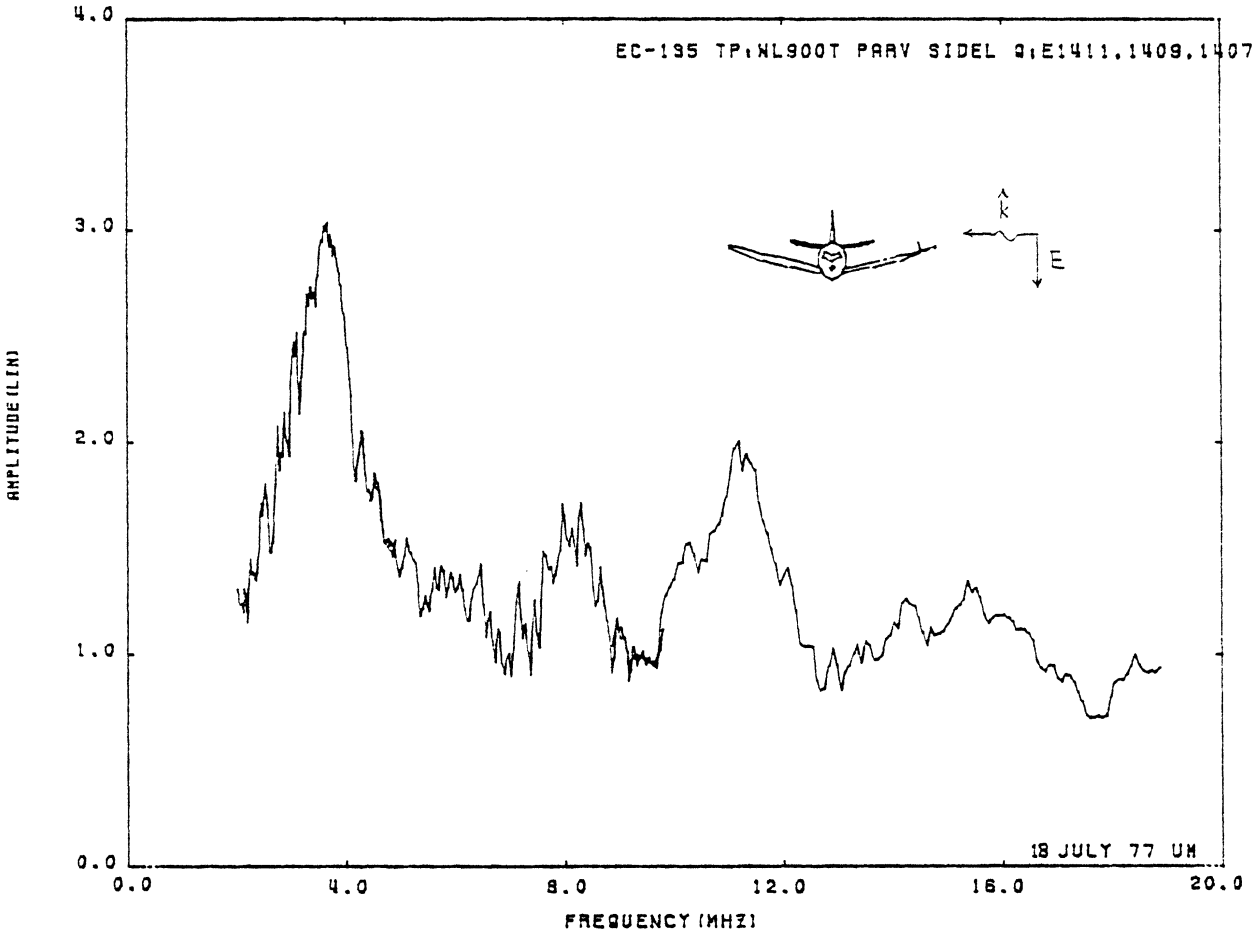

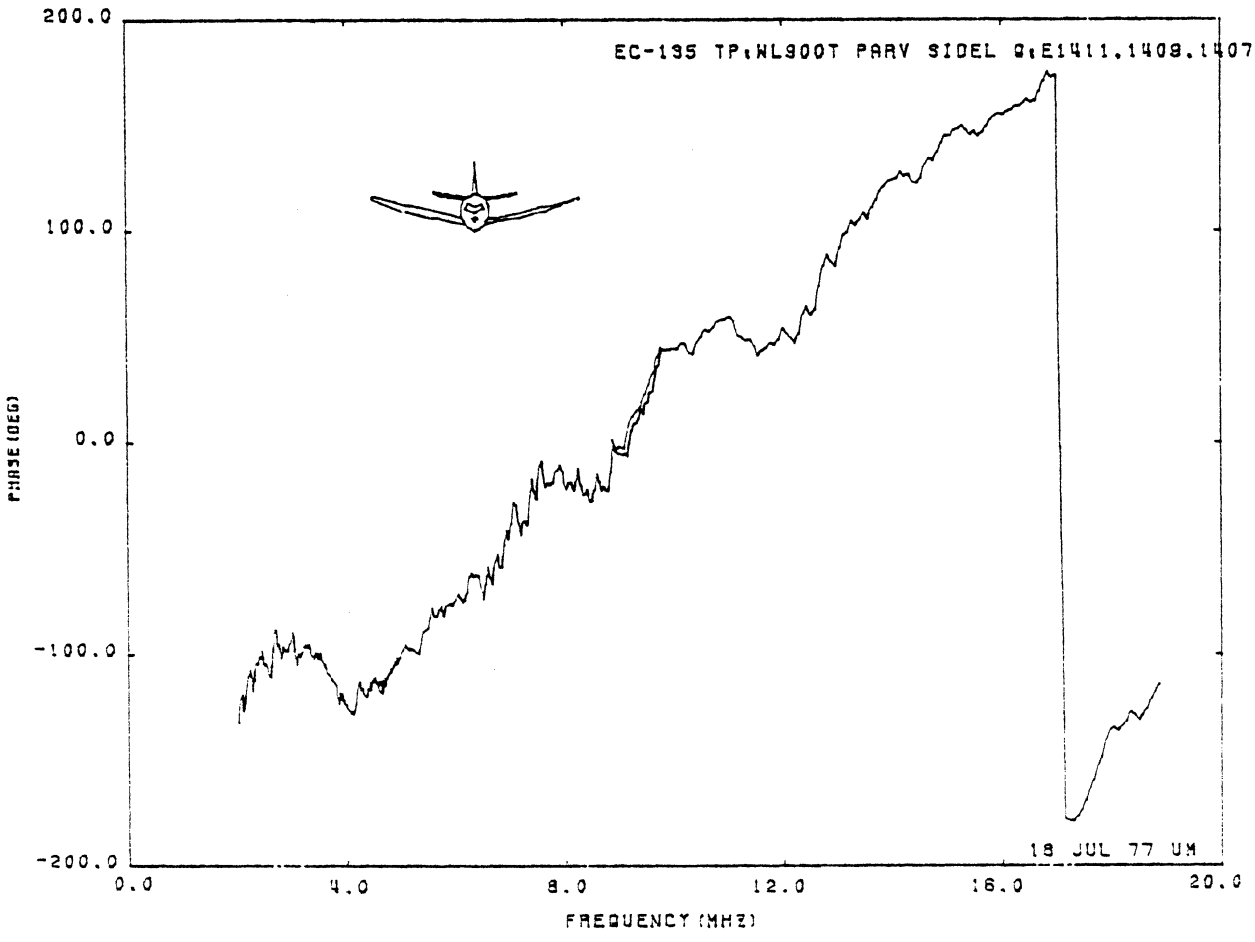

Figure 62: Charge at TP:WL900T, Orientation 4.

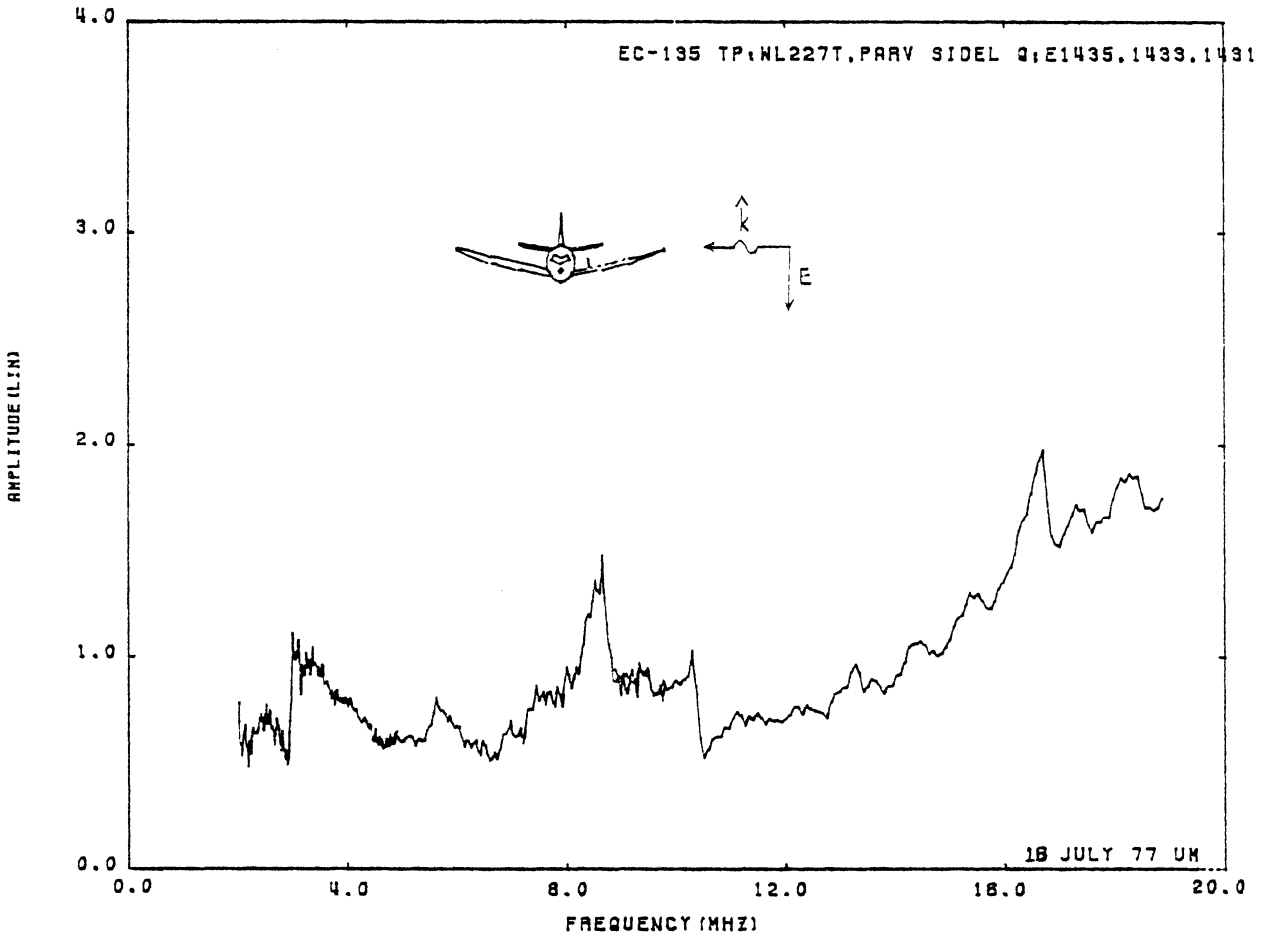

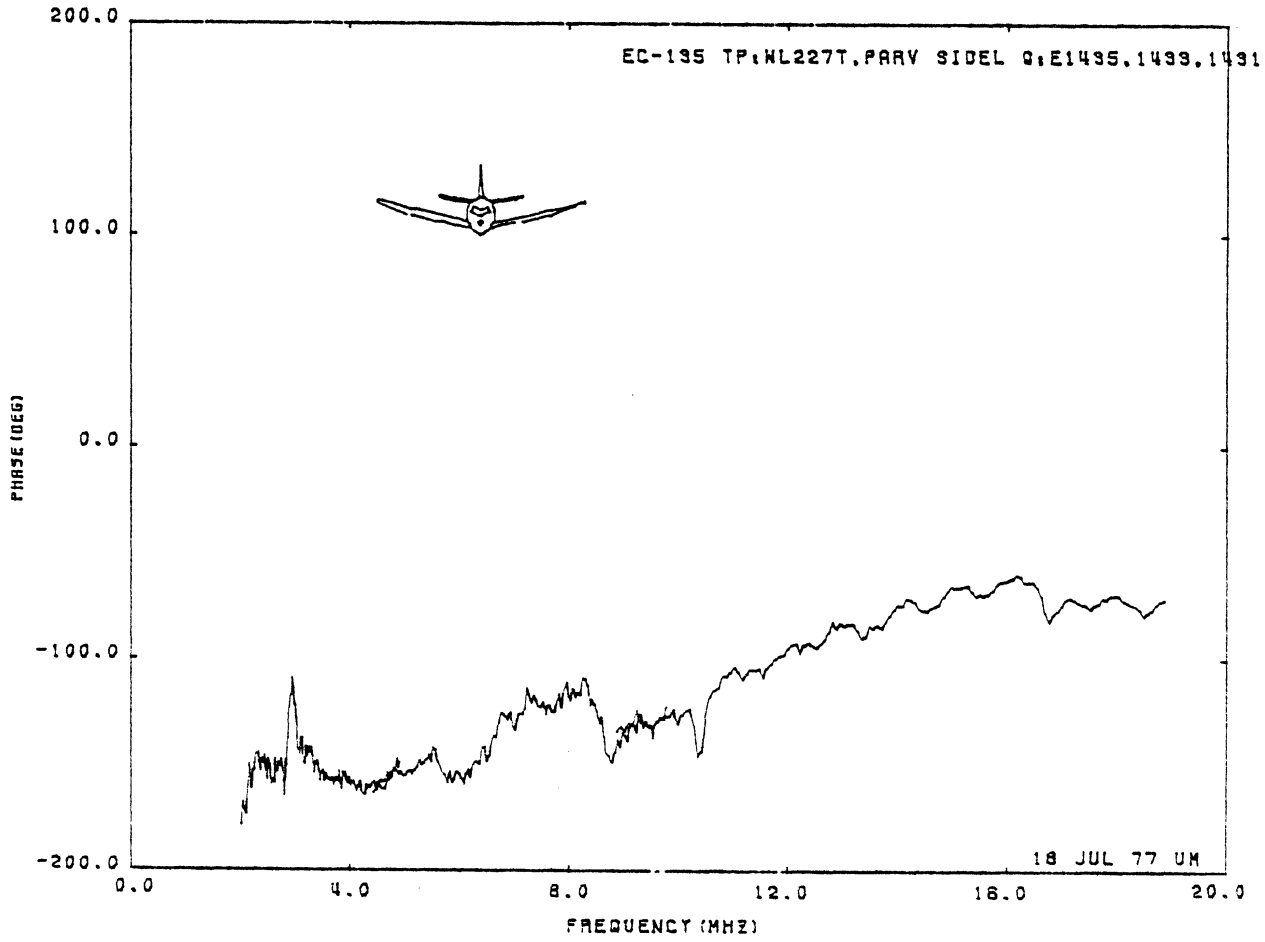

Figure 63: Charge at TP:WL227T, Orientation 4.

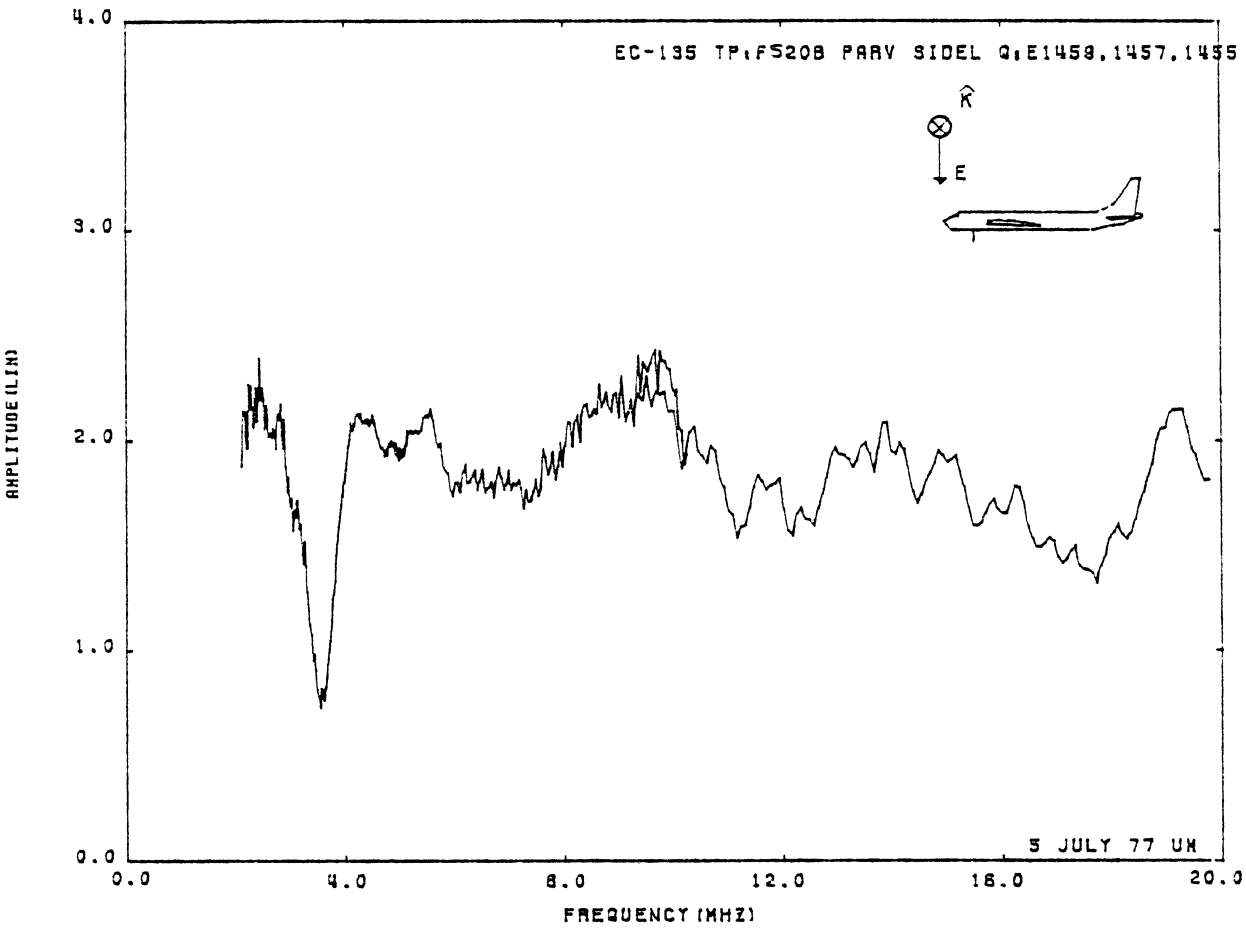

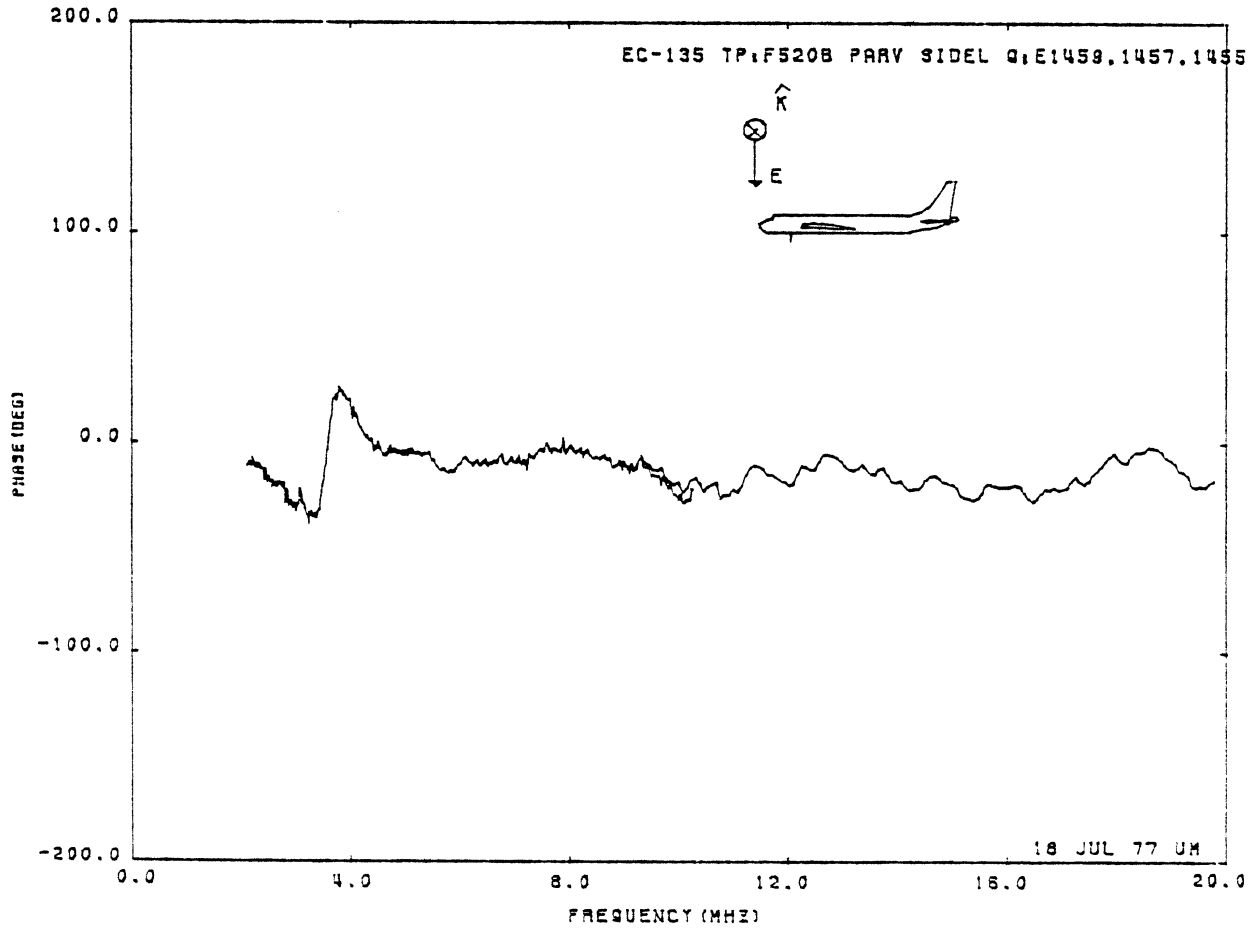

Figure 64: Charge at TP:F520B, Orientation 4.

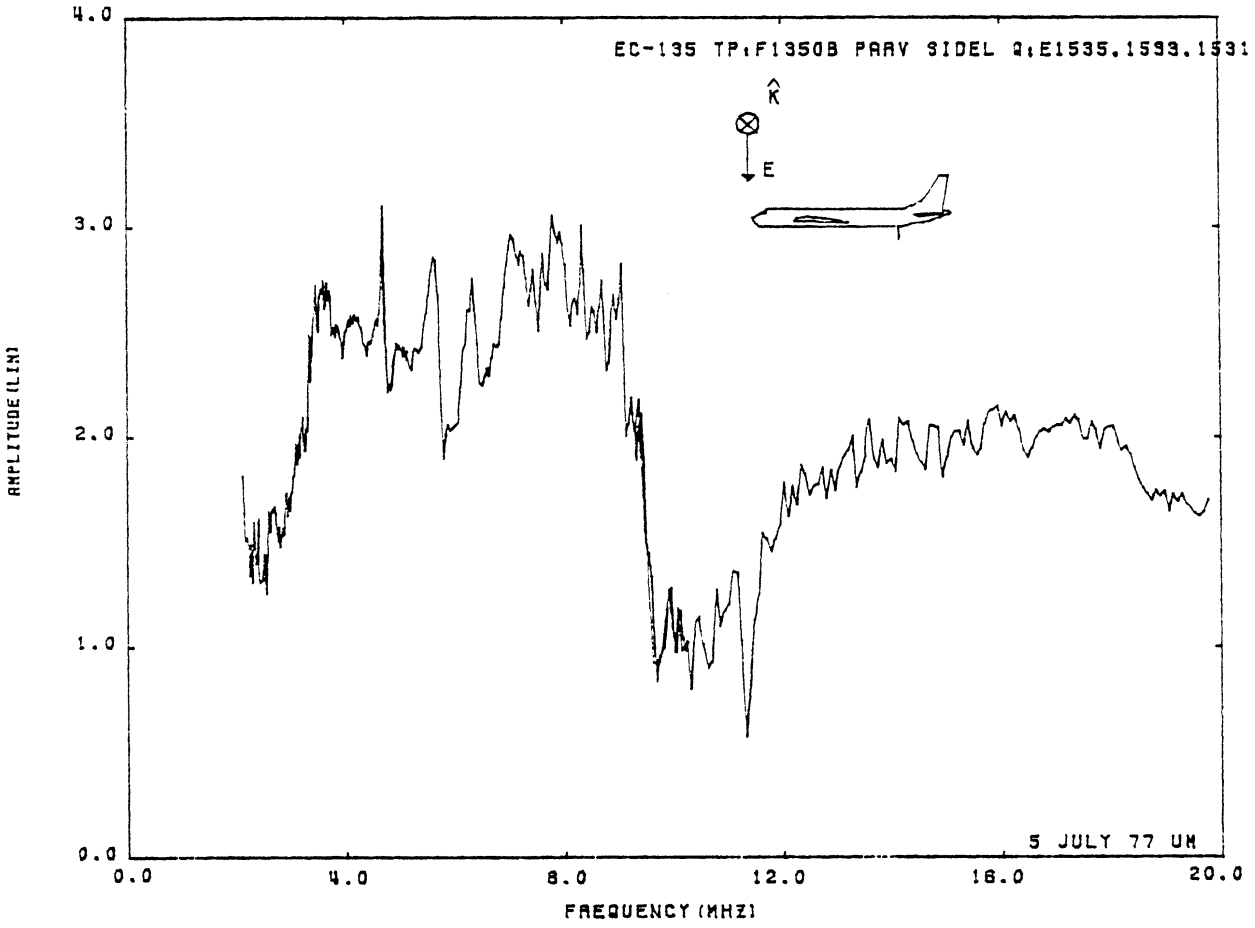

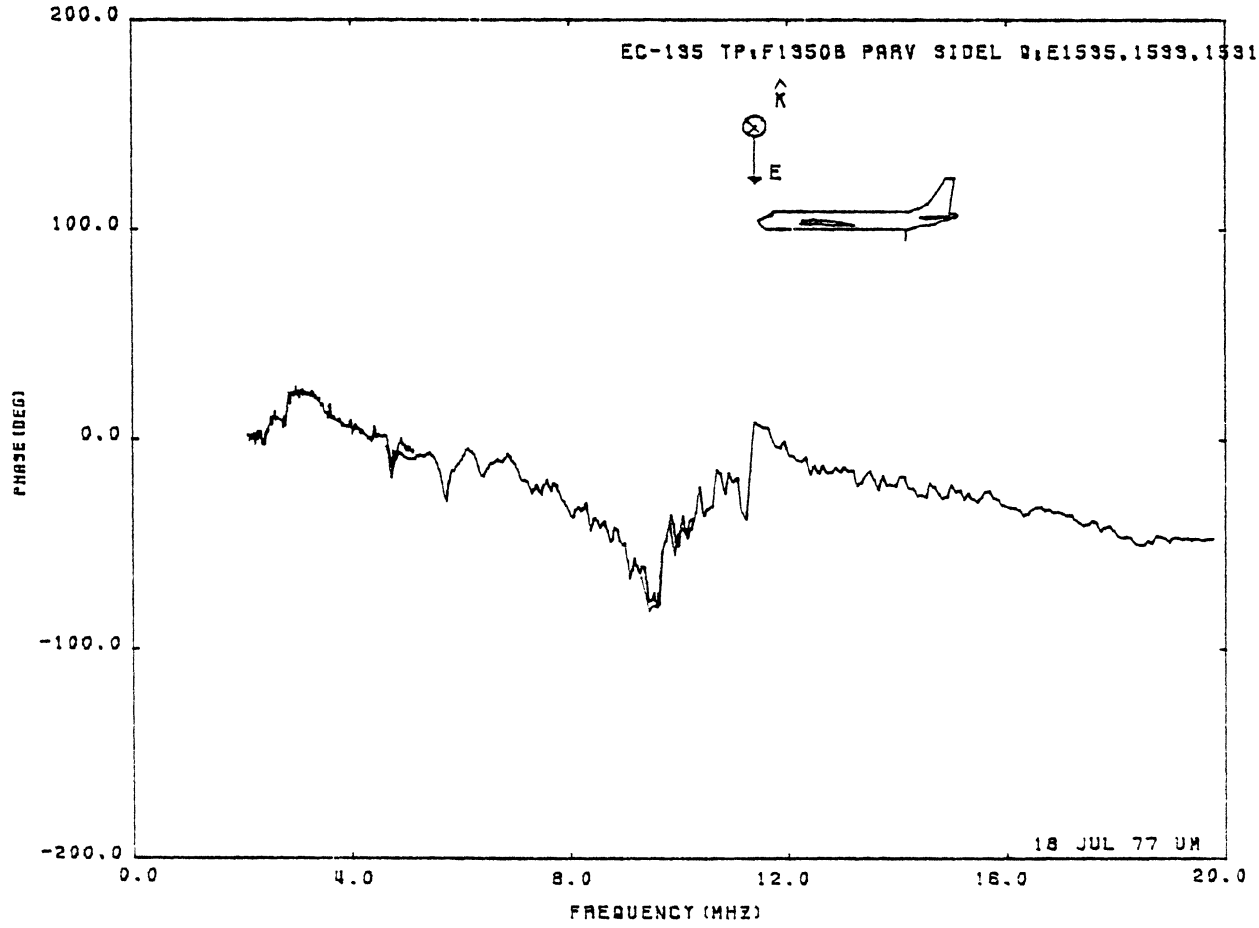

Figure 65: Charge at TP:F1350B, Orientation 4.